Comprehensive techno-econo-environmental modelling of renewable hydrogen supply chains

Tubagus Aryandi Gunawan, M.Sc., B.Eng.

Supervised by Dr Rory Monaghan

A thesis submitted to the National University of Ireland, Galway
as the requirement to obtain the degree of Doctor of Philosophy
in the College of Science and Engineering.

Mechanical Engineering

National University of Ireland, Galway

August 2021

Abstract

The research in this thesis has explored, investigated, and analysed renewable hydrogen supply chain opportunities and optimisation through techno-econo-environmental modelling. The modelling incorporates capital and operational costs and greenhouse gas emissions for all equipment and/or vehicles needed in hydrogen production, transportation, dispensing, and consumption. The key parameters for optimisation and evaluation include annual hydrogen production capacity, levelised cost of hydrogen (LCOH), total costs of vehicle ownership, and carbon abatement. Hydrogen can be produced from wind or solar via distributed or centralised electrolyser and compressed before storing or using it. The electrolyser operations are generally modelled under three different modes: (1) curtailed wind operation, (2) available wind operation, and (3) full capacity operation. Different electrolyser technologies and electricity prices are also investigated. The capacity and cost of hydrogen transportation using tube trailers from the production site to its closest end-user location are modelled and evaluated. In addition, location-allocation algorithms in a Geographic Information System environment are applied to optimise transportation routes. Applications of hydrogen investigated in this study include gas grid injection, heating, and transport. The modelling works in this thesis find that wind and solar can produce 100% green hydrogen. Curtailed, exportable, and available wind electricity are used in the modelling. The integration of wind and solar with additional batteries can increase hydrogen production capacity and reduce the LCOH. The LCOH can be used to size the equipment for producing hydrogen. The optimum equipment sizes are selected at the minimum LCOH. Using cost-effective hydrogen, the operational costs of some hydrogen-fuelled buses, trucks, and refuse collectors are almost as competitive as diesel.

Dissemination

Journal articles

- Gunawan, T.A.; Singlitico, A.; Blount, P.; Burchill, J.; Carton, J.G.; Monaghan, R.F.D. At What Cost Can Renewable Hydrogen Offset Fossil Fuel Use in Ireland's Gas Network?. Special Issue Computational Analysis of Natural Gas Supply Chains. Energies, Volume 13, Issue 7, Page 1798. 2020. (Chapter 3).
- Gunawan, T.A; Cavana, M; Leone P; Monaghan, R.F.D. Solar Hydrogen for High Capacity, Dispatchable, Long-Distance Energy Transmission – A Case Study for Injection in the Greenstream Natural Gas Pipeline. In preparation. (Chapter 4).
- Gunawan, T.A; Williamson, I.; Raine, D.; Monaghan, R.F.D. Decarbonising City Bus Networks in Ireland with Renewable Hydrogen. Special Issue on Hydrogen Energy Systems. International Journal of Hydrogen Energy, Volume 46, Issue 57, Pages 28870-28886. 2021. (Chapter 6).
- Gunawan, T.A; Monaghan, R.F.D. Techno-Econo-Environmental Comparisons of Zero- and Low-Emission Heavy-Duty Trucks Integrated with Wind Electricity – Case Study for a Quarrying Fleet in Ireland. Under review by the Elsevier Journal of Applied Energy. (Chapter 8).
- Gunawan, T.A; Monaghan, R.F.D. Decarbonisation Costs of Multiple Vehicles by A Regional Hydrogen Hub – Case Study in Galway, Ireland. In preparation. (Chapter 9).

Conference articles

- Gunawan, T.A.; Singlitico, A.; Blount, P.; Burchill, J.; Carton, J.G.; Monaghan, R.F.D. Towards techno-economic evaluation of renewable hydrogen production from wind curtailment and injection into the Irish gas network. Proceedings of the 32nd International Conference on Efficiency, Cost, Optimization, Simulation and Environmental Impact of Energy Systems (ECOS), Wroclaw, Poland 2019.
- Gunawan, T.A.; Monaghan, R.F.D. Decarbonising City Bus Networks in Ireland with Hydrogen from a Hybrid Wind-Photovoltaic-Battery-Electrolyser System. The 23rd World Hydrogen Energy Conference (WHEC2020), Istanbul, Turkey 2020.
- Moran, C.; Moylan, E.; Reardon, J.; Gunawan, T.A.; Monaghan, R.F.D. Can regional hubs make green hydrogen viable? – A case study for Ireland. Applied Energy Symposium: MIT A+B, Cambridge, USA 2021.

Public and stakeholder engagement

- A techno-economic modelling of hydrogen supply chain for Energy Co-operatives Ireland. (Chapter 5)
- An online map-based Decision Support Tool (DST) of Community Hydrogen Forum (CH2F) at http://communityh2.eu/dst/. (Chapter 7)
- A techno-economic modelling of hydrogen production for Robinson Quarry Masters Ltd, Northern Ireland. (Chapter 8)
- An investigation of hydrogen-fuelled agricultural tractors for the Association of Farm and Forestry Contractors in Ireland (FCI Ireland). (Chapter 9)

Acknowledgements

First of all, I would like to thank my dedicated supervisor, Dr Rory Monaghan, for the tremendous amount of help and assistance, countless fruitful discussions, and endless guidance during my intellectual journey at the National University of Ireland Galway. I am grateful and honoured to have been a postgraduate researcher in the GENCOMM project. It adds another milestone to my work experience. Rory has helped my research direction, linked me to key people in related topics, guided me on writing proposals, journal papers, and my thesis, and provided me with plenty of opportunities for capacity building. I am eternally grateful to Rory for his support and supervision.

I would like to express my gratitude to the following individuals for their generosity in sharing their knowledge and data; Dr Alessandro Singlitico, Dr James Carton, Dr Shane McDonagh, Dr Bodo Gross, Dr Wulf Clemens, Prof. Lionel Estel, Paul McCormack, Ian Williamson, Diana Raine, Paul Blount, James Burchill, James Robinson, Amanda Lyne, John O'Sullivan, Niamh Keogh and Cian Moran. It would have been impossible to complete my research and study without them. Finally, I would like to extend my gratitude to my Indonesian colleagues in Galway for the talks and Indonesian foods, Dr Febrimarsa, Andi Egon and Abdul Kadir. A distance of 12,000 km feels closer than ever.

I am grateful and indebted to funding institutions for supporting my research and study, including the European Union (EU) Interregional Cooperation (INTERREG) Northwest Europe (NWE) programme through the GENerating energy secure COMMunities through smart renewable hydrogen (GENCOMM) project (NWE 334), and the Sustainable Energy Authority of Ireland (SEAI) through research programme (RDD 445).

Also, I gratefully acknowledge the everlasting support and dedication of my daddy, Tubagus Iwan Gunawan; my mommy, Yennie Roesli; my big brothers, Tubagus Ardian

Gunawan and Tubagus Adimas Gunawan; my sisters in law, Dian Safarini and Yuniar Heriani; my nephews and niece, Zidane Rafif Ramzaki, M. Al Fatih Arsyanendra, Janitra Zahran Ibrahimovic, and Diandra Putri Andinar; my aunty, Dr Rennie Roesli; my cousin and her husband, Anastasia Wahyuni and Andrew Gibbons. Thank you to my beloved friends, Endra, Endry, Stanislaus Joze, Uray Irzandi, Adiesta Panjiesha and the saviour of my heart, Sofia Tjatradiningrat. I would never have grown to be who I am today without them.

I would like to thank the wind, the sunshine, the water, the beaches, the rivers, the forests, and the mountains. Although they can never speak and are threatened by human activities, they are always there to refresh my mind. Let’s hope the best for the future of our planet.

Table of contents

List of figures

List of tables

Nomenclature

Latin symbols

c	Specific cost, €/kWh or €/kW
C	Total cost, €
$\dot{C}$	Kilometric cost, €/km
Cp	Specific heat, kJ/kgK
CoP	Coefficient of Performance
d	Fuel economy, km/kWh
D	Operational distance, km
DoD	Depths of discharge
E	Energy, kWh
$\dot{E}$	Average refuelling energy delivered per minute, kWh/minute
$\tilde{E}$	Average hourly fuel demand, kWh/hour
$\bar{E}$	Average daily fuel demand, kWh/day
f	Fuel consumption, (DB) km/litre or (FCEB) km/kg
H_A	Total time of available hoses, minutes per filling
H_O	Total time of occupied hoses, minutes per filling
k	Specific heat ratio
K	Temperature, Kelvin
L	Distance between wind farm and HRS, km
$LCOH_D$	Levelised cost of hydrogen dispensing, €/kg
$LCOH_F$	Levelised cost of hydrogen fuel from whole system, €/kg
$LCOH_P$	Levelised cost of hydrogen production, €/kg
$LCOH_T$	Levelised cost of hydrogen transportation, €/kg
m	Average hourly mass flow rate, kg/hour
$\dot{m}$	Average filling capacity, kg/ filling

m'	Average molar flow rate, kgmol/second
M	Annual mass capacity, kg/year
$\dot{M}$	Average daily mass capacity, kg/day
n	Year of *n*, year
N	Number, unit
O_D	Operation distance, km/day/bus
O_T	Operation time, days/year/bus
p	Pressure, barg
P	Nominal power, MW_e
r	Discount rate, %
R	Gas constant, J/°K·mol
t	Time, hour
t'	Time, minute
T	Time, year
x	Fraction
Z	Compressibility factor

Greek symbols

α	Specific energy consumption, kWh/km
η	Efficiency, %
λ	Capacity factor, %
μ	Specific energy consumption, kWh/kg
τ	Economic lifetime, year

Abbreviations

AGI	Above ground installation
AMB	Ambient temperature
AW	Available wind
BESS	Battery energy storage subsystem
BET	Battery electric heavy-duty truck
BSV	Buffer storage vessel
CAPEX	Capital expenditure
CS	Charging system
CCUS	Carbon dioxide capture utilisation and storage
CW	Curtailed wind
DB	Diesel bus
DS	Dispensing system
DF	Diesel fuel
DFET	Diesel-hydrogen dual-fuel engine heavy-duty truck
DS	Dispenser system
DT	Diesel truck
DQ	Dispatch quantity
EB	Electric battery
EC	Electric compressor
EL	Electricity
EMU	Energy management unit
ENG	Engineering
EG	Electricity grid
EW	Exportable wind
F	Fuel

FCEB	Fuel cell electric bus
FCET	Hydrogen fuel cell electric heavy-duty truck
FP	Filling process
FOM	Fixed operation and maintenance
GIS	Geographic information system
GNI	Gas Networks Ireland
H_2	Hydrogen gas
H_2O	Water
HESS	Hydrogen energy storage subsystem
HD	Hydrogen gas at dispensing subsystem
HDT	Heavy-duty truck
HFSC	Hydrogen fuel supply chain
HOF	Hose occupation factor
HP	Hydrogen gas at production subsystem
HRS	Hydrogen refuelling station
HT	Hydrogen gas at transportation subsystem
HX	Heat exchanger
I	Refuelling infrastructure
IN	Inlet condition
INV	Investment capital
ICET	Diesel internal combustion engine truck
ICS	Interconnection, commissioning, and start-up
LP	Lingering process
M	Maintenance
MG	Metered generation
MPC	Major powertrain components

NMC	Nickel Manganese Cobalt Oxide
NO	Nitric oxide
NO_2	Nitrogen dioxide
NO_x	Nitrogen oxide
O_2	Oxygen gas
OPEX	Operation and maintenance expenditure
OPT	Optimum size
OH	Other expenditure
OM	Operation and maintenance
OT	Operation time
out	Outlet condition
PH	Peak hour
PHET	Plug-in hybrid electric heavy-duty truck
PV	Photovoltaic
PROD	Production
R	Resale
RC	Additional retail cost
RT	Retest of tube trailer
RU	Refrigeration unit
SEMO	Single Electricity Market Operator
SCR	Selective Catalytic Reduction
SR	Electrolyser stack replacement
SOC	State of charge
SV	Storage vessel
TOTAL	Summary of production and transportation
TRANS	Transportation

TRIP	Occurrence of hydrogen delivery
TCO	Total cost of truck ownership
TCA	Total cost of carbon abatement
TTW	Tank-to-wheel
TT	Tube trailer
UR	Utilisation rate
V	Vehicle
VOM	Variable operation and maintenance
VRF	Vanadium Redox Flow
WE	Water electrolyser
WF	Wind farm
WHS	Wind-hydrogen system
WPBES	Wind-photovoltaic-battery-electrolyser system
WT	Wind turbines
WTT	Well-to-tank
WTW	Well-to-wheel
ZLET	Zero- or low-emission trucks

“I believe that water will one day be employed as fuel, that hydrogen and oxygen which constitute it, used singly or together, will furnish an inexhaustible source of heat and light, of an intensity of which coal is not capable”.

Jules Verne, the Mysterious Island, 1875

Chapter 1. Introduction

1.1. Hydrogen and climate target

In Paris at the end of 2015, members of the Conference of the Parties (COP) 21 of the United Nations Framework Convention on Climate (UNFCCC) agreed to limit global warming to below 1.5 or 2°C, compared to pre-industrial levels. To achieve this ambitious target, we must significantly reduce greenhouse gas (GHG) emissions over the years. The Intergovernmental Panel on Climate Change (IPCC) identified the key pathways to reduce GHG emissions in energy-intensive sectors. They include increased efficiency, resource circularity, substituting existing polluting technologies with electrification, hydrogen, bio-based fuels, and, when necessary, additional carbon dioxide capture utilisation and storage (CCUS) [1]. These pathways are aligned with several Sustainable Development Goals (SDGs) such as the development of health (goal 3), clean energy (goal 7), cities and communities (goal 11), responsible consumption and production (goal 12) and oceans (goal 14). However, these pathways will cause trade-offs with poverty (goal 1), water (goal 6) and energy access (goal 7) if poorly managed [1].

In moving towards a climate-neutral economy in the region, the European Union (EU) set key targets to be achieved by 2030, (1) 40% reduction of GHG emissions, compared to 1990 levels, (2) 32% contribution of renewable energy, and (3) 32.5% improvement in

energy efficiency [2]. These targets have recently been strengthened to a 55% GHG emissions cut by 2030 [3]. To achieve these targets, the EU can substitute their polluting energy system with the hydrogen-based energy system, particularly for harder-to-abate sectors. These sectors can eliminate one-third of total global GHG emissions and require relatively higher abatement costs than the rest of the economic sectors [4]. Hydrogen has a potential role in decarbonising energy-intensive industries like cement, steel, and plastics as well as heavy transport and shipping, which might not easily be done by electrification entirely. Hydrogen can be used to produce steel via direct reduction of iron (DRI), electricity via fuel cells or turbines, heat via boilers, and chemical feedstocks. One of the strategies to accomplish this is deploying hydrogen as envisioned in the EU Hydrogen Strategy [5]. It is necessary to improve the economic competitiveness and feasibility of the green hydrogen value chain. Therefore, the EU aims to scale up its hydrogen production capacity, boosts hydrogen demand, and build more hydrogen-based infrastructure, including distribution via pipelines, trucks, or ships, storage via salt cavern or tube trailers, and dispensing for vehicles via hydrogen refuelling station [5].

1.2. Hydrogen production routes

Hydrogen can be produced from a wide range of primary energy sources through various technological routes. Hydrogen is often classified using some variation of the colour scheme shown in Table 1.1, even though hydrogen gas is colourless. A review by Shahbaz et. al. summarised the emerging technologies to produce green hydrogen from biomass via (1) biochemical processes that include biophotolysis and fermentation, and (2) thermochemical processes such as pyrolysis, gasification, combustion, and liquefaction [6]. Green hydrogen can also be produced using renewable electricity from wind, solar, hydro, geothermal, wave and tidal via water electrolysis [7]. In addition, hydrogen production directly from water driven by sunlight can also be performed with

photoelectrochemical approaches [8]. However, hydrogen generated from electrolysis can be categorised as pink and yellow if the primary sources are nuclear and electricity of mixed origin, respectively. Natural gas can be converted through steam methane reforming (SMR), a thermochemical process, to blue hydrogen if the emitted carbon dioxide is captured by carbon dioxide capture utilisation and storage (CCUS), or grey hydrogen if it is not. In addition, Noussan et. al. described turquoise hydrogen generated from natural gas through pyrolysis, where solid carbon resulted as the by-product [9]. Additionally, hydrogen production from waste plastic (polyethylene) using pyrolysis is also investigated and developed by Aminu et. al. [10]. Finally, black or brown hydrogen comes from the gasification of black or brown coal.

Table 1.1. The industrial terminology for hydrogen colour according to the technology and primary energy, reproduced from [6], [7], [9], [11], [12]

Terminology	Primary energy	Key technology
Green hydrogen	Biomass	Various biochemical, thermochemical and/or chemical processes
	Renewable electricity (wind, solar, hydro, geothermal, tidal, wave)	Electrolysis
Purple/ Pink hydrogen	Nuclear electricity	
Yellow hydrogen	Mixed-origin grid electricity	
Blue hydrogen	Natural gas	Steam methane reforming and carbon capture storage
	Coal	Gasification and carbon capture storage
Turquoise hydrogen	Natural gas	Pyrolysis
Grey hydrogen	Natural gas	Steam methane reforming
Brown hydrogen	Brown coal (lignite)	Gasification
Black hydrogen	Black coal	

1.3. Hydrogen supply and demand

Most hydrogen today is produced from fossil fuels - thus emitting carbon dioxide- because of the low production cost (1.4 €/kg on average) of SMR. SMR is responsible for 70% of global hydrogen supply [11]. Hydrogen demand is primarily in the ammonia, oil refining, and methanol industries at 55%, 25% and 10% of total global demand, respectively [11]. This indicates that, currently, hydrogen is mainly used as a feedstock

for fertilisers and refineries. Regionally, the total hydrogen demand is equivalent to 1% of Europe's final energy demand [11].

Hydrogen Europe[1] estimates that hydrogen demand will increase to 6% of total energy demand in the EU by 2030 and up to 24% by 2050 [13]. This projection can only be reached if other applications of hydrogen (i.e. transportation, heat and power) become economically competitive compared to fossil fuel-based conventional technologies. Indeed, the Hydrogen Council[2] predicts that the economic competitiveness of hydrogen as industrial feedstock will be followed by other new applications such as transportation by 2025, heat and power for buildings by 2030, and industry by 2040 [14]. Thus, it is imperative to implement a strategic plan to move hydrogen usage from the domination of chemical industries to some shares of transportation and heat; and to move hydrogen production from carbon emitting sources to renewable sources.

1.4. Renewable hydrogen projects in Europe

The EU supports several renewable hydrogen development projects as part of the EU Interregional Cooperation (INTERREG) Northwest Europe (NWE) and Horizon 2020 Research and Innovation Program. Funded by INTERREG NWE, the GENCOMM (GENerating energy secure COMMunities through smart renewable hydrogen) project is building a total of 1,250 kW_e of electrolyser capacity in three different locations as listed in Table 1.2. In the same table, the BIG HIT (Building Innovative Green Hydrogen systems in an Isolated Territory) project currently operates a total of 1,500 kW_e of electrolyser capacity to produce hydrogen using wind electricity on remote islands in

[1] Hydrogen Europe is an umbrella association representing more than 200 European companies, 90 research organisations, and 26 national associations in the hydrogen and fuel cell sector.
[2] Hydrogen Council is a global CEO-led initiative of 92 energy, transport, industry, and investment companies to develop the hydrogen economy.

Scotland, UK. These renewable hydrogen projects indicate the transformation of hydrogen usage from industrial to transportation and hydrogen production from fossil fuels to renewable sources in Europe.

In addition to these projects, there are multiple ongoing renewable hydrogen projects and studies in Europe. These include HUGE (Hydrogen Utilization and Green Energy) to facilitate remote and rural communities with the assessment tool and business model to use hydrogen for housing, transport, and industry, SEAFUEL (Sustainable Integration of Renewable Fuels in Local Transportation) to use seawater as the water source to produce hydrogen, hydrogen for industries in the 2x40 GW initiative by Hydrogen Europe, as well as the development of a regional hydrogen hub by ORION (Opportunity for Renewables Integration with Offshore Networks).

Table 1.2. Renewable hydrogen development status in Europe

Project	Location	Funding from	Electrolyser		Current status	Energy source	Hydrogen end-user
			Size in kWe	Technology*			
BIG HIT	Shapinsay Island, Scotland	European Union's Horizon 2020	1,000	PEMWE	Operational	Wind	Boiler in Shapinsay
BIG HIT	Eday Island, Scotland	European Union's Horizon 2020	500	PEMWE	Operational	Wind and tidal	Van fleet and heat and power in Kirkwall
Brande Hydrogen	Brande, Denmark	Siemens Gamesa	400	AWE	Operational	Wind	Taxi fleet
GENCOMM	Antrim, Northern Ireland	INTERREG Northwest Europe	1,000	PEMWE	Under construction	Wind	City bus
GENCOMM	Saarbrucken, Germany	INTERREG Northwest Europe	50	PEMWE	Under construction	Solar	Private car
GENCOMM	Stornoway, Scotland	INTERREG Northwest Europe	200	PEMWE	Operational	Biomass	Refuse collector
Green Hysland	Mallorca, Spain	Fuel Cells and Hydrogen Joint Undertaking	7,500	PEMWE	Planning	Solar	Transport, heat, power, and gas network
H2FUTURE	Linz, Austria	Fuel Cells and Hydrogen 2 Joint Undertaking	6,000	PEMWE	Operational	Wind and solar	Grid services and steel manufacturing process
REFHYNE	Rheinland, Germany	Fuel Cells and Hydrogen Joint Undertaking	10,000	PEMWE	Operational	Low CO_2 electricity	Refinery
SEAFUEL	Tenerife, Spain	INTERREG Atlantic Area	35	PEMWE	Planning	Wind and solar	Van fleet

*) *PEMWE = Proton Exchange Membrane Water Electrolyser, AWE = Alkaline Water Electrolyser*

1.5. Thesis motivation

Hydrogen can only be classified as renewable fuel if generated using renewable energy sources, and only then can potentially be used to decarbonise the harder-to-abate sectors [4], [15]. To do this, the cost of owning and operating renewable hydrogen-fuelled vehicles must be competitive to diesel-fuelled vehicles. So that, renewable hydrogen can achieve substantial decarbonisation of conventional heavy-duty vehicles. Therefore, to reduce the cost of owning and operating hydrogen-fuelled vehicles, the value chain of renewable hydrogen, comprising production, transportation, and dispensing, needs to be optimised [16]. To achieve this, the EU already has a roadmap of hydrogen development. In addition, at least 12 countries worldwide have published hydrogen strategies as part of their drives to carbon neutrality by 2050 [17]. The motivation of this thesis is to use a novel integrated modelling approach to investigate and discuss the opportunities and challenges of renewable hydrogen supply chains to cost-effectively achieve substantial decarbonisation of energy systems.

1.6. Thesis aims and objectives

The overall aims of this thesis are (1) to model the renewable hydrogen supply chains that reduce fossil fuel consumption and carbon emissions, (2) to optimise overall renewable hydrogen costs making it more affordable as a clean and sustainable energy supply, (3) to enable sector coupling between renewable power, heating, transportation, and gas networks, and (4) to support communities and industries in energy security and transition. These aims are achieved by meeting technical research objectives, which are:

1. Modelling of renewable hydrogen supply chains that comprises hydrogen production, transportation, dispensing and consumption.

2. A comprehensive modelling framework, including technical, economic, and environmental aspects of the renewable hydrogen supply chain.
3. Ability to handle multiple energy sources (wind, solar, curtailed, exportable, and grid electricity), system designs (distributed and centralised systems, on- and off-grid electricity system, and on- and off-site hydrogen production), distribution options (tube trailers and gas networks), and end-users (transportation and heating).
4. Optimisation techniques to minimise delivered hydrogen costs via component selection and sizing, as well as distribution routes and allocation.
5. Assess the framework for a wide range of configurations on system designs and value chains, technologies, time frames (parameters for 2020 and 2030), capacities, and locations.

1.7. Thesis outline

The thesis is written based on five journal articles, two of which have been published, one under review, and two in preparation, and four public engagement activities. The thesis is presented in ten chapters as follows.

Chapter 1 presents the general background of the research. It covers the global issues of climate change and current hydrogen development. The research objectives and thesis outline are also provided in this chapter.

Chapter 2 presents the literature review of the state-of-the-art technology and costs of hydrogen production, transportation, dispensing and vehicles. Additionally, this chapter covers the recent literature on the integration of wind and solar electricity and sector coupling between power and transport sectors. Chapters 3 to 9 present the application of the modelling framework to various value chain case studies.

Chapter 3 presents system design, techno-economic modelling, and optimisation of hydrogen production from wind electricity for gas grid injection on the island of Ireland.

Chapter 4 presents the same for hydrogen production from solar electricity for gas grid injection in Libya to be transmitted to Italy via the Greenstream gas corridor.

Chapter 5 presents techno-economic modelling of hydrogen production from wind electricity for heating and transportation in a remote community in Ireland.

Chapter 6 presents system design, techno-economic modelling, optimisation and integration of hydrogen production using wind and solar electricity for city bus networks on the island of Ireland.

Chapter 7 presents the same analysis for the 38 largest cities in northwest Europe. Chapter 8 presents the system design, techno-econo-environmental modelling, optimisation and integration on hydrogen production using wind electricity to fuel zero- and low-emission heavy-duty trucks for quarry activities.

Chapter 9 presents the same analysis applied to the decarbonisation of various types of vehicles in Galway, Ireland.

Chapter 10 presents the conclusion of the thesis and several key findings during the research. Additionally, it makes suggestions for potential studies in the future.

Chapter 2. Literature Review

2.1. Overview

Renewable hydrogen has a potential role to decarbonise the energy system. This chapter reviews the most recent and relevant studies to achieve the aims and objectives described in the previous chapter. A wide range of journal articles on the modelling of hydrogen value chains have been reviewed. The reviewed studies are categorised into (1) hydrogen production, transportation, and dispensing (2) hydrogen mobility and energy systems. The research gaps from the modelling-related studies are found on the types of modelling aspects, optimisation techniques, systems, hydrogen end-users, analysis, and the scope areas. Not all the studies included hydrogen production, transportation, dispensing, and consumption in the technical models. Moreover, there is a missing link between techno-economic modelling with the environmental aspect of the abated GHG emission. Additionally, the optimisation is partial, focusing mostly on the hydrogen production side. Also, most of the literature overlooks the importance of including production, transportation and dispensing to total hydrogen fuel costs. Therefore, this thesis suggests the modelling framework that integrates technical, economic, and environmental aspects of renewable hydrogen supply chains.

2.2. Introduction

This chapter aims to (1) define the current opportunities and challenges on the modelling of renewable hydrogen supply chains, and (2) provide a modelling framework to achieve the aims and objectives of this thesis. Hence, the objectives of this chapter are to:

- review hydrogen production, transportation, and dispensing,
- review modelling methods, system designs, and optimisation techniques,
- identify current research gaps, and
- propose potential modelling frameworks.

A total of 48 journal articles on the modelling of hydrogen supply chains have been reviewed. The studies cover the at least one of the following aspects, technical, economic, and emission. The opportunities and challenges found in the reviewed studies are highlighted and discussed in two categories of (1) hydrogen production, transportation, and dispensing (2) hydrogen mobility and energy systems. Studies on hydrogen production, transportation, and dispensing are broke down to hydrogen from wind electricity, hydrogen from solar electricity, hydrogen from hybrid power systems, hydrogen for grid injection, hydrogen for transportation, and hydrogen refuelling infrastructures. Each of these classifications is discussed in the subsection 2.3.1. to 2.3.6. Hereafter, studies on hydrogen mobility and energy systems are classified to electrification of transportation, decarbonisation of heavy-duty trucks, and on-grid and off-grid electricity systems. Each of these classifications is covered in the subsection 2.4.1. to 2.4.4. The modelling gaps are classified to (1) technical models, (2) optimisation, (3) systems, (4) economic models, (5) emission models, (6) hydrogen end-users, (7) analysis types, and (8) the coverage areas. All the important opportunities, challenges, research gaps, and suggestions for modelling frameworks are summarised in conclusion section.

2.3. Hydrogen production, transportation, and dispensing

2.3.1. Hydrogen from wind electricity

Most wind curtailment occurs in countries with wind penetration above 10% [18]. In Ireland, dispatch-down of wind energy refers to the amount of wind energy that is available at wind farms but cannot be used by the electricity networks due to limitations of system-wide networks (curtailment) and local networks (constraints) [19]. According to WindEurope, the overall wind curtailment is caused by two factors: (1) low wind demand in the electricity market, and (2) low capacity of electricity networks. The low wind demand is caused by (1) must-run capacities of conventional power plants, and (2) wind supply limitation to maintain system stability [20]. The low transmission capacity is caused by (1) transmission congestion, and (2) network constraint [20]. Beccali et al. simulated wind curtailment using electricity demand and wind speed data and then defined optimum system size from minimum hydrogen production cost [21]. The study found that the cost of hydrogen production using an electrolyser with 75% wind electricity and 25% grid electricity is between 4 and 7 €/kg. Zhang et al. advanced the optimisation by using real time data from a wind farm and introduced the need of a grid electricity supply to maintain minimum power for the electrolyser to run idle [22]. However, in Zhang's study, the algorithm is designed to replace curtailed wind with grid electricity whenever curtailed wind does not meet the minimum power to run electrolyser. Thus, some curtailed wind is still wasted. The analysed system did not include a compressor, which also consumes energy. A novel approach to optimise the system capacity of hydrogen production is required, where curtailed wind is prioritised to power the electrolyser and compressor. Available exportable electricity from the wind farm and grid electricity also can used as backup energy sources.

2.3.2. Hydrogen from solar electricity

Currently, renewable electricity can be commercially generated from solar energy through photovoltaic (PV) and concentrated solar power (CSP) technologies. The global average levelised cost of electricity (LCOE) for PV and CSP in 2020 are 57 and 108 USD/MWh, respectively [23]. The global average installed PV system cost for utility-scale systems is 883 USD/kW [23]. A wide range of studies estimates the costs of solar electricity can be reduced due to the decrease of capital expenditure (CAPEX) of PV in the future [24]–[26]. When the CAPEX of PV reaches 458 USD/kW in 2030, the LCOE of PV could be 23 to 28 USD/MWh [26].

Hydrogen can be produced using PV electricity via a water electrolyser system. Modelling work by Kikuchi et. al. found that an additional battery to the hydrogen production from PV electricity can improve the productivity of the electrolyser [27]. This finding is aligned with those from a pilot PV-based hydrogen plant described by Dispenza et. al [28]. The study found that the addition of a battery can store excess PV electricity to be used by the electrolyser later, for example at night. Thus, when the system is connected to the grid, the battery can reduce grid electricity usage as well as the carbon intensity of hydrogen production. In addition, Berckmans et. al. estimated the cost of lithium-ion batteries will be less than 100 USD/kWh by 2030 due to the rapid growth of the battery market [29].

2.3.3. Hydrogen from hybrid power systems

A hybrid power system combines two or more electricity sources such as wind and solar, with or without additional battery, and with or without backup by grid electricity. In their study of power-to-gas, McDonagh et al. describe hydrogen from grid electricity as a potential clean fuel for transport in Ireland. The evaluation shows electricity purchased at

a low bid price can reduce the carbon intensity (gCO_2/kWh) of hydrogen produced, due to larger shares of renewables in the grid at these times mainly from surplus renewable electricity [30]. To produce hydrogen electrochemically, Schmidt et al. describes that a proton exchange membrane (PEM) electrolyser is able to use intermittent renewable electricity, with very short response times, and produce high purity hydrogen [31]. In terms of power sources for electrolysers, evaluation by Abdin et al. describes that integration of wind and solar can increase the energy to generate more hydrogen and minimise hydrogen production cost despite larger capital costs [32]. When the costs of batteries are added in wind- or PV-only systems, studies by Papadopoulos et al. and Kikuchi et al. show significant advantages from installing batteries to increase electrolyser capacity factor to reduce hydrogen production cost [27], [33].

2.3.4. Hydrogen for gas grid injection

Spatial analysis through the use of Geographic Information System (GIS) software on the evaluation of hydrogen production capacity from wind energy enables identification of high potential sites [34]. Quarton et al. described current hydrogen projects that focus on grid injection and emphasised the need for incorporating spatial analysis in future hydrogen studies [35]. In Ireland, the potential of hydrogen production from wind curtailment integrated with biogas production to create biomethane was evaluated by Vo et al. [36]. The study found the maximum capacity of biomethane production is limited by the level of hydrogen capacity from curtailed wind. McDonagh et al. investigated hydrogen production from grid electricity and found that incorporating wind curtailment within the analysis can reduce the carbon intensity of the hydrogen produced [30]. Singlitico et al. spatially assessed the techno-economics of biomass-derived synthetic natural gas (bio-SNG) injection into the Irish gas network and optimised the design of the supply chain for economic performance using a geographic information system (GIS) [37]. The authors further expanded their work to include supply chain optimisation for

environmental performance and explored trade-offs between these two optima [38]. The current study also aims to fill a literature gap on how much hydrogen can be optimally and economically produced in respect to the reduction of wind curtailment and efficiently supplied to gas injection sites. As recently published by [39], the Irish gas grid operator, Gas Networks Ireland (GNI), plans to directly inject hydrogen into the gas network after 2030.

Cavana et al. investigated the technical challenges of injecting and blending different volume fractions of hydrogen produced from PV electricity in a long-distance gas transmission pipeline [40]. The study modelled the hydrogen production at two separate locations in Libya to be injected together to meet hydrogen demands imposed by different fixed volume fraction requirements at the Melittah gas terminal for export to Italy. It did not consider the costs of delivering these quantities of hydrogen. Gas-separation technologies such as pressure swing adsorption, membrane separation, and electrochemical hydrogen separation can be used to extract hydrogen from mixtures in natural gas pipelines.

2.3.5. Hydrogen for transportation

For the transport sector, hydrogen can be distributed to customers at hydrogen refuelling stations (HRS). Hydrogen can be (1) produced, stored, and dispensed on-site at HRSs or (2) produced off-site, transported via tube trailer or dedicated pipeline to HRSs, where it is stored and dispensed. In both on-site and off-site hydrogen production, the required energy to operate the electrolyser can be supplied from grid electricity, renewable electricity, or a combination of both. For on-site hydrogen production, evaluation by Dispenza et al. shows the reduction of hydrogen production costs after adding photovoltaics (PV) and battery to a grid-supplied HRS. In addition to the carbon reduction benefit, the hydrogen production cost can be reduced by more than half compared with all

grid electricity [28]. In another study, hydrogen from an on-site wind-photovoltaic-battery-electrolyser system (WPBES) specifically dedicated to HRS fuelling is techno-economically modelled by Gökçek et al [41]. The study shows that such a system is feasible for the evaluated site in Turkey. The model is then extended by the same author to integrate the WPBES and HRS [42]. The evaluation finds that hydrogen total cost from a WPBES is less expensive than if the system operated without the battery as part of the combination. The improved system capacity factor more than offsets the additional capital cost of the batteries. Capacity factor of electrolyser represents the productivity of electrolyser that is calculated using input energy to electrolyser divided by its maximum nominal power of electrolyser.

For off-site hydrogen supply, a recent study by Sun et al. evaluates distributed hydrogen production from non-renewable sources to meet regional demand of HRS [43]. The study finds the benefit of having multiple hydrogen sources to optimise the hydrogen supply chain. In hydrogen transportation, a review by Moradi et al. concludes that gaseous delivery with tube trailers is economically preferable to pipeline or liquid delivery for short distances and low demand [44]. For the transportation distances between 161 and 483 km, Reddi et al. finds compressed hydrogen gas transport via tube trailer is more cost-effective for hydrogen capacity less than 1,000 kg per day, which suits the low to medium capacity of HRSs [45]. For larger capacities of more than 1,000 kg per day, pipeline or liquid delivery is preferable [45]. Assessment by Mayer et al. concludes that transporting liquid hydrogen than dispensing it in the form of compressed gas gives lower dispensing cost than entirely using compressed gas in transporting and dispensing processes. However, liquefaction can increase the production cost at the production site [46]. In another work, Reddi et al. [47] applies a techno-economic model of a HRS to evaluate the cost of dispensing hydrogen from off-site production. The study finds that larger HRSs can significantly decrease dispensed hydrogen costs due to economies of scale. The total

actual costs of providing the hydrogen for fuel cell electric vehicles (FCEVs) in California was between 13 and 15 $/kg in 2017 [47].

2.3.6. Hydrogen refuelling infrastructures

One of the conclusions of a study by Iordache et al. emphasizes the importance of having an adequate number of HRSs to promote deployment of fuel cell electric cars [48]. This is one of the “chicken and egg” problems commonly associated with hydrogen and fuel cell electric vehicles (FCEV). The other side is that HRSs are less likely to be viable without enough FCEVs on the road. A study by He et al. identifies a suitable number of HRSs and their locations along an expressway in Beijing, China [49]. This can be determined from the most appropriate nearby hydrogen source and transport route. As one of the strategies to increase the number of HRSs in big cities, Campíñez-Romero et al. evaluates the potential of HRSs for hydrogen-fuelled taxi fleets [50]. Fleets of FCEVs are desirable for HRSs because they offer large numbers of vehicles at a single fuelling location with relatively predictable fuel consumption. The study proposes that more than 10,000 conventional taxis can be replaced by fuel cell electric taxis that can be fuelled in over 100 new HRSs in Madrid, Spain. Another work on HRSs dedicated to carsharing by Grüger et al. finds that refuelling frequency and the number of vehicles are essential factors to optimise the size of HRSs to reduce overall costs [51]. For heavy-duty vehicles, Li et al. specifically analyse the feasibility of HRSs for fuel cell electric trucks (FCET) [52]. The US-based analysis shows that a 10% penetration of FCETs into the diesel truck fleet results in up to 25% reduction in dispensed hydrogen cost when compared to costs for those seen with 1% penetration.

2.4. Hydrogen mobility and energy systems

2.4.1. Electrification of transportation

Electrification of transportation replaces the internal combustion engine with an electric motor to perform the mechanical work. In connecting the electricity and transport sectors, Thellufsen et. al. [53] found that cross-sector interconnection increases overall system efficiency and utilisation of renewable energy. Victoria et. al. found that another benefit of this sector coupling is that more carbon emissions can be avoided in advance of the commercial availability of large-scale storage technologies [54].

Battery electric vehicles (BEVs) and hydrogen fuel cell electric vehicles (FCEVs) are investigated as options for sector coupling between power and transport. One of the advantages of BEVs is that BEVs have a higher overall energy efficiency than FCEVs, due to hydrogen needs to be converted from electricity at the production site, and hydrogen is then converted again to electricity at the vehicle. In terms of costs, the vehicle and fuel costs of BEVs are lower than FCEVs. Moreover, BEVs are supported by the widespread recharging facilities compared to the limited number of refuelling infrastructure for FCEVs. However, hydrogen gas, which is the form of a chemical substance, makes FCEVs' refuelling speed faster than charging BEVs, due to BEVs highly depend on the chemical reaction within the battery [55]. Hydrogen also enables surplus electricity from intermittent renewables to be harvested and stored through hydrogen production for FCEVs. In comparison, BEVs have to be charged during high penetration of renewables to maximise the share of renewable electricity [55].

In terms of powering vehicles using renewable electricity, Ruhnau et. al. used the terminologies of direct electrification, which encompasses BEVs, and indirect

electrification, which encompasses FCEVs [56]. The study advises the future study of holistic electrification scenarios to understand the impact of directly or indirectly electrified vehicles. In another study, Yue et. al. supported a fuel diversification strategy, which includes the use of hydrogen, rather than direct electrification of all vehicles [57]. Another study by Helgeson et. al. [58] expected that power-to-x (PtX) fuels would primarily supply energy demand for heavy-duty trucks (HDTs) in Europe by 2050, especially in countries with high penetration of variable renewables. PtX covers multiple routes to produce various fuel types from renewable power to hydrogen, liquid hydrogen, or synthetic fuels [58].

2.4.2. Decarbonisation of heavy-duty trucks

A review of decarbonisation pathways by Inkinen et. al. [59] summarises that the emissions from HDTs can be significantly reduced by using (1) new planning for route and traffic volume, (2) new transport modes such as replacement with rail, and (3) new technologies or fuels. In the United Kingdom, Liimatainen et. al. [60] found that traffic volume and emissions can be reduced by using longer and heavier vehicles to carry more payload per journey. In the United States, Sen et. al. evaluated mixed fleets of HDTs for different sectors such as food products, beverages, household durables, oil and gas, and automotive [61]. Combinations of battery-electric, hybrid, and diesel HDTs can optimise environmental, economic, and social impacts. Another study by Gao et. al. found that HDT technology can be improved by (1) load reduction approaches (aerodynamic drag, rolling resistance, accessory load reduction, and light-weighting), and (2) efficiency approaches (engine efficiency, hybridisation, and waste heat recovery) [62]. For alternative fuels, Elgowainy et. al. emphasised that future fuels such as biofuels, electricity, and hydrogen with low carbon intensities can reduce carbon emissions significantly [63]. Modelling work by Mulholland et. al. [64] estimated that more than half of the needed global emission reductions of HDTs could be made by fuel switching by

2050. Renewable electricity and hydrogen produced by electrolysis powered by renewable electricity (green hydrogen) are potentially to be evaluated as fuels for fleets of HDTs.

HDT missions, which are specific tasks or functions to be executed, can be classified as on-road and off-road. The following examples are based on use cases of HDTs according to the FCH 2 JU. On-road missions are for (1) delivery of logistics and materials for manufacturing and chemical industries, (2) distribution of wholesale and retail goods, and (3) transporting garbage. Off-road missions are for (1) agricultural transport of wood and grain, and (2) mining transport for raw material extraction, ore transport and quarry haulage [65]. For on-road delivery missions in a relatively small country like Switzerland, a study by Liimatainen et. al. [66] found that BETs may be viable due to the mostly short operational distances for domestic delivery. On the other hand, Brown et. al. [67] suggest FCETs can potentially travel long-range journeys or as haulage trucks where charging stations for BETs along the roads are unavailable. In terms of the total cost of ownership (TCO), Lajevardi et. al. found that TCO for BETs and FCETs are very competitive, particularly for short distance drayage for delivering cargo from port to the respective warehouses and operation in a flat highway [68]. Also, Smallbone et. al. recommended that BETs operate at a maximum distance of 400 km to avoid impractically large battery size [69]. The study also found the more extended operational range of FCETs, the lower gravimetric energy density (kg/km) and volumetric energy density (l/km) compared to BETs. Hence, FCETs have the potential for long-distance operations of up to 500 km range.

Diesel-electric hybridisation combines internal combustion engine fuelled by diesel and electric motor fuelled by electricity to power plug-in hybrid electric heavy-duty trucks (PHETs). It can reduce CO_2 emissions up to 20% [70], improve fuel economy (km/kWh)

up to 8% [62] compared to diesel-only trucks. Likewise, diesel-hydrogen dual-fuel engine heavy-duty trucks (DFETs) show significant emissions reduction, proportional to the diesel displacement ratio [71]. Moreover, the study indicates the combination of diesel with hydrogen fuel can provide potential cost savings.

2.4.3. On-grid and off-grid electricity systems

As mentioned in the previous section, some HDTs work for off-road missions. For example, quarry sites can typically be powered by the electricity grid (on-grid) or by standalone energy systems (off-grid). In an on-grid system, the quarry can employ renewable sources to supply on-site energy demand, and the grid provides the remaining electricity. An off-grid system for quarry is usually found in remote or isolated locations, where connection to the grid is not possible or too expensive [72]. Therefore, normally an off-grid system relies on a diesel generator to meet the entire on-site energy demand. An off-grid system integrated with renewable electricity is also a viable option to provide clean energy in a quarry. It can lower emissions and operating costs while improving reliability [65]. In addition, battery electric heavy-duty trucks (BETs) and FCETs can be options for quarries to decarbonise transport emissions in quarry activities [74].

For on-grid systems, Phadke et. al. found that charging costs, the total levelised cost of charging equipment and electricity, of 60 $/MWh can make BETs very competitive with diesel internal combustion engine heavy-duty trucks (ICET) [75]. This cost can be achieved if BETs are charged during periods of low electricity prices and if charging stations are operated for at least 8 hours every day. For hydrogen systems, a study by Rose et. al. used grid electricity at a low price to produce hydrogen so that production cost can be minimised [76]. In another study, Liu et. al. also found that hydrogen refuelling cost can be reduced by economies of scale of HRSs [52]. These large HRSs' capacities are required for large hydrogen demand. The demand for at least 10% penetration of

FCETs increases the economic competitiveness of FCETs relative to ICETs, assuming no change in electricity price.

However, the high penetration of either BETs that rely on on-grid charging or FCETs that depend on on-grid refuelling significantly impacts the electricity network. The cost of electricity supply can increase because of the impact of the additional infrastructure costs needed to expand electricity transmission due to high electricity demand to produce hydrogen for FCETs [76]. The significant impact on electricity transmission also applies to BETs, particularly for the electricity grid close to BET charging stations, requiring high charging power capacities [66]. Greater electrification demand for the transport sector also implies more significant investments in the required electricity generation capacities [58].

In terms of refuelling performance, FCETs can avoid electricity load peaks caused by concurrent charging of BETs, due to the time flexibility to produce hydrogen via electrolysis [77]. A study by the International Council on Clean Transportation [78] recommended using on-site batteries at charging stations to secure energy supply for BETs at peak demand times and on-site renewable electricity supplies to reduce energy costs and increase the security of supply. By adding a renewable energy generator to the system to meet the internal energy demand, the system can be termed a “prosumer”, implying it performs as an energy producer as well as an energy consumer. However, the physical space required for the battery would be very large compared to hydrogen due to the lower energy density of batteries [79]. If the vehicles can only be charged during the night, Keller et. al. found that storing large amounts of energy in batteries lead to significant costs compared to hydrogen, even though both result in similar emissions reductions [80].

2.5. Conclusions

From 48 journal articles on the modelling of hydrogen production, transportation, dispensing and consumption that have been reviewed, the modelling approach and research gaps can be identified in those studies. In terms of modelling approach, most hydrogen production from wind curtailment was modelled using wind speed data (m/s) as mentioned in Section 2.3. For the modelling works in this thesis, historical data of wind curtailment is used to represent the actual characteristic of wind curtailments, such as its occurrence and capacity (MWh) at different wind farms throughout the year. Additionally, the most recent data of capital costs for equipment to produce hydrogen is also applied in the model. From the reviewed modelling works on hydrogen transportation and dispensing in Section 2.3.5. and 2.3.6, it is crucial to integrate the modelling of hydrogen transportation and dispensing with hydrogen production to obtain the total costs of delivered renewable hydrogen. For transportation, the model in this thesis also considers the distributed locations of hydrogen supply and demand. Thus, the distance to transport hydrogen and allocation for each demand can be optimised. Furthermore, the equipment sizes and costs to dispense hydrogen can also be calculated using the number of operational buses. Using this approach, it is expected that the model provides a realistic dispensed hydrogen fuel cost from a required hydrogen refuelling station.

The levelised cost of hydrogen (LCOH) is used because it shows the lifetime investment and operation costs required to produce renewable hydrogen. Additionally, most reviewed studies evaluate and optimise their model using this parameter. However, due to the unintegrated technical models in most studies, LCOHs only represent either production or dispensing costs. Even though the overall model can result in the total costs of hydrogen dispensed, the benefit of hydrogen as an efficient energy carrier

cannot be fully assessed by solely using LCOH. Moreover, most current LCOHs are relatively high. Therefore, total costs of vehicle ownership (TCOs) play an essential role in investigating hydrogen vehicles' operating costs. In addition, the model can include the overall GHG emissions to calculate the total costs of carbon abatement (TCAs). TCA explains how much it costs to reduce vehicle emissions using renewable hydrogen. The development details of modelling methods are described in the methodology section of each chapter from Chapter 3 to Chapter 9.

From the reviewed studies, the gaps can be categorised as being in (1) technical models, (2) optimisation, (3) systems, (4) economic models, (5) emission models, (6) hydrogen end-users, (7) analysis types, and (8) the coverage areas, as shown in Table 2.1 and Table 2.2. Renewable hydrogen production modelling studies are widely spread from using only wind or solar electricity to integrating both with an additional battery. However, not all the studies included hydrogen production, transportation, dispensing, and consumption in the technical models. For instance, there are literature gaps in investigations of HRSs for FCEBs and an integrated evaluation of the off-site hydrogen production at WPBES, transportation via tube trailer and dispensing at an HRS. Therefore, this thesis includes modelling of city bus fleets fuelled by hydrogen produced by electrolysers at existing wind farms. It also explores the addition of PV arrays and batteries to improve hydrogen productivity and reduce production costs.

Only a few studies explored the optimisation opportunities from electrolyser operation, geospatial supply chain design, and renewable energy integration. Even fewer studies investigated the total carbon abatement costs in their economic models, showing the decarbonisation performance and costs of hydrogen. Most of the studies do not have emission models in their studies. Additionally, there are still research gaps in evaluating HDTs in off-grid settings, quarry haulage HDTs, the techno-economic performance of

diesel-hydrogen dual-fuel engine heavy-duty trucks (DFETs), and the design of energy systems for prosumers in the HDT sector. This thesis also contributes to the modelling of zero- and low-carbon quarry trucks, on- and off-grid wind power system, direct and indirect electrification of wind power to HDTs, the hydrogen and diesel DFET, and TCO and total cost of abatement (TCA) of HDTs at the prosumer system.

Moreover, the hydrogen studies in the literature are mostly oriented towards the transport sector, even though heating and gas injection also have the potential to be investigated. Other gaps are found in the included analysis, such as technological comparison, current and future performances, sensitivity analysis, and the coverage area of the studies. This PhD thesis covers all the mentioned research gaps, as also shown in the same table.

2.6. Final remarks

In this chapter, the broad literature on the modelling of renewable hydrogen from production to consumption is reviewed. There is a missing link between techno-economic modelling with the environmental aspect of the abated GHG emission. Additionally, the optimisation is partial, focusing mostly on the hydrogen production side. Also, most of the literature overlooks the importance of including production, transportation and dispensing to total hydrogen fuel costs. Therefore, the modelling work in this thesis builds an integrated techno-econo-environmental model of renewable hydrogen as described in detail from Chapter 3 to Chapter 9, comprising different locations.

As an initial step, the modelling of hydrogen capacities and costs in production and transportation from the existing wind farms for natural gas grid injection in Ireland is explained in Chapter 3.

Table 2.1. Research gaps in the literatures (part one)

Author	Ref.	Technical models					Optimisation techniques				Systems		Economic models				
		Renewable electricity	Hydrogen production	Hydrogen transportation	Hydrogen dispensing	Hydrogen demand	Electrolyser operations	Equipment sizing	Geospatial supply chain	Renewable's integration	Distributed	Centralised	Capital and operation costs of equipment	Capital and operation costs of vehicles	Levelised cost of hydrogen fuel	Total vehicle ownership cost	Total carbon abatement cost
Beccali et al.	[21]	✓	✓		✓	✓	✓	✓				✓	✓		✓		
McDonagh et. al.	[30]	✓	✓									✓			✓		
Reddi et. al.	[45], [47]			✓	✓						✓	✓	✓				
Kuczynski t. al.	[81]					✓		✓			✓						
Ma et. al.	[82]	✓	✓	✓		✓			✓		✓		✓				
Samsatli et. al.	[35], [83], [84]	✓	✓	✓	✓	✓		✓	✓		✓		✓	✓			✓
Elgowainy et. al.	[63], [85]				✓	✓		✓			✓		✓			✓	
Gökçek et. al.	[41], [42]	✓	✓	✓	✓	✓		✓	✓	✓	✓		✓		✓		
Zhang et. al.	[22]	✓	✓			✓	✓	✓			✓		✓		✓		
You et. al.	[86]	✓	✓	✓	✓	✓				✓	✓		✓		✓		
Kim et. al.	[87]	✓	✓	✓	✓	✓	✓		✓		✓	✓	✓		✓		
Pfeifer et. al.	[88]	✓	✓		✓	✓			✓		✓		✓	✓		✓	
Hao et. al.	[89]	✓	✓	✓	✓							✓			✓		
Morrison et. al	[90]					✓										✓	
Liu et. al.	[91]				✓												
Zhao et al.	[70]					✓										✓	
Hannach et al.	[71]																
Lajevardi et. al.	[68]					✓			✓		✓					✓	✓
Smallbone et. al.	[69]					✓								✓			
Cavana et. al.	[40]	✓	✓			✓						✓					
Ashrafi et. al.	[34]	✓	✓						✓		✓						
Schmidt et. al.	[31]		✓										✓				
Abdin et. al.	[32]	✓	✓			✓	✓	✓		✓		✓	✓		✓		
Papadopoulos et. al.	[33]	✓	✓								✓		✓				
Kikuchi et. al.	[27]	✓	✓				✓				✓		✓				
Dispenza et. al.	[28]	✓	✓		✓		✓						✓				
Sun et. al.	[43]		✓		✓			✓	✓		✓		✓		✓		
Moradi et. al.	[44]			✓							✓	✓					
Mayer et. al.	[46]				✓	✓					✓		✓		✓		
Iordache et. al.	[48]				✓	✓			✓		✓		✓				
He et. al.	[49]			✓	✓	✓			✓		✓		✓		✓		
Campíñez et. al.	[50]				✓	✓			✓		✓		✓		✓		
Grüger et. al.	[51]	✓	✓		✓	✓					✓		✓		✓		
Liu et. al.	[52]					✓			✓		✓		✓		✓	✓	
Inkinen et. al.	[59]					✓											
Victoria et. al.	[54]	✓	✓			✓			✓	✓		✓	✓				
Ruhnau et. al.	[56]		✓			✓						✓					
Helgeson et. al.	[58]	✓	✓			✓		✓	✓	✓		✓	✓				
Rose et. al.	[76]	✓	✓		✓	✓		✓	✓	✓	✓		✓				
Sterchele et. al.	[77]	✓				✓				✓	✓			✓			
Bünger et. al.	[79]		✓		✓	✓					✓		✓		✓		
Keller et. al.	[80]	✓	✓		✓					✓		✓	✓				
Brown et. al.	[67]	✓				✓			✓	✓		✓	✓				
This PhD thesis		✓	✓	✓	✓	✓	✓	✓	✓	✓	✓	✓	✓	✓	✓	✓	✓

Table 2.2. Research gaps in the literatures (part two)

Author	Ref.	Emission models		Hydrogen end-users			Analysis types				Coverage areas				
		Well-to-tank	Tank-to-wheel	Transport	Heating	Gas injection	Technology comparison	Current and future performances	Gravimetric, volumetric, and energetic	Sensitive parameters	Remote island	City/ regional	National	Trans-national	Inter-continental
Beccali et al.	[21]			✓					✓			✓			
McDonagh et. al.	[30]			✓				✓		✓			✓		
Reddi et. al.	[45], [47]			✓				✓	✓			✓			
Kuczynski t. al.	[81]					✓			✓	✓				✓	
Ma et. al.	[82]					✓		✓	✓				✓		
Samsatli et. al.	[35], [83], [84]			✓	✓			✓	✓				✓		
Elgowainy et. al.	[63], [85]	✓	✓	✓			✓		✓			✓	✓		
Gökçek et. al.	[41], [42]			✓					✓			✓			
Zhang et. al.	[22]								✓				✓		
You et. al.	[86]			✓			✓		✓	✓		✓			
Kim et. al.	[87]			✓			✓		✓		✓				
Pfeifer et. al.	[88]			✓			✓	✓	✓		✓				
Hao et. al.	[89]			✓			✓		✓				✓		
Morrison et. al	[90]			✓			✓			✓			✓		
Liu et. al.	[91]		✓	✓					✓						
Zhao et al.	[70]			✓			✓								
Hannach et al.	[71]	✓	✓	✓			✓								
Lajevardi et. al.	[68]	✓	✓	✓			✓		✓	✓		✓			
Smallbone et. al.	[69]	✓	✓	✓			✓	✓	✓	✓					
Cavana et. al.	[40]					✓			✓						✓
Ashrafi et. al.	[34]								✓				✓		
Schmidt et. al.	[31]						✓	✓							
Abdin et. al.	[32]											✓			
Papadopoulos et. al.	[33]								✓			✓			
Kikuchi et. al.	[27]								✓						
Dispenza et. al.	[28]			✓					✓			✓			
Sun et. al.	[43]			✓					✓			✓			
Moradi et. al.	[44]			✓			✓			✓		✓			
Mayer et. al.	[46]			✓			✓	✓	✓			✓			
Iordache et. al.	[48]			✓					✓					✓	
He et. al.	[49]			✓			✓		✓				✓		
Campíñez et. al.	[50]			✓			✓		✓			✓			
Grüger et. al.	[51]			✓					✓	✓		✓			
Liu et. al.	[52]			✓									✓		
Inkinen et. al.	[59]			✓			✓								
Victoria et. al.	[54]			✓	✓				✓					✓	
Ruhnau et. al.	[56]			✓	✓		✓		✓				✓		
Helgeson et. al.	[58]			✓			✓	✓	✓					✓	
Rose et. al.	[76]			✓					✓				✓		
Sterchele et. al.	[77]			✓			✓					✓			
Bünger et. al.	[79]			✓			✓			✓		✓			
Keller et. al.	[80]			✓			✓		✓				✓		
Brown et. al.	[67]			✓	✓		✓		✓					✓	
This PhD thesis		✓	✓	✓	✓	✓	✓	✓	✓	✓	✓	✓	✓	✓	✓

Chapter 3. Hydrogen Production from Wind Electricity for Gas Network

3.1. Overview

The results of a techno-economic model of distributed wind-hydrogen systems (WHS) located at each existing wind farm on the island of Ireland are presented in this chapter. Hydrogen is produced by water electrolysis from wind energy and backed up by grid electricity, compressed before being temporarily stored, then transported to the nearest injection location on the natural gas network. The model employs a correlation-based approach to select an optimum electrolyser capacity that generates a minimum levelised cost of hydrogen production ($LCOH$) for each WHS. Three scenarios of electrolyser operation are studied: (1) curtailed wind, (2) available wind, and (3) full capacity. Additionally, two sets of input techno-economic parameters are used: current and future. Finally, two electricity prices are considered: low and high. A closest facility algorithm in a geographic information system (GIS) package identifies the shortest route from each WHS to its nearest injection point. Using current parameters, results show that small wind farms are not suitable to run electrolysers under curtailed or available wind operation. They must be run at full capacity to achieve sufficiently low $LCOH$. At full

capacity, the future average $LCOH$ is 6–8 €/kg with total hydrogen production capacity of 49 kilotonnes per year, or equivalent to nearly 3% of Irish natural gas energy consumption. This potential will increase significantly due to the projected expansion of installed wind capacity in Ireland from 5 GW in 2020 to 10 GW in 2030.

3.2. Introduction

The global installed capacity of wind energy increased by nearly four times from 2008 to 2018, accounting for a quarter of global renewable installed capacity in 2018 [92]. Over the same period, wind power installed capacity on the island of Ireland rose by three times to nearly 5 GW. Wind accounts for 29% of national electricity generation, the third highest in the world after Denmark and Uruguay [19]. Currently, Ireland has a government policy to deliver 70% renewable electricity through the Renewable Electricity Support Scheme (RESS), mostly from wind, by 2030 [93], [94].

In 2018, 707 GWh or 6% of available wind energy was lost due to curtailment. Wind curtailment in Ireland may increase to 7–14% as a result of a higher penetration of wind energy in the future [95]. Distributed and long-term energy storage can help to reduce wind energy losses, particularly that caused by low transmission capacity. Hydrogen has the potential to be generated through electrolysis using curtailed wind power and used as a clean energy carrier [22]. Hydrogen production can be placed and operated at each existing wind farm. For relatively small quantities and short distances, hydrogen can be economically transported to demand locations in the form of compressed gas [45]. It can be blended with natural gas and transported longer distances through the existing gas grid [96]. In 2018, natural gas contributed 30% of total primary energy requirement in Ireland [97]. In the same year, 52% of electricity and 41% of heat demands were supplied by natural gas [97]. If produced at wind farms and transported to the gas network,

hydrogen could be used to (1) reduce wasted available wind energy, (2) decarbonise the gas network, and eventually (3) increase renewable supply for power and heat generation and transportation.

The objectives of this chapter are primarily (1) to model and optimise the system size of hydrogen production that prioritises wind curtailment as its energy source, (2) to evaluate hydrogen production capacity and its costs at all existing Irish wind farms, and (3) to optimise the cost of hydrogen transportation from wind farm to gas grid. The following method section describes the hydrogen production system from wind energy as well as three scenarios to evaluate the effect of using different electricity sources in the hydrogen production system. This section also lists the essential techno-economic parameters, explains the system sizing approach, describes the wind curtailment data preparation, and explains the hydrogen transportation submodel. Results are shown in the results and discussion section, which presents detailed system size optimisation at a sample wind farm and summaries for all Irish wind farms. The section also covers energy analysis, levelised cost of hydrogen ($LCOH$) analysis, share of hydrogen in the natural gas network, sensitivity analysis, and a discussion of technical challenges for hydrogen injection. All the significant findings and suggestions for future work are summarised in conclusions section.

3.3. Methodology

3.3.1. System and scenario description

In this study, the system of hydrogen production from wind energy is named the wind-hydrogen system (WHS) and, because it is intended to reduce curtailment and constraint, is proposed to be located at each existing wind farm in Ireland. The WHS comprises subsystems such as energy management, electrolyser, compressor, storage

and transport subsystems. As illustrated in Figure 3.1, the energy management subsystem controls, converts and distributes curtailed electricity (E_{CW}) and exportable electricity (E_{EW}) from the wind farm, as well as grid electricity (E_{EG}) to the water electrolyser (E_{WE}) and electric compressor (E_{EC}) subsystems. The next subsystem is the electrolyser to convert water (M_{H2O}) to hydrogen (M_{H2}) and oxygen (M_{O2}). The electrolyser subsystem includes a power supply, water pump, water treatment, safety devices, heat exchanger, water electrolyser stacks, demisters, gas separators, and dryers [98]. Afterwards, hydrogen is compressed and cooled in the subsequent subsystem before temporarily being stored in the storage subsystem. Operating conditions of the subsystems are described in the technical parameters in the subsection of techno-economic submodel. The last subsystem, the transport subsystem aims to deliver hydrogen to the nearest gas grid injection point via tube trailer with energy requirement (E_{TT}) from a diesel-fuelled truck, which is described in the subsection of transportation submodel. The modelling is performed by using Microsoft Excel for all the calculations except optimisation of renewable hydrogen supply chains, which is done using ArcGIS. This is explained in the subsection on the transportation submodel.

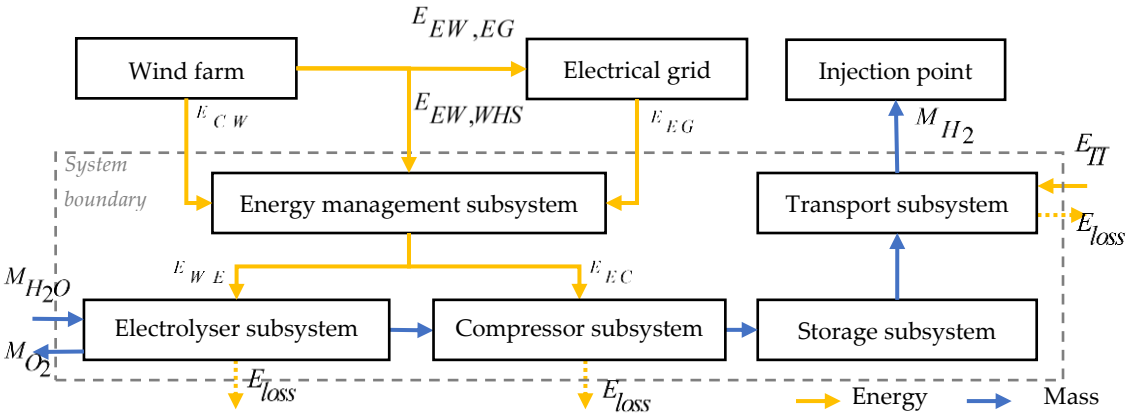

Figure 3.1. Block diagram of a wind-hydrogen system (WHS) modelled at each wind farm in Ireland

Three scenarios for electrolyser operation mode are defined to analyse the impacts of (1) primarily utilising curtailed electricity in “curtailed wind” operation, (2) additionally using exportable electricity to increase the electrolyser capacity factor (λ_{WE}, defined in Equation (3.1)) in “available wind” operation, and (3) maximising λ_{WE} by additionally using grid electricity in “full capacity” operation. Due to the intermittency of curtailed electricity profiles, grid electricity is required as a backup whenever electrolyser minimum input energy is not met. The maximum possible operational time of the electrolyser (t_{WE}) is 8,760 hours, i.e. the number of hours in a year. A minimum 5% of electrolyser nominal power (P_{WE}) is used to maintain the economic lifetime of the electrolyser stack [99].

$$\lambda_{WE} = \frac{E_{CW} + E_{EW} + E_{EG}}{t_{WE} \cdot P_{WE}} \tag{3.1}$$

A. First Scenario: Curtailed Wind Operation

In curtailed wind operation at a sample 15-MW wind farm, electrolyser operation is dependent on the occurrence of curtailed electricity and is backed up by grid electricity to produce hydrogen. This is illustrated in Figure 3.2.a for a 0.1 MW_e electrolyser operating over three days. Due to exportable electricity not being considered in this scenario, this results in very low electrolyser capacity factor, which in turn results in high production cost.

B. Second Scenario: Available Wind Operation

This operation mainly relies on the availability of wind energy. In addition to curtailment, the WHS also receives extra energy input from exportable electricity to increase its electrolyser capacity factor. The electrolyser is also assisted by grid electricity to cover

its minimum energy input in the absence of wind energy as shown in Figure 3.2.b This results in lower production costs than the first scenario.

C. Third Scenario: Full Capacity Operation

To maximise hydrogen production, the electrolyser can be operated at full capacity. To achieve this, in addition to curtailed and available wind electricity, the supply of grid electricity to electrolyser is increased so that electrolyser capacity factor can reach 100%, as illustrated in Figure 3.2.c.

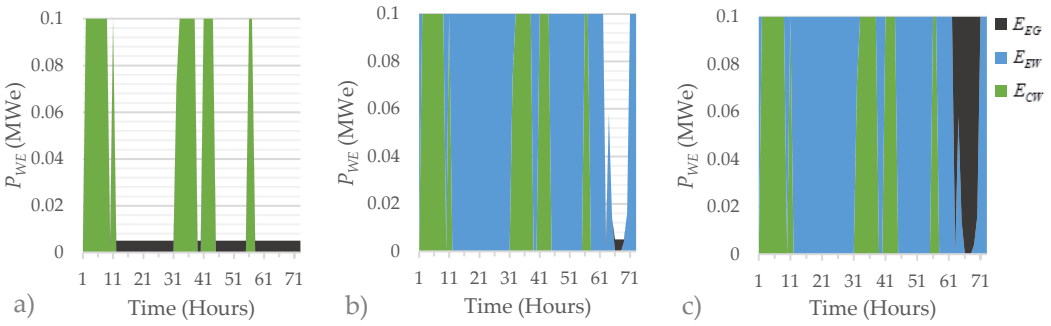

Figure 3.2. Scenarios of electrolyser operation mode: (a) curtailed wind operation, (b) available wind operation, and (c) full capacity operation at a sample wind farm

3.3.2. Techno-economic submodel

Levelized cost of hydrogen ($LCOH$) is defined as the key techno-economic parameter in the optimisation [100]–[102]. The total LCOH ($LCOH_{total}$) is the sum of LCOH for production ($LCOH_{prod}$) and transport ($LCOH_{trans}$) as expressed in Equation(3.2). $LCOH_{prod}$ represents the total discounted present value of investment, operation, and maintenance costs during system lifetime per unit mass of hydrogen produced. Equation (3.3) shows how $LCOH_{prod}$ is calculated. Ideally, the cost of hydrogen injection is included in the analysis. However, the price to facilitate hydrogen injection from gas network operators is not available at the moment. Additionally, there is no regulation on how much hydrogen can be injected to gas grid. The allocation of hydrogen in volume percentage in the gas

network is important for sizing the additional equipment for handling hydrogen at injection points. Such equipment includes additional buffer storage and pressure expanders. A review by Quarton et al. emphasises the strong relation between permitted hydrogen injection (vol%) and injection cost [35].

$$LCOH_{total} = LCOH_{prod} + LCOH_{trans} \tag{3.2}$$

$$LCOH_{prod} = \frac{\sum_{T=0}^{T=\tau_{WHS}} \frac{C_{Inv} + C_{FOM} + C_{VOM}}{(1+r)^T}}{\sum_{T=0}^{T=\tau_{WHS}} \frac{M_{H2}}{(1+r)^T}} \tag{3.3}$$

The total expenses of hydrogen production include the total investment capital cost (C_{Inv}), and fixed (C_{FOM}) and variable (C_{VOM}) operation and maintenance costs. The model assumes a discount rate (r) of 6% over a 20-year system economic lifetime (τ_{WHS}) [21]. The discount rate reflects the financial return and project risk [103]. In a recent study of hydrogen production from wind, Glenk et al. uses discount rates between 4 and 6% [104]. Equation (3.4) shows how C_{Inv} is calculated.

$$C_{Inv} = C_{WE} + C_{EC} + C_{SV} + C_{EM} + C_{ICS} + C_{Eng} + C_{Other} \tag{3.4}$$

Investment capital cost comprises costs for the water electrolyser (C_{WE}), electric compressor (C_{EC}), storage vessel (C_{SV}), energy management unit (C_{EM}), interconnection, commissioning and start-up (C_{ICS}), engineering (C_{Eng}) and other items (C_{Other}). Evaluation by Schmidt et al. mentions that innovations in an inexpensive and more efficient catalyst can decrease the cost of the electrolyser [31]. Additionally, a review by Proost et al. shows significant potential cost reduction from new arrangements of electrolyser stacks

in the future [105]. Modelling work by Glenk et al. estimates that electrolyser cost can fall to half of its current cost in the future [104]. Two sets of parameters are considered: (1) current and (2) future techno-economic parameters. Current techno-economic parameters include all the available technologies today as well as their cost. Future techno-economic parameters consider published learning curves and projections for upcoming technology and their costs in 2030. The values and respective references used for these costs are presented in Table 3.1.

Fixed operation and maintenance cost includes the electrolyser ($C_{OM,WE}$), compressor ($C_{OM,EC}$) and storage ($C_{OM,SV}$), together with a stack replacement (C_{SR}), as shown in Equation (3.5). Variable operation and maintenance costs includes electricity (C_{EL}) and water costs (C_{H2O}), as shown in Equation (3.6).

$$C_{FOM} = C_{OM,WE} + C_{OM,EC} + C_{OM,SV} + C_{SR} \tag{3.5}$$

$$C_{VOM} = C_{EL} + C_{H2O} \tag{3.6}$$

The calculation of C_{EL} is calculated from annual energy consumption of curtailed electricity, exportable electricity and grid electricity and their respective annual average electricity prices, as expressed in Equation (3.7).

$$C_{EL} = (E_{CW} \times c_{CW}) + (E_{EW} \times c_{EW}) + (E_{EG} \times c_{EG}) \tag{3.7}$$

According to [102], [106], [107], electricity price has a significant impact on $LCOH_{prod}$. Therefore, this study identifies and applies representative electricity prices (c) based on each energy source. There are two electricity markets considered in this study: (1) the retail market in which electricity is purchased by end users from electricity suppliers, and

(2) the wholesale market in which electricity is purchased by electricity suppliers from electricity generators [108]. As illustrated in Figure 3.3, the price for grid electricity (c_{EG}) follows the electricity price in the retail market. The electricity price in the wholesale market is defined as the price for exportable electricity (c_{EW}). Curtailed electricity is considered to be purchased at the minimum selling price of wind electricity as represented by the average levelized cost of electricity ($LCOE$) of onshore wind (c_{CW}). The low and high values of each electricity price are listed in Table 3.1.

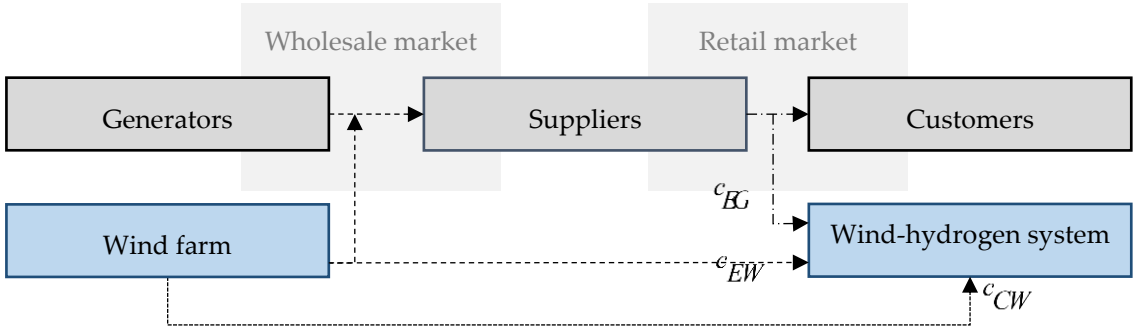

Figure 3.3. Electricity prices in the wind-hydrogen system

Curtailed, exportable and grid electricity each comprise input energy to electrolyser and compressor as expressed in Equation (3.8), (3.9), and (3.10) respectively.

$$E_{CW} = \left(E_{CW,WE} + E_{CW,EC}\right) \tag{3.8}$$

$$E_{EW} = \left(E_{EW,WE} + E_{EW,EC}\right) \tag{3.9}$$

$$E_{EG} = \left(E_{EG,WE} + E_{EG,EC}\right) \tag{3.10}$$

The water price (P_{H2O}) and annual water consumption (M_{H2O}) are used to calculate C_{H2O} as expressed in Equation (3.11). The price used for water can be found in Table 3.1.

$$C_{H2O} = (M_{H2O} \times P_{H2O}) \tag{3.11}$$

Annual water consumption can be calculated using Equation (3.12) from total input energy for the electrolyser (E_{WE}) and specific energy consumption of the electrolyser system (μ_{WE}). The method to calculate optimum electrolysers size at each WHS is explained in subsection of system sizing submodel.

$$M_{H2,WE} = \frac{E_{CW,WE} + E_{EW,WE} + E_{EG,WE}}{\mu_{WE}} \tag{3.12}$$

For each wind farm, each electrolyser operation scenario has different portions of curtailed, exportable and grid electricity to the electrolyser. In the first scenario, the curtailed and grid electricity portion for electrolyser is calculated using Equation (3.13) and Equation (3.14).

$$E_{CW,WE} = \sum_{t=0}^{T} P_{CW,WE}(t) \times \Delta t(t) \tag{3.13}$$

$$E_{EG,WE} = \sum_{t=0}^{T} P_{EG,WE}(t) \times \Delta t(t) \tag{3.14}$$

There are two conditions to calculate curtailed power. The first is when curtailed wind power (P_{CW}) at time (t) exceeds electrolyser rated power (P_{WE}). In this case, P_{CW} is set to the size of electrolyser rated power in kW_e (P_{WE}). It means some curtailed wind can be wasted at small electrolyser sizes. The second condition is to accommodate when P_{CW} is lower than P_{WE}. These two conditions are is expressed in Equation (3.15). P_{WE} is started from 0.01 MW_e to the size of wind farm (P_{WF}). In the first scenario, exportable wind is not introduced to the WHS. Therefore, exportable electricity equals zero. When grid

electricity is required to maintain a minimum of 5% of P_{WE}, it is expressed in Equation (3.16), which is the same approach used in a previous study by [22].

$$P_{CW,WE}(t) = \min\left(P_{WE}, P_{CW}(t)\right) \tag{3.15}$$

$$P_{EG,WE}(t) = \min\left(5\%P_{WE}, P_{CW,WE}(t)\right) \tag{3.16}$$

In the second scenario of available wind operation, curtailed, exportable and grid electricity are calculated with Equation (3.13), (3.17), and (3.14), respectively.

$$E_{EW,WE} = \sum_{t=0}^{T} P_{EW,WE}(t) \times \Delta t(t) \tag{3.17}$$

Curtailed power is calculated using Equation (3.15). Equation (3.18) shows the calculation of exportable wind power (P_{EW}). The calculation of back-up power from the grid is expressed in Equation (3.19).

$$P_{EW,WE}(t) = \min\left(P_{WE} - P_{CW,WE}(t), P_{EW}(t)\right) \tag{3.18}$$

$$P_{EG,WE}(t) = \min\left(5\%P_{WE}, P_{CW,WE}(t) + P_{EW}(t)\right) \tag{3.19}$$

In the third scenario of full capacity operation, curtailed, exportable and grid electricity are calculated from Equation (3.13), (3.17), and (3.14), respectively. Power from curtailed wind, exportable wind and grid can be calculated using Equation (3.15), (3.18), and (3.20), respectively.

$$P_{EG,WE}(t) = P_{WE} - P_{CW,WE}(t) - P_{EW,WE}(t) \tag{3.20}$$

Table 3.1. Economic parameters in WHS, calculated using cost curve data from [31], [98], [104], [105], [109]

Cost component	Symbol	Unit	Values		Ref
Investment cost			Current	Future	
Electrolyser	C_{WE}	€	$2498 \times P_{WE,n}^{0.925}$	$1249 \times P_{WE,n}^{0.925}$	[31], [104], [105]
Compressor	C_{EC}	€	$4948 \times P_{WE,n}^{0.66}$	$4948 \times P_{WE,n}^{0.66}$	[98], [109]
Storage vessel	C_{SV}	€	$470 \times (\dot{M}_{H2} \times t_{SV})$	$470 \times (\dot{M}_{H2} \times t_{SV})$	[98], [109]
Main equipment	C_{ME}	€	$C_{WE} + C_{EC}$	$C_{WE} + C_{EC}$	[98]
Energy mgt. unit	C_{EM}	€	$10\% \times C_{ME}$	$10\% \times C_{ME}$	[98]
Interconnection	C_{ICS}	€	$20\% \times C_{ME}$	$20\% \times C_{ME}$	[98]
Engineering	C_{Eng}	€	$15\% \times C_{ME}$	$15\% \times C_{ME}$	[98]
Other cost	C_{Other}	€	$1.5652 \times P_{WE,n}^{-0.154} \times C_{ME}$	$1.5652 \times P_{WE,n}^{-0.154} \times C_{ME}$	[98]
Operation and maintenance cost			Current	Future	
Electrolyser	$C_{OM,WE}$	€	$0.2011 P_{WE}^{-0.23} \times C_{WE}$	$0.2011 P_{WE}^{-0.23} \times C_{WE}$	[98]
Compressor	$C_{OM,EC}$	€	$2\% \times C_{EC}$	$2\% \times C_{EC}$	[98]
Storage vessel	$C_{OM,SV}$	€	$2\% \times C_{SV}$	$2\% \times C_{SV}$	[98]
Stack replacement	C_{SR}	€	$874 \times P_{WE,n}^{0.925}$	$437 \times P_{WE,n}^{0.925}$	[104], [105]
Electricity and water prices in Ireland			Low	High	
Grid electricity	c_{GE}	€/MWh	104	157	[110]
Exportable wind	c_{EW}	€/MWh	72	93	[111]
Curtailed wind	c_{CW}	€/MWh	50	65	[112]
Water	c_{H2O}	€/m^3	2.38	2.38	[113]

Total required energy input to the electric compressor (E_{EC}) is the summary of curtailed, exportable and grid electricity that are used to operate compressor as expressed in Equation (3.21).

$$E_{EC} = E_{CW,EC} + E_{EW,EC} + E_{EG,EC} \tag{3.21}$$

The calculation of each annual curtailed, exportable and grid electricity can be seen in Equation (3.22), (3.23) and (3.24).

$$E_{CW,EC} = \sum_{t=0}^{T} P_{CW,EC}(t) \times \Delta t(t) \tag{3.22}$$

$$E_{EW,EC} = \sum_{t=0}^{T} P_{EW,EC}(t) \times \Delta t(t) \tag{3.23}$$

$$E_{EG,EC} = \sum_{t=0}^{T} P_{EG,EC}(t) \times \Delta t(t) \tag{3.24}$$

Required curtailed power at time t follows Equation (3.25). There are two conditions to prioritise the use of curtailed wind. The conditions are when curtailed power is larger than the required power to run the electrolyser and compressor, and when curtailed power is larger than the required power to run the electrolyser, but not enough to run the compressor. The contribution of exportable power at time t is calculated with Equation (3.26). The back-up power from the grid is added when energies from curtailed and exportable winds are not enough to run the compressor as expressed in Equation (3.27). The power demand to compress hydrogen can be calculated from flow rate (m_{H2}) at time t and the specific energy consumption of the electric compressor (μ_{EC}).

$$P_{CW,EC}(t) = \min\left(\left(m_{H2}(t) \times \mu_{EC}\right), P_{WE} - P_{CW}(t)\right) \quad (3.25)$$

$$P_{EW,EC}(t) = \min\left(\left(m_{H2}(t) \times \mu_{EC}\right) - P_{CW}(t), P_{EW}(t) - P_{WE} - P_{CW}(t)\right) \quad (3.26)$$

$$P_{EG,EC}(t) = \left(m_{H2}(t) \times \mu_{EC}\right) - P_{CW,EC}(t) - P_{EW,EC}(t) \quad (3.27)$$

In terms of technical parameters, this study models proton exchange membrane (PEM) electrolyser technology mainly due to its fast response time to intermittent power like wind, compared to alkaline or solid oxide electrolysis cells [31], which operate at higher temperatures. Alkaline operates at lower pressure than PEM. Output pressures of 30 barg for alkaline and 60 barg for PEM are under development by Fuel Cells and Hydrogen 2 Joint Undertaking (FCH 2 JU) [98]. These output pressures are in line with other publications by Papadopoulos et al. [33] and Schmidt et al. [31]. The material in an electrolyser stack can degrade with time [31], which affects the stack lifetime. A study by [31] predicts that the specific energy consumption (μ_{WE}) and degradation of the electrolyser may be lower in the future. The detailed technical parameters of the WHS are shown in Table 3.2.

Table 3.2. Technical parameters in WHS

Parameters	Symbol	Units	Values		Ref.
Electrolyser subsystem			Current	Future	
Electrolyser rated power	$P_{WE,n}$	MW_e	0.01 to P_{WF}	0.01 to P_{WF}	[98]
Operating pressure	p_{WE}	barg	30	30	[33]
Sp. energy consumption	μ_{WE}	kWh_e/kg	55	47	[31], [114], [115]
Water consumption	ρ_{WE}	L/kg	15	15	[98]
Stack lifetime	τ_{SR}	years	5	8	[31]
Compressor subsystem			Current	Future	
Pressure input	$p_{EC,in}$	barg	30	30	[98]
Pressure output	$p_{EC,out}$	barg	300	300	[98]
Sp. energy consumption	μ_{EC}	kWh_e/kg	1.7	1.7	[98], [116]
Storage subsystem			Current	Future	
Operating pressure	p_{SV}	barg	300	300	[101]

Reciprocating compressors are widely used in the hydrogen industry mainly due to their high compression ratio, so are used in this study. Hydrogen is compressed from 30 barg to 300 barg. It requires two intercooled stages to preserve a temperature of 135 °C at the discharge point [98], [116], [117].

For buffer storage, bundles of steel cylinders are selected due to their capability to store hydrogen gas up to 300 barg from 10 hours to many months [98]. Hydrogen is modelled as being stored in the storage system before it is delivered to the nearest gas grid injection point by truck. The model does not include additional equipment needed to reduce the pressure to 80 barg [96] and blend the hydrogen gas safely with the natural gas.

3.3.3. System sizing submodel

Several WHS pilot plants already operate across Europe. The electrolyser comprises up to 40% of total capital expenditure, followed by the compressor and storage vessels [102], [118]. Therefore, in the design of the WHS, the electrolyser is sized first. Compressor and storage vessel sizes are scaled according to the electrolyser.

When cost curves from the literature [31], [98], [104], [105], [109] are employed, this has the effect of turning all components' costs into functions of electrolyser size ($\mathrm{PWE,n}$), as presented in Table 3.2. For each wind farm capacity (P_{WF}) larger than 10 MW_e, $LCOH_{prod}$ is calculated using Equation (3) with different electrolyser sizes from n = 0.01 MW_e to P_{WF} with increments of 0.05 MW_e for each scenario. The trend of $LCOH_{prod}$ is examined, with the electrolyser size that results in the minimum $LCOH_{prod}$ ($P_{WE,opt}$). This is deemed to be the optimum for that wind farm as illustrated in Figure 3.4.

After calculating the optimum electrolyser size for all wind farms larger than 10 MW_e, a statistical model, which is described below, is developed to find $P_{WE,opt}$ for those smaller than 10 MW_e. Data collection for all sizes of wind farm is described in the subsection of wind curtailment submodel.

3.3.4. Wind curtailment submodel

The most influential aspects to WHS's economic performance are the hydrogen production system capacity and annual curtailed electricity, which also depend on wind farm size [119]. Ireland's Single Electricity Market Operator (SEMO) stores the required data to calculate curtailed electricity profiles of large Irish wind farms (P_{WF} > 10 MW_e).

Therefore, in this study, the calculation of curtailed electricity is divided into two segments, (1) for wind farms larger than 10 MW_e, and (2) for those smaller than 10 MW_e.

A. Wind Farms Larger than 10 MWe

This accounts for 74 out of the 312 wind farms currently operating in Ireland. There are three types of hourly data that can be obtained from the SEMO website: actual availability of wind power that can be delivered to the electrical grid (P_{AW}), quantity of dispatch instruction from SEMO (P_{DQ}) and metered generation of exported power by a wind farm (P_{MG}) [120]. In practice, P_{MG} can be different from P_{DQ}, known as uninstructed imbalance. The calculation of total annual curtailed, exportable and grid electricity are shown in Equation (3.28), (3.29), and (3.30), respectively [121].

$$E_{AW} = \sum_{t=0}^{T} P_{AW}(t) \times \Delta t(t) \tag{3.28}$$

$$E_{EW} = \sum_{t=0}^{T} P_{EW}(t) \times \Delta t(t) \tag{3.29}$$

$$E_{CW} = \sum_{t=0}^{T} P_{CW}(t) \times \Delta t(t) \tag{3.30}$$

The hourly power from curtailed, exportable and grid are calculated using Equation (3.31), (3.32), and (3.33), respectively. In condition of $P_{AW} \leq P_{DQ}$, curtailed wind energy at time *t* is equal to zero.

$$P_{AW}(t) = P_{AW}(t) \text{ , if } P_{AW}(t) > P_{DQ}(t) \tag{3.31}$$

$$P_{EW}(t) = max\left(P_{DQ}(t), P_{MG}(t)\right) \text{ , if } P_{AW}(t) > P_{DQ}(t) \tag{3.32}$$

$$P_{CW}(t) = P_{AW}(t) - P_{EW}(t) \tag{3.33}$$

B. Wind Farms Smaller than 10 MWe

Since not all of wind farms have this level of hourly data available from SEMO[1], E_{CW} can also be approximated from regional annual average values for wind curtailment rate ($E_{CW,\%}$) and E_{AW} as shown in Equation (3.34). E_{AW} is approximated from the reported P_{WF} and the average capacity factor for the wind farm's macro-region (λ_{WF}) and operational time of wind farm (t_{WF}), as represented in Equation (3.35).

$$E_{CW} = E_{CW,\%} \times E_{AW} \tag{3.34}$$

$$E_{AW} = t_{WF} \times P_{WF} \times \lambda_{WF} \tag{3.35}$$

The current average of $E_{CW,\%}$ in the island of Ireland is 6%, as reported in [19]. It regionally varies between 4.1% and 9.4% [19]. According to [93], the average $E_{CW,\%}$ could be up to 7% in the future. Current capacity factor in the Republic of Ireland (RoI) and Northern Ireland (NI) are 28% and 22%, respectively [19]. This study assumes the same values of capacity factor in the future.

3.3.5. Transportation submodel

A submodel is presented here that calculates the transportation cost of moving hydrogen from each wind farm to its nearest grid injection location. Evaluation by [122], [123] identify at least 42 locations of above ground installations (AGIs) that can potentially be used for gas injection into the gas network in the Republic of Ireland [124]; 10 AGIs are spread across Northern Ireland. In total, there are 52 potential injection locations in the island of Ireland.

A 300-barg tube trailer is operated to deliver 500 kg hydrogen per trip [125]. The tube trailer is built from steel cylinders, which is considered to be mature technology. Therefore, the techno-economic parameters in hydrogen transport with a steel-based tube trailer is not expected to change in the future, as listed in Table 3.3 [98]. The tube trailer is hauled by diesel truck to the injection location and returned to the wind farm. The required energy to transport hydrogen (E_{TT}) is calculated using specific energy consumption per kilometric (α_{TT}) of the diesel truck and the total distance as expressed in Equation (3.36). The model assumes a third-party company operates the truck to haul the tube trailer.

$$E_{TT} = \left(\alpha_{TT} \times L_{AGI} \times N_{trip} \times 2 \right) \tag{3.36}$$

The closest-facility algorithm in the ArcGIS Geographic Information System (GIS) software does two measurements: (1) identification on each WHS to be directed to suitable AGI based on its nearest distance, and (2) identification of the shortest road route from WHS to its respective AGI. For wind farms, this study identifies 238 locations in RoI [126] and 74 locations in NI [127]. The detailed road network in the island of Ireland is obtained from [128], which includes motorway, primary road, secondary road, tertiary road and trunk road. The parameters used to determine transportation costs are obtained from [98], [103], [125] and listed in Table 3.3. The $LCOH_{trans}$ is the total discounted present value of investment in tube trailers ($C_{Inv,TT}$), and operation and maintenance costs ($C_{OM,TT}$), during system lifetime per kg of hydrogen, as shown below.

$$LCOH_{trans} = \frac{\sum_{t=0}^{t=\tau_{WHS}} \frac{C_{Inv,TT}}{(1+r)^t} + \sum_{t=0}^{t=\tau_{WHS}} \frac{C_{OM,TT}}{(1+r)^t}}{\sum_{t=0}^{t=\tau_{WHS}} \frac{M_{H2}}{(1+r)^t}} \quad (3.37)$$

Equation (3.38) is used to calculate total operation and maintenance cost of the tube trailer. In these equations, $C_{O,TT}$ is the operational cost per kilometre, $C_{M,TT}$ is the maintenance cost per kilometre, L_{AGI} is the shortest distance between wind farm and injection point, N_{trip} is the total trip numbers per year (the return trip is represented by 2) and $C_{R,TT}$ is a ten-yearly tube trailer retesting cost.

$$C_{OM,TT} = \left(\left(\dot{C}_{O,TT} + \dot{C}_{M,TT}\right) \times L_{AGI} \times N_{trip} \times 2\right) + C_{R,TT} \quad (3.38)$$

To minimise travel costs for each wind farm, N_{trip} is measured with the average length of storage time (t_{SV}) which is based on hourly average production kg/hr (m_{H2}) and tube trailer capacity (M_{TT}), as shown below.

$$N_{trip} = \frac{365}{t_{SV}/24} \quad (3.39)$$

$$t_{SV} = \frac{M_{TT}}{m_{H2}} \quad (3.40)$$

Table 3.3. Techno-economic parameters in the transportation submodel

Parameters	Symbol	Unit	Values		Ref
Economic parameters			Current	Future	
Tube trailer cost	$C_{Inv,TT}$	€	232,000	232,000	[103]
Operational cost	$\dot{C}_{O,TT}$	€/km	1.9	1.9	[103]
Maintenance cost	$\dot{C}_{M,TT}$	€/km	0.13	0.13	[103]
Retest cost	$C_{R,TT}$	€	$30\% \times C_{TT}$	$30\% \times C_{TT}$	[98]
Technical parameters			Current	Future	
Tube trailer capacity	M_{TT}	kg	500	500	[125]
Operating pressure	p_{TT}	barg	300	300	[125]
Kilometric energy consumption	α_{TT}	kWh/km	1.77	1.77	[129]
Trip numbers	N_{trip}	Trips/year	Calculated by Equation (3.41)		
WHS distance to AGI	L_{AGI}	km	Determined by GIS closest-facility algorithm for each wind farm		
Average production per hour	m_{H2}	kg/hour	m_{H2} calculated by Equation (3.12), then divided with 8,760 hours		

3.3.6. Solution algorithm overview

WHSs are designed to be decentralized and placed at each Irish wind farm to maximize the usage of curtailed and constrained electricity throughout the island. The hourly power generation data from at least 74 wind farms are accessible at the SEMO website. For each wind farm, electrolyser sizes (P_{WE}) from 0.01 MW_e to the wind farm's rated capacity (P_{WF}) are used to compute the levelized cost of hydrogen production ($LCOH_{prod}$) as described above. The electrolyser size that minimises $LCOH_{prod}$ is defined as $P_{WE,opt}$. Afterwards, the $LCOH_{trans}$ is calculated as described above and added to the $LCOH_{prod}$ to obtain $LCOH_{total}$. As shown in Figure 3.4, essential values are indicated by square boxes, where submodels are illustrated in round edge boxes. To aid understanding of the algorithm, data preparation are coloured with light red, system sizing for all scenarios with dark blue, hydrogen production with light blue, and hydrogen transportation with yellow.

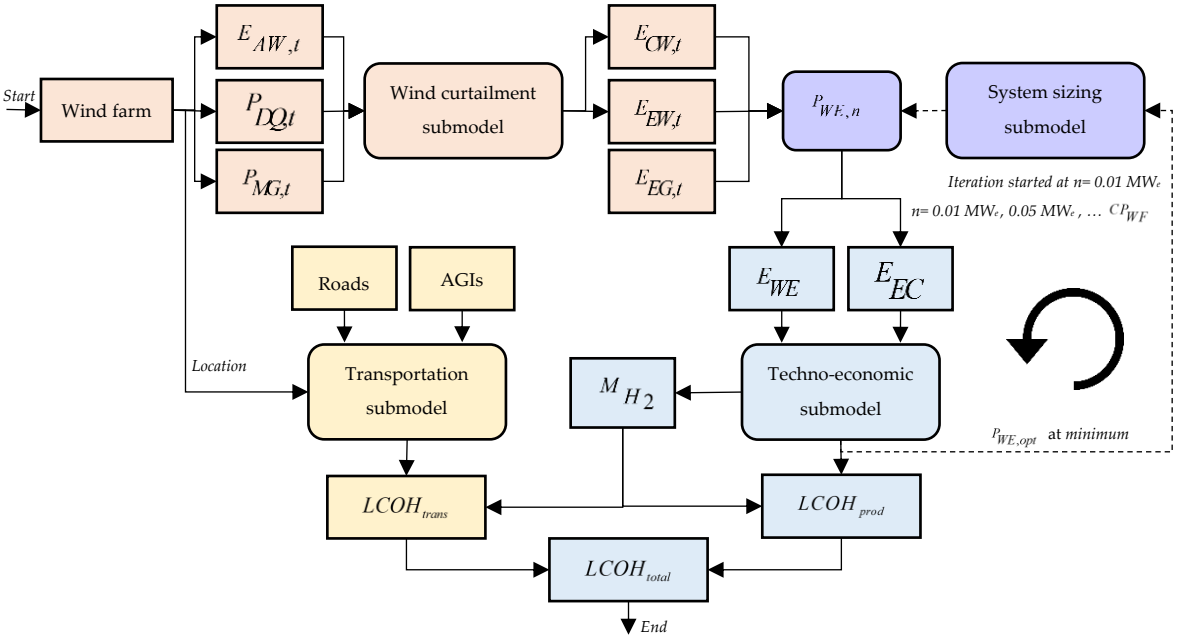

Figure 3.4. Algorithm to calculate the $LCOH_{Total}$

3.4. Results and discussion

3.4.1. System sizing for a sample wind farm

The cumulative available wind energy profile (curtailed plus exportable electricity) of Ballincollig Hill wind farm in 2015 is illustrated in Figure 3.5. The grey area shows exportable electricity to the grid, and black indicates curtailed electricity. The wind farm capacity, capacity factor and curtailment rate are 15 MW, 31% and 13%, respectively. Curtailment significantly occurs during winter, starting from 7,000 hours onwards. 50% of curtailment is less than 2.2 MW of instantaneous power. The highest rate of curtailed power is 11 MW.

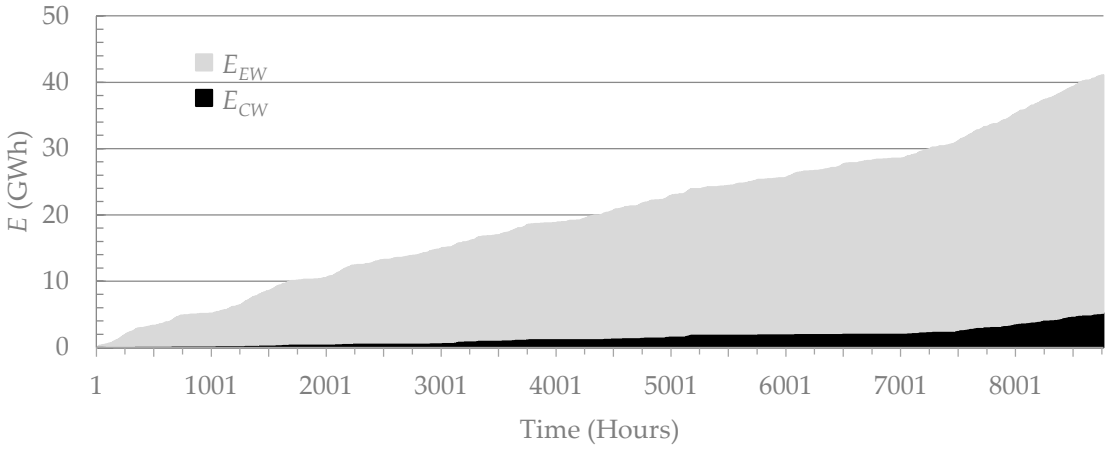

Figure 3.5. Cumulative wind power profile of a sample wind farm

$LCOH_{prod}$ of curtailed wind operation drops from 40 €/kg for a 0.01-MW_e (10-kW_e) electrolyser to its lowest level of 18–20 €/kg for a 1.5-MW electrolyser, as illustrated in Figure 3.6. The $LCOH_{prod}$ is relatively high due to a low electrolyser capacity factor of 20%. When exportable electricity is also introduced to the WHS in the second scenario, the minimum $LCOH_{prod}$ drops to 7 €/kg for the same electrolyser size but with an electrolyser capacity factor near 80%. In the third scenario, $LCOH_{prod}$ further reduces to 6 €/kg due to the fact that more hydrogen can be produced at a capacity factor of 100%. The system sizing model optimally prioritised E_{CW} to be the energy source of the electrolyser and compressor, and found the optimal electrolyser size for all scenarios of 1.5 MW_e. Hydrogen production from an electrolyser smaller than 0.5 MW_e fails to benefit from economies of scale. For electrolysers larger than 1.5 MW_e, operating in the curtailed electricity only scenario, electrolyser capacity factor decreases and $LCOH_{prod}$ dramatically increases. This does not significantly affect the second scenario due to the supply of exportable wind to the electrolyser. The increase of $LCOH_{prod}$ in the second scenario can be seen at electrolyser sizes beyond 7.5 MW_e, where all curtailed electricity is consumed by the electrolyser. The $LCOH_{prod}$ of the third scenario shows a slight

decrease due to more hydrogen being produced when electrolyser capacity factor is maintained at 100%.

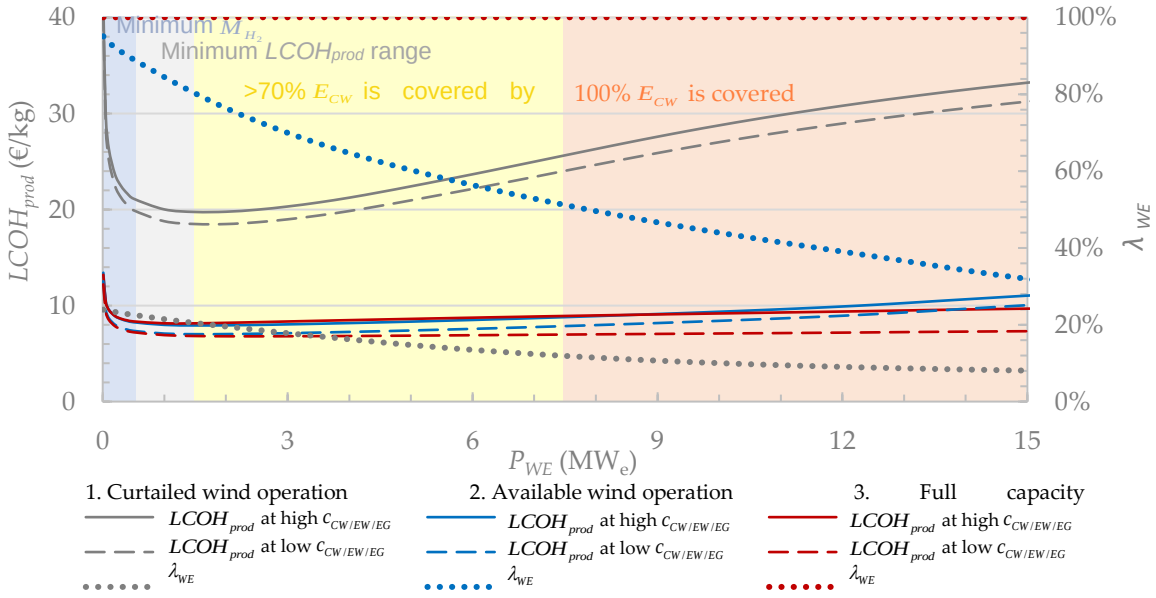

Figure 3.6. Calculated $LCOH_{prod}$ for Ballincollig Hill wind farm as a function of electrolyser size for all operation scenarios

In comparison to the result from Beccali et al. [21], if wind penetration and wind curtailment rate in Sicily, Italy are 41% and 10%, respectively, then the optimum hydrogen production cost by using only curtailed wind is 33 €/kg at electrolyser size of 0.5 MW$_e$. On the other hand, it is difficult to compare the study from Zhang et al. [22] due to the fact that hydrogen production cost is not used as the main parameter, but hydrogen price and payback period. Based on payback period, 6 MW$_e$ is used to utilise a wind curtailment rate of 28% with a hydrogen price in the range of 3 to 4 €/kg in full capacity operation, without compression and storage. Details of the cost contribution to $LCOH$ can be seen in the subsection of the sensitivity analysis of the techno-economic parameters.

3.4.2. Optimal system sizing for all Irish wind farms

In total, there are 312 wind farms the island of Ireland, of which only 74, with rated output of over 10 MWe have detailed hourly data. Therefore, a method is developed to size electrolysers for the rest of the 238 wind farms. Based on the results from the 74 wind farms, statistical curve-fitting models are derived and used for optimal electrolyser sizing and annual hydrogen production for the remainder. These models are shown in Equations (3.41) and (3.42), respectively.

$$P_{WE,opt} = 0.3868 \times E_{CW} + 0.01 \tag{3.41}$$

$$M_{H2} = 22.426 \times E_{CW}{}^{0.8503} \tag{3.42}$$

Annual curtailed electricity and optimum electrolyser sizes for all Irish wind farms are shown in Figure 3.7. Optimum electrolyser sizes are found to range between 10 kWe and 8 MWe. From this point, the annual hydrogen production capacity can be calculated for all existing Irish wind farms. With current techno-economic parameters, each scenario results is indicated in Figure 3.8. The total annual hydrogen production capacity for first, second, and third scenarios are 13, 32, and 39 kilotonnes per year, respectively. Using future parameters, the hydrogen capacity slightly increases for each WHS due to higher electrolyser efficiency. In this case, the total production capacity for first, second, and third scenarios are 16, 39, and 49 kilotonnes per year, respectively.

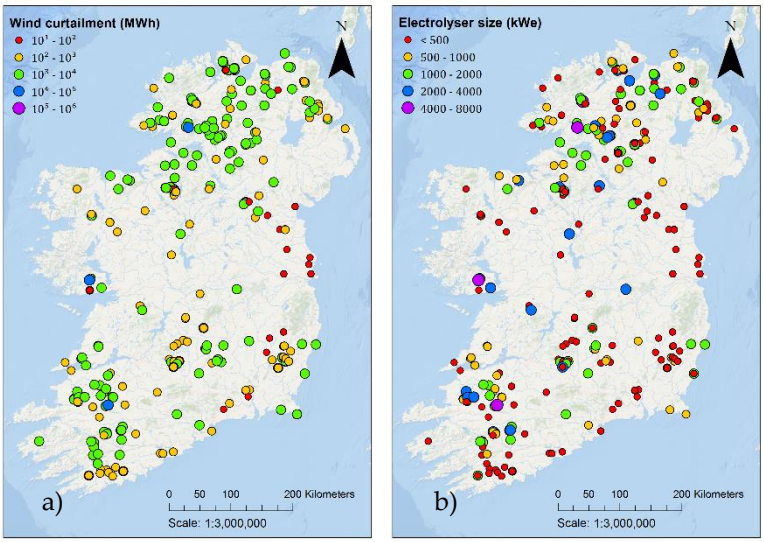

Figure 3.7. Wind farm distribution on the island of Ireland: (a) total energy of curtailed wind (E_{CW}) and (b) optimum electrolyser size ($P_{WE,opt}$) at each wind farm in Ireland

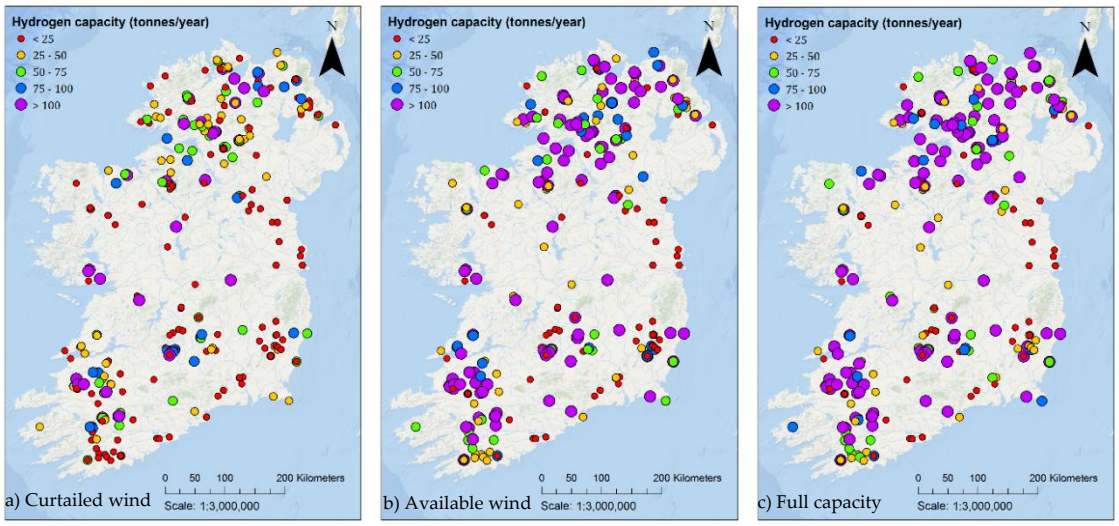

Figure 3.8. Capacity of annual hydrogen production (M_{H2}) with current parameters of (a) curtailed wind operation, (b) available wind operation, and (c) full capacity operation, calculated by the techno-economic submodel for all wind farms in the island of Ireland

3.4.3. Energy analysis for all scenarios

In the curtailed wind operation scenario, 87% of energy input to electrolyer is from curtailed electricity and the rest is backed up by grid electricity to maintain electrolyser

idle power, as illustrated in the Sankey diagram in Figure 3.9. In the available wind operation scenario, exportable electricity dominates hydrogen production at 63%, followed by curtailed and grid electricity at 36% and <1%, respectively. When electrolysers at all WHSs run at full capacity, the relative contributions of curtailed, exportable, and grid electricity are 29%, 51% and 19%, respectively. By using the higher heating value hydrogen of 39.41 kWh/kg, the overall system efficiencies at all existing Irish wind farms for current and future technologies are 71% and 83%, respectively.

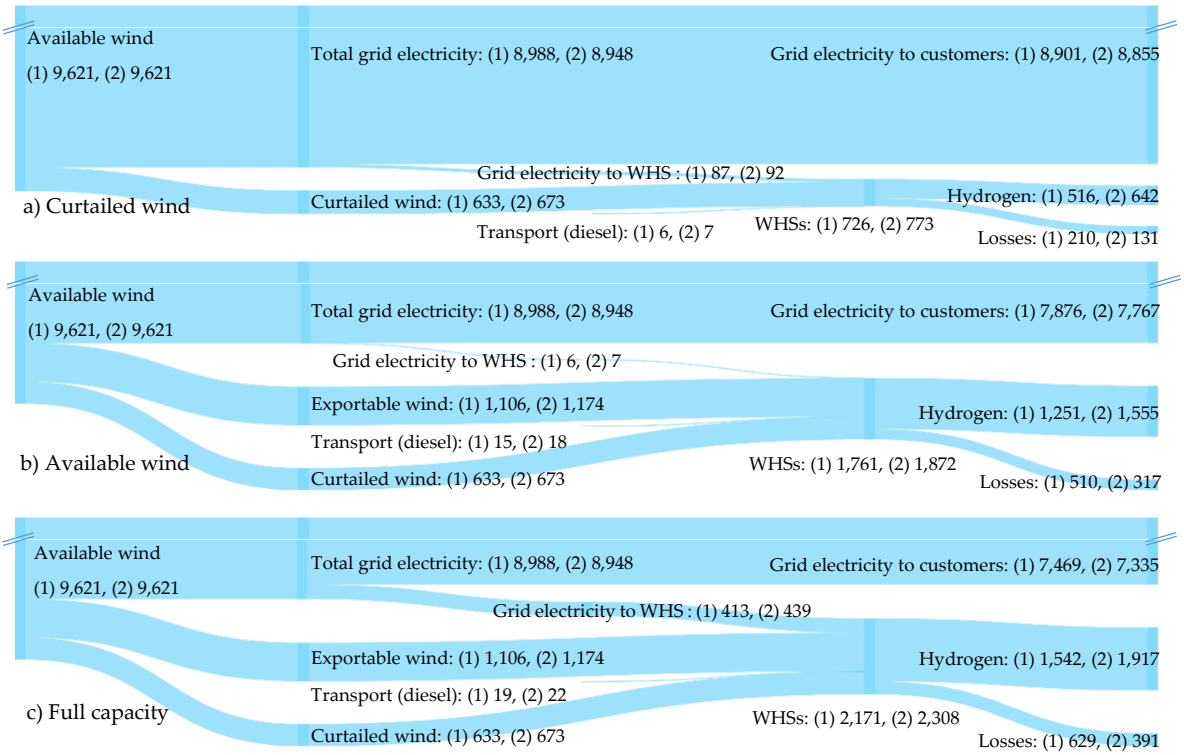

Figure 3.9. Energy flows (GWh) using (1) current and (2) future techno-economic parameters to all WHSs in Ireland of (a) curtailed wind operation, (b) available wind operation, and (c) full capacity operation

3.4.4. LCOH analysis for all scenarios

The $LCOH_{total}$ for each WHS using current and future techno-economic parameters can be seen in Figure 3.10 and Figure 3.11, respectively. Each figure represents a different scenario and electricity price. At low or high electricity prices, the $LCOH_{total}$ at

most of wind farms in the first scenario (curtailed only) is higher than 13 €/kg with averages of 23 €/kg and 24 €/kg for low and high electricity prices. This figure is mostly contributed to by wind farms with capacity of below 5 MW_e. When exportable wind is also included in the second scenario, the average $LCOH_{total}$ drops to 10–11 €/kg. Only wind farms smaller than 1 MW_e have $LCOH_{total}$ higher than 13 €/kg, due to insufficient hydrogen production to cover investment, operation, maintenance, and transportation expenses. When maximum electrolyser capacity factor is maintained in the third scenario, the average $LCOH_{total}$ of all Irish wind farms is 9–11 €/kg, with only few wind farms below 0.1 MW_e left with $LCOH_{total}$ higher than 13 €/kg. By 2030, hydrogen production at WHS becomes more attractive, with average $LCOH_{total}$ for first, second, and third scenarios of 14–15 €/kg, 7–8 €/kg and 6–8 €/kg, respectively.

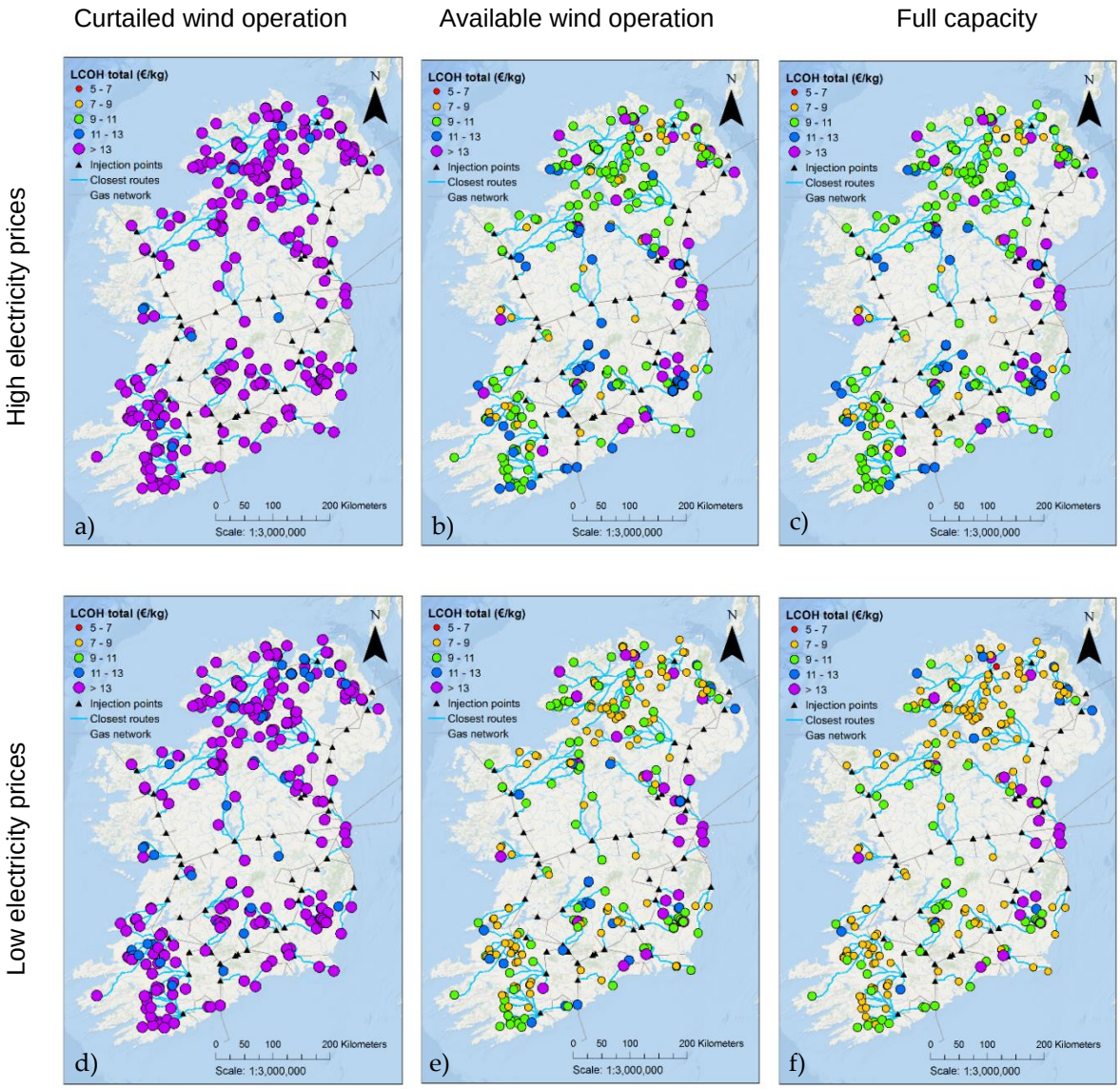

Figure 3.10. Current $LCOH_{total}$ of (a) curtailed wind operation at high electricity prices, (b) available wind operation at high electricity prices, and (c) full capacity operation at high electricity prices, (d) curtailed wind operation at low electricity prices, (e) available wind operation at low electricity prices, and (f) full capacity operation at low electricity prices, calculated by the WHS model for all wind farms in Ireland

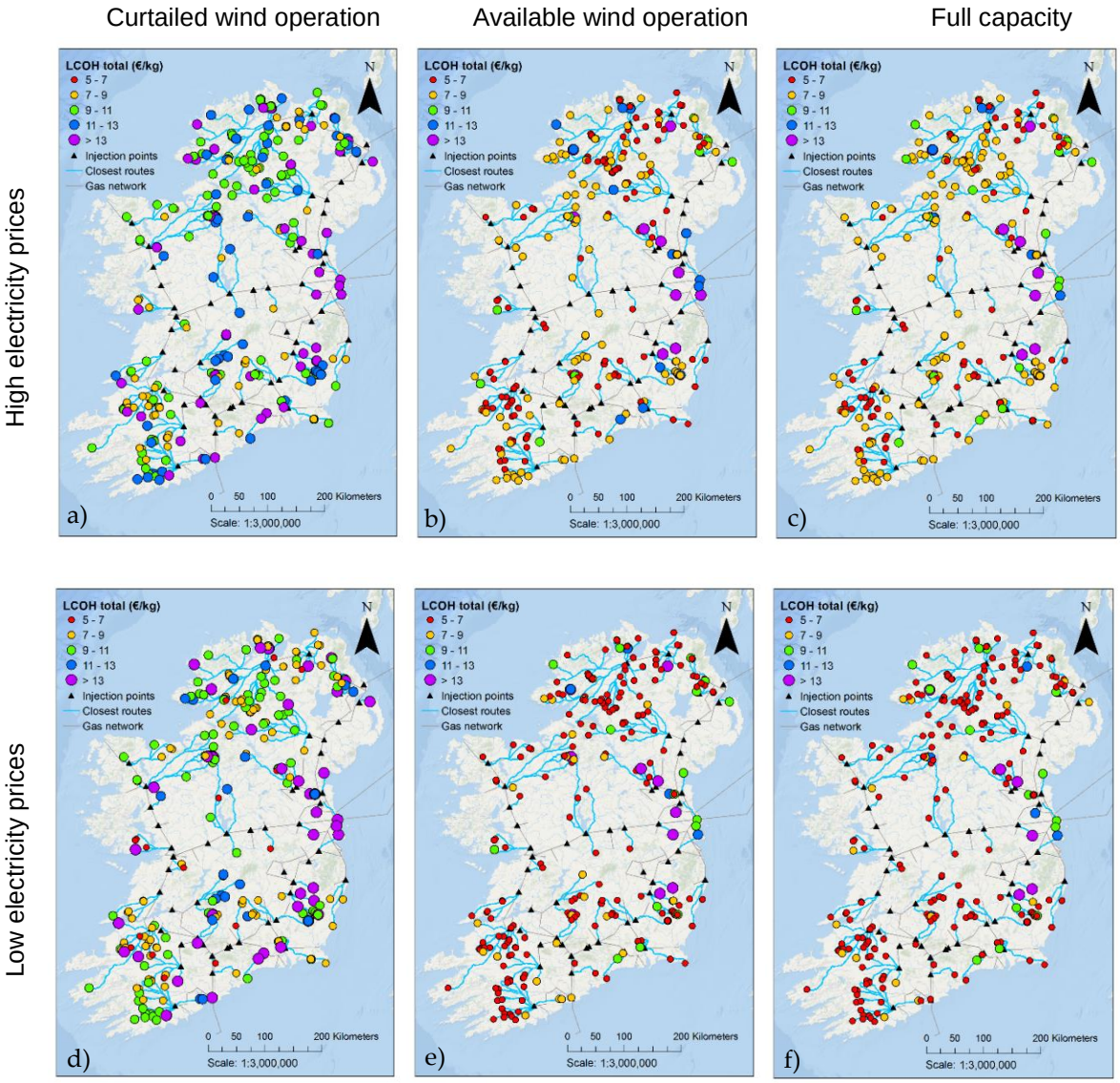

Figure 3.11. Future $LCOH_{total}$ of (a) curtailed wind operation at high electricity prices, (b) available wind operation at high electricity prices, (c) full capacity operation at high electricity prices, (d) curtailed wind operation at low electricity prices, (e) available wind operation at low electricity prices, and (f) full capacity operation at low electricity prices, calculated by the WHS model for all wind farms in Ireland

3.4.5. Overall share of hydrogen in natural gas network

Figure 3.12 shows that at least 84% of hydrogen capacity is located not more than 100 km from the nearest gas injection location, with the longest distance reaching 195 km. The total hydrogen production potential using current techno-economic parameters at all existing wind farms in the island of Ireland for full capacity operation reaches 39 kilotonnes. This increases to 49 kilotonnes using future techno-economic parameters. This is equivalent to nearly 3% of current natural gas energy demand. When additional wind capacity of more than one-hundred percent of today's capacity and curtailment rate of 7% in the future [93] are considered, the potential of wind-produced hydrogen to substitute energy from natural gas reaches almost 6%.

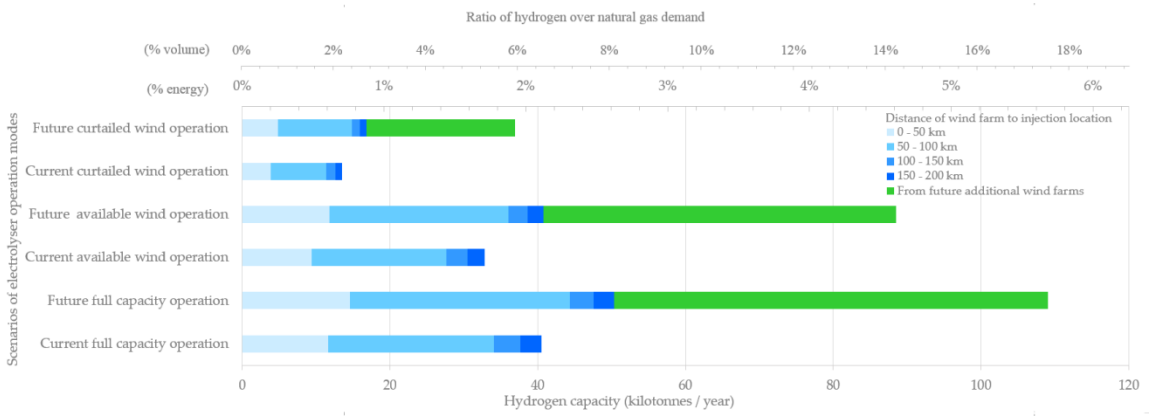

Figure 3.12. Distribution of hydrogen capacity relative to Irish natural gas demand, as functions of distance from WHS to injection points

3.4.6. Sensitivity analysis of techno-economic parameters

The results of sensitivity analysis for Screggagh wind farm with capacity of 20 MW_e are shown in Figure 3.13. The technical parameters in the analysis include curtailment percentage, stack lifetime and electrolyser specific energy consumption. The economic parameters in the analysis are discount rate, capital cost of electrolyser, and electricity

price. The value of each parameter is changed by −50% and 50% of its initial value. Electrolyser specific energy consumption accounts for the most sensitive parameter for all scenarios, followed by curtailment percentage and stack lifetime. The $LCOH_{total}$ will further decrease when economic parameters such as capital cost of electrolyser decreases in the future. The cost share of different cost components to $LCOH_{total}$ can also be seen in Figure 3.13. The relative increase in the importance of electricity price as electrolyser operating hours increase from curtailed only operation to full time operation is notable.

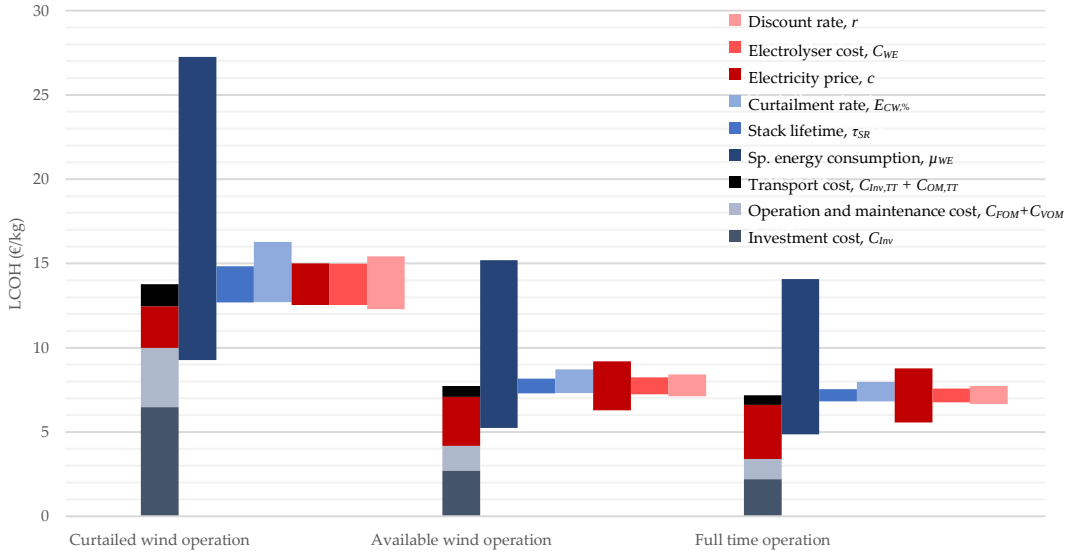

Figure 3.13. Sensitivity analysis of the techno-economic parameters

3.4.7. Technical challenges for injection into the natural gas network

In hydrogen injection into natural gas network, several challenges are encountered from (1) technical, (2) economic, and (3) the regulatory perspectives. The two main technical perspectives are from the gas network operator and the final consumer. The gas network operator implements parameters to maintain gas quality such as the Wobbe Index. The Wobbe index (MJ/m³) is the ratio of gross calorific value to relative density. It indicates

the rate of heat flow from the gas burner. Low Wobbe Index results in increased propensity for flame lift and flame extinction, leading to incomplete combustion and hazardous emissions. High Wobbe Index results in over-heating and carbon monoxide formation [130]. The increase of hydrogen concentration in natural gas reduces volumetric gross calorific value and relative density, which eventually affect Wobbe Index. Therefore, the parameters for gas quality in transmission and distribution have to be improved for more hydrogen to be transported by the gas grid in the future. The other technical aspect in gas transmission and distribution is gas handling at the injection location. The required equipment and installation have to be identified to safely transfer hydrogen from tube trailer to gas pipeline. Each AGI might have different technical characteristics and capacity to accommodate hydrogen. As shown previously in Figure 10 and Figure 11, each AGI is connected to different numbers of WHSs, where each WHS has a different hydrogen capacity. If curtailed wind and available wind operations are considered, the daily hydrogen supply is highly dependent on wind availability. This means additional storage at each AGI is required to ensure the continuity and stability of gas supply. Further studies are required to quantify the hydrogen storage and other required equipment at AGIs. Additionally, it is necessary to ensure the hydrogen concentration to be equivalent across the pipeline at different locations with gas metering. At final consumer locations, when the concentration of hydrogen at natural gas is high, system adjustment may be required as studied by Leicher et al. [131]. A review by Vries et al. [132] shows hydrogen must be preserved at a certain fraction to maintain the performance of domestic appliances in the residential and commercial sectors. In the power sector, modern gas turbine power plants can burn over 50% hydrogen by volume in natural gas. But by and large, such plants require modification to the combustion system when the fuel contains high levels of hydrogen, as evaluated by Andersson et al. [133].

In terms of economic challenges, the injection cost is difficult to estimate due to as yet unidentified injection equipment. The specification of required equipment can assist the formulation of hydrogen injection costs. The additional cost of injection and distribution in the gas network is required to be added to $LCOH_{total}$. As described in the subsection of techno-economic submodel, current analysis only includes hydrogen production and transportation to the injection location.

Hydrogen from future onshore and offshore wind farms has even greater potential to be delivered to the Irish gas network. However, hydrogen is not yet regulated in the same way as biomethane injection into the gas network. To facilitate biomethane injection, Ireland introduced an injection price [134] as well as gas quality parameters [135]. The same approach is required for hydrogen in the near future.

3.5. Conclusions

A wind-hydrogen system (WHS) is designed to harness either curtailed wind power or a combination of curtailed and exportable wind with support from grid electricity to produce hydrogen and transport it to the Irish natural gas grid. Electrolyser operation is modelled under three different scenarios: (1) curtailed wind operation, (2) available wind operation and (3) full capacity operation. $LCOH$ is used as the key techno-economic parameter in the techno-economic optimisation and evaluation of WHS. In designing a WHS capacity, a novel algorithm is used to prioritise the use of curtailed wind to power electrolyser and compressor. All the equipment costs for hydrogen production are made to be functions of electrolyser size.

The calculation of optimum electrolyser size, giving the minimum production costs for 74 wind farms (>10 MW_e), is performed iteratively from 10 kW_e to its wind farm capacity by

using an hourly curtailed wind profile at each wind farm. From these results, a statistical model is defined to calculate optimum electrolyser power capacity for the remaining 238 smaller wind farms in Ireland. The minimum hydrogen production cost can be calculated using a statistical model from three essential values of wind farm capacity, percentage of curtailed wind and wind farm capacity factor. Afterwards, GIS is used to pair each WHS with its nearest AGI and identify the shortest road route between them. Low and high electricity prices are also used in the evaluation. The opportunity of having more competitive equipment costs and technical performance in the future is also considered.

As a result, most existing Irish wind farms that rely only on curtailed wind have a hydrogen production and transportation cost of more than 13 €/kg. When an electrolyser operates with available wind or at full capacity, WHSs show better techno-economic performance, as reflected by its lower hydrogen cost. As indicated by high hydrogen production and transportation costs, it is found that some of wind farm capacities are not suitable for hydrogen production and transportation to the gas network. Wind farm capacities lower than 5 MW_e are not suitable to be operated only with curtailed wind, wind farms below 1 MW_e are not suitable to depend on available wind, and wind farms below 0.1 MW_e are not suitable even when the electrolyser is operating at full capacity. Results also show that 84% of the hydrogen supply potential in Ireland is located not more than 100 km to the nearest injection point with the total costs of 9–11 €/kg at full capacity operation. In the future, the total cost can reach 6–8 €/kg at the same operation scenario. With this hydrogen production cost, the WHS also provides additional economic value to a wind farm due to the fact that curtailed wind is purchased as much as the average $LCOE$ of onshore wind farms. The most sensitive parameters of WHS that possibly change in the future are the percentage of curtailed wind, stack lifetime, electrolyser efficiency, and electrolyser capital cost. The future potential of hydrogen capacity from current wind capacities reaches 49 kilotonnes which is equivalent to nearly

3% energy demand of natural gas in Ireland. Additional wind capacities in the future can even elevate the potential of hydrogen to substitute energy from natural gas to almost 6%, or slightly higher than current natural gas supply from Kinsale gas field. This potential can be fully exploited after technical, economic, and regulation challenges in hydrogen injection at potential sites are answered. The recommendation to energy stakeholders is to structure and establish a regulation for hydrogen injection to the gas grid. This can motivate further study and development on hydrogen injection and eventually stimulate more renewables in the gas network, particularly from renewable hydrogen.

The future stage of this work is to reduce dependency on grid electricity by system integration to other renewable sources. It is also essential to advance the developed hydrogen production model by modifying the arrangement of the electrolyser with multiple different electrolyser sizes and combining the existing design with a battery system. Alternative hydrogen transportation mechanisms such as liquid hydrogen and a dedicated hydrogen pipeline from the wind farm are also necessary to be technically and economically compared. At an injection location, details of new required equipment and installation at the AGI are necessary to be investigated for a secure and stable hydrogen supply.

3.6. Final remarks

In this chapter, the techno-economic performances are modelled using equipment' techno-economic parameters and optimised through sizing using $LCOH$ (€/kg) as the key parameter. The historical curtailed and exportable wind electricity are prepared and used as input to the hydrogen production model. An algorithm in GIS is used to optimise the supply chain between supply and demand sites.

In Chapter 4, hydrogen production is also modelled for gas grid injection. However, solar electricity generated from PV arrays is used instead of wind electricity. Hydrogen production in Libya for Italy via the Greenstream corridor is selected as a case study to evaluate the impact of long-distance gas transmission capacity.

Chapter 4. Hydrogen Production from Solar Electricity for Long-Distance Gas Transmission

4.1. Overview

This chapter presents the results of the techno-economic model for hydrogen production from a photovoltaic battery electrolyser system (PBES) for injection into a natural gas transmission line. Mellitah in Libya, connected to Gela in Italy by the Greenstream subsea gas transmission line, is selected as the location for a case study. The PBES includes the photovoltaic (PV) arrays, battery, electrolyser, compressor, and large-scale hydrogen storage to maintain constant hydrogen volume fraction. Simulated hourly PV electricity generation is used to calculate the specific hourly capacity factor of a hypothetical PV array in Mellitah. This capacity factor is then used at different PV sizes for sizing the PBES. The levelised cost of hydrogen production ($LCOH_P$) is used as the key techno-economic parameter to optimise the size of the PBES by equipment sizing. The costs of all equipment, except the PV array and batteries, are made to be a function of electrolyser size. The equipment sizes are deemed optimal if PBES meets hydrogen demand at a minimum $LCOH_P$. The techno-economic performance of the PBES is evaluated for four scenarios of fixed and constant hydrogen volume fraction targets in

the pipeline: 5%, 10%, 15%, and 20%. The PBES can produce up to 106 kilotonnes of hydrogen per year to meet 20% target at $LCOH_P$ of 2.28 €/kg using optimum equipment sizes. The energy intensity of hydrogen production is from 50 to 63 kWh/kg, including a small share of energy necessary to produce desalinated water for the PBES.

4.2. Introduction

The European Union (EU) aims by 2030 to install 40 GW of electrolyser capacity within its member states and a further 40 GW in neighbouring regions, specifically North Africa and Ukraine, to supply the EU [5]. Large scale of electrolysers at wind and solar hydrogen production sites can potentially generate low-carbon hydrogen at levelised production costs as low as 1.5 to 2.0 €/kg by 2025. The hydrogen produced in these neighbouring regions can be transmitted to the EU via existing natural gas transmission infrastructure. North African countries including Algeria and Libya currently provide 24 billion cubic meters (bcm) of natural gas to the EU, equivalent to 5% of total natural gas consumed in the bloc in 2019 [136].

The objectives of this study are (1) to model hydrogen production from a photovoltaic battery electrolyser system (PBES), (2) to evaluate the impact on production cost of different equipment sizes, and (3) to determine the optimum size of PBES techno-economically. The following section describes the methods used to achieve these objectives. It covers the explanations of how the model handles the photovoltaic electricity, the levelised cost of hydrogen, hydrogen supply, desalinated water supply, and hydrogen demand. Following that, the results and discussion section comprises the description of techno-economic performance for PV arrays, battery, electrolyser, and storage, the optimum equipment sizes for all scenarios, hydrogen supply from the

optimum equipment, and energy intensity of hydrogen production. Finally, the overall findings of the work and impacts on the extensive size hydrogen production system are presented in the conclusions section.

4.3. Methodology

4.3.1. Systems and scenario description

Hydrogen can potentially be generated using a photovoltaic battery electrolyser system (PBES) in a region with high solar energy potential like North Africa. As a case study, this work models renewable hydrogen production from solar energy in North Africa and its injection into the existing subsea gas transmission pipeline between Libya and Italy. The hydrogen is assumed to be produced and injected at the Mellitah Gas Compression Station (MGCS) in Libya, transported through the 520-km Greenstream subsea natural gas transmission pipeline and delivered to the Gela receiving terminal in Italy, as shown in Figure 4.1. In the PBES, photovoltaic (PV) electricity is generated by PV arrays. This electricity can be temporarily stored in battery system and/or used to produce hydrogen via water electrolysis. Hydrogen is compressed to 80 barg for storage and/or injection to the gas transmission pipeline, as illustrated in Figure 4.2. Hydrogen production is modelled to meet demand required by hydrogen volume fractions of 5%, 10%, 15% and 20% in the Greenstreram pipeline.

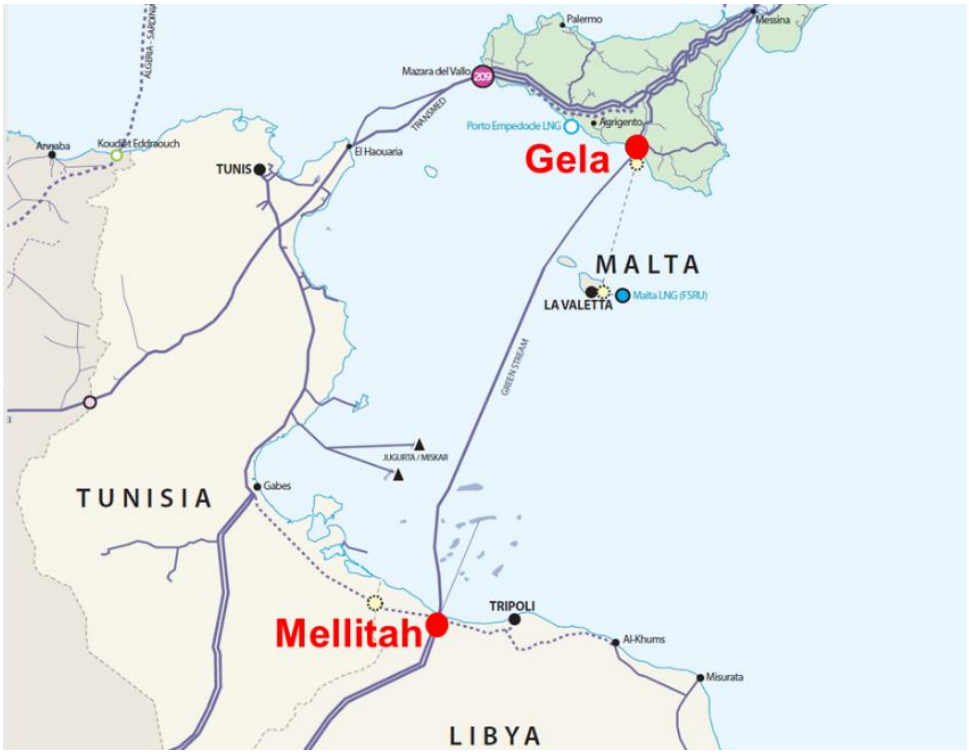

Figure 4.1. Mellitah and Gela gas terminals are connected by the 520-km Greenstream subsea natural gas transmission pipeline [137]

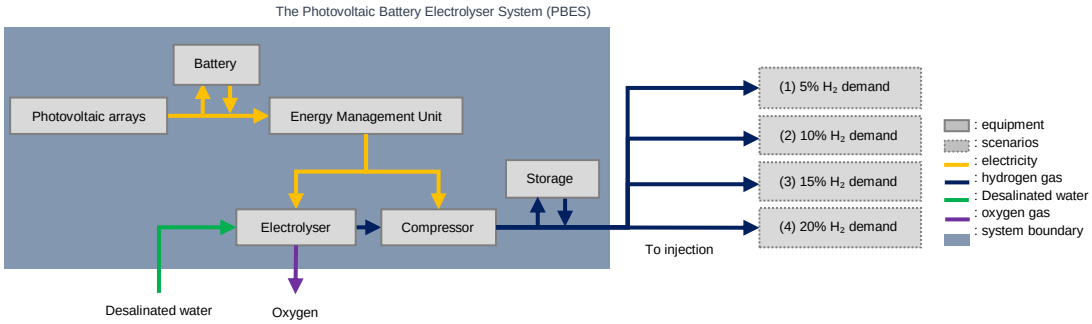

Figure 4.2. The equipment of a photovoltaic battery electrolyser system (PBES) for hydrogen gas injection

4.3.2. Photovoltaic electricity

PV electricity production for the coordinates of Mellitah, Libya is simulated using the PV Performance tool (PVT) from the European Union Photovoltaic Geographical Information System (EU-PVGIS) [138]. The solar radiation database collected by Surface Solar

Radiation Data Set - Heliosat (SARAH) and recorded by the European Organisation for the Exploitation of Meteorological Satellites (EUMETSAT) Climate Monitoring Satellite Application Facility (CM SAF) from 2005 to 2015 are used in the simulation. PVT optimises the slope and azimuth of the fixed mounting PV arrays in the simulation of PV electricity. The PV technology, installed peak PV power (P_{PV}), and system losses are crystalline silicon, 1,000 kW_e, and 14%, respectively. The average hourly PV electricity (E_{PV}) is then calculated from these ten years of data. The PV capacity factor for time t ($\lambda_{PV,(t)}$) can be calculated using Equation (4.1).

$$\lambda_{PV(n)} = \frac{E_{PV(n)}}{P_{PV} \times t_{(n)}} \tag{4.1}$$

4.3.3. Levelised cost of hydrogen

The levelised cost of hydrogen production ($LCOH_P$) and annual hydrogen production ($M_{H2,HP}$) are used as the key parameters to optimise the equipment sizes of PBES techno-economically. $LCOH_P$ is calculated from total capital ($C_{CAPEX,HP}$), operational and maintenance expenditure ($C_{OPEX,HP}$), and total hydrogen produced (M_{H2}) for the year (T) using Equation (4.2). The PBES lifetime (τ_{PBES}) is defined to operate for 20 years with an assumed discount rate (r) of 5% for renewable energy projects in Libya [139]. Annual hydrogen production is described in the following subsection of hydrogen supply.

$$LCOH_P = \frac{\sum_{T=0}^{T=\tau_{PBES}} \frac{C_{CAPEX,HP} + C_{OPEX,HP}}{(1+r)^T}}{\sum_{T=0}^{T=\tau_{PBES}} \frac{M_{H2,HP}}{(1+r)^T}} \tag{4.2}$$

The $C_{CAPEX,\,HP}$ includes the capital costs of PV array (C_{PV}), battery (C_{EB}), water electrolyser (C_{WE}), electric compressor (C_{EC}), hydrogen storage vessels (C_{SV}), energy management unit (C_{EMU}), interconnection, commissioning, and start-up (C_{ICS}), engineering (C_{ENG}) and other (C_{OH}) as expressed by Equation (4.3). The $C_{OPEX,\,HP}$ comprises the operational and maintenance costs of PV arrays ($C_{OM,PV}$), water electrolyser ($C_{OM,WE}$), electric compressor ($C_{OM,EC}$), and hydrogen storage vessel ($C_{OM,SV}$), as well as the stack replacement (C_{SR}) and water consumption (C_{H2O}) as shown by Equation (4.4). All the costs are made to be a function of electrolyser size in kWe (P_{WE}), except for PV and battery costs, which are independent variables. Capital costs for electrolyser and batteries are projected to decrease by 50% and 60% in 2030, respectively [104] [27]. All techno-economic parameters in 2030 of the PBES constituent equipment are listed in Table 4.1.

$$C_{CAPEX,HP} = C_{PV} + C_{EB} + C_{WE} + C_{EC} + C_{SV} + C_{EMU} + C_{ICS} + C_{ENG} + C_{OH} \tag{4.3}$$

$$C_{OPEX,HP} = C_{OM,PV} + C_{OM,WE} + C_{OM,EC} + C_{OM,SV} + C_{SR} + C_{H2O} \tag{4.4}$$

Table 4.1. Techno-economic parameters of hydrogen production at photovoltaic battery electrolyser system (PBES)

Parameters, Symbol	Value/ Unit/ Reference					
Equipment	**Water Electrolyser (WE)**			**Electric Compressor (EC, HP)**		
Technology	Alkaline			Reciprocating		
Sp. energy cons., μ	48	kWh/kg	[140]	0.7	kWh/kg	[115]
Lifetime, τ	20 (system), 11 (stack)	years	[31]	10	years	[115]
Efficiency, η	69%	(LHV_{H2})	[115]	73%	(isentropic)	[46]
Outlet pressure, p	30	barg	[115]	80	barg	[141]
CAPEX, C_{CAPEX}	3645 x $P_{WE}^{0.783}$	€	[17]	4342 x $P_{WE,n}^{0.66}$	€	[98]
OPEX, C_{OPEX}	0.2011 $P_{WE,n}^{-0.23}$ x $C_{CAPEX,WE}$		[115] [104]	2%		[115]
ICS	20% x (C_{WE} + C_{EC})		[98]			
Engineering	15% x (C_{WE} + C_{EC})		[98]			
Other cost, $C_{OH, HP}$	1.5652 $P_{WE,n}^{-0.154}$ x $C_{CAPEX,WE}$	€	[98]			
Equipment	**Photovoltaic (PV)**			**Energy management unit (EMU)**		
Technology	Polycrystalline silicon			Converter and controller		
Lifetime, τ	30	years	[42]	15	years	[42]
Efficiency, η	10-15%		[138]	90%		[42]
Capacity factor, λ	Calculated using Equation (4.1)					
CAPEX, C_{CAPEX}	450 x P_{PV}		[24], [26]	10% x (C_{WE} + C_{EC})	€	[98]
OPEX, C_{OM}	1.5%		[27]			
Equipment	**Electric Battery (EB)**			**Storage Vessel (SV, HP)**		
Technology	Lithium Nickel Manganese Cobalt Oxide			Pressure vessels		
Lifetime, τ	20	years	[33]	20	years	[98]
Efficiency, η	90%		[27]	-		
DoD	100%		[33]	-		
C-rate	1C		[33]	-		
CAPEX, C_{CAPEX}	3283 x $E_{EB,n}^{0.7108}$	€/kWh	[142]	0.6 x $m_{H2,max}$	€	[140]
OPEX, C_{OPEX}	Not considered		[27]	2%		[98]

4.3.4. Hydrogen supply

Annual hydrogen production ($M_{H2,HP}$) is calculated from the electricity (E_{WE}) used by the electrolyser and its specific electricity consumption (μ_{WE}) as expressed in Equation (4.5) [143]. The electrolyser operates with electricity from the PV array ($E_{PV,WE}$) and battery ($E_{EB,WE}$), as shown in Equation (4.6).

$$M_{H2,HP,(t)} = \frac{E_{WE,(t)}}{\mu_{WE}} \tag{4.5}$$

$$E_{WE,(t)} = E_{PV,WE,(t)} + E_{EB,WE,(t)} \tag{4.6}$$

The modelling of electrolyser and compressor performance is done in the same manner as in Gunawan et. al [143]. There are two conditions to calculate electricity flow from the PV array to the electrolyser. The first is when the PV power (P_{PV}) at time (t) exceeds electrolyser rated power size (P_{WE}). The second is the P_{PV} is equal to the size of electrolyser rated power (P_{WE}). It means some PV power output can generate surplus power at small electrolyser sizes. The surplus power over time can be stored in the battery to be used in the second condition. The second condition is when P_{PV} is lower than P_{WE}. These two conditions are expressed in Equation (4.7). Equation (4.8) shows how battery electricity can be calculated to support hydrogen production when there is enough stored energy in the battery.

$$E_{PV,WE,(t)} = \min\left(P_{WE}, P_{PV,(t)}\right) \times \Delta t(n) \tag{4.7}$$

$$E_{EB,WE,(t)} = \min\left(E_{WE,(t)} - E_{PV,WE,(t)}, E_{WE,(t)}\right) \tag{4.8}$$

Like the water electrolyser, the electric compressor is also operated using PV array ($E_{PV,EC}$) and battery ($E_{EB,EC}$) electricity, as shown in Equation (4.9). If PV electricity is larger than the electricity demand for an electrolyser, the contribution of PV electricity for the compressor can be calculated using Equation (4.10). The electricity stored in the battery can also be used to operate the compressor when PV electricity is insufficient, as expressed in Equation (4.11). The electricity demand for compressing hydrogen gas can be calculated from the flow rate at time t ($M_{H2,(t)}$) and the specific electricity consumption of the compressor (μ_{EC}).

$$E_{EC,(t)} = E_{PV,EC,(t)} + E_{EB,EC,(t)} \tag{4.9}$$

$$E_{PV,EC,(t)} = \min\left(M_{H2,(t)} \times \mu_{EC}, E_{PV,(t)} - E_{PV,WE,(t)}\right) \tag{4.10}$$

$$E_{EB,PV,(t)} = \min\left(M_{H2,(t)} \times \mu_{EC}, \left(M_{H2,(t)} \times \mu_{EC}\right) - E_{PV,EC}\right) \tag{4.11}$$

The modelling of battery and hydrogen storage performance is done in the same manner as in Ma et. al. [144] and Song et al. [145]. The PV electricity charges the battery when PV electricity exceeds the electricity consumption for both electrolyser and compressor, and therefore can be calculated using Equation (4.12). Equation (4.13) shows the calculation during battery discharge, supplying the electrolyser and compressor.

$$E_{EB,(t)} = E_{EB(t-1)} + \left(\left(E_{PV,(t)} - E_{PV,WE,(t)} - E_{PV,EC,(t)}\right) \times \eta_{EB}\right) \tag{4.12}$$

$$E_{EB,(t)} = E_{EB(t-1)} + \left(\left(E_{EB,WE,(t)} + E_{EB,EC,(t)}\right) \times \eta_{EB}\right) \tag{4.13}$$

In this study, the hydrogen storage, the type I made from fully metallic pressure vessels [44], is modelled to supply the hourly hydrogen injection demand ($M_{H2,HD,(t)}$). Hydrogen is

stored when its production surpasses the hourly demand expressed in Equation (4.14). Hydrogen is released from storage when the hourly hydrogen production is less than hydrogen demand and can be calculated using Equation (4.15). The maximum of all hourly (at time t) stored hydrogen capacities ($M_{H2,SV,(t)}$) throughout the year determines the required storage size. In terms of equipment sizing, the $LCOH_P$ calculation is performed iteratively for ranges of minimum and maximum for each piece of equipment as listed in Table 4.2. The equipment size combination for the minimum $LCOH_P$ is selected as the optimum system design.

Table 4.2. The ranges for equipment sizing of photovoltaic battery electrolyser system (PBES)

		Formula	Scenarios			
			5%	10%	15%	20%
PV array sizes, P_{PV} (MWe)	Minimum	= $M_{H2}/(\mu_{WE}+\mu_{EC})/(\lambda_{PV}*8760)$	735	1454	2229	3064
	Maximum	= $P_{PV,minimum}/\eta_{EB,roundtrip}$	918	1817	2786	3830
Electrolyser sizes, P_{WE} (MWe)	Minimum	= $M_{H2}/(\mu_{WE}+\mu_{EC})/8760$	140	276	424	582
	Maximum	= $P_{PV,maximum}$	918	1817	2786	3830
Battery sizes, E_{EB} (MWh)	Minimum	= 5	5	5	5	5
	Maximum	= $P_{PV,maximum}$	918	1817	2786	3830

$$M_{H2,SV,(t)} = M_{H2,SV,(t-1)} + \left(\left(\frac{E_{PV,WE,(t)} + E_{EB,WE,(t)}}{\mu_{WE}} \right) - M_{H2,HD,(t)} \right) \quad (4.14)$$

$$M_{H2,SV,(t)} = M_{H2,SV,(t-1)} - min\left(\left(M_{H2,HD,(t)} - \left(\frac{E_{PV,WE,(t)} + E_{EB,WE,(t)}}{\mu_{WE}} \right) \right), M_{H2,HD,(t)} \right) \quad (4.15)$$

4.3.5. Water supply

Mellitah is chosen as the location for the PBES because (1) it has an existing gas terminal that could potentially be used for hydrogen injection, and (2) it is situated near the Mediterranean coast, which is favourable for water supply from a hypothetical desalination plant. There are at least two desalination technologies to convert seawater to desalinated water, (I) multiple-effect desalination (MED) and (II) seawater reverse osmosis (SWRO). The World Bank reported that the total annualised cost of desalinated seawater using Mediterranean seawater is 0.57 €/m^3 for MED and 0.39 €/m^3 for SWRO, all for plant capacity of 100,000 m^3 per day [146]. Energy use for desalination plants in the Middle East and North Africa (MENA) accounts for 10% of total MENA primary energy usage. The typical energy consumption of SWRO is 1.8 kWh per m^3 of desalinated water.

Desalinated water production from seawater using solar energy has been widely investigated in several studies. Palenzuela et. al. modelled the integration of MED and concentrating solar power (CSP) using seawater from the Mediterranean Sea [147]. The study found the levelised cost of water production is between 0.92 and 1.05 €/m^3. In another study, El-Bialy et. al. analysed a wide range of desalination systems using direct solar energy [148]. The study found various techniques to produce desalinated water from brine using passive or active solar stills. Typically, the passive solar still relies on the evaporation process with different configurations of condensers, absorbers, and reflectors. Desalinated water production can be optimised using active solar stills by harnessing more thermal energy through additional collectors or concentrators. These processes have potential to be the options for water supply in the future, especially when the capacity and cost of water production are significantly improved from current levels. This study assumes that the water for electrolysis is supplied from a hypothetical SWRO,

which is outside the boundary of the techno-economic assessment, at a price of 0.39 €/m^3.

4.3.6. Hydrogen demand

Hourly data for natural gas flow and hydrogen demand for four hydrogen volume fraction scenarios for the Greenstream transmission pipeline is obtained from Cavana et. al. [40]. These scenarios are chosen because most of the natural gas network value chains in the EU can deliver up to 20% share of hydrogen [149]. The total equipment sizes from two locations of hydrogen production in Libya by Cavana et. al. are listed in Table 4.3. In this study, the PBES is located in Mellitah to meet the annual hydrogen demands listed in Table 4.4. Hourly hypothetical hydrogen demand profiles for one week for each of the four scenarios are shown in Figure 4.3.

Table 4.3. Total required equipment sizes from previous study by Cavana et. al. [40]

		Hydrogen volume fraction target			
Parameter	Unit	5%	10%	15%	20%
PV array capacity	MW_e	1,570	3,278	5,111	7,092
Electrolyser capacity	MW_e	1,049	2,191	3,415	4,739
H_2 storage capacity (mass)	kilotonnes	0.1	0.2	0.3	0.4
H_2 storage capacity (volume)	million Sm^3	1.3	2.5	3.8	5.5

Table 4.4. Summary of annual hydrogen demand for all scenarios

Parameters	Unit	Demand scenarios			
		5%	10%	15%	20%
Gravimetric of H_2	kilotonnes/ year	25.47	50.41	77.29	106.24
Volumetric of H_2	million Sm^3/ year	299.56	592.81	908.90	1,249.26

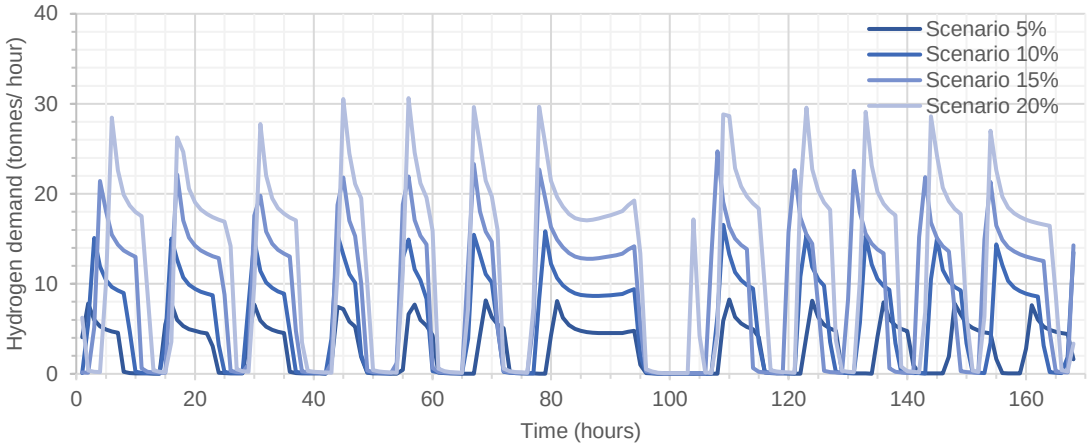

Figure 4.3. Hourly hydrogen demand profiles for one representative week for the Greenstream transmission pipeline

4.3.7. Overall model

A photovoltaic battery electrolyser system (PBES) is modelled to produce hydrogen for blending with natural gas. The PBES includes the PV arrays to generate electricity, a battery to temporarily store the electricity when needed, an electrolyser to produce hydrogen, a compressor to compress the hydrogen to 80 barg, and hydrogen storage to maintain the required injection flow rate. The total capital, operational, and maintenance costs and total hydrogen produced PBES during its lifetime are used to calculate the $LCOH_P$. Each combination of equipment sizes results in specific $LCOH_P$. Therefore, the $LCOH_P$ is iteratively calculated using different equipment sizes. The optimum equipment size of PBES is found at minimum $LCOH_P$. The equipment sizing for PBES is performed to meet four different hydrogen volume fractions for blending at the Greenstream pipeline, as illustrated in Figure 4.4.

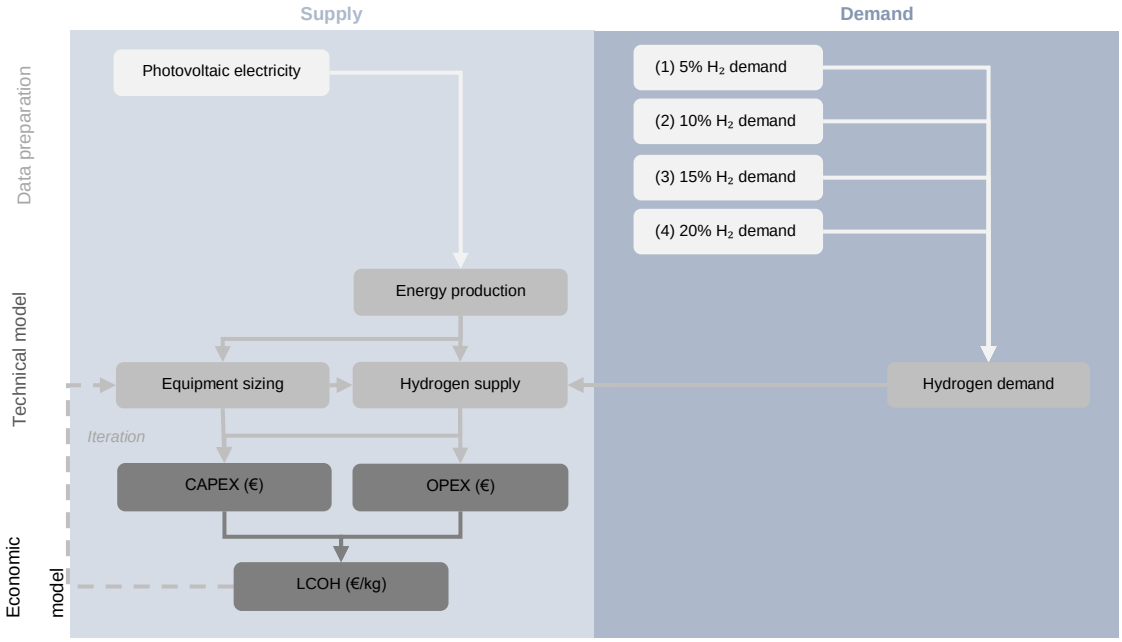

Figure 4.4. Overall model to calculate the levelised cost of hydrogen production ($LCOH$) from a photovoltaic battery electrolyser system (PBES)

4.4. Results and discussion

4.4.1. Impact of PV array, battery, and electrolyser sizes on techno-economic performance

The selection of electrolyser size significantly impacts the techno-economic performances of PBES. When a 1,000-MW_e PV array and a 500-MWh battery are coupled with a 10-MW_e electrolyser, the capacity factor of the electrolyser reaches 100%, as also illustrated in Figure 4.5.a for three days of electrolyser operation. However, 97% of the PV electricity is unable to be converted to hydrogen due to the small size of the electrolyser. As a result, the $LCOH_P$ for this simplified case is very high at 25 €/kg. When the same sizes of PV arrays and battery are integrated with a 100-MW_e, there are some hours where the electrolyser cannot operate due to the absence of electricity supply from both PV and battery. Hence the capacity factor of the electrolyser is 60%, as shown in Figure 4.5.b. The surplus PV electricity and $LCOH_P$ are 76% and 5 €/kg, respectively.

Figure 4.5.c shows the electrolyser performance using the same sizes of PV array and battery with a 500-MW_e electrolyser. Even though the capacity factor of the electrolyser is only 35%, the $LCOH_P$ is calculated at 2.4 €/kg due to fact that 91% of the PV electricity can be used. Therefore, it is more crucial to reduce the surplus of PV electricity rather than increase the electrolyser's capacity factor in designing a cost-effective PBES.

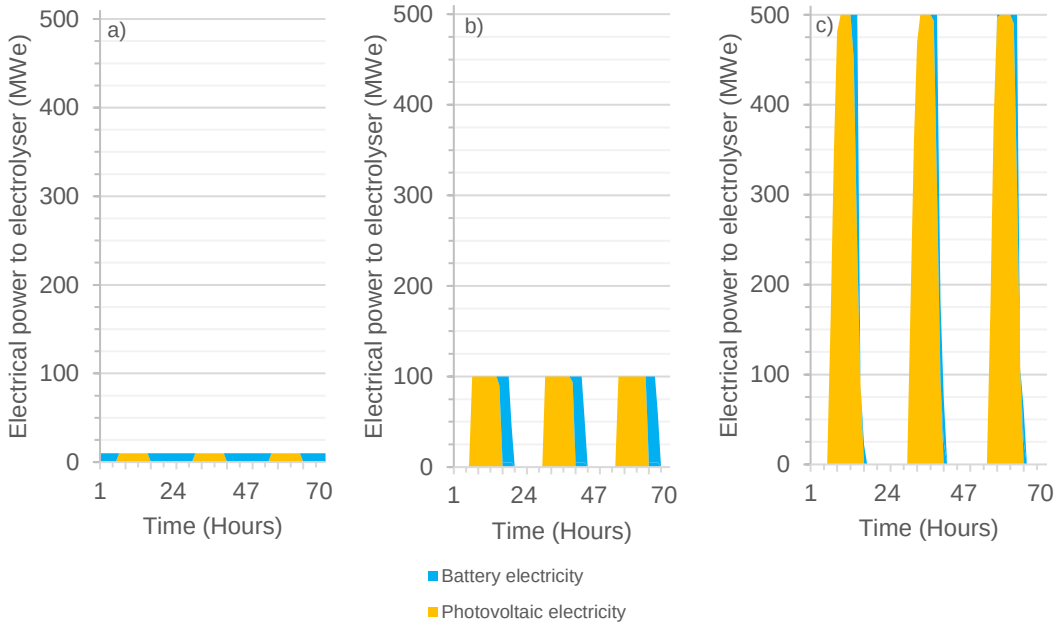

Figure 4.5. Impact of electrolyser size (a) 10 MW_e, b) 100 MW_e and c) 500 MW_e) on electrolyser operational hours for a 1,000-MW_e PV array and 500-MWh_e battery

To evaluate the impacts of different sizes of PV array and battery, Figure 4.6.a shows the $LCOH_P$ for 1,000, 2,000 and 3,000 MW_e PV arrays that each of it is coupled without, with 3,000 or 6,000 MWh battery. The increase of PV and battery capacities results in the reduction of $LCOH_P$ at large electrolyser sizes due to the fact more hydrogen is produced, as shown in Figure 4.6.b. The capacity factor of the electrolyser and surplus PV electricity are also depicted in Figure 4.7.a and Figure 4.7.b, respectively. The PBES operates at high capacity factor as well as high surplus PV electricity at electrolyser sizes of lower than 700, 2,000 and 4,000 MW_e when integrated with PV arrays of 1,000, 3,000 and 6,000 MW_e, respectively.

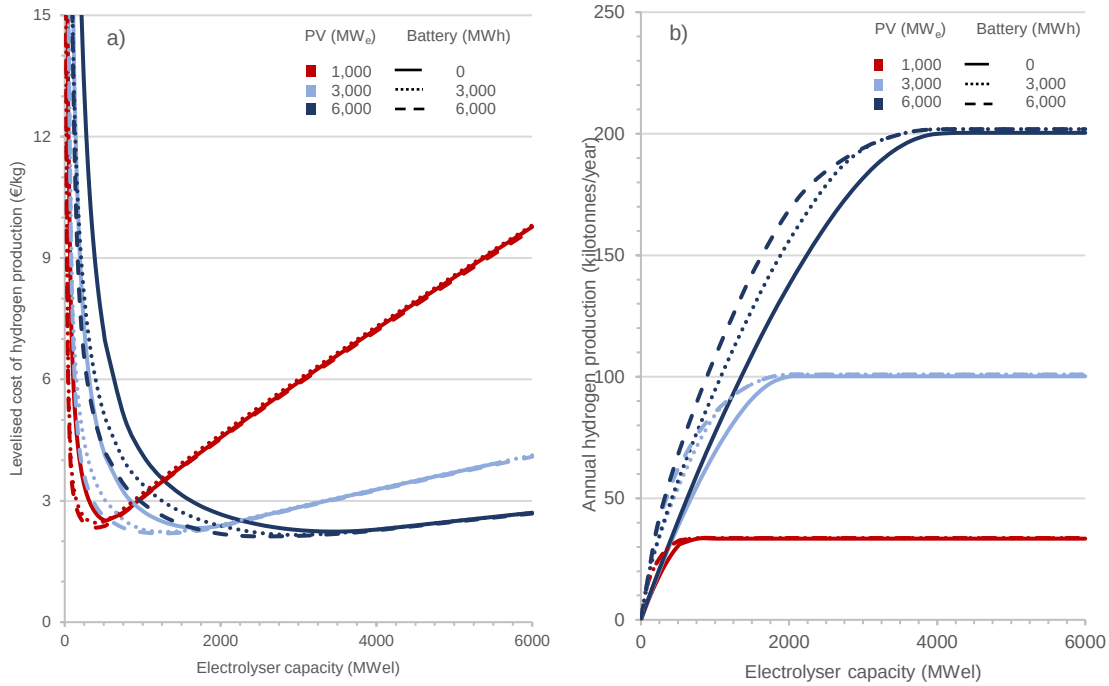

Figure 4.6. Impact of the sizes of PV array, battery, and electrolyser on a) levelised cost of hydrogen production (€/kg) and b) annual hydrogen production (kilotonnes/year)

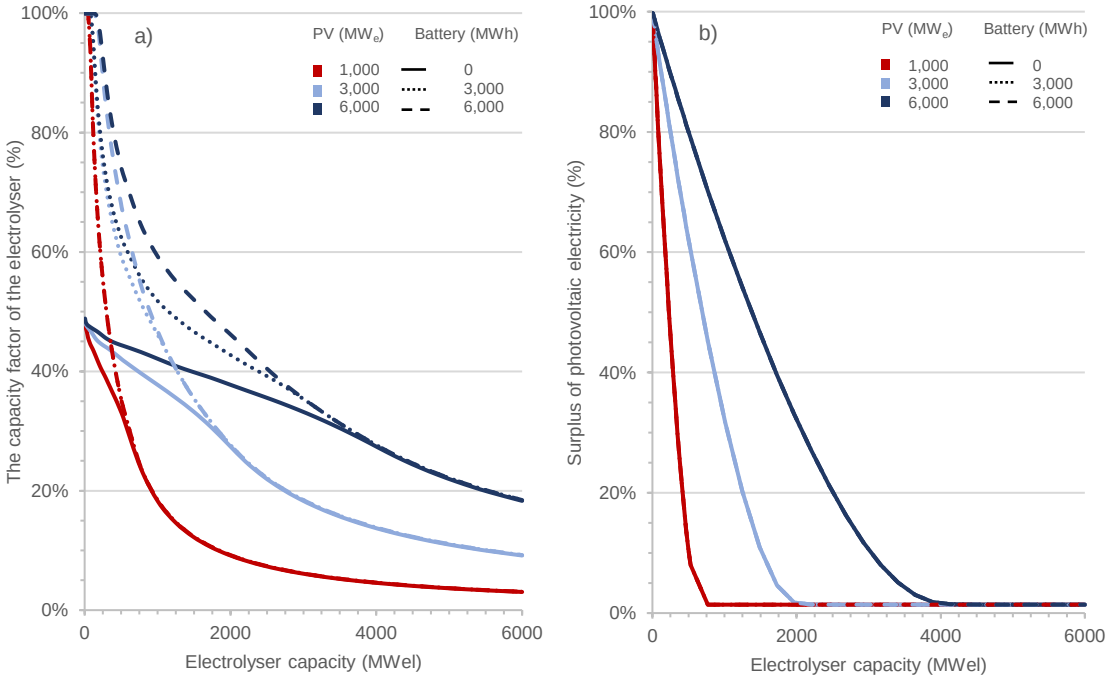

Figure 4.7. Impact of the sizes of PV array, battery, and electrolyser on a) the capacity factor of the electrolyser (%) and b) surplus of photovoltaic electricity (%)

4.4.2. Optimum equipment sizes for all scenarios

Results show the minimum $LCOH_P$ to meet the hydrogen blending demand can be found with a particular combination of PV, electrolyser, and battery sizes. The $LCOH_P$ to deliver the hydrogen volume fraction of 5% is 2.56 €/kg, 10% is 2.43 €/kg, 15% is 2.33 €/kg, and 20% is 2.28 €/kg. The optimum equipment sizes to meet hydrogen demand at minimum $LCOH_P$ are listed in Table 4.5. These optimum equipment sizes in this study are lower than the total sizes of the required equipment calculated by Cavana et. al., except for hydrogen storage size. The large sizes of hydrogen storage in this study are due to the accommodation of hydrogen supply demand during the whole year, which implies a need for hydrogen storage to act as seasonal storage. Seasonal storage can play a role to store most of the storable hydrogen production in summer and then release it to meet most of the hydrogen demand in winter.

Table 4.5. Summary of the optimum equipment sizes for all scenarios

Parameters	Unit	Demand scenarios			
		5%	10%	15%	20%
Hydrogen demand	kilotonnes/ year	25.47	50.41	77.29	106.24
$LCOH_P$	€/kg	2.56	2.43	2.33	2.28
Photovoltaic array size	MWe	765	1,515	2,325	3,195
Surplus photovoltaic electricity	%	1.51%	1.52%	1.55%	1.60%
Electrolyser size	MWe	470	930	1,425	1,955
Electrolyser capacity factor	%	29.69%	29.70%	29.72%	29.78%
Battery size	MWh	45	85	115	180
Hydrogen storage size (mass)	kilotonnes	1.44	2.84	4.34	5.97
Hydrogen storage size (volume)	million Sm^3	16.94	33.42	51.10	70.23

4.4.3. Hydrogen supply from the optimum equipment

Figure 4.8 shows a 3-day hydrogen supply performance from the PBES for each blending scenario at the Greenstream pipeline. The solid colours represent the hydrogen flow for grid injection, and pattern colours indicate the hydrogen flow to storage. The hydrogen flow for grid injection can be from storage as indicated by dark red and from the electrolyser, using PV electricity (yellow) or battery electricity (blue). It can be seen that hydrogen production using direct PV electricity follows the solar energy profile during the day, with some additional hours of battery electricity afterwards. Part of the hydrogen produced during the day is kept in storage for supply during the absence of sunlight. Therefore, the PBES can deliver the hourly hydrogen demand throughout the year. The hydrogen storage performance for all scenarios is illustrated in Figure 4.9. It can be seen that the storage profiles for all scenarios are similar in that most surplus hydrogen is produced and stored during summer and released during winter.

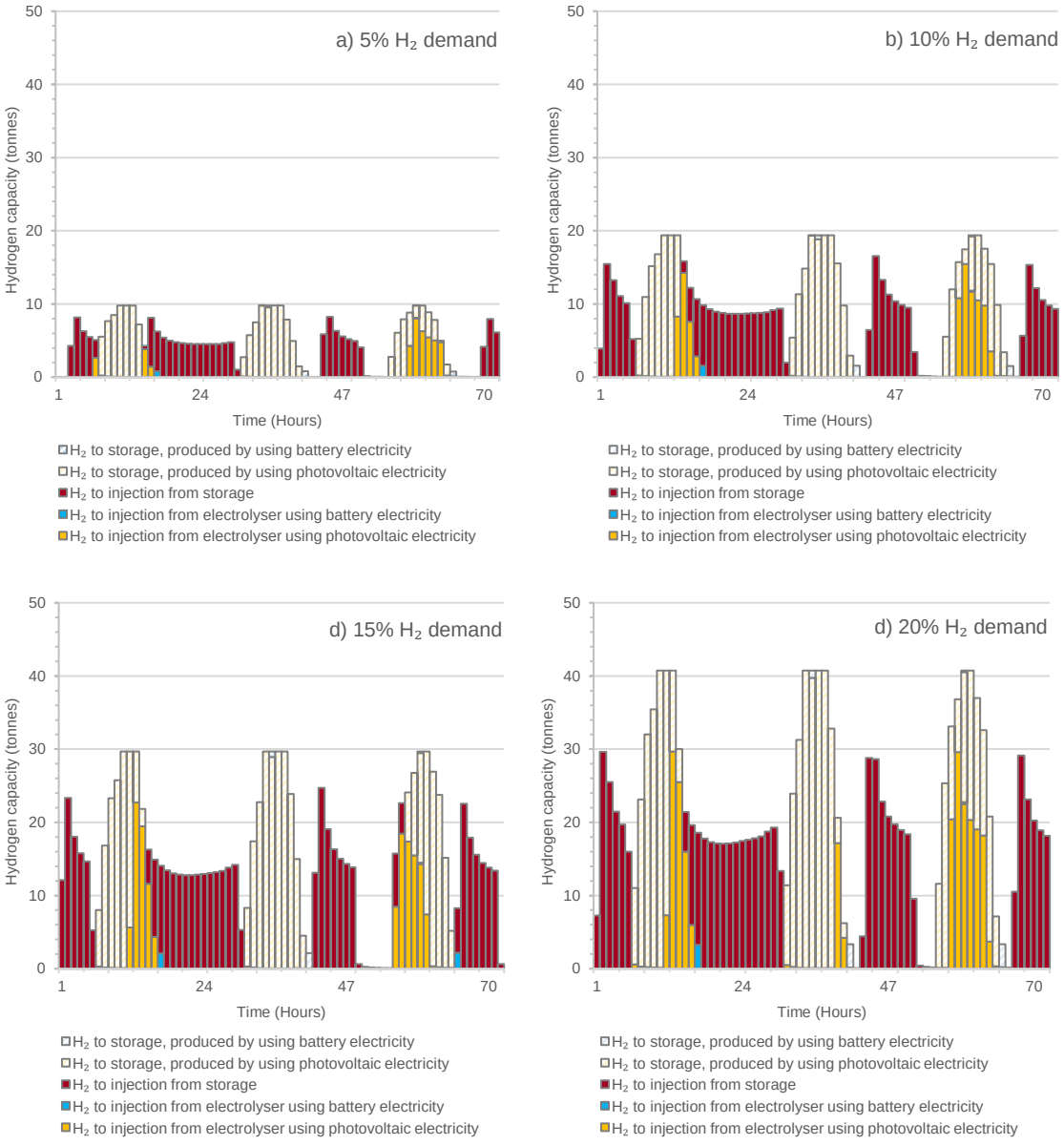

Figure 4.8. Hourly hydrogen supply performance during a 3-days operation in winter for all hydrogen demand scenarios

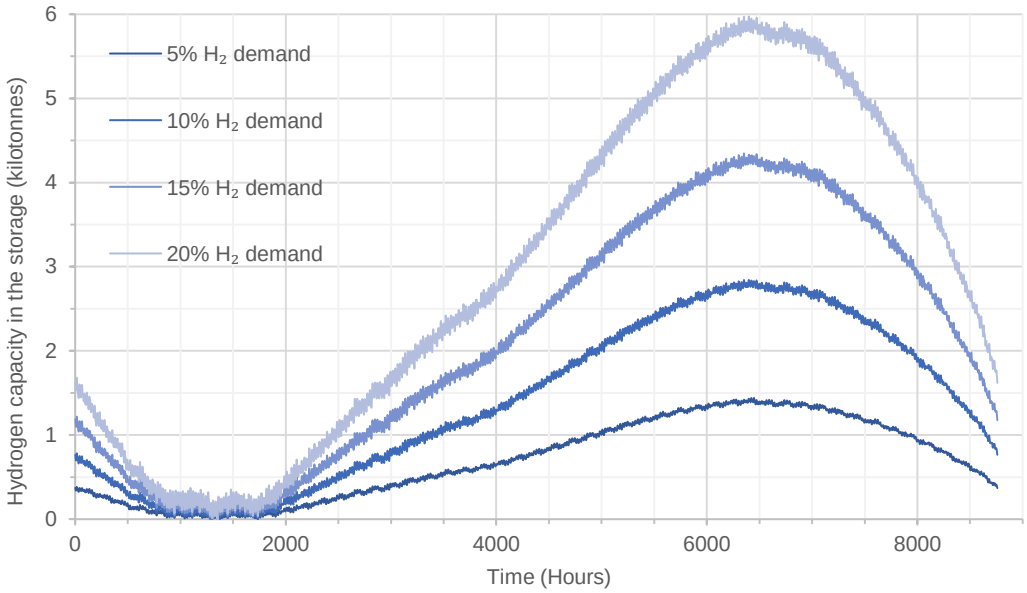

Figure 4.9. Hydrogen storage profiles for all hydrogen demand scenarios

4.4.4. Energy intensity of hydrogen production

The overall energy efficiency in converting PV electricity to compressed hydrogen gas is 53% using the lower heating value of hydrogen (LHV_{H2}). The shares of energy for hydrogen production to meet 5% hydrogen demand are 98.6% for the electrolyser 1.3% for the compressor, and 0.1% for the desalinated water supply. Thus, the total energy intensity of hydrogen production is between 63 and 50 kWh/kg, including the small share of energy consumption to produce desalinated water to meet 5% and 20% hydrogen demand scenarios, respectively.

4.5. Conclusions

A techno-economic model of hydrogen production from a photovoltaic battery electrolyser system (PBES) for injection and blending into a natural gas transmission pipeline was performed in this study. Mellitah in Libya is selected as the location for this case study. The PBES includes a polycrystalline silicon photovoltaic (PV) array to

generate electricity, a lithium-ion battery to temporarily store PV electricity, an alkaline water electrolyser to produce hydrogen, a reciprocating compressor to compress the hydrogen to 80 barg, and large-scale hydrogen gas storage to maintain the flow rate of hydrogen gas injection. Hourly PV electricity output was simulated using the European Union Photovoltaic Geographical Information System (EU-PVGIS). The levelised cost of hydrogen production ($LCOH_P$) and hydrogen blending demand are used as the key parameters to optimise the size of PBES through equipment sizing. The hydrogen blending demand at the Greenstream subsea natural gas transmission pipeline are evaluated for four hydrogen volume fractions of 5%, 10%, 15%, and 20%.

Results show the selection of PV, electrolyser and battery sizes can significantly impact the techno-economic performances of PBES, as indicated by $LCOH_P$. Therefore, the equipment of PBES are sized through iterative calculation of $LCOH_P$ for different combination of equipment sizes. The optimum equipment sizes of PBES are selected at minimum $LCOH_P$. The $LCOH_P$ and hydrogen production capacity from optimum system to meet the 5% to 20% hydrogen blending demand are in the range of 2.28 to 2.56 €/kg and 25 to 106 kilotonnes per year, respectively. The large capacity of this system and the use of expected future technology parameters for the PBES result in the significant reduction of $LCOH_P$. The PBES requires the large hydrogen storage capacities between 1 and 6 kilotonnes. The large sizes of hydrogen storage in this study are due to most of the storable hydrogen is produced in summer to meet the annual demand for hydrogen blending.

Future studies can explore the hydrogen production using a concentrated solar power (CSP). An alternative mechanism to store hydrogen at a substantial capacity like 20% hydrogen blending demand for long-distance natural gas transmission is necessary to investigate. The compressed hydrogen gas storage at salt caverns, depleted natural gas

reservoirs, hydrogen liquefaction, methanol, ammonia, and liquid organic hydrogen carriers (LOHC) are the potential options to be evaluated and compared with the current study. The integration of PBES and hydrogen-fuelled vehicles for local use have the potential to be studied.

4.6. Final remarks

This chapter presents the results of techno-economic modelling of hydrogen production from PV electricity. The $LCOH$ (€/kg) and hydrogen demand are used as the key parameters to size the PBES equipment. PV electricity is simulated for calculating the capacity factor of PV arrays. The capacity factor is then used for calculating PV electricity from different PV sizes. The impact of various sizes on PV arrays, electrolyser, battery, and storage are also discussed in this chapter.

In Chapter 5, hydrogen production is modelled for various energy demands in a remote island community. Multiple scenarios are investigated to source the hydrogen for decarbonising the local energy system.

Chapter 5. Hydrogen Production from Wind/Grid Electricity for Heating & Transport in a Remote Community

5.1. Overview

This chapter presents the results of techno-economic modelling of hydrogen production using curtailed and exportable wind electricity on- or off-island as well as using grid electricity. Valentia Island, in County Kerry, in the southwest of Ireland, is selected as a suitably remote location for a case study. The hydrogen production scenarios are (1) at a nearby wind farm with transportation to Valentia Island, (2) at a hypothetical wind farm located on Valentia Island, and (3) at the electrical substation on Valentia Island. The electrolyser is modelled to operate for three different modes: curtailed wind, available wind, and full capacity. The energy demands to be met by hydrogen include process heating in a factory, space heating for a large public and a large private building, and transport fuel for delivery vehicles, rural buses, and a small car ferry. Results show the hydrogen demand can be supplied from all three production scenarios. The $LCOH_P$ of green hydrogen from on-island wind farm would be 8 €/kg if the electrolyser operated at full capacity with current technology. In comparison, the hydrogen from grid electricity

results in the lowest production cost at 6 €/kg. However, it must be noted that the carbon intensity of this hydrogen is higher than green hydrogen.

5.2. Introduction

Energy Co-operatives Ireland, a co-operative renewable energy consultancy promoting community access to the benefits of renewable energy [150], is currently investigating the opportunities of using hydrogen as a zero-emission fuel for transportation and heating in remote communities in Ireland. Valentia Island is located in County Kerry, in the southwest of Ireland. The island has an area of 26 km^2 and a population of 657 inhabitants, according to the 2016 census. In 2019, Valentia Island residents and businesses consumed 143,590 litres of liquid fuels for transportation. This breaks down as 50% diesel for passenger vehicles and holiday homes, 39% diesel for a ferry to the mainland, 5% petrol for passenger vehicles, 4% diesel for road freight vehicles, and 2% diesel for buses [151].

Valentia Island has a strong potential to generate electricity from wind power. The wind speed at 20 m is in the range of 7 to 13 m/s and 8.5 to 9 m/s for on-shore and off-shore, respectively [151]. It is connected the mainland by a road bridge and a car ferry. Six onshore wind farms within 150 km of Valentia Island supply electricity to the grid. The curtailed electricity from these nearby wind farms has the potential to be the electricity source for hydrogen production.

The objectives of this chapter are (1) to design the system and scenarios of hydrogen supply to Valentia Island, and (2) to model the capacity and costs of hydrogen production and transportation to Valentia Island. The following section covers the methodology, including the description of the system and scenarios, energy demand, and techno-

economic modelling of hydrogen production and transportation. Finally, the results and discussion section presents the optimum electrolyser sizes, capacities, and costs of hydrogen production and transportation.

5.3. Methodology

5.3.1. System and scenario description

Seven scenarios are developed to meet the energy demand in Valentia Island. The hydrogen can be produced (1) at existing nearby onshore wind farms and transport to Valentia Island, (2) at a hypothetical wind farm located on Valentia Island, or (3) at the electrical substation on Valentia Island. This study investigates the potential of producing hydrogen using (I) curtailed wind electricity only, (II) available wind, comprising both curtailed and exportable electricity, and (III) full capacity operation using grid electricity to supply any electrolyser electrical demand unmet by II. The scenarios are summarised in Table 5.1.

Table 5.1. Scenario description for hydrogen supply in Valentia Island

Scenario			**Electricity source for the electrolyser**		
Number	Supply location	Electricity source	Curtailed wind	Exportable wind	Grid supplied
1A	Off-island	Nearby wind farms	✓	-	-
1B			✓	✓	-
1C			✓	✓	✓
2A	On-island	Hypothetical wind farm	✓	-	-
2B			✓	✓	-
2C			✓	✓	✓
3		Without wind farm	-	-	✓

5.3.2. Energy demands replaced by hydrogen

The energy demand potentially supplied by hydrogen in Valentia Island has been investigated by Energy Co-operatives Ireland. The equivalent energy demand is calculated based on the lower heating value of hydrogen (LHV_{H2}), as shown in Table 5.2. The heating demand includes process heating at a plastics factory, and space heating at large public and private buildings. The electrification of heating in Valentia Island is not included because the electricity grid is relatively underdeveloped, and the buildings have poor thermal insulation, which might lead to high retrofit costs for heat pumps [151]. The hydrogen produced from wind energy can potentially replace heating oil that supplies current heating demand. Therefore, the replacement of heating fuel with renewable hydrogen is a long-term opportunity included in this study [151]. Additionally, fuel demand covers 5 delivery vans, 3 single-decker buses, and a ferry to transport passengers and cars to and from the island. The energy demand for transportation are calculated using utilisation rate and fuel economy of hydrogen vehicles in Valentia Island as reported in [151].

Table 5.2. Energy demand for heating and transportation in Valentia Island

Energy demand		Energy demand (MWh/year)	Assumption (kWh/kg)	Hydrogen demand (tonnes/year)
Heating	Factory	533	LHV_{H_2} = 33.33	16
	Large public building	33		1
	Large private building	156		5
Transportation	Delivery vehicle	69		2
	Buses	30		1
	Ferry	58		2
Total		879		26

5.3.3. Hydrogen production and transportation

The levelised cost of hydrogen production and transportation ($LCOH_T$) for off-island supply (in scenario 1A, 1B, and 1C) is calculated using Equation (3.2). Where hydrogen is supplied on-island (in scenario 2A, 2B, 2C, and 3), the levelised cost of hydrogen production ($LCOH_P$) is calculated using Equation (3.3). Hydrogen capacities for all scenarios are calculated using Equation (3.37). These Equations are presented previously in Chapter 3.

This study uses the techno-economic parameters listed in Table 3.1 and Table 3.2, also shown in Chapter 3. The *Closest Facility* algorithm is also used to identify the shortest route from nearby wind farms to Valentia Island for scenarios 1A, 1B and 1C. The average hourly wind capacity factor is obtained from the Eirgrid report [19] for average wind farms in Ireland and used to estimate the hourly wind power for hypothetical wind farms. The required hypothetical wind farm (P_{WF}) to operate the electrolyser in scenarios 2A, 2B, and 2C can be calculated using Equation (5.1), where E_{H2}, t_{WE}, and λ_{WF} are the hydrogen energy demand, maximum possible operational time of electrolyser (8,760 hours in a year), and wind farm capacity factor (typically 30%), respectively. Finally, the required electrolyser size in scenario 3 can be estimated using Equation (5.2). The efficiency of the electrolyser (η_{WE}) is assumed at 61% for PEM in 2020 [17].

$$P_{WF} = \frac{E_{H2}}{t_{WE} \times \lambda_{WF}} \tag{5.1}$$

$$P_{WE} = \frac{E_{H2}}{t_{WE}} \Big/ \eta_{WE} \tag{5.2}$$

5.4. Results and discussion

5.4.1. Off-island hydrogen supply

The hydrogen production capacity and $LCOH_T$ for scenario 1A, 1B and 1C are given in Figure 5.1, Figure 5.2, and Figure 5.3, respectively. It can be seen that the hydrogen production capacities vary from 4 to 31 tonnes per year in scenario 1A. By adding the exportable wind electricity to the electrolyser in scenario 1B, the hydrogen production capacity can reach 10 to 74 tonnes per year with lower $LCOH_T$ than scenario 1A. The largest production capacity and minimum $LCOH_T$ can be achieved in scenario 1C, where the productivity of the electrolyser is maximised. In summary, the delivered hydrogen costs ($LCOH_T$) for scenario 1A, 1B, and 1C are in the range of 17.83 to 19.50 €/kg, 8.58 to 9.13 €/kg, and 6.95 to 7.26 €/kg, respectively. Where the hydrogen production capacities for scenario 1A are between 4 and 31 tonnes per year, for scenario 1B are between 10 and 74 tonnes per year, and for scenario 1C are between 14 and 96 tonnes per year.

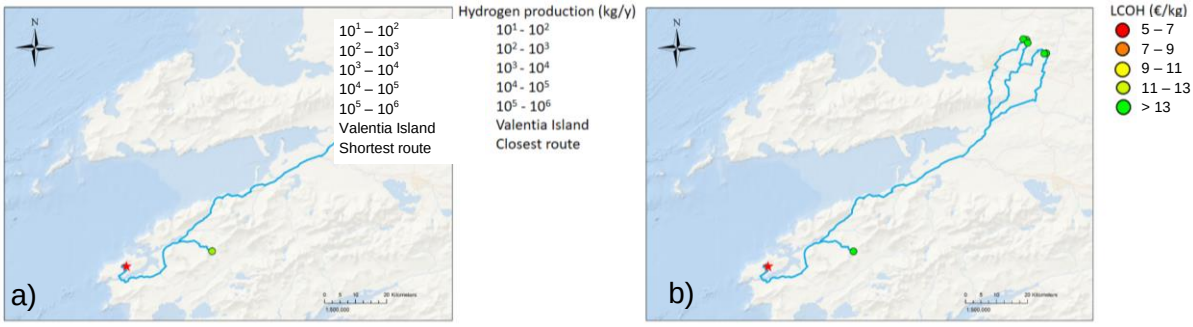

Figure 5.1. a) Hydrogen production capacities and b) hydrogen production and transportation costs for curtailed wind operation of off-island (scenario 1A)

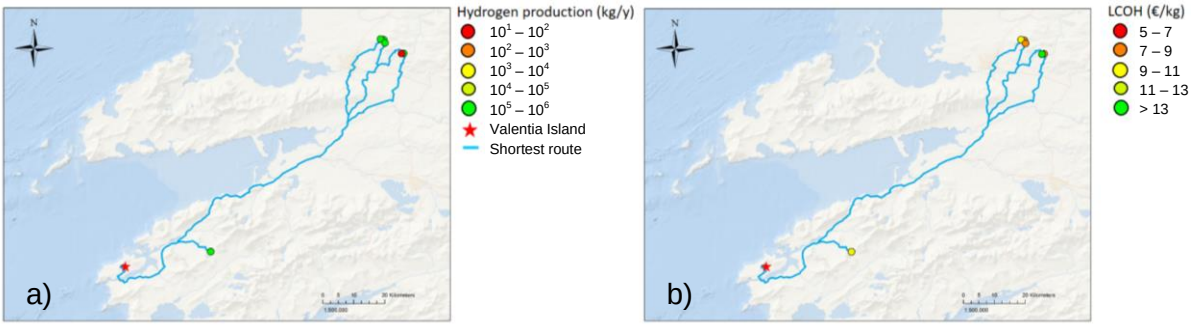

Figure 5.2. a) Hydrogen production capacities and b) hydrogen production and transportation costs for available wind operation of off-island (scenario 1B)

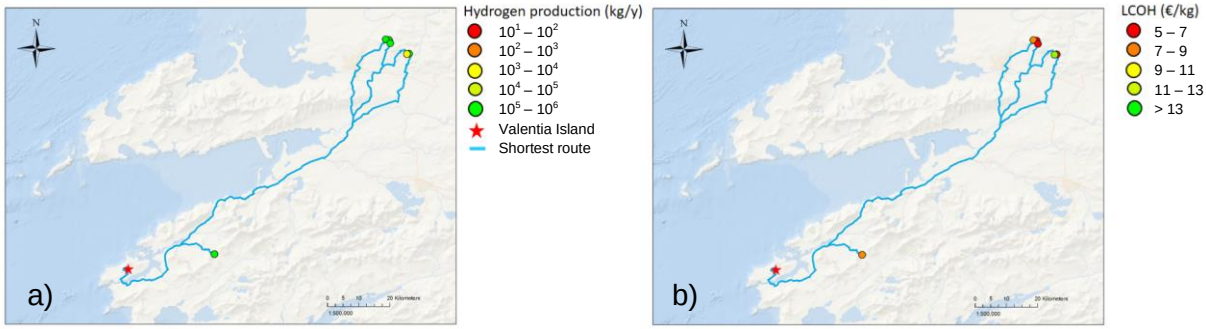

Figure 5.3. a) Hydrogen production capacities and b) hydrogen production and transportation costs for full capacity operation of off-island (scenario 1C)

However, hydrogen production capacity from a single electrolyser located at a nearby wind farm is not sufficient to meet the overall energy demand. Thus, multiple hydrogen supplies might be required depending on the production scenario, as illustrated in Figure 5.4. Therefore, the increase in $LCOH_T$ reflects the additional hydrogen supply from different wind farm and the consequence on the longer distance of the additional wind farm, as shown in Figure 5.5. The results show that higher hydrogen production capacities result in lower $LCOH_T$. But on the other hand, additional buyers must be found for the excess hydrogen.

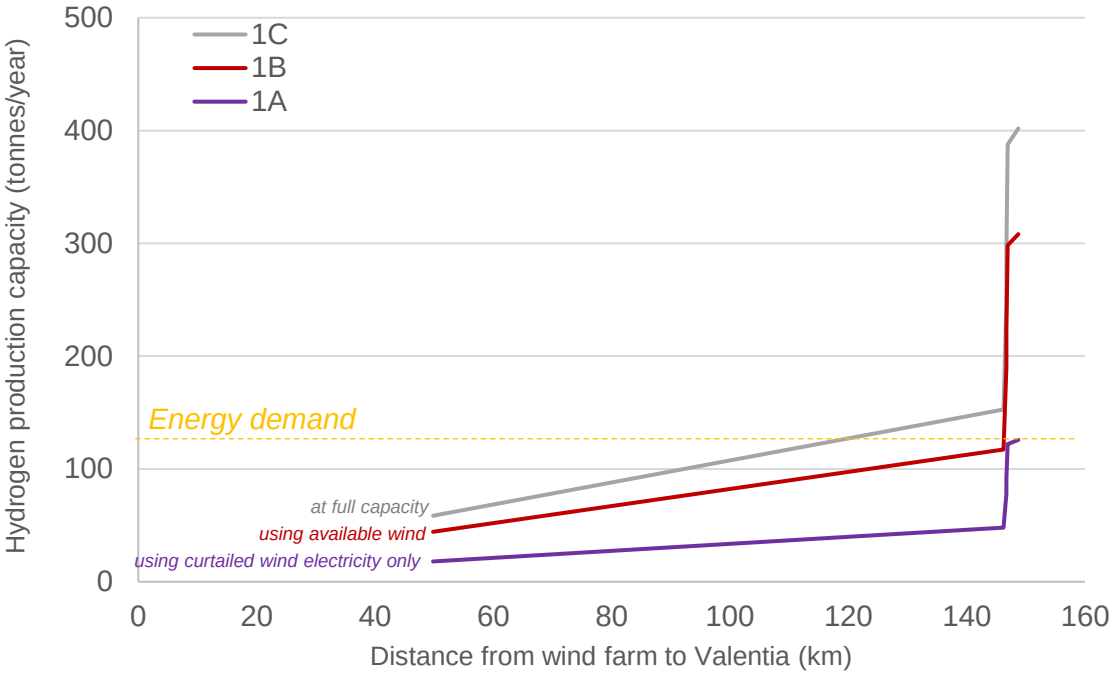

Figure 5.4. Hydrogen production capacity, compared to total energy demand

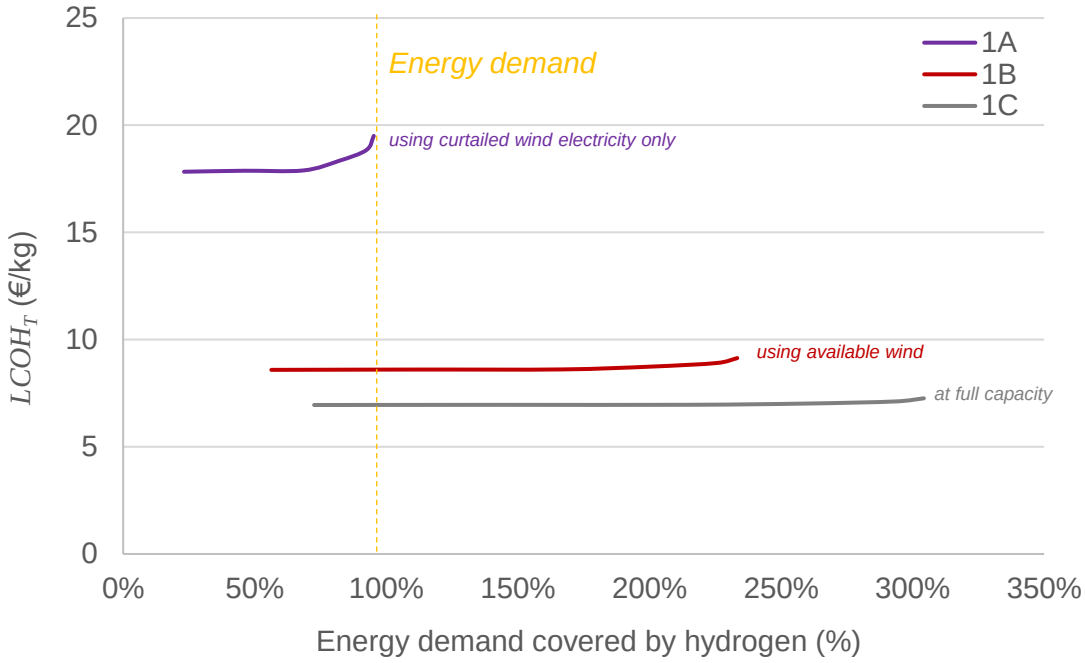

Figure 5.5. Hydrogen production and transportation cost to meet the total energy demand

5.4.2. On-island hydrogen supply

The hydrogen can also be supplied from a hypothetical wind farm in Valentia Island. Since no wind farm exists on the island, this study calculates the required size of the wind farm theoretically. A large wind farm is needed in scenario 2A due to requirement to produce hydrogen from curtailed wind electricity only. The required wind farm and electrolyser sizes in scenario 2B are smaller because the electrolyser operates with the available wind electricity. Lower $LCOH_P$ is also achieved when the electrolyser operates at the maximum capacity factor with the support of grid electricity in scenario 2C.

This study also investigates the opportunity on producing hydrogen by using only grid electricity in scenario 3. It shows that the lowest $LCOH_P$ can be achieved in scenario 3 with $LCOH_P$ of 6 €/kg. Therefore, the carbon intensity on the hydrogen from scenario 3 will only be as green as the grid electricity used in Valentia Island. The summary of results for all scenarios can also be found in Table 5.3.

Table 5.3. The optimum electrolyser sizes and LCOH for hydrogen supply in Valentia Island

Scenario			Parameters		
Number	Supply location	Energy source	Electrolyser Size (kW)	Wind farm (MW_e)	$LCOH$ (€/kg)
1A	Off-island	Nearby wind farms	260 - 575	2 - 15	$LCOH_T$ = 17.83 – 19.50
1B			260 - 575	2 - 15	$LCOH_T$ = 8.58 – 9.13
1C			260 - 575	2 - 15	$LCOH_T$ = 6.95 – 7.26
2A	On-island	Hypothetical wind farm	2,459	66	$LCOH_P$ = 12.98
2B			1,026	4	$LCOH_P$ = 8.42
2C			1,026	4	$LCOH_P$ = 8.19
3		Without wind farm	821	-	$LCOH_P$ = 6.31

5.5. Conclusions

A techno-economic model of hydrogen production using wind or grid electricity for a remote community is presented in this chapter. Valentia Island is selected as the location for a case study. The hydrogen can be produced (1) at existing nearby wind farms and transported to Valentia Island, (2) at a hypothetical wind farm located on Valentia Island, or (3) at the electrical substation on Valentia Island. This study investigates the potential of producing hydrogen solely using (I) curtailed wind electricity, (II) available wind electricity, comprising both curtailed and exportable electricity, and (III) full capacity operation by using grid electricity to fill the remaining required electricity for the electrolyser. The heating demand includes process heating at a plastics factory, and space heating at large public and private buildings. Additionally, fuel demand covers 5 delivery vans, 3 single-decker buses, and a ferry to transport passengers and cars to and from the island.

Results show the hydrogen can be supplied from both off- or on-island to meet the hydrogen demand. The $LCOH_P$ of green hydrogen from off-island wind farm would be 7 €/kg if the electrolyser operated at full capacity with current technology. Besides building a dedicated wind turbine on the island, the wind electricity also can be sourced from nearby wind farms located 50-150 km away from Valentia Island. In comparison, hydrogen from a grid-connected electrolyser results in the cheapest production cost at 6 €/kg. However, it must be noted that the carbon intensity of this hydrogen is greater than for green hydrogen. It is clear that for small capacity, the use of current technology results in relatively high hydrogen production costs. However, subsidies on the capital investment of electrolysers, incentives on the wind-based hydrogen fuel for heating and transport, and greater hydrogen demand might eventually reduce the costs of producing hydrogen. Plans are underway in Valentia to support the development of a very large

offshore wind farm that would be used to produce hydrogen at scale. The cost of the small amount hydrogen required for Valentia Island would be much lower in this case.

For future work, the costs of providing heat using a hydrogen boiler can be included in the model and compared with conventional technologies (€/MWh). In the transport sector, the costs of dispensing hydrogen (€/kg) via a hydrogen refuelling station (HRS) and hydrogen vehicle ownership (€/km) can be investigated. In addition to the wind, solar electricity can potentially be generated via a floating PV located nearby the island to produce hydrogen.

5.6. Final remarks

This chapter presents the performances of techno-economic modelling on hydrogen production from wind or grid electricity and transportation via tube trailers to meet energy demand on a remote island. In Chapter 6, hydrogen dispensing is also modelled and integrated into the developed techno-economic model. Public city bus networks on the island of Ireland are used as a case study.

Chapter 6. Hydrogen Production from Wind and Solar Electricity for City Bus Networks

6.1. Overview

This chapter presents techno-economic modelling results of a nationwide hydrogen fuel supply chain (HFSC) that includes renewable hydrogen production, transportation, and dispensing systems for fuel cell electric buses (FCEBs) in Ireland. Hydrogen is generated by electrolysers located at each existing Irish wind farm using curtailed or available wind electricity. Additional electricity is supplied by on-site photovoltaic (PV) arrays and stored using lithium-ion batteries. At each wind farm, sizing of the electrolyser, PV array and battery is optimised system design to obtain the minimum levelised cost of hydrogen ($LCOH$). Results show the average electrolyser capacity factor is 64% after the integration of wind farm-based electrolysers with PV arrays and batteries. A location-allocation algorithm in a geographic information system (GIS) environment optimises the overall hydrogen supply chain from each wind farm to a hypothetical hydrogen refuelling station in the nearest city. Results show that hydrogen produced, transported, and dispensed using this system can meet the entire current bus fuel demand for all the studied cities, at a potential $LCOH$ of 5 to 10 €/kg by using available wind electricity. At this $LCOH$, the future operational cost of FCEBs in Belfast, Cork and Dublin can be competitive with public buses

fuelled by diesel, especially under carbon taxes more reflective of the environmental impact of fossil fuels.

6.2. Introduction

In 2018, wind supplied nearly 30% of electricity demand on the island of Ireland (Northern Ireland [NI] and the Republic of Ireland [ROI]). As a consequence, at least 6% of available wind energy was lost to curtailment [19]. Irish government policy is to double the 2020 wind installed capacity by 2030 [94]. It is projected that Ireland will still experience curtailment of at least 6% over the next decade [93]. This creates an even higher volume of curtailment (in MWh) as a result of higher installed capacity. This wasted electricity can potentially be stored in the form of hydrogen gas that is produced through the water electrolysis process. As an energy carrier, in parallel to exported electricity to the grid, hydrogen can store and carry the energy to other end uses, thereby enabling sector integration.

Ireland is the third-largest greenhouse gas emission contributor per capita in the European Union [152]. Almost 40% of total energy-related emissions in Ireland are from the transport sector [153]. In Europe as a whole, more than a quarter of transport emissions are from heavy duty trucks and buses [154]. This has encouraged one-third of the 94 countries represented in C40, a consortium of the mayors of the world's megacities, to ban diesel buses and pledge to operate zero-emission buses from 2025 [155], [156]. Fuel cell electric buses (FCEB) are one technology that could help to meet this challenge. They have refuelling times similar to those of diesel buses at 10 minutes, compared to 3-5 hours for all-electric buses [157], [158]. At least 90 FCEBs were in operation across European cities in 2018, with an additional 100 buses planned [159]. Foshan city in China also planned to operate at least 300 hydrogen buses from 2018 [160].

According to the International Energy Agency, China operates more than 5,300 FCEBs in 2021 [161].

If the hydrogen is produced via electrolysis powered by surplus renewable electricity, this presents an opportunity for hydrogen to (1) maximise wind energy outputs, (2) be a reliable carrier of renewable energy in parallel with the existing electricity grid, (3) enable sector coupling between power and transport, and eventually (4) decarbonise public city buses with zero-carbon fuel.

Most of the cited hydrogen production modelling studies calculate the optimum size of equipment based on generated power from weather data such as wind speed and irradiance. The sizing of the production system in the current study uses historical data of curtailed and available wind power as modelled by Gunawan et al. [143] and integrates it with the potential of solar power for each wind farm location in Ireland. The sizing of HRSs uses the theoretical hydrogen capacity equivalent to energy demand for the current number of public buses operated by the cities in Ireland. These cities account for more than two million people, or nearly 35% of the population on the island of Ireland in 2017 [162], [163].

The objectives of this chapter are (1) to model the hydrogen fuel supply chain (HFSC) that consists of WPBES, hydrogen transportation and HRS, (2) to analyse the techno-economic performance of the model by using current and future parameters, (3) to evaluate the operation and capacity of WPBES, and (4) to calculate the cost of dispensed hydrogen fuel at sized HRSs in major cities in Ireland. Hydrogen production, transportation, dispensing, and overall model solution algorithm are described in the following section. The results and discussion section covers hydrogen production from optimum equipment size, fuel supply network and transportation, and hydrogen dispensing and bus operational

cost. The overall findings of the work and impacts on transportation decarbonisation are presented in the conclusions section.

6.3. Methodology

6.3.1. Overall system design and operation scenarios

The HFSC is divided into three main subsystems for (1) production, (2) transportation and (3) dispensing. The production subsystem is a WPBES that consists of PV array, energy management system (EMU), battery, electrolyser, compressor, and hydrogen storage that is situated at every wind farm on the island of Ireland. Since this work uses already operational wind farms, they are not included within the subsystem boundary. Hydrogen is produced through water electrolysis in a PEM electrolyser. Due to the low occurrence of wind curtailment over some periods of time, solar electricity from the PV array is added to improve the electrolyser capacity factor (λ_{WE}). λ_{WE} is calculated from the energy sources to run an electrolyser of size (P_{WE}) in kW_e. These sources include curtailed wind (E_{CW}), exportable wind (E_{EW}), PV (E_{PV}), electric battery (E_{EB}), as shown in Equation (6.1). The maximum possible operational time of the electrolyser (t_{WE}) is 8,760 hours, i.e. the number of hours in a year. An EMU converts wind energy from AC to DC and controls the energy flow from wind energy, solar energy and battery energy to the electrolyser and compressor as illustrated in Figure 6.1. To evaluate the impact of the PV array and battery on electrolyser productivity, the electrolyser operation is evaluated in eight scenarios as shown in Table 6.1. The techno-economic submodel of the WPBES and its sizing are described in the subsection of hydrogen production. In all scenarios, after the hydrogen is produced by the electrolyser, it is compressed to 300 barg and temporarily stored in steel storage cylinders.

$$\lambda_{WE} = \frac{E_{CW} + E_{EW} + E_{PV} + E_{EB}}{t_{WE} \cdot P_{WE}} \quad (6.1)$$

Table 6.1. The operational scenarios of the electrolyser

Scenario	Name	Energy source for electrolyser			
		Wind farm		PV array	Battery
		Curtailed electricity	Exportable electricity		
1	Curtailed wind operation	✓			
2	Curtailed wind assisted by battery operation	✓			✓
3	Curtailed wind assisted by PV array operation	✓		✓	
4	Curtailed wind assisted by PV array and battery operation	✓		✓	✓
5	Available wind operation	✓	✓		
6	Available wind assisted by battery operation	✓	✓		✓
7	Available wind assisted by PV array operation	✓	✓	✓	
8	Available wind assisted by PV array and battery operation	✓	✓	✓	✓

The second subsystem is hydrogen transportation via tube trailer hauled by diesel truck to a hypothetical bus refuelling station in the city nearest to the wind farm at which the WPBES is situated. Details on this submodel are given in the subsection of hydrogen transportation.

In the hydrogen dispensing subsystem, compressed hydrogen is transferred to a 300-barg storage tank connected to a booster compressor to meet the typical delivery pressure of 350 barg and temperature of 15 °C for FCEBs [164], [165]. The techno-economic parameters of the subsystem are further explained in the hydrogen dispensing subsection.

The techno-economic performance of the whole system and its subsystems are evaluated by calculating levelised cost of hydrogen ($LCOH$). The total $LCOH$ of fuel delivered by the HFSC ($LCOH_F$) is the sum of $LCOH$ production ($LCOH_P$), transportation ($LCOH_T$) and dispensing ($LCOH_D$) as shown in Equation (6.2). The whole system lifetime (τ) and discount rate (r) in the model are 20 years and 6%, respectively [104]. Three electricity prices are used in this study, (1) 4 euro cent per kilowatt hour (c/kWh) for curtailed electricity [110], (2) 8 c/kWh to purchase exportable wind and sell surplus solar electricity [111] and (3) 10 c/kWh for grid electricity to operate the HRS [110].

$$LCOH_F = LCOH_P + LCOH_T + LCOH_D \tag{6.2}$$

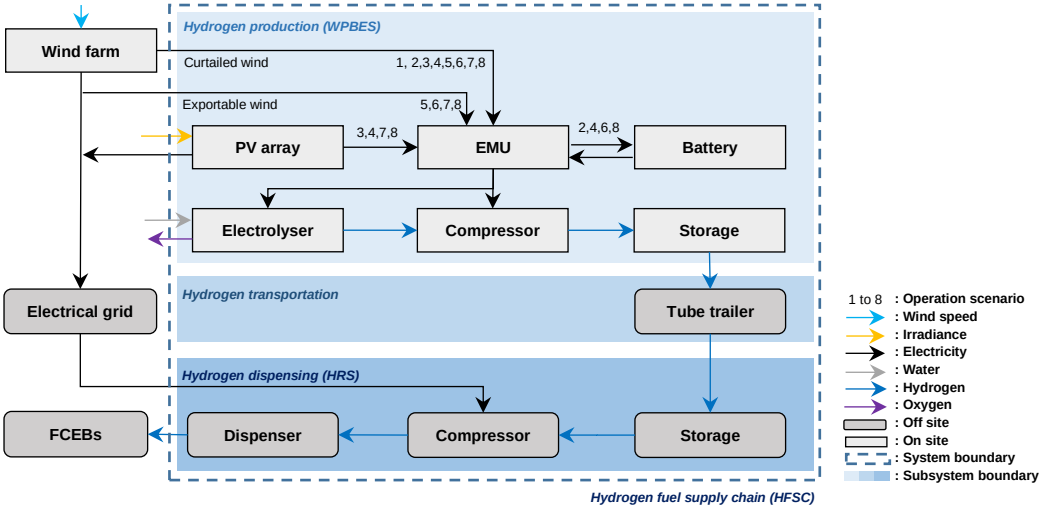

Figure 6.1. The whole hydrogen system for producing, transporting, and dispensing hydrogen fuel.

6.3.2. Hydrogen production

In the WPBES, $LCOH_P$ accounts for the discounted total present values of capital investment, operation and maintenance costs per discounted total mass of hydrogen produced, as expressed in Equation (4.2).

$$LCOH_P = \frac{\sum_{T=0}^{T=\tau_{WPBES}} \frac{C_{CAPEX,HP} + C_{OPEX,HP}}{(1+r)^T}}{\sum_{T=0}^{T=\tau_{WPBES}} \frac{M_{H2,HP}}{(1+r)^T}} \quad (6.3)$$

The capital investment ($C_{CAPEX,\ HP}$) and operation and maintenance costs of hydrogen production ($C_{OPEX,\ HP}$) are calculated by using Equation (6.4) and Equation (6.5), respectively. The techno-economic parameters for each piece of equipment are listed in Table 6.2. Installation and engineering costs are set to 20% and 15% of total capital costs of electrolyser and compressor, respectively [98]. Capital costs for electrolyser and batteries are assumed to decrease by 50% and 60% in 2030, respectively [104] [27].

$$C_{CAPEX,HP} = C_{WE} + C_{EC,HP} + C_{SV,HP} + C_{EMU} + C_{ICS,HP} + C_{ENG,HP} + C_{OH,HP} \quad (6.4)$$

$$C_{OPEX,HP} = C_{OM,WE} + C_{OM,EC,HP} + C_{OM,SV,HP} + C_{SR} + C_{EL,HP} + C_{H2O} \quad (6.5)$$

Hourly wind power data for 74 Irish wind farms larger than 10 MW_e in 2017 are obtained from the Single Electricity Market Operator website (www.lg.sem-o.com). Using this data, curtailed (P_{CW}) and exportable power (P_{EW}) are calculated using the method described by Gunawan et al. [143]. Hypothetical hourly PV outputs (P_{PV}) at each wind farm location are simulated at www.renewables.ninja. This tool was developed by Pfenninger et al. [166] using the meteorological dataset of Modern-Era Retrospective analysis for

Research and Applications 2 (MERRA-2) for 2017. The coordinates of the wind farms are required in the simulation and obtained from Sustainable Energy Authority of Ireland (SEAI) [167]. Different PV array capacities at intervals of 0.5 MW_e are modelled at each wind farm. PV system losses of 10% from cable, connection and environmental conditions, tilt angle of 35°, azimuth of 180°, and no tracking system are assumed. In the selection of battery technology, Papadopoulos et al. finds Lithium Nickel Manganese Cobalt Oxide (Lithium NMC) is better than Vanadium Redox Flow (VRF) for integration with wind and solar power [33]. Lithium NMC has higher charge and discharge rates (C-rate) and efficiency compared to VRF. Hence, Lithium NMC is able to provide larger energy than VRF in the same period of time and capacity. Detailed parameters for the battery and other equipment are listed in Table 6.2. The annual hydrogen production is calculated from the input energy to the electrolyser and its specific energy consumption as expressed in Equation (6.6) [143].

$$M_{H2,HP} = \frac{E_{WE}}{\mu_{WE}} \tag{6.6}$$

The next process is to calculate $LCOH_P$ using these data with a techno-economic model for each scenario. To size the equipment in a WPBES, the cost of EMU, compressor and storage are functions of electrolyser size [143]. $LCOH_P$ is calculated using Equation (6.3) iteratively at different equipment sizes as listed in Table 6.3. The optimum equipment sizes for each scenario are determined at the minimum $LCOH_P$. The optimum operation scenario of WPBES is selected at maximum hydrogen capacity.

Table 6.2. Techno-economic parameters of hydrogen production at wind-photovoltaic-battery-electrolyser system (WPBES)

Parameters, Symbol	**Value/ Unit/ Reference**					
Equipment	**Water Electrolyser (WE)**			**Electric Compressor (EC, HP)**		
Technology	Proton exchange membrane			Reciprocating		
Sp. energy cons., μ	55	kWh/kg	[115]	1.7	kWh/kg	[115]
Lifetime, τ	20 (system), 5 (stack)	years	[31]	10	years	[115]
Efficiency, η	61%	(LHV_{H2})	[115]	73%	(isentropic)	[46]
Outlet pressure, p	60	barg	[115]	300	barg	[141]
CAPEX, C_{CAPEX}	2498 x $P_{WE}^{0.925}$	€	[98]	4948 x $P_{WE}^{0.66}$	€	[98]
OPEX, C_{OPEX}	0.2011 $P_{WE}^{-0.23}$ x $C_{CAPEX,WE}$	€	[115]	2%	of C_{CAPEX}	[115]
Other cost, $C_{OH,HP}$	1.5652 $P_{WE}^{-0.154}$ x $C_{CAPEX,WE}$	€	[98]			
Equipment	**Photovoltaic (PV)**			**Energy management unit (EMU)**		
Technology	Polycrystalline silicon			Converter and controller		
Lifetime, τ	30	years	[42]	15	years	[42]
Efficiency, η	90%		[166]	90%		[42]
Capacity factor, λ	10 to 13%		[166]			
CAPEX, C_{CAPEX}	1400 x P_{PV}	€	[27]	10% x (C_{WE} + C_{EC})	€	[98]
OPEX, C_{OPEX}	1.5%	of C_{CAPEX}	[27]			
Equipment	**Electric Battery (EB)**			**Storage Vessel (SV, HP)**		
Technology	Lithium Nickel Manganese Cobalt Oxide			Steel cylinder		
Lifetime, τ	20	years	[33]	20	years	[98]
Efficiency, η	90%	(round)	[27]	-		
DoD	100%		[33]	-		
C-rate	1C		[33]	-		
CAPEX, C_{CAPEX}	115 x E_{EB}	€	[27]	470 x m_{H2} x 12	€	[98]
OPEX, C_{OPEX}	Not considered		[27]	2%	of C_{CAPEX}	[98]

Table 6.3. The range of equipment sizes used to calculate $LCOH_P$

Scenario	The range of equipment sizes		
	Electrolyser (MWe)	PV array (MWe)	Battery (MWh)
1	0.01 to 20		
2	0.01 to 20		1 to 20
3	0.01 to 20	0.5 to 20	
4	0.01 to 20	0.5 to 20	1 to 20
5	0.01 to 20		
6	0.01 to 20		1 to 20
7	0.01 to 20	0.5 to 20	
8	0.01 to 20	0.5 to 20	1 to 20

6.3.3. Hydrogen transportation

Hydrogen produced by WPBESs is transported to HRSs in the six main cities across the island of Ireland; Belfast in NI, and Cork, Dublin, Galway, Limerick, and Waterford in the ROI. The cost of hydrogen transportation, $LCOH_T$, is calculated using Equation (6.7).

$$LCOH_T = \frac{\sum_{T=0}^{T=\tau_{WHS}} \frac{C_{CAPEX,HT} + C_{OPEX,HT}}{(1+r)^T}}{\sum_{T=0}^{T=\tau_{WHS}} \frac{M_{H2,HT}}{(1+r)^T}} \quad (6.7)$$

The operation and maintenance costs ($C_{OPEX,HT}$) of hydrogen transportation is calculated using Equation (6.8). The capital cost of tube trailer ($C_{CAPEX,HT}$) and other techno-economic parameters of hydrogen transportation can be seen in Table 6.4.

$$C_{OPEX,HT} = \left(\dot{C}_{OPEX,TT} \times L \times \frac{365 \text{ days}}{\frac{\dot{m}_{TT}}{m_{H2,P}} \Big/ 24 \text{ hours}} \times 2 \right) + C_{R,TT} \quad (6.8)$$

Table 6.4. Techno-economic parameters of hydrogen transportation via tube trailer

Parameters	Symbol	Value	Unit	Ref.
Capacity	$\dot{m}_{TT}$	500	kg	[125]
Pressure	p_{TT}	300	barg	[125]
Fuel consumption	α_{TT}	1.77	kWh/km	[129]
CAPEX	$C_{CAPEX,\,HT}$	232,000	€	[103]
OPEX	$\dot{C}_{OPEX,\,TT}$	2.03	€/km	[103]
Retest cost	$C_{R,\,TT}$	30%xC_{TT}	€	[98]

This study uses the coordinates of (1) 312 existing onshore wind farms to locate WPBESs, (2) the road network, and (3) the six largest cities in Ireland as HRSs locations. Hydrogen at each HRS is supplied from multiple WPBESs. The distance (L) between WPBES and HRS is calculated using the *Maximise Capacitated Coverage* function [168], described below, of the location-allocation algorithm in geographic information system (GIS) to maximise hydrogen supply from WPBES and hydrogen demand at each HRS. The working principles of the algorithm are: (1) all hydrogen demand must be met, (2) each WPBES selects the most suitable HRS to supply, provided that the most of the WPBES capacity can be delivered without exceeding the selected HRS capacity, and (3) if both criteria are met by several WPBESs, the WPBES closest to the HRS is selected.

6.3.4. Hydrogen dispensing

In Ireland, there are three operators of publicly-owned bus networks (1) Dublin Bus in greater Dublin, (2) Translink in NI, and (3) Bus Éireann in the ROI outside Dublin. The number of operational public buses in each city (N_{DB}) are listed in Table 6.5. It is assumed that all the public bus fleets are equally distributed among the number of bus depots (N_{BD}) in each city. In this model, HRSs are considered to be built at each bus depot to dispense the hydrogen fuel to FCEBs. The current capacity of operational HRSs in the

world ranges from 100 to 1,000 kg/day, which is sufficient to fuel 4 to 40 buses per day. Higher capacity is expected in future following the growth of the hydrogen market [169].

Table 6.5. Number of the operational public city bus network in Ireland in 2018

City	City bus network		
	N_{DB} (Unit)	N_{BD} (Depot)	Ref.
Dublin	1,011	7	[170]
Cork	130	1	[170]
Limerick	40	1	[170]
Galway	44	1	[170]
Waterford	17	1	[170]
Belfast	296	2	[171]

As evaluated by Carr et al. [172], one of the essential parameters to optimise hydrogen dispensing cost is the number of vehicles refuelled per day, therefore providing the hydrogen demand. At high hydrogen demand, the study finds the electrolyser can be operated more frequently at low electricity price periods. Hydrogen demand is calculated by using the bus operational parameters listed in Table 6.6. FCEBs and diesel buses are determined to have the same utilisation rate and operation time. As the detailed information of current bus types of single- and double-decker is not available, all buses are assumed to be double-decker buses to evaluate maximum hydrogen demand of each HRS. The operation time of each bus (O_T) is limited to 358 days per year, to account for public holidays and maintenance. The hypothetical number of FCEBs in each city is set equal to the number of operational diesel buses. The number of HRSs in each city is set equal to N_{BD}.

In the calculation of hydrogen dispensing cost at each HRS, $LCOH_D$ represents the discounted total present value of the capital investment, operation, and maintenance costs per discounted total mass of hydrogen dispensed at the HRS as shown in Equation (6.9).

$$LCOH_D = \frac{\sum_{T=0}^{T=\tau_{WHS}} \frac{C_{CAPEX,HD} + C_{OPEX,HD}}{(1+r)^T}}{\sum_{T=0}^{T=\tau_{WHS}} \frac{M_{H2,HD}}{(1+r)^T}} \quad (6.9)$$

Table 6.6. Techno-economic parameters of a diesel bus and fuel cell electric bus in the evaluation

	Diesel bus (DB)			Hydrogen bus (FCEB)		
Technical parameters						
Fuel consumption, *f*	2	km/litre	[158]	10	km/kg	[173]
Utilisation rate, O_D	250	km/day/bus	[158]	250	km/day/bus	[158]
Lifetime, *τ*	10	years	[158]	10	years	[174]
Fuel cell power, *P*				150	kW_e	[175]
Tank capacity, *m*				50	kg	[164]
Tank pressure, *p*				350	barg	[164]
Economic parameters						
CAPEX, *C*	250,000	€/unit	[176]	400,000	€/unit	[157]
OPEX, *Ċ*	0.26	€/km	[176]	0.40	€/km	[175]
Stack replacement, *C*	-			60,000	€/ 3 years	[157]

The capital investment ($C_{CAPEX,HT}$) and operation and maintenance costs ($C_{OPEX,HT}$) of each HRS are expressed in Equation (6.10) and Equation (6.11), respectively. The techno-economic parameters of each component are listed in Table 6.7. The costs of installation, engineering and other systems are 40%, 15% and 50% of total installed equipment, respectively [46], [177]. Dispensers and compressors can have greater cost reduction potential; up to 60% of the current cost by 2030 [47].

$$C_{CAPEX,HD} = C_{SV,HD} + C_{EC,HD} + C_{DU} + C_{ICS,HD} + C_{ENG,HD} + C_{OT,HD} \quad (6.10)$$

$$C_{OPEX,HD} = C_{OM,SV,HD} + C_{OM,EC,HD} + C_{OM,DU} + C_{EL,HD} \quad (6.11)$$

A study by Grüger et al. [51] emphasizes the importance of demand profile to optimise the size of an HRS for FCEV. The current study uses the hourly demand profile of bus refuelling, as illustrated in Figure 6.2. Bus refuelling mostly occurs during the night as most of bus operational hours are during the day.

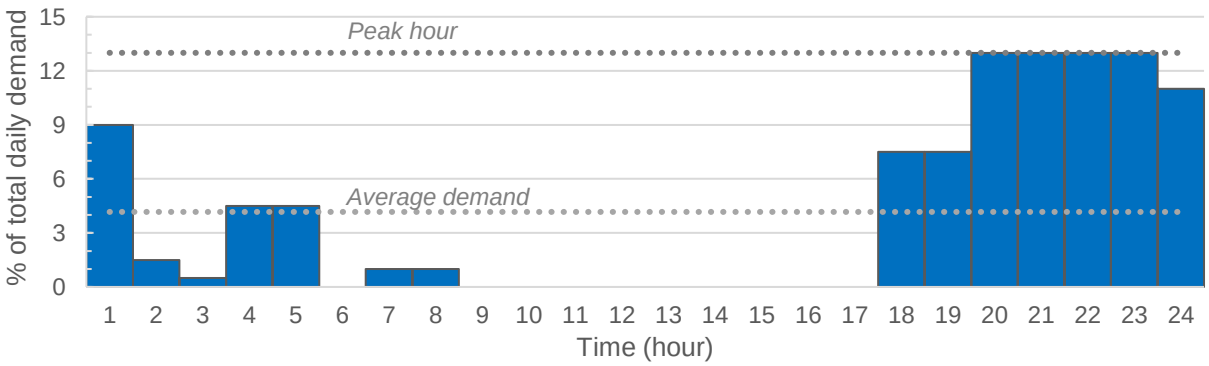

Figure 6.2. The daily bus refuelling profile in Europe [178]

The total number of dispensers at each HRS($N_{DU,HRS}$) is then calculated using Equation (6.12). This study considers two hoses attached to each dispenser. The total number of required hoses (N_H) is calculated using Equation (6.13).

$$N_{DU,HRS} = \frac{N_H}{2} \Big/ N_{HRS} \quad (6.12)$$

$$N_H = \frac{H_A}{60 \text{ minutes}} \quad (6.13)$$

An inadequate number of hoses during peak hour is avoided using hose occupation fraction (HOF) that is set at 50% [47]. The flow rate of the hose is 2 kg per minute [85],

which is categorised as the normal fuelling rate in the SAE J2601/2 fuelling protocol for gaseous hydrogen powered heavy duty vehicles [179]. The total time of available hoses (H_A) is calculated using HOF and the total time of occupied hoses (H_O) as shown in Equation (6.14).

$$H_A = \frac{H_O}{HOF} \tag{6.14}$$

Equation (6.15) shows how H_O is calculated from the average filling capacity of 25 kg per refuelling ($\dot{m}_{FP}$) [43], 12.5 minutes of the filling time (t'_{FP}), 3 minutes of the lingering time between continuous FCEB fills (t'_{LP}) [47], hydrogen daily demand per HRS ($\dot{M}_{H2,D}$), and peak hour fraction (X_{PH}). Annual hydrogen capacity at each HRS is calculated using Equation (6.16).

$$H_O = \frac{\left(\dot{M}_{H2,HD} \times X_{PH}\right)}{\dot{m}_{FP}} \times \left(t'_{FP} + t'_{LP}\right) \tag{6.15}$$

$$M_{H2,HD} = \frac{O_{D,FCEB} \times T_{FCEB} \times N_{FCEB}}{f_{FCEB}} \Big/ N_{HRS} \tag{6.16}$$

The required size of the compressor (P_{EC}) can be calculated using Equation (6.17). In this model, the compressibility factor (Z), specific heat ratio (k), specific heat of hydrogen (Cp_{H2}), gas constant (R) are 1.2, 1.41, 14.7 kJ/kg°K, and 8.314 J/°K·mol, respectively [180]. The compressor size is multiplied by operation time to obtain the required electrical energy.

$$P_{EC} = Z \times m'_{H2,HD} \times R \times K_{AMB} \times N_{CS} \times \frac{1}{\eta_{EC}} \times \frac{k}{k-1} \times \left[\left(\frac{p_{out}}{p_{in}} \right)^{\frac{k-1}{N_{CS} \times k}} - 1 \right] \quad (6.17)$$

Table 6.7. Techno-economic parameters of hydrogen dispensing at the hydrogen refuelling station (HRS)

Parameters, symbol	**Value/ Unit/ Ref.**					
Equipment	**Dispenser unit (DU)**			**Electrical compressor (EC, HD)**		
Technology	Hydrogen dispenser			Reciprocating		
Lifetime, τ	10	years	[42]	10	years	[115]
Efficiency, η				73%	(isentropic)	[46]
Stages, N_{SC}				2	stages	[47]
Pressure, p	350	barg	[177]	350	barg	[47]
Flow rate, m''_{H2}	2	kg/min	[85]			
Dispensing temp., K_{DU}	233	K	[177]			
CAPEX, C_{CAPEX}	67,595	€	[177]	17670 x $P_{EC}^{0.6089}$	€	[47]
OPEX, C_{OPEX}	2%	of C_{CAPEX}	[46]	2%	of C_{CAPEX}	[47]
Equipment	**Storage vessel (SV, HD)**					
Technology	Steel vessel					
Lifetime, τ	20	years	[98]			
Working pressure, p	300	barg	[98]			
CAPEX, C_{CAPEX}	470 x $\dot{M}_{H2}$	€	[98]			
OPEX, C_{OPEX}	2%	of C_{CAPEX}	[46]			

6.3.5. Overall algorithm

The HFSC consists of hydrogen production, transportation and dispensing subsystems. $LCOH_F$ is used as the key parameter to evaluate the techno-economic performance of the HFSC. $LCOH_F$ is the summary of $LCOH_P$, $LCOH_T$, and $LCOH_D$. In sizing equipment for the WPBES, the equipment costs are set to be the functions of the electrolyser size. $LCOH_P$ is iteratively calculated by using different sizes of electrolyser, photovoltaic and battery. The minimum $LCOH_P$ indicates the optimum equipment sizes, where the maximum hydrogen capacity means the optimum operation scenario. In the hydrogen transportation subsystem, a location-allocation algorithm in GIS is used to identify

suitable hydrogen distribution network as well as the distance between WPBES and HRS. In the hydrogen dispensing subsystem, the HRS is sized by hydrogen demand of FCEBs.

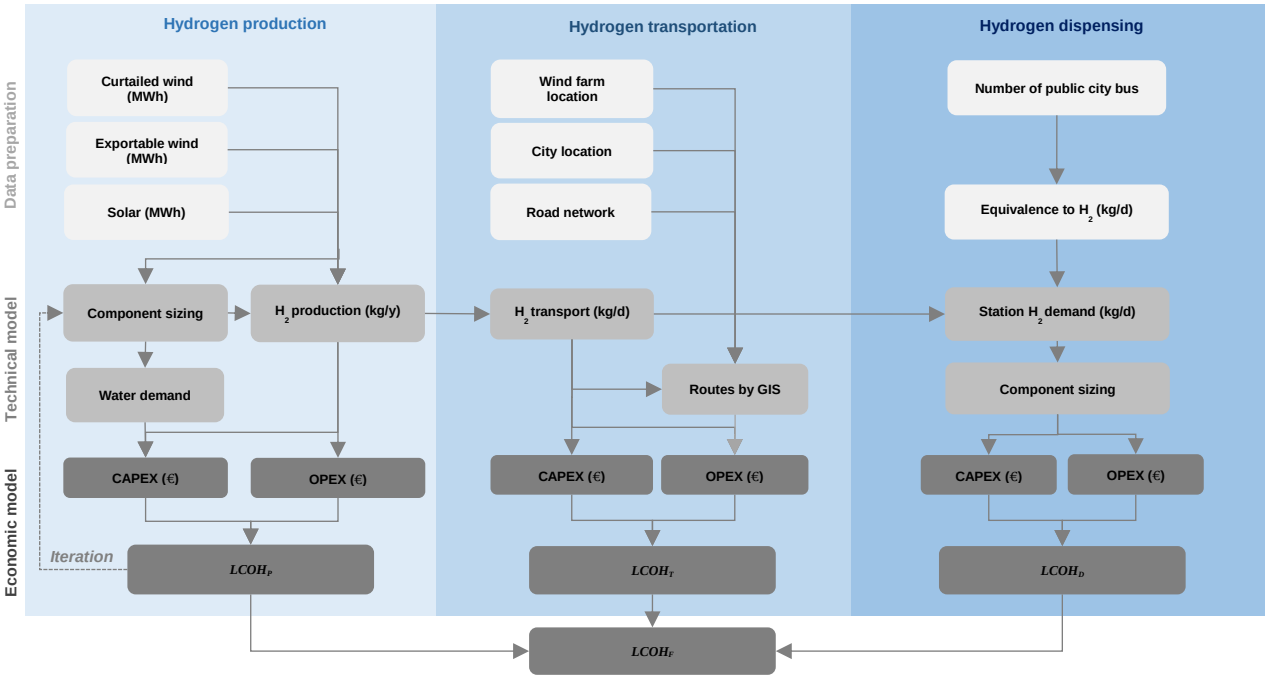

Figure 6.3. Block diagram to calculate levelised cost of hydrogen fuel from hydrogen fuel supply chain ($LCOH_F$)

6.4. Results and discussion

6.4.1. Hydrogen production from optimum equipment size

Figure 6.4 shows the three-day operation scenarios of 3-MW_e electrolyser at a sample Irish wind farm, the 15-MW_e Tursillagh wind farm, which had 8,613 MWh of wind curtailment in 2017.Figure 6.4.b, 4.d, 4.f, and 4.h show the use of additional 3-MWh battery to capture the surplus renewable power limited by electrolyser size. Figure 6.4.c, 4.d, 4.g, and 4.h show the additional 3.5-MW_e PV improves the electrolyser productivity during the unavailable or low wind power. The total capacity factor for scenario 8 is 51%.

The total annual contribution of curtailed wind, exportable wind, PV and battery are 43%, 36%, 16%, and 5%, respectively. The hourly cumulative energy from each source is depicted in Figure 6.5.

Figure 6.6 shows the techno-economic results of all scenarios to operate a hydrogen production system at the same sample wind farm. As shown in Figure 6.6.a and Figure 6.6.b, either by adding a 10-MWh battery to a 1.5-MW_e electrolyser, or a 5-MW_e PV array to a 2.5-MW_e-electrolyser, minimum $LCOH_P$ reduces from 29 to 13-14 €/kg. As illustrated in Figure 6.6.c, a combination of a 6-MWh battery and 5.5-MW_e PV array further decreases minimum $LCOH_P$ to 12 €/kg for a 2.5-MW_e electrolyser. This occurs due to a higher electrolyser capacity factor of 45% for scenario 4, compared to 27-41% for scenarios 1-3. The capacity of hydrogen production for all scenarios are listed in Table 6.8. Supplying the electrolyser with exportable wind energy further decreases the minimum $LCOH_P$ from 14 to 10 €/kg, due to the increase of hydrogen production from a more productive electrolyser. As shown in Figure 6.6.d and Figure 6.6.e, either by adding a 5-MWh battery, a 5-MW_e PV array, or a combination of a 3-MWh battery and a 3.5-MW_e PV array to a 3-MW_e-electrolyser, minimum $LCOH_P$ rises by less than 1 €/kg, but provides more hydrogen capacity.

In curtailed wind operation, 65 tonnes of hydrogen is produced annually in scenario 1. This capacity increases by 20% in scenario 2. In scenario 3, the capacity is double compared to scenario 1. The combination of optimum battery and PV array sizes at scenario 4 results in larger capacity, which nearly triples the capacity of scenario 1. In available wind operation, the capacity of hydrogen in scenario 5 is 112 tonnes per year (t/y). This capacity increases by 62% in scenario 6. There is no significant difference between capacities in scenario 5 and 7. Scenario 8 has the largest hydrogen capacity of 248 t/y.

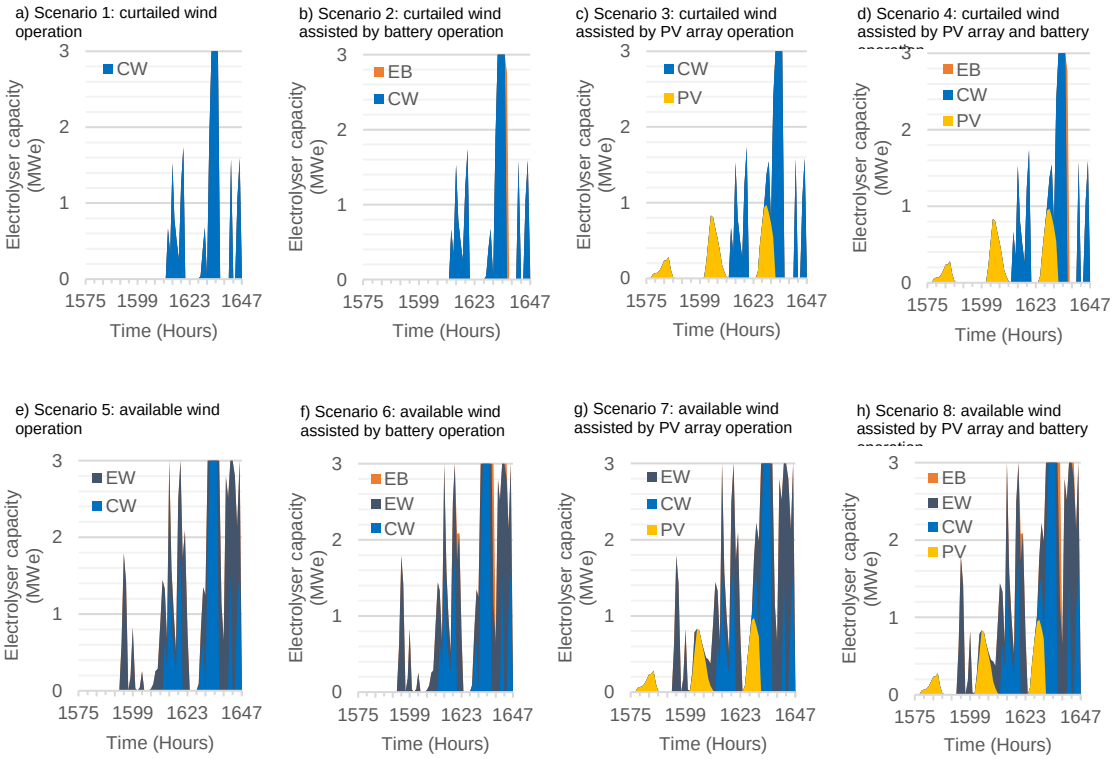

Figure 6.4. Operational of the electrolyser for (a) scenario 1, (b) scenario 2, (c) scenario 3, (d) scenario 4, (e) scenario 5, (f) scenario 6, (g) scenario 7, and (h) scenario 8 at Tursillagh wind farm

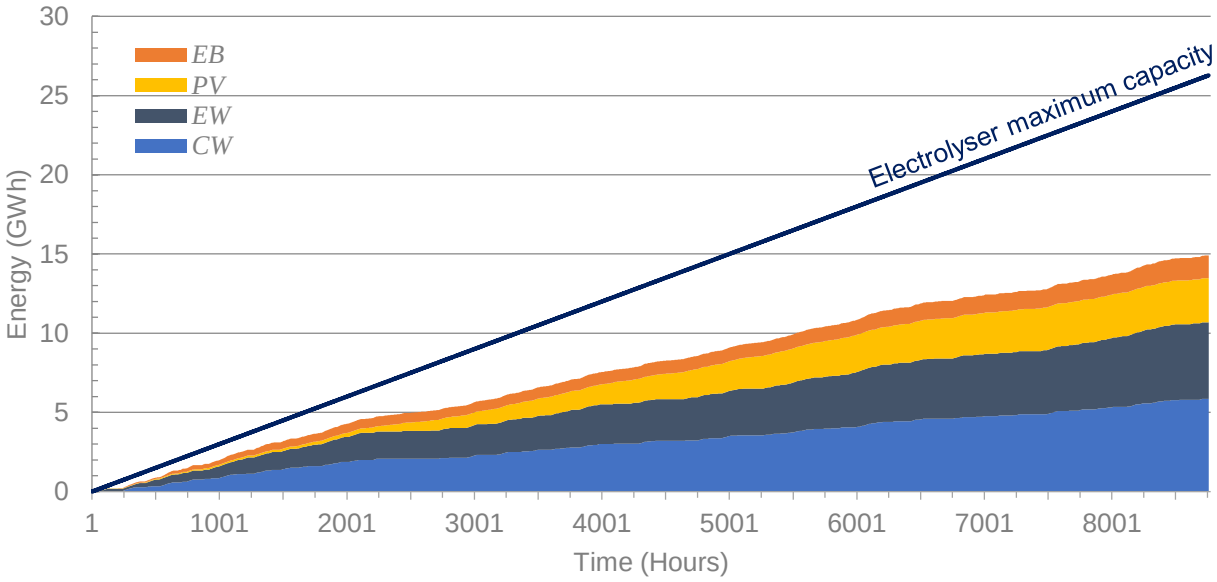

Figure 6.5. Cumulative energy profile to the electrolyser at Tursillagh wind farm in scenario 8

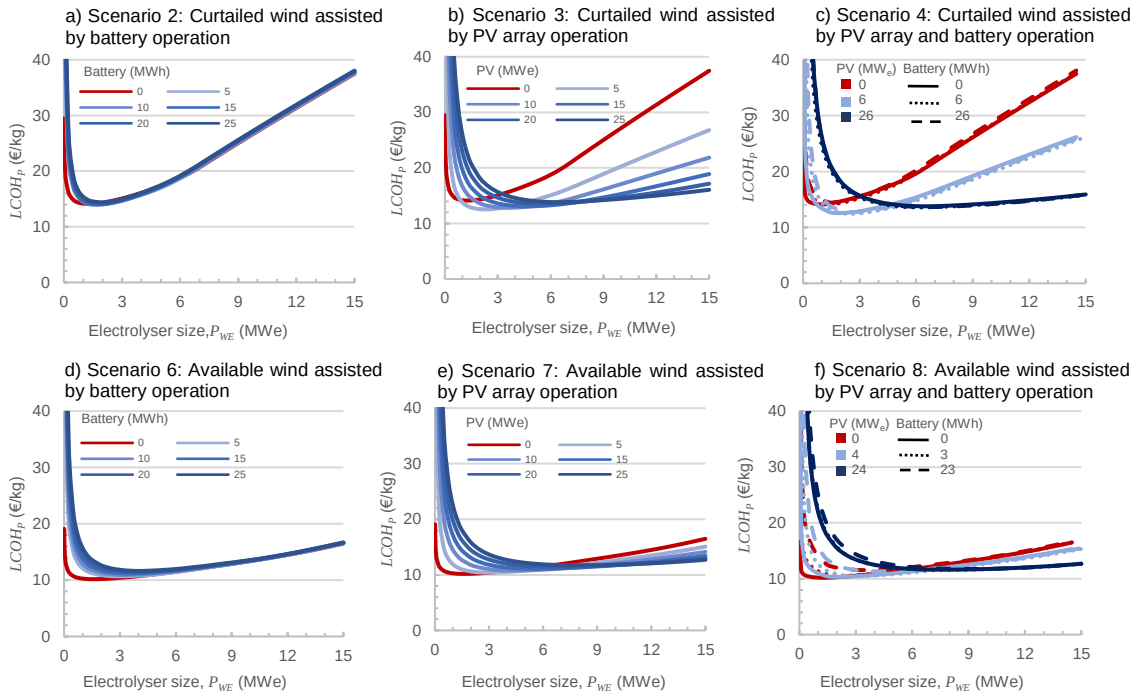

Figure 6.6. The impact of curtailed wind operation on $LCOH_P$ of (a, scenario 2) battery sizing, (b, scenario 3) PV array sizing, and (c, scenario 4) battery and PV array sizing. The impact of available wind operation on $LCOH_P$ of (d, scenario 6) battery sizing, (e, scenario 7) PV array sizing, and (f, scenario 8) battery and PV array sizing

Table 6.8. Optimum equipment sizes for each scenario at Tursillagh wind farm

	Unit	Operation scenario							
		1	2	3	4	5	6	7	8
$LCOH_P$	€/kg	14.16	13.99	12.47	12.32	10.17	10.53	10.20	10.47
Electrolyser capacity factor	%	27%	33%	41%	45%	46%	45%	48%	51%
Optimum electrolyser	MW_e	1.5	1.5	2.0	2.5	1.5	2.5	1.5	3
Optimum battery	MWh	-	10	-	6	-	3	-	3
Optimum photovoltaic	MW_e	-	-	4	5.5	-	-	0.5	3.5
Hydrogen production	t/y	65	78	132	180	112	181	117	248

The optimum equipment sizes of WPBESs that minimise $LCOH_P$ for all large (>10 MW_e) wind farms in Ireland are shown in Figure 6.7. The ratio of optimum electrolyser capacity to wind farm capacity as a function of curtailment volume for curtailed and available wind operation are shown in Figure 6.7.a and Figure 6.7.d, respectively. The different capacities of batteries at curtailed and available wind operation are shown in Figure 6.7.b

and Figure 6.7.e, respectively. Since the output of the PV array depends on the WPBESs' locations, the optimum PV size varies widely, as illustrated in Figure 6.7.c. However, WPBESs require smaller PV sizes when the system operates with available wind, as can be seen in Figure 6.7.f.

The maximum, average and minimum capacity factor for all large wind farms are 73%, 64% and 42%, respectively. The average of $LCOH_p$ for scenario 8 at all the WPBESs by using the current and future techno-economic parameters are 9 €/kg and 5 €/kg, respectively.

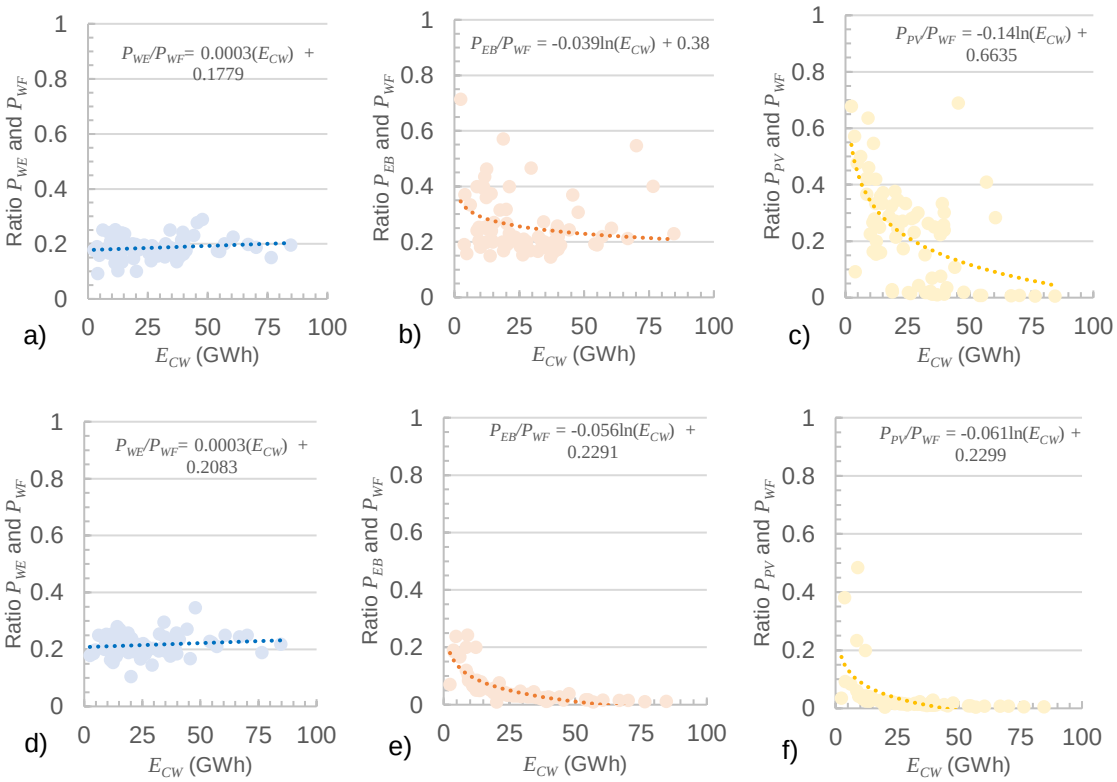

Figure 6.7. The optimum sizes of equipment at curtailed wind operation (scenario 4) for large wind farms are shown by (a) ratio of P_{WE} and P_{WF}, (b) ratio of P_{EB} and P_{WF}, (c) ratio of P_{PV} and P_{WF}. The optimum sizes of equipment at available wind operation (scenario 8) for large wind farms are shown by (d) ratio of P_{WE} and P_{WF}, (e) ratio of P_{EB} and P_{WF}, (f) ratio of P_{PV} and P_{WF}.

6.4.2. Hydrogen transportation and supply network

One tube trailer is used for a WPBES with average hydrogen production of less than 50 kg/hour. While the tube trailer is in transit, on-site hydrogen storage can be used at the WPBES. This can reduce the $LCOH_T$ for small WPBESs. At least two tube trailers are used for WPBES with the capacities larger than 50 kg/hour. More tube trailers are necessary when the trip time is longer than the filling time. Trip time includes travel time between WPBES and HRS for round-trip and the assumption of two hours for discharge time and other extra time at the HRS. Figure 6.8 illustrates the three-day operation stages of 3 tube trailers operated at Golagh wind farm and its hydrogen filling level at each tube trailer. These tube trailers consecutively deliver hydrogen over 164 km to Belfast. By using an average truck speed of 50 km/hour [103], the trip time is around 9 hours per tube trailer.

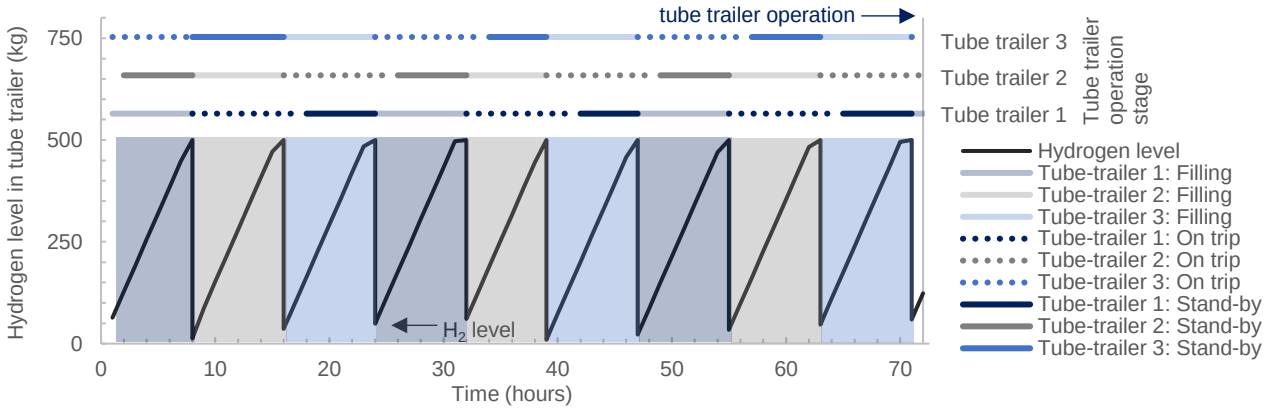

Figure 6.8. The operation of tube trailers over time at sample WPBES

Figure 6.9 shows the hydrogen supply network of distributed WPBESs to meet fuel demand for public bus networks in the six largest cities across Ireland. For clarity, the exact road routes of hydrogen transportation are not shown, but the straight lines indicate which WPBESs are allocated to each HRS. The total hydrogen demand of 13.7 kilotonnes per year can be supplied by 130 WPBESs in curtailed wind operation, and 104 WPBESs in available wind operation. The essential parameters in hydrogen

transport are the distance between WPBES and HRS, and daily transported hydrogen capacity, as illustrated in Figure 6.10. Shorter distance and more frequent daily hydrogen transportation reduces $LCOH_T$.

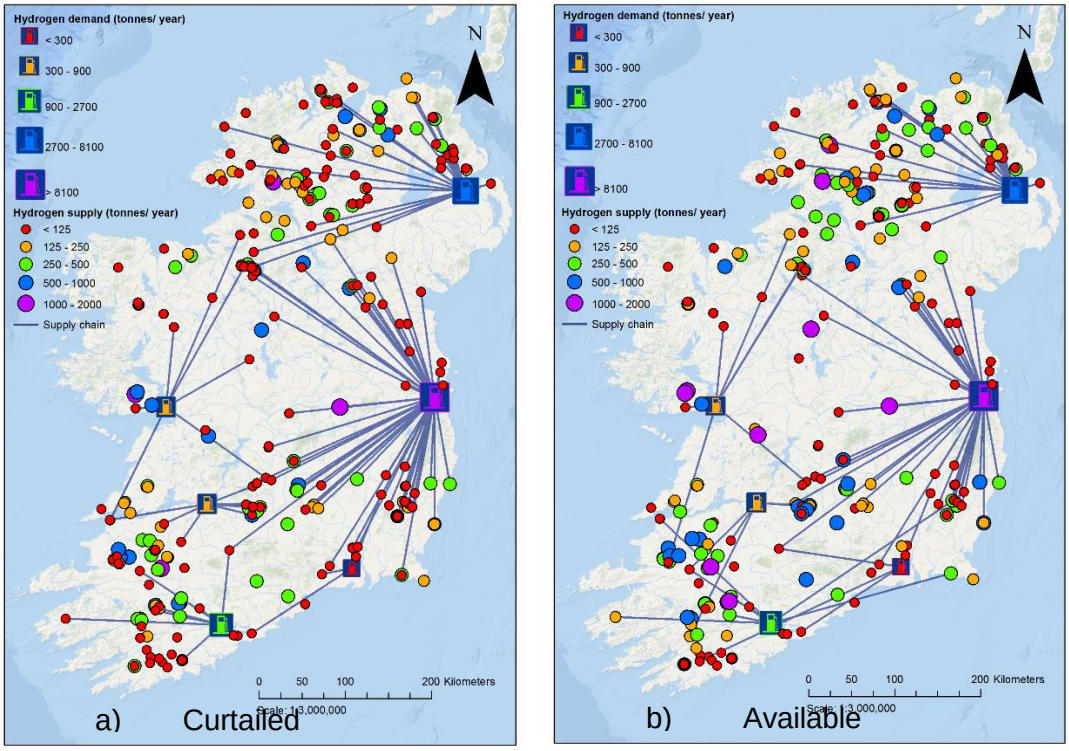

Figure 6.9. Hydrogen fuel supply chain: a) WPBES at curtailed wind operation, and (b) WPBES at available wind operation

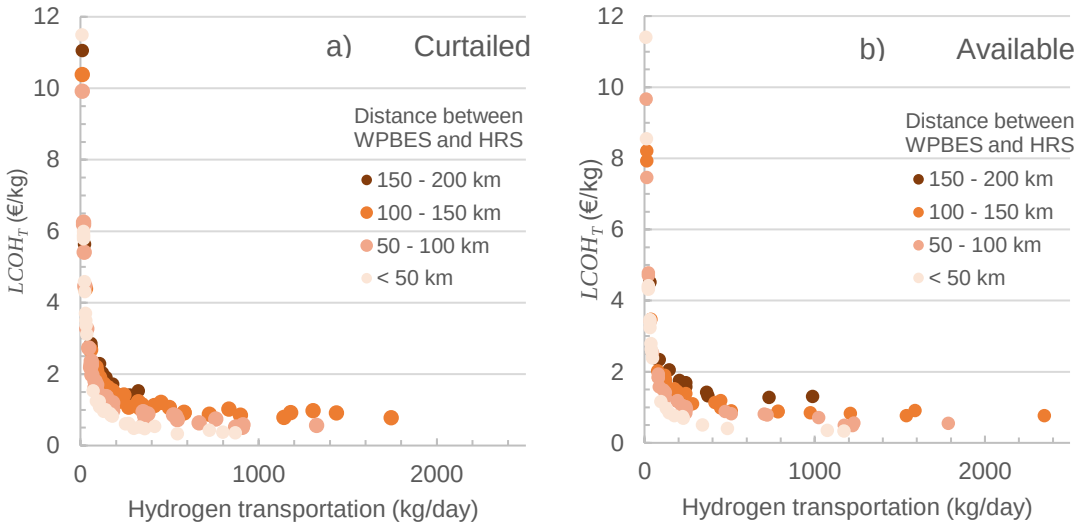

Figure 6.10. Distribution of hydrogen transportation capacity across all existing Irish onshore wind farms

6.4.3. Hydrogen dispensing and bus operational cost

Figure 6.11 shows the $LCOH_D$ of HRSs in Belfast, Cork, Dublin, Galway, Limerick, and Waterford. $LCOH_D$ varies from 2 to 4 €/kg. Based on the number of bus depots and operational public bus fleets in each major city, HRS capacity across Ireland range from 500 to 4,500 kg/day. The larger hydrogen capacity of the HRS, the lower the unit cost to distribute hydrogen fuel for FCEBs.

The $LCOH_F$ and decarbonisation potential can be seen in Figure 6.12. To decarbonise entire public bus fleets in the evaluated cities, $LCOH_F$ of curtailed operation are in the range of 11 to 22 €/kg using current techno-economic parameters (solid lines), and 7 to 15 €/kg using future parameters (dashed lines), in Figure 6.12.a. When the WPBES also use exportable electricity in available wind operation, $LCOH_F$ for current and future parameters are 8 to 17 €/kg and 5 to 10 €/kg, respectively, as shown in Figure 6.12.b.

$LCOH_F$ represents the minimum evaluated cost of hydrogen under certain scenarios. Using this value, the comparison between operational costs of FCEBs and diesel buses is shown in Figure 6.13. The operational cost of diesel buses is shown for carbon taxes from 27 to 320 €/tonnes of CO_2. The operational cost of public buses with current and future techno-economic parameters for curtailed and available wind operations are shown in Figure 6.13.a and Figure 6.13.b, respectively. The range of operational cost using curtailed wind operation and current parameters across evaluated cities is between 3.4 and 3.7 €/km. When future parameters are considered, the operational cost decreases by 27%. When WPBES is operated by using available wind, the current average operational cost is 2.8 €/km or nearly 50% higher than current operational cost of diesel bus with carbon tax of 27 €/tonnes of CO_2. In the future, operational cost of FCEBs fuelled by renewable hydrogen from WPBESs using available wind is 2% to 32% higher than diesel bus.

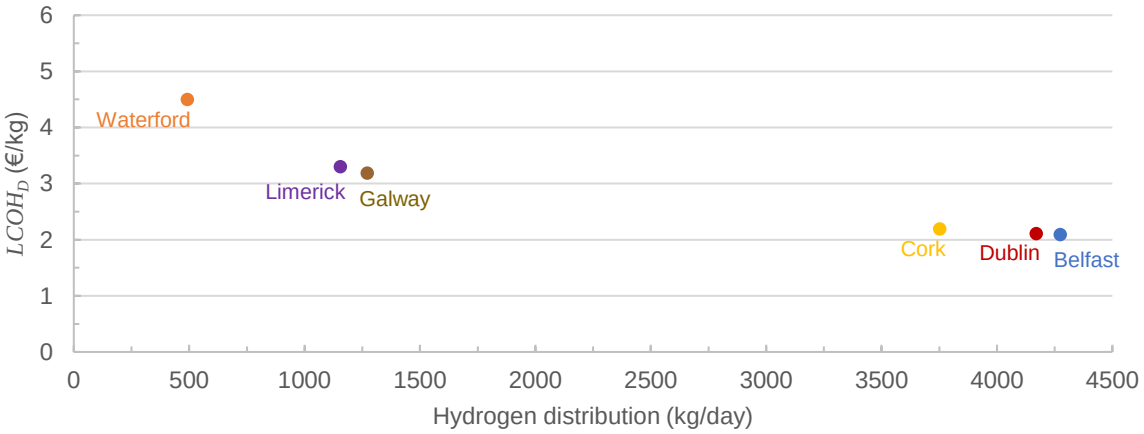

Figure 6.11. Distribution of hydrogen dispensing capacities and costs across Irish cities

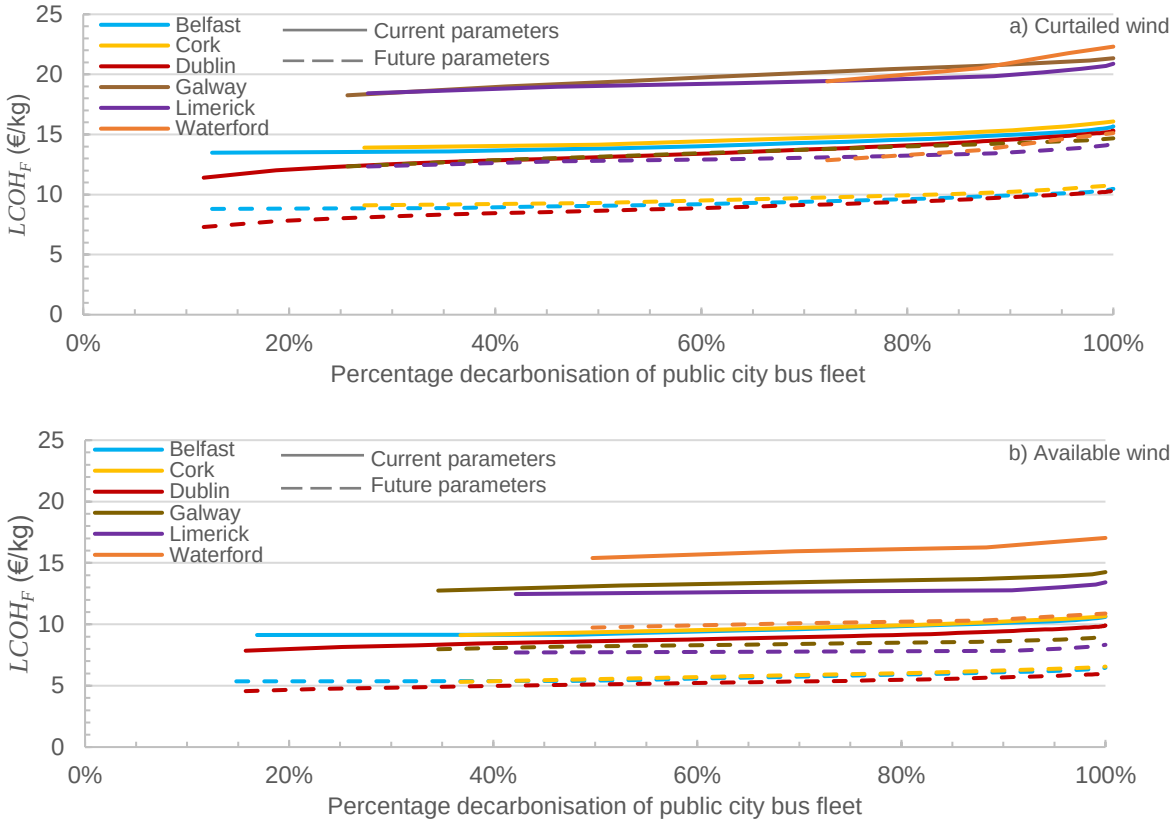

Figure 6.12. The potential percentage decarbonisation of public city bus fleets using (a) curtailed and (b) available wind operation using current (solid lines) and future (dashed lines) techno-economic parameters

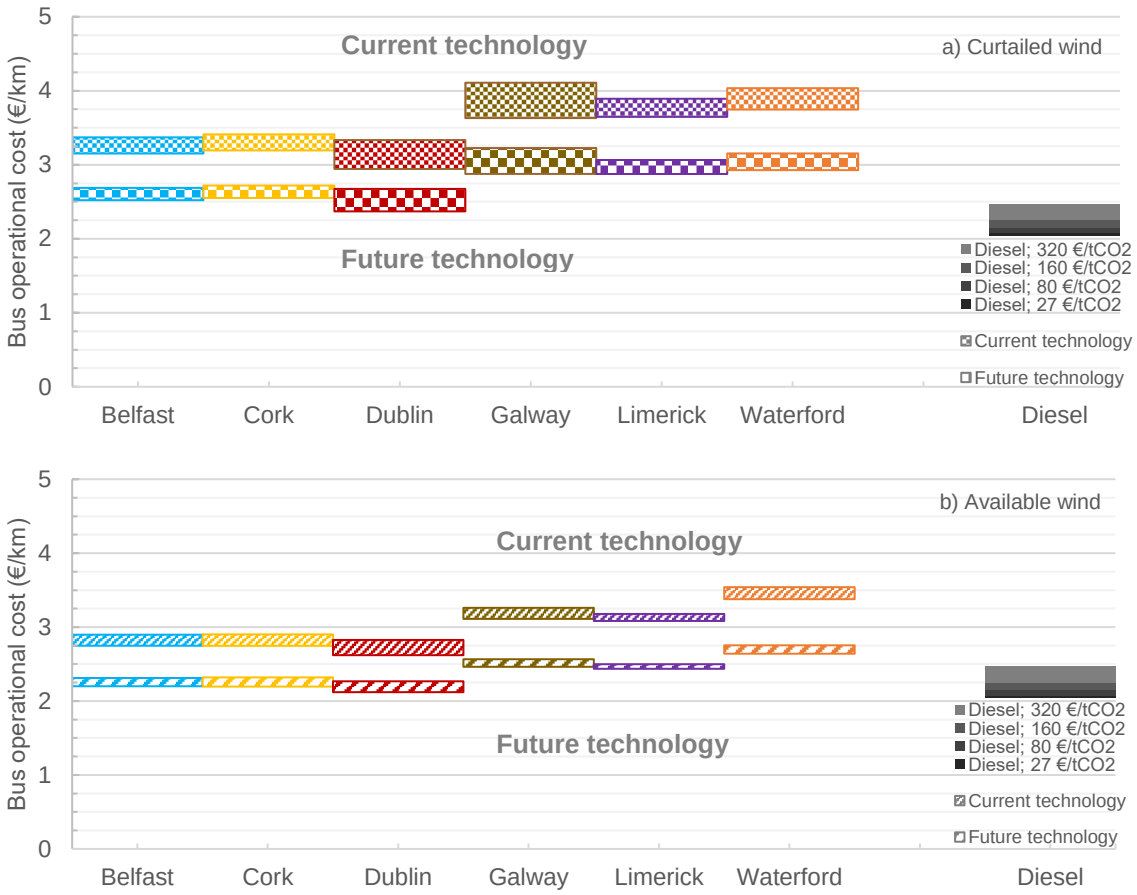

Figure 6.13. Hydrogen bus operational costs (€/km) for each city using current and future techno-economic parameters under (a) curtailed and (b) available wind operation, compared to conventional diesel buses with various diesel carbon taxes

6.5. Conclusions

This chapter models a hydrogen fuel supply chain (HFSC) for the island of Ireland that consists of hydrogen production, transportation, and dispensing subsystems. The levelised cost of hydrogen fuel ($LCOH_F$) of the HFSC is used to evaluate the techno-economic performance of the system. $LCOH_F$ is the sum of levelised costs of hydrogen production ($LCOH_P$), transportation ($LCOH_T$), and dispensing ($LCOH_D$). In the hydrogen production subsystem, $LCOH_P$ of the wind-photovoltaic-battery-electrolyser system (WPBES) is iteratively calculated at different sizes of electrolyser, photovoltaic array, and battery. The optimum equipment sizes are indicated by the minimum $LCOH_P$. In the

hydrogen transportation subsystem, a location-allocation algorithm in a geographic information system (GIS) environment is applied to allocate hydrogen distribution from each WPBES to the most suitable HRS. In the hydrogen dispensing subsystem, hydrogen refuelling stations (HRS) are sized by hydrogen demand of fuel cell electric buses (FCEBs) in the major cities of Belfast, Cork, Dublin, Galway, Limerick, and Waterford. By using $LCOH_F$, operational costs of hydrogen-fuelled public buses throughout the largest Irish cities are evaluated and compared to existing diesel-fuelled buses.

Results show the addition of lithium-ion batteries and PV arrays can produce 100% green hydrogen at the average $LCOH_F$ of 15 €/kg for the available wind operation. The integration of wind electricity with solar electricity and battery usage increases the productivity of the electrolyser, compared to using only wind electricity. PV outputs improve power input to electrolyser in the absence of wind electricity. Batteries optimise the overall performance due to its flexibility to store PV outputs and the surplus of curtailed wind when WPBES is limited by electrolyser size. If future techno-economic parameters are considered, the $LCOH_F$ even reduces to the range of 5 and 10 €/kg for the available wind operation. By using the available wind operation, the bus operational cost parity between diesel and hydrogen fuelled city buses can be achieved by 2030 in Dublin. The hydrogen fuel demand of public bus networks in all evaluated cities can be met by hydrogen produced using curtailed or available electricity produced at Irish wind farms. However, with current techno-economic parameters, the hydrogen produced by WPBES operated with curtailed or available wind is not yet competitive with existing diesel-fuelled bus fleets. The competitiveness of renewable hydrogen from WPBES improves with forecast improvements in the techno-economics parameters of key pieces of equipment. Therefore, more supportive policies, incentives, and projects are necessary to stimulate further research to reduce capital and operating costs of

production, transportation, and distribution of hydrogen and the operation of hydrogen-fuelled buses.

In reviewing the cost-reduction potential, oxygen as a by-product of the water electrolysis process may also be evaluated for utilisation and value for multiple purposes in a future study. HRSs equipped with PV arrays, batteries and/or fuel cells can also be evaluated to reduce carbon emissions from the operation of HRS. Due to large hydrogen capacity at available wind operations exceeding the hydrogen demand of the public bus network, new potential hydrogen demands require further investigation and evaluation in the future. The potential of regional or centralised hydrogen production system is also necessary to be explored and evaluated.

6.6. Final remarks

This chapter presents the results of techno-economic modelling of hydrogen production, transportation and dispensing from an integrated wind and solar electricity generation system supported by batteries. A location-allocation algorithm in a Geographic Information System (GIS) environment is applied to design hydrogen distribution chains between supply and demand sites. In addition, this chapter describes a method of sizing hydrogen refuelling stations (HRSs) that uses the theoretical hydrogen demand equivalent to the energy demanded by the current number of public buses operating in the largest cities in Ireland.

In Chapter 7, this integrated techno-economic modelling approach is applied to a much larger region; Northwest Europe. Like Chapter 6, hydrogen can also be sourced from the existing wind farms in the region and integrated with additional PV arrays and battery systems to increase the hydrogen supply capacity as well as drive cost reduction.

Chapter 7. Renewable Hydrogen Supply Chains for City Bus Networks across Northwest Europe

7.1. Overview

This chapter presents the results of techno-economic modelling of the renewable hydrogen supply from existing wind farms across northwest Europe (NWE) to fuel bus fleets in the region's largest cities. Hydrogen production at the wind farms is augmented with hypothetical photovoltaic (PV) arrays and batteries. The region of NWE is used as a case study of transnational renewable hydrogen supply chains. The model includes evaluation of the deployment potential of hydrogen-fuelled city buses throughout the 37 main cities across NWE and the possibility of hydrogen supply from 4,252 wind farms in the region. The electrolyser operation scenarios included in the model are (1) curtailed wind operation with high electricity price, (2) curtailed wind with low electricity price, (3) full time operation with high electricity price, (4) full time operation with low electricity price, (5) curtailed wind operation combined with solar with high electricity price, (6) curtailed wind operation combined with solar with low electricity price, (7) renewable intensification with additional PV electricity with high electricity price, and (8) renewable intensification with additional PV electricity with low electricity price. The levelised cost

of hydrogen fuel ($LCOH$) is used to evaluate the minimum delivered cost of hydrogen and calculate the bus operational costs. The minimum LCOH is found for the optimum equipment sizes to produce hydrogen. For hydrogen transportation, the closest facility algorithm in a geographic information system (GIS) environment is applied to allocate hydrogen distribution from each hydrogen production site (existing wind farm) to the most suitable hypothetical hydrogen refuelling system (HRS) in a large city. The operational costs of hydrogen-fuelled city buses are individually calculated for each major city in NWE using $LCOH$. They are compared to models for existing operational costs for diesel-fuelled city buses. Results show that additional lithium-ion batteries and PV arrays to the existing wind farms in NWE can produce 100% green hydrogen and meet the fuel demand for most major cities in the region. The operational costs of hydrogen-fuelled city buses are calculated to be 25% higher than current conventional diesel-fuelled buses when the electrolyser is operated at full capacity and electricity price is assumed to be low. The full results can also be accessed online at the Decision Support Tool (DST) at the webpage of the Community Hydrogen Forum http://communityh2.eu/dst/. This site was established under the GenComm project for public engagement with investors, academics, communities, and the public.

7.2. Introduction

As already mentioned in Chapter 6, European cities are beginning to impose diesel vehicle bans. In other words, current conventional diesel bus fleets must be replaced with zero-emissions alternatives in a number of European cities. Hydrogen buses have the potential to replace diesel buses due to their relatively high technological readiness and similar refuelling times with diesel, as already described in Chapter 6. According to Eudy et al. [175], the technology readiness level (TRL) of Fuel Cell Electric Bus (FCEB) reached a TRL of 7 in 2016, meaning that prototypes have been operated in actual

operational environments and they are moving towards full commercialisation. Buses powered by hydrogen fuel cells are a potential solution to greenhouse gas emissions and air quality problems in NWE cities. City buses are an ideal end-user of renewable hydrogen due to the significant and predictable fuel demands, the relatively small numbers of fuel buyers necessary to have impact, and the fact that buses are refuelled in centralised depots. A small numbers of city bus operators adopting hydrogen would substantially impact the overall hydrogen demand in NWE.

By its nature, renewable energy resources are distributed across NWE. However, not all of the available renewable electricity can be transferred to the grid. The technical challenges of operating electricity grids with high levels of variable renewable energy lead to surplus renewable electricity. This curtailed electricity can be converted via electrolysis to hydrogen and then used for transport, heating, or stored for future power generation. This study demonstrates hydrogen's potential for fuelling the city bus fleets.

The objectives of this chapter are (1) to model the hydrogen production capacity and its costs from wind, solar, and grid electricity at each NWE's wind farm, and (2) to model the hydrogen demand from FCEBs across major cities in NWE as well as the hydrogen supply sources

7.3. Methodology

7.3.1. Systems and scenarios

Figure 7.1 shows the renewable hydrogen supply chain that is integrated with the road networks, locations of major cities and wind farms, and the supply and demand quantities and costs. The region of Northwest Europe (NWE) is used as a case study of

transnational scale. Wind farm capacities and locations in Ireland, the United Kingdom, France, Belgium, the Netherlands, and Germany are presented in the following subsection of renewable electricity in Northwest Europe. This section also explains how to model hydrogen production capacity and costs. The techno-economic evaluation of hydrogen production is performed for eight scenarios, as listed in Table 7.1. Hydrogen production can be powered by curtailed wind electricity only, or with curtailed, exportable and grid electricity to maximise electrolyser productivity. In addition, electricity stored by hypothetical batteries is also added in some scenarios. Moreover, the contribution of renewable in hydrogen production can be increased by adding hypothetical collocated photovoltaic arrays, referred as renewable intensification in two scenarios. Two electricity prices are also used to understand the limits of hydrogen production costs. The electricity prices of 4 and 8 c/kWh are used as low and high electricity prices, respectively [111], [112]. The evaluated major cities are described in major cities in Section 7.3.4. That section also explains how to model hydrogen demand from public city buses operated in major cities across NWE. Finally, the use of road networks in a Geographic Information System environment is explained in Section 7.3.5.

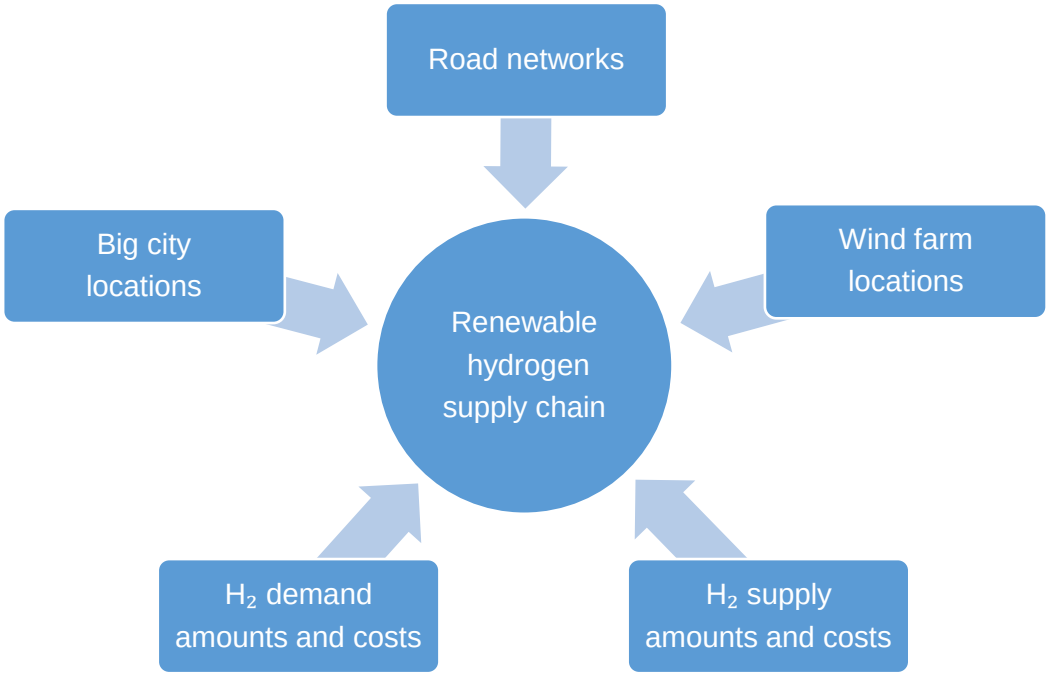

Figure 7.1. The integrated model for renewable hydrogen production from renewable powers for public city bus across cities in Northwest Europe

Table 7.1. Scenario description on renewable hydrogen production in Northwest Europe

No.	Short description of the electrolyser operation scenario	Electricity source				Electricity price	
		Curtailed wind	Exportable wind	Grid electricity	Photovoltaic array	Low	High
1	Curtailed wind with high electricity price	✓					✓
2	Curtailed wind with low electricity price	✓				✓	
3	Full time with high electricity price	✓	✓	✓			✓
4	Full time with low electricity price	✓	✓	✓		✓	
5	Curtailed wind combined with solar with high electricity price	✓			✓		✓
6	Curtailed wind combined with solar with low electricity price	✓			✓	✓	
7	Renewable intensification with high electricity price	✓	✓	✓	✓		✓
8	Renewable intensification with low electricity price	✓	✓	✓	✓	✓	

7.3.2. Renewable Electricity in Northwest Europe

Wind farms in Northwest Europe are suitable for hydrogen production due to their widespread distribution and relatively large installed capacity. This study uses 4,507 wind farms throughout NWE. The capacities and locations of wind farms, and the number of wind farms in each country are shown in Table 7.2. The average wind capacity factor for each country is applied to all wind farms within that country. Ireland, France, and Germany report the curtailment problem is more than 4% in 2018. However, countries like France, Netherlands, and Belgium with a small share of wind electricity have not yet reported experiencing curtailment. The annual national percentage of wind energy curtailed is available and reported in Table 7.2, with citations, for Ireland, the UK and Germany. Such figures are not available for France, the Netherlands and Belgium, which has lower wind penetration rates, so this study uses the assumption of 3% wind curtailment for these three countries. The national average capacity factors of solar energy is used in the calculation of additional solar electricity for the electrolyser.

Table 7.2. The performances of current wind electricity and the potential of solar electricity for each country in Northwest Europe region

Country	Wind						Solar	
	Curtailment		Capacity factor		Number of farms		Capacity factor	
Ireland	5%	[19]	27%	[19]	238	[167]	11%	[166]
United Kingdom	6%	[181]	20%	[182]	894	[127]	11%	[166]
France	3%	*	23%	[182]	138	[183]	14%	[166]
Belgium	3%	*	19%	[182]	112	[184]	13%	[166]
Netherlands	3%	*	22%	[182]	493	[185]	13%	[166]
Germany	4%	[181]	19%	[182]	2632	[186]	13%	[166]

7.3.3. Renewable hydrogen production, transportation, and dispensing

This chapter uses the same techno-economic model that has been described in Chapter 6. The levelised cost of hydrogen ($LCOH$) production, transportation, and dispensing are calculated using Equations (6.3), (6.7), and (6.9), respectively. The techno-economic parameters used in this chapter are given in Table 6.2.

7.3.4. Public City Buses in Northwest Europe

Cities with more than 400,000 inhabitants in Northwest Europe have been included in this study as major cities. In addition, Luxembourg, which has lower population, is still studied as it is one of the NWE region's capital cities. These major cities are the most likely first adopters of large-scale hydrogen fuel cell electric buses (FCEBs). However, only a few cities publicly disclose the number of buses they operate, as illustrated in Figure 7.2. Therefore, a function, which is shown in the same figure, is used to estimate operational buses based on city population.

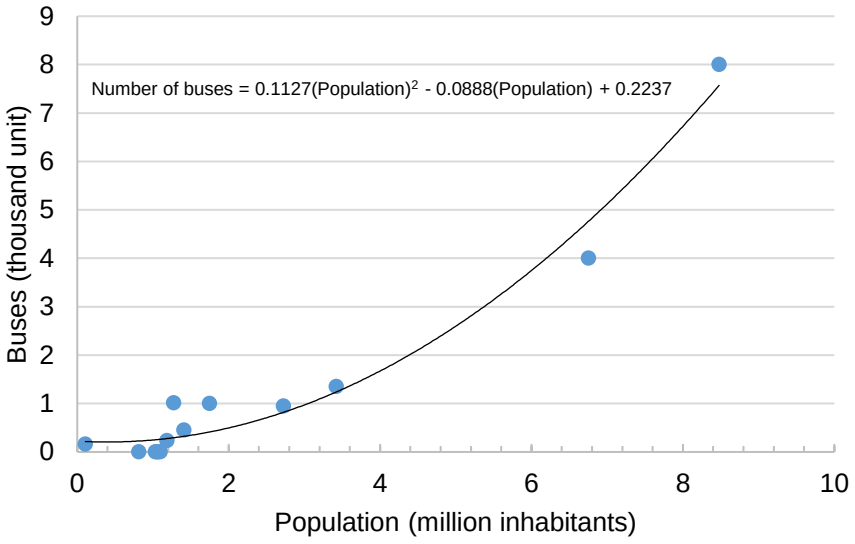

Figure 7.2. Relation population and number of buses in largest cities across NWE [175], [187]–[190]

The hydrogen fuel demand can be calculated based on the calculated number of public city bus number for each major city. The method to calculate the fuel demand for each bus is explained in hydrogen dispensing subsection in Chapter 6. The techno-economic parameters to calculate this are given in Table 6.6. The bus operational cost represents the total costs of capital, operation, maintenance, and fuel for the bus during its economic lifetime per total operational distance (€/km). Table 6.6 also shows the parameter to calculate the bus operational costs.

7.3.5. Renewable Hydrogen Supply Chain in Northwest Europe

As mentioned in systems and scenarios subsection, road networks in NWE are used in the Geographic Information System (GIS) [128]. The primary and secondary roads form the transportation route between hydrogen sources, located at wind farms, and hydrogen demand, located in the major cities. The closest routes algorithm in GIS is used to obtain the shortest available transportation distance, which is used in Equation (6.8) to calculate the transportation cost. The techno-economic parameters for hydrogen transportation used in the model are given in Table 6.4.

7.3.6. Overall algorithm

The overall algorithm shown in Figure 7.3 performs the techno-economic calculations for hydrogen production for this study. The hydrogen production scenarios are: The electrolyser operation scenarios included in the model are (1) curtailed wind operation with high electricity price, (2) curtailed wind with low electricity price, (3) full time operation with high electricity price, (4) full time operation with low electricity price, (5) curtailed wind operation combined with solar with high electricity price, (6) curtailed wind operation combined with solar with low electricity price, (7) renewable intensification with

additional PV electricity with high electricity price, and (8) renewable intensification with additional PV electricity with low electricity price. The required electrolyser size for each wind farm is calculated using Equation (3.41) and is based on available statistics of curtailed electricity available at the farm. Overall system efficiency is calculated to find the quantity of hydrogen produced at each wind farm. It enables compressed gas storage to be sized and the frequency of delivery to city bus fleets to be determined. Capital and operating costs are applied to each component in the hydrogen production and delivery chain. Finally, the model also calculates the operational cost of running fuel cell buses powered by the hydrogen produced at the wind farms and compares this with running diesel buses.

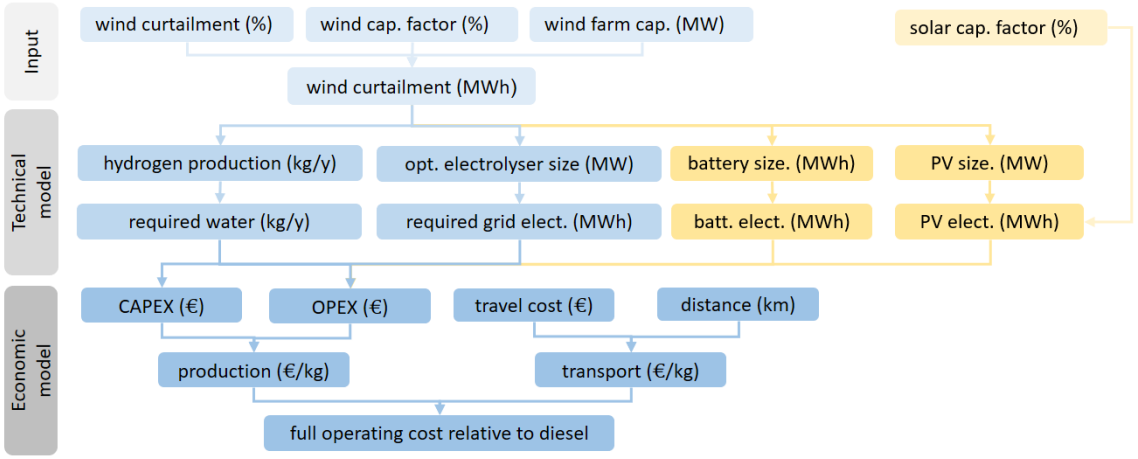

Figure 7.3. The overall algorithm in techno-economic modelling of hydrogen supply chain in Northwest Europe

7.4. Results and discussion

7.4.1. Renewable hydrogen production capacity for all wind farms

The distributed curtailed wind energy at each wind farm in NWE is depicted in Figure 7.4. It can be seen that western Ireland, western and northern United Kingdom and

northern Germany have the largest amounts of curtailed wind energy. Using this curtailed wind, the techno-economic model can calculate the optimum electrolyser size for each wind farm as depicted in Figure 7.5. Electrolysers with capacities of 10 MW_e or less predominate. The potential annual hydrogen production capacity for all wind farms is shown in Figure 7.6. The results show that most wind farms can produce more than 100 tonnes of hydrogen per year. It is important to note that the capacities of most wind farms in the eastern part of Ireland and the Netherlands are small which require relatively small electrolyser sizes.

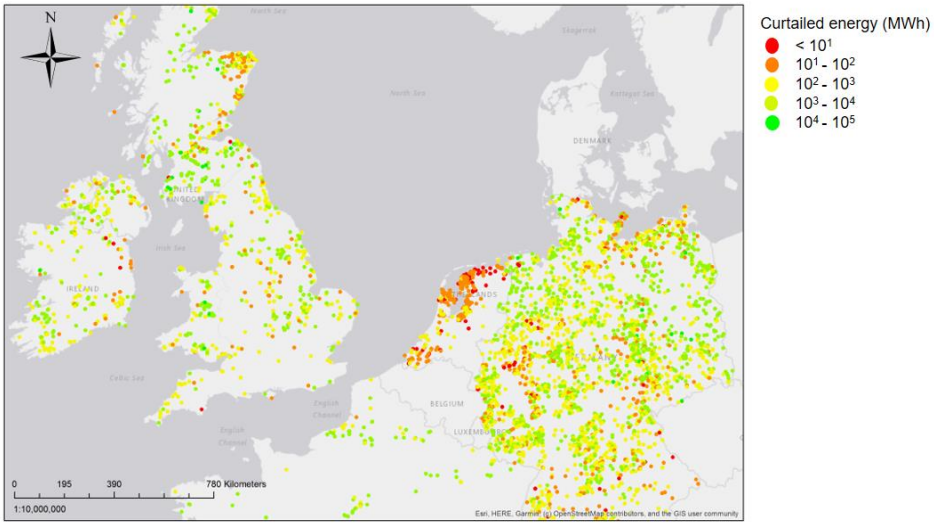

Figure 7.4. Annual wind curtailed energy at Northwest Europe's wind farms

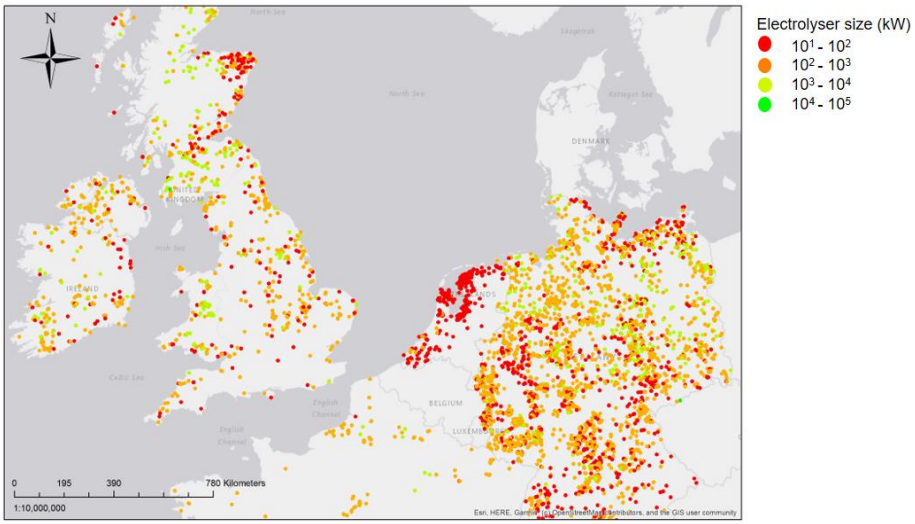

Figure 7.5. Optimum electrolyser size for wind curtailment-based hydrogen production at Northwest Europe's wind farms

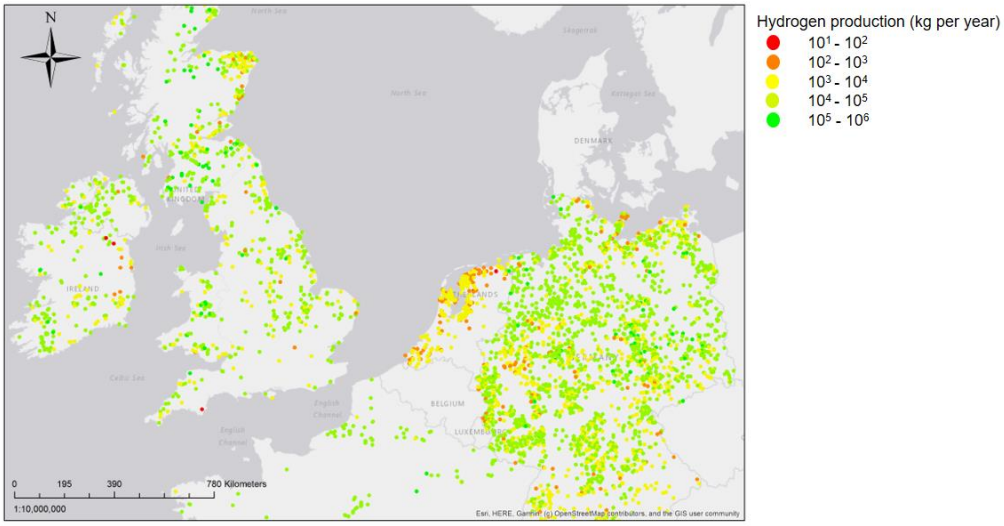

Figure 7.6. Annual wind curtailment-based hydrogen production at Northwest Europe's wind farms

7.4.2. Renewable hydrogen supply chain network

There are 46 cities with more than 400,000 people across the seven countries in the region. However, the region of NWE in this study, which coincides with the Interreg administrative region of Northwest Europe, covers only the northern part of France.

Therefore, only 37 cities are considered in the evaluation. Figure 7.7 shows the calculated transportation routes of hydrogen supplies to each wind farm's nearest major cities, as shown in. Wind farms located on the Scottish islands and the south of France are not connected to any city.

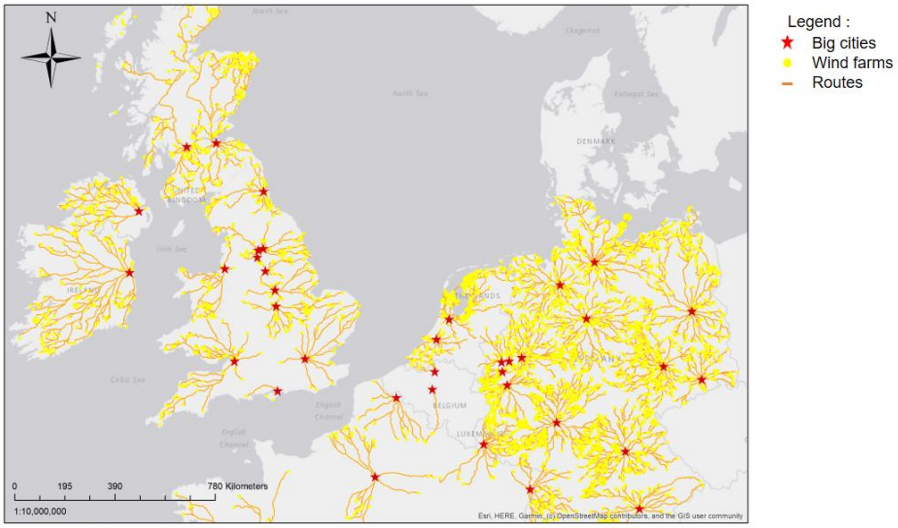

Figure 7.7. Supply routes of curtailment-based hydrogen to Northwest Europe's big cities

Figure 7.8 shows the distances from hydrogen sources to public city bus fleets in Dublin. The five horizontal bars indicate the percentages of hydrogen coming from different distance bands. The bands are 50 kilometres wide and go from 0 to 200+ kilometres. In the same figure, it can be seen that over 80% of the hydrogen available to fuel the city bus fleet must be transported over 200 kilometres. In many cases, this transport distance is considered too far. However, the results show that the wind resources for most of major cities are so favourable that this distance is practical. Similar results for the rest of the studied cities are provided in Appendix A.

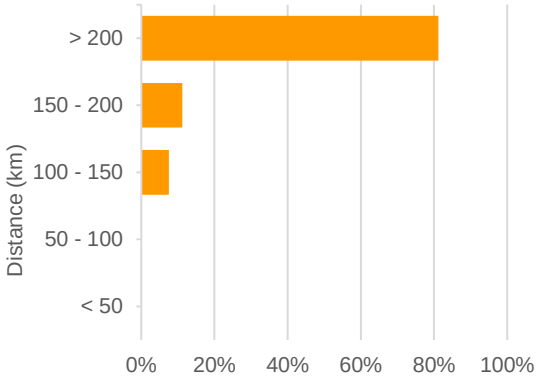

Figure 7.8. Distances from hydrogen sources to city bus fleet in Dublin, Ireland

7.4.3. City bus fuel displaceable by renewable hydrogen

Figure 7.9 shows the modelled bus fleet sizes of the 37 cities studied. They vary from less than 500 to more than 2,000 buses. The diesel fuel capable of being displaced by renewable hydrogen can be calculated using the hydrogen capacity for the respective supply chain network shown in Section 6.3.4.

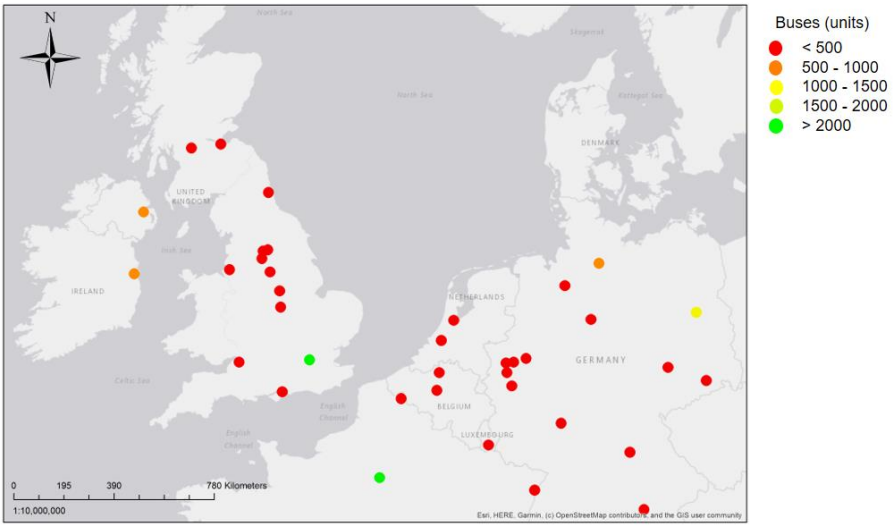

Figure 7.9. Bus fleet sizes for Northwest Europe's' largest cities

Figure 7.10 shows the percentage of the Dublin city's bus fleet fuel use that could be displaced by hydrogen produced by electrolysis at all nearby onshore wind farms. The left-hand bar shows the percentage of fuel that could be replaced if hydrogen is produced by curtailed electricity only. Since curtailment only happens a small portion of the time, the electrolysers would not operate to their full capacities. The right-hand bar shows the percentage of fuel that could be displaced if those same electrolysers are maximised their productivity to the fullest by using electricity from the grid so that they can operate full-time.

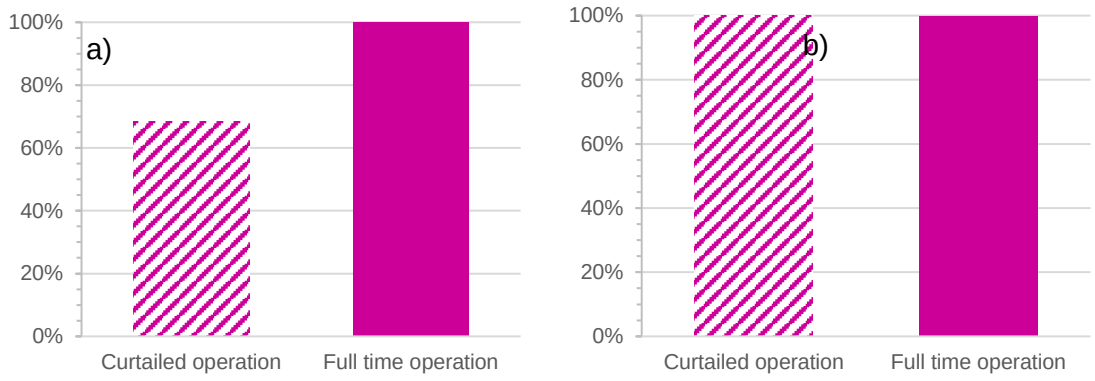

Figure 7.10. The percentage of city bus fuel displaceable by renewable hydrogen in Dublin for different electrolyser operation modes by using a) wind electricity and b) wind and solar electricity

In the same figure, results show that by using wind electricity, hydrogen would displace 70% of bus fleet fuel use with the curtailed operation of the electrolyser or >100% with full time operation. In comparison, hydrogen would replace >100% of total fuel use with the curtailed operation of the electrolyser and additional solar power and battery. Similar results for the rest of the cities are provided in Appendix A.

7.4.4. Operational costs for hydrogen buses

Figure 7.11 shows five bars that signify the operational cost per kilometre travelled of a fuel cell city bus powered by hydrogen produced under a range of scenarios relative to a diesel bus. The operating cost for a diesel bus is shown as 100% on the far right-hand side. The diesel costs do not account for planned rises in carbon taxes or for impending bans on diesel-fuelled vehicles in many European cities and countries. As shown in the same figure, by using wind electricity, a fuel cell city bus could operate with costs from 26% higher than diesel (for full time electrolyser operation with low electricity price) to 67% higher (for curtailed wind operation with high electricity price). In comparison, a fuel cell bus could operate with costs from 25% higher than diesel (renewable intensification with solar, with low electricity price) to 41% higher (curtailed wind combined with solar, with high electricity price). Similar results for the rest of the cities are provided in Appendix A.

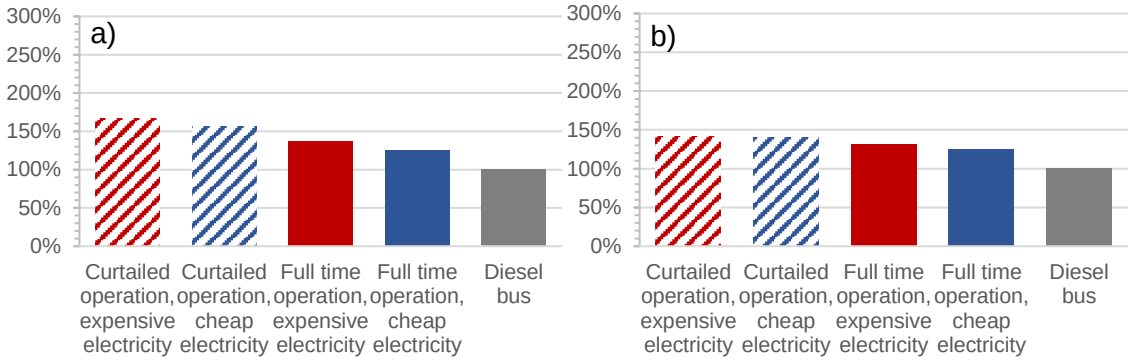

Figure 7.11. The percentage of operational costs for hydrogen buses in Dublin for different electricity prices and electrolyser operation modes by using a) wind electricity and b) wind and solar electricity, relative to diesel

7.5. Conclusions

This chapter presents techno-economic modelling of renewable hydrogen supply from existing wind farms with additional photovoltaic (PV) arrays and batteries in Northwest Europe (NWE) to decarbonise major city bus networks. The levelised cost of hydrogen fuel ($LCOH$) is used to evaluate the hydrogen production and transportation techno-economic performances and calculate bus operational costs. The minimum LCOH indicates the optimum equipment sizes to produce hydrogen. In hydrogen transportation, the closest facility algorithm in a geographic information system (GIS) environment is applied to allocate hydrogen distribution from each hydrogen production site to a hypothetical hydrogen refuelling system (HRS) in the nearest major city. Finally, the operational costs of hydrogen-fuelled city buses throughout NWE are calculated using $LCOH$ and compared to existing diesel-fuelled city buses.

Results show that the additional lithium-ion batteries and PV arrays to the existing wind farms in NWE can produce 100% green hydrogen and meet the fuel demand for most cities in the region, except for London and Paris. These two largest cities modelled to operate more city buses than their relatively small existing onshore renewable sources could support. However, there is a potential for these two capital cities to source their hydrogen demand from offshore wind electricity, for instance, from the North Sea. In general, the transnational approach benefits the major cities where the nearby renewable sources are limited or even unavailable. The hydrogen can still be sourced from the nearby renewable sources in neighbour countries, particularly in the eastern countries of NWE. The operational costs of hydrogen-fuelled city buses for most of the cities in NWE are at least 25% higher than current conventional diesel-fuelled buses when electrolyser is operated at full capacity under the assumption of a low average electricity price.

The lack of publicly available data causes the limitation of modelling to use national average wind capacity factors. Some improvements can be performed for future study when the historical exported and curtailed wind electricity data for each wind farm and the number of public city buses in the region are available. The recommendations are to model the hydrogen supply chain regionally via hubs, compare FCEB to other zero- and low-emission buses, and the carbon abatement costs. Future studies can also investigate the impacts of the wind used to produce hydrogen rather than export to the grid.

7.6. Final remarks

This chapter presents the results of techno-economic modelling on hydrogen production and transportation from an integrated wind and solar electricity generation supported with the battery system for the transnational scope. Northwest Europe (NWE) is used as a case study to represent the transnational scale. Results show that hydrogen fuel demand to operate hydrogen-fuelled city buses for most major cities in the region can be met by wind and solar electricity.

In Chapter 8, the developed techno-economic model is integrated with a GHG emissions model to perform full techno-econo-environmental modelling for heavy-duty truck fleets. Quarry trucks in Ireland are used as a case study to represent generic truck fleets in other countries.

Chapter 8. Hydrogen Production from Wind Electricity for Heavy-Duty Trucks

8.1. Overview

This chapter presents the results of techno-econo-environmental modelling of options to decarbonise fleets of four-axle trucks in the quarrying sector. The key parameter used to evaluate the performance of transitioning from diesel heavy-duty trucks (HDT) to zero- or low-emission heavy-duty trucks (ZLETs) is the total cost of carbon abatement (TCA). TCA is calculated by using the total cost of truck ownership on a discounted cost per km basis (TCO) and well-to-wheel (WTW) life-cycle greenhouse gas (GHG) emissions. TCO includes the costs of the vehicle, infrastructure, fuel, maintenance, and resale, and is evaluated for five different powertrain configurations: (1) battery electric heavy-duty truck (BET), (2) plug-in hybrid electric heavy-duty truck (PHET), (3) diesel internal combustion engine heavy-duty truck (ICET), (4) diesel-hydrogen dual-fuel engine heavy-duty truck (DFET), and (5) hydrogen fuel cell electric heavy-duty truck (FCET). Combinations of wind and/or grid electricity supply BETs and PHETs. Hydrogen is also produced from the same energy sources via electrolysis for DFETs and FCETs. Hourly electricity and hydrogen production and refuelling performance for each powertrain are assessed for on- and off-grid systems. The production capacity and costs can be optimally sized using the

total number of trucks, annual operational distance, and fuel economy to meet the annual fuel demand for each powertrain. Results show the fuel cost is the largest contributor to TCOs for all powertrains except the BET, which is dominated by vehicle and infrastructure costs. The TCOs for all powertrains in off-grid systems are higher compared to on-grid systems. This is because the required equipment sizes are smaller for on-grid systems compared to off-grid systems. In contrast, more WTW emissions for all powertrains can be abated by off-grid system compared to on-grid system. The minimum TCAs for fleets of 100 trucks in on- and off-grid systems are found for BETs and DFETs, respectively. The total number of trucks has a significant impact on the reduction of TCO and TCA. Higher carbon tax (€/ tonne of CO_2 emitted) in the future can also help the ZLETs to be more competitive.

8.2. Introduction

The heavy-duty truck (HDT) class is one of the harder-to-abate transportation sectors, together with shipping and aviation [4]. These sectors are classified as harder-to-abate due to their significant greenhouse gas (GHG) abatements cost compared to others [4]. HDTs contributed around 4% of global GHG emissions in 2018 [191]. At the current pace of growth, GHG emissions from HDTs can be doubled by 2050 [191]. Therefore, several countries began to tighten emission regulations to reduce GHG emissions from HDTs. For instance, India, Japan, China, and the United States target to tighten the mandatory CO_2 emission standards per HDT by up to 5%, 10%, 25%, and 40% lower than 2010 by 2025, respectively [192]. In the European Union, several HDT types must pay financial penalties if they fail to achieve 15% reductions in 2019 CO_2 emissions per HDT by 2025 [193]. This regulation also incentivises the transformation of diesel heavy-duty truck (DTs) to zero- and low-emission heavy-duty trucks (ZLETs).

The objectives of this chapter are to (1) model the techno-econo-environmental system and parameters of electricity and hydrogen supply to meet the energy demand of HDTs, (2) assess the life-cycle or well-to-wheel (WTW) or overall GHG emissions, and (3) evaluate TCA for all powertrain options using a novel approach based on TCO and WTW emissions. The techno-econo-environmental system is an arrangement of multiple types of equipment needed in the evaluation associated with the capital and operational costs and its overall GHG emission resulting during the system economic lifetime. Therefore, key parameters include the fuel production capacity (with units of kWh/year), fuel production cost (with units of €/kWh) and carbon abatement cost (with units of €/ tonne of CO_2 emitted). As a case study, this chapter evaluates the data for Ireland as a representative of similar quarry settings throughout the world.

The following section describes the methods used to achieve these objectives. It covers the explanation of the energy systems, scenarios, modelling of fuel production, refuelling infrastructure and its performance, heavy-duty truck powertrain technologies and their costs, life-cycle emission for all scenarios and the overall model. Following that, the results and discussion section comprises the analysis of refuelling performance, truck ownership costs, carbon abatement costs, and sensitivity analysis. Finally, conclusions are drawn specifically for the case study of Ireland and more generally for any location in which similar fleets and energy systems operate.

8.3. Methodology

8.3.1. Systems and scenarios

This study compares the techno-econo-environmental performance of five different powertrain configurations: (1) battery electric heavy-duty truck (BET), (2) plug-in hybrid

electric heavy-duty truck (PHET), (3) diesel internal combustion engine heavy-duty truck (ICET), (4) diesel-hydrogen dual-fuel engine heavy-duty truck (DFET), and (5) hydrogen fuel cell electric heavy-duty truck (FCET) in the setting of a quarry in Ireland. The fuel, energy storage and energy conversion technology for each powertrain is shown in Table 8.1.This study uses the technologies in 2030 for all scenarios. The total cost of carbon emission abatement (TCA) is used as a parameter to compare the overall techno-econo-environmental performance. TCA, which is expressed in Equation (8.1), represents the cost of moving from conventional diesel internal combustion engine heavy-duty trucks ($_{ICET}$) to zero or low-emission heavy-duty trucks ($_{ZLET}$) while still driving the same distance annually. It has units of €/kg of CO_2 eq. abated [194], [195]. The further descriptions to calculate TCO (with units of €/km) and operational distance (D) are explained in the next paragraph. Carbon emissions (M_{WTW}, units of gCO_2 eq./kWh) for ICETs and ZLETs are described in the life-cycle emission subsection.

$$TCA = \frac{\left(TCO_{ZLET} - TCO_{ICET}\right) \times D}{M_{WTW,ICET} - M_{WTW,ZLET}} \tag{8.1}$$

Based on these fuels, production and refuelling infrastructure are defined as depicted in Figure 4.2. In scenario 1, diesel-fuelled ICETs are determined as the baseline scenario. In scenario 2, the electricity generated by wind turbines is converted via an energy management unit (EMU) and supplied to BETs via a 350 kW fast charger at refuelling time. When the wind electricity is not enough to satisfy the demand of HDTs, battery and/or grid electricity is supplied as a back-up. A battery is installed to store the surplus wind power when the demand is low. In scenario 3, the energy system is the same as scenario 2 but with additional diesel supplied to PHETs. In scenario 4, hydrogen is generated from water and wind electricity, compressed to 350 barg, stored when needed

and supplied to FCETs via a dispenser. In scenario 5, the system is the same as scenario 4 but with diesel supplied to DFETs.

Table 8.1. Onboard truck technology for each scenario

	Powertrain scenarios				
		ZLET			
	1) ICET	2) BET	3) PHET	4) FCET	5) DFET
Energy source					
Diesel	✓		✓		✓
Electricity		✓	✓		
Hydrogen				✓	✓
Energy storage					
Diesel fuel tank	✓		✓		✓
Battery		✓	✓		
Compressed H_2 tank				✓	✓
Energy conversion					
Internal combustion engine	✓		✓		✓
Electrical motor		✓	✓	✓	
Fuel cell				✓	

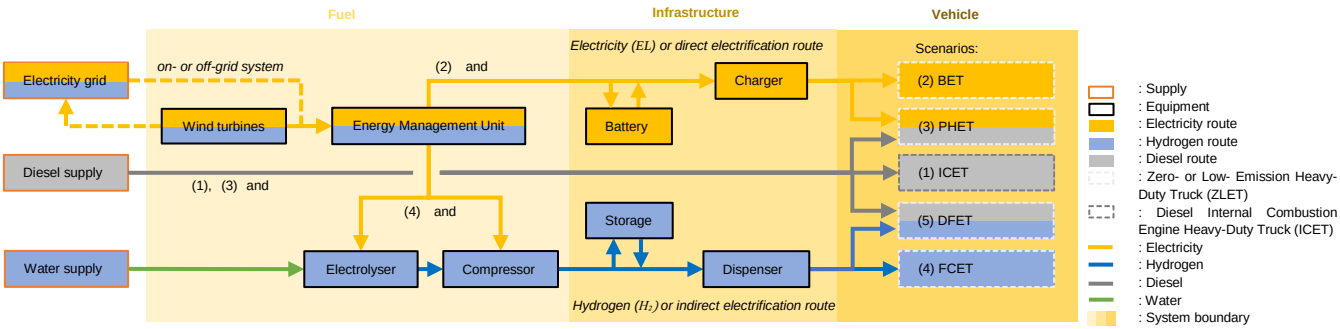

Figure 8.1. Block diagram of equipment for each energy system scenario

The equipment described above can be categorised into fuel production equipment, refuelling infrastructure equipment, and vehicle technology. These categories are used for the calculation of TCO, as shown in Equation (8.2) [90], [196], [197].

$$TCO = \left(\frac{C_F + C_V + C_I + C_M - C_R}{D} \right) \tag{8.2}$$

The fuel cost (C_F) is calculated using Equation (8.3), where c_F is the specific cost of fuel (€/kWh), D_n is the operational distance (km) in year n, d is fuel economy (km/kWh), r is the discount rate (%), T is economic lifetime, and n is the number of years. Further explanation of fuel production is given in more detail in the fuel supply subsection. The calculation of vehicle cost (C_V) is described in the heavy-duty truck subsection. The total cost of infrastructure equipment (C_I) is explained in the refuelling infrastructure subsection.

$$C_F = \sum_{T=0}^{T=n} \frac{c_F \times D_n}{d \times (1+r)^{(n-1)}} \tag{8.3}$$

The maintenance cost (C_M) can be calculated using Equation (8.4), where c_M is the specific cost of maintenance (€/km), and N_{HDT} is the number of HDTs (units). The economic parameters are given in the heavy-duty truck subsection. The resale (C_R) value is assumed to be 38% of vehicle cost [90].

$$C_M = \sum_{T=0}^{T=n} \frac{c_M \times D_n \times N_{HDT}}{(1+r)^{(n-1)}} \tag{8.4}$$

The operational distance (D) is calculated using Equation (8.5). The value of typical operational distance in quarry application is given in the heavy-duty subsection.

$$D = \sum_{T=0}^{T=n} \frac{D_n \times N_{HDT}}{(1+r)^{(n-1)}} \tag{8.5}$$

8.3.2. Fuel production

The spatially averaged hourly wind capacity factor in Ireland is simulated at www.renewable.ninja. The wind electricity for scenarios 1 and 2 are directly supplied to the refuelling infrastructure. In scenarios 4 and 5, the wind electricity is converted to hydrogen by using the electrolyser. The total fuel specific costs (c_F) of (1) electricity for BETs, (2) electricity and diesel for PHETs, (3) diesel for ICETs, (4) hydrogen and diesel for DFETs, and (5) hydrogen for FCETs are calculated using Equation (8.6). All the units of energy costs are set as €/kWh, so that the energy in the form of electricity, hydrogen and diesel can be equally calculated and compared. The total energy demand for HDTs (E_{HDT}) is calculated by using Equation (8.7). Depending on the fuel ratio (R) for each scenario, E_{HDT} from wind in the form of either electricity ($_{EL}$) or hydrogen ($_{H2}$), and E_{HDT} from diesel fuel ($_{DF}$) can be calculated using Equation (8.8), (8.9), and (8.10). The N_{HDT} is calculated for the range of 10 to 1000 units, where the R, D and d are given in the heavy-duty truck subsection.

$$c_F = \frac{\left(\left(LCOE_{EL/H2} \times E_{HDT,EL/H2}\right) + \left(LCOE_{DF} \times E_{HDT,DT}\right)\right)}{E_{HDT}} \tag{8.6}$$

$$E_{HDT} = \frac{N_{HDT} \times D}{d} \tag{8.7}$$

$$E_{HDT} = E_{HDT,EL/H2} + E_{HDT,DF} \tag{8.8}$$

$$E_{HDT,EL/H2} = E_{HDT} \times R_{EL/H2} \tag{8.9}$$

$$E_{HDT,DF} = E_{HDT} \times R_{DF} \tag{8.10}$$

In this study, the levelised cost of energy ($LCOE$) of diesel fuel after extracted, transported across oceans, refined, freighted to Ireland, stored, and delivered locally is

assumed at 0.6 €/litre, excluded all taxes [198]. The $LCOE$ of electricity or hydrogen is calculated using Equation (8.11). The calculation of total capital expenditure ($C_{CAPEX,EL}$) and its operation and maintenance expenditure ($C_{OPEX,EL}$) of providing electricity for HDTs are expressed in Equation (8.12) and (8.13), respectively. The calculation of total capital expenditure ($C_{CAPEX,H2}$) and its operation and maintenance expenditure ($C_{OPEX,H2}$) of providing hydrogen for HDTs are expressed in Equation (8.14) and (8.15), respectively. All projected techno-economic parameters for the equipment for 2030 are given in Table 8.2. The diesel cost is estimated at 0.8 €/litre after excluding all taxes except the projected carbon tax of 80 € per tonne of CO_2 emitted in 2030 [199]. The grid electricity price and discount rate are 0.13 €/kWh and 5%, respectively [200]. Installation, engineering, and other costs are set to 20%, 15%, 50% of total capital costs, respectively [98].

$$LCOE_{EL/H2} = \frac{\sum_{T=0}^{T=n} \frac{C_{CAPEX,EL/H2} + C_{OPEX,EL/H2}}{(1+r)^T}}{\sum_{T=0}^{T=n} \frac{E_{HDT,EL/H2}}{(1+r)^T}} \tag{8.11}$$

$$C_{CAPEX,EL} = C_{WT} + C_{EMU} + C_{ICS} + C_{ENG} + C_{OH} \tag{8.12}$$

$$C_{OPEX,EL} = C_{OM,WT} + C_{EL,EG} \tag{8.13}$$

$$C_{CAPEX,H2} = C_{WT} + C_{WE} + C_{EC} + C_{EMU} + C_{ICS} + C_{ENG} + C_{OH} \tag{8.14}$$

$$C_{OPEX,H2} = C_{OM,WT} + C_{OM,WE} + C_{OM,EC} + C_{SR} + C_{EL,EG} + C_{H2O} \tag{8.15}$$

For the hydrogen production, the water electrolyser size in kWe (P_{WE}) can be calculated by using the required hydrogen fuel for HDTs ($E_{HDT,H2}$), the maximum possible operational time of electrolyser (t_{WE}) is 8,760 hours in a year, and the electrolyser efficiency (η_{WE}) as shown in Equation (8.16). The installed capacity of wind turbines (P_{WT}) required to

provide electricity or hydrogen is calculated using Equation (8.17). The maximum possible operational time of the wind farm (t_{WF}) is 8,760 hours, i.e. the number of hours in a year. When equipment sizes in off-grid system do not meet the electricity and hydrogen demands, the optimal equipment size is iteratively calculated with larger equipment sizes until the entire demand is met by the fuel supply at minimum TCO.

$$P_{WE} = \frac{E_{HDT,H2}}{t_{WE}} \Big/ \eta_{WE} \tag{8.16}$$

$$P_{WT} = \frac{E_{HDT,EL/H2}}{t_{WF} \times \lambda_{WF}} \tag{8.17}$$

Table 8.2. Techno-economic parameters of the equipment for fuel production

Parameters, Symbol	Value/ Unit/ Reference					
Equipment	**Water electrolyser (WE)**			**Electric compressor (EC)**		
Technology	Alkaline water electrolyser			Reciprocating		
Specific energy consumption, μ	48	kWh/kg	[140]	3.4	kWh/kg	[55]
Lifetime, τ	20 (system), 10 (stack)	years	[31]	10	years	[115]
Efficiency, η	69%	(LHV_{H2})	[140]	73%	(isentr.)	[46]
Outlet pressure, p	30	barg	[115]	350	barg	[201]
CAPEX, $C_{WE/EC}$	1734 x $P_{WE}^{0.841}$	€	[31], [98]	4785 x $P_{WE}^{0.66}$	€	[98]
OPEX, $C_{OM,WE/EC}$	0.2011 $P_{WE}^{-0.23}$ x $C_{CAPEX,WE}$	€	[115]	2%	of C_{CAPEX}	
Stack rep., C_{SR}	353 x $P_{WE}^{0.929}$	€/ n	[31], [98]			
Equipment	**Wind turbines (WT)**			**Energy management unit (EMU)**		
Technology	Horizontal axis wind turbine			Converter and controller		
Lifetime, τ	25	years	[202]	15	years	[42]
Efficiency, η				90	%	[42]
CAPEX, $C_{WT/EMU}$	840 x P_{WT}	€/kW	[202]	8% x C_{WT}	€	[203]
OPEX, $C_{OM,WT}$	3% x C_{WT}	€/year	[202]			

8.3.3. Refuelling infrastructure

There are several refuelling strategies for supplying electricity as fuel such as (1) fast charging using 350 kW_e charger [66], (2) overnight charging using 50 kWe charger [66], (3) on-road charging using catenary wires [68], (4) dynamic induction grid [204] and (5) battery swapping [205]. Bünger et. al. found that the infrastructure cost can be significantly larger for deploying large electric fleets compared to hydrogen fleets [79]. The study suggests the detailed refuelling infrastructures for electricity charging and hydrogen refuelling have to be evaluated and compared in more detail. In this study, the fast-charging technology is considered as charging infrastructure for the BETs and PHETs. The hydrogen dispenser is used to refuel FCETs and DFETs. The daily refuelling and charging profile is illustrated in Figure 8.2. This profile is used to support the operational of HDTs during day, where 80% HDTs can be refuelled and charged from 10 pm to 6 am. By distributing these activities in 8 hours, the peak hours can be minimised to reduce the required number of chargers and dispensers needed. The rest of refuelling and charging activities occur in the morning and afternoon during inactivity periods of several HDTs [78].

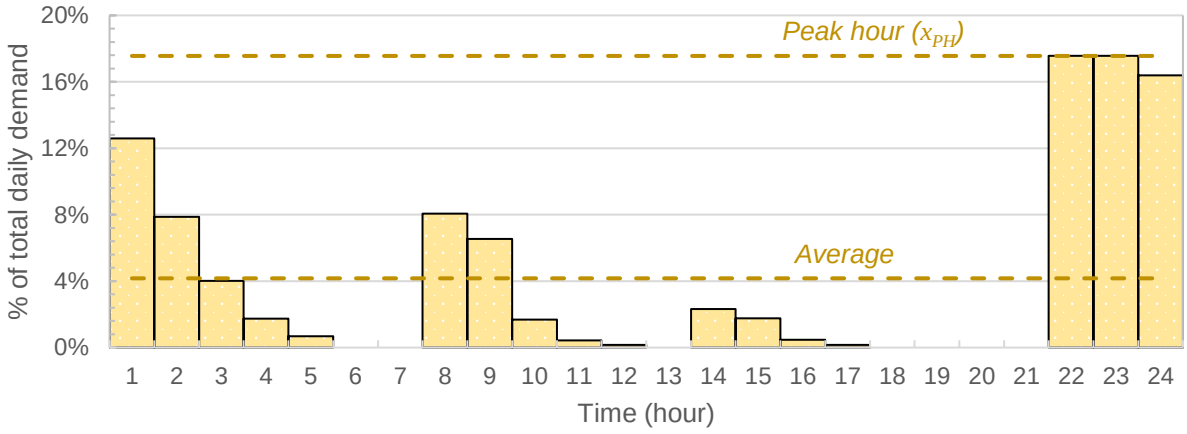

Figure 8.2. Daily refuelling and charging profile for HDTs [78]

The refuelling infrastructure cost (C_I) is calculated using Equation (8.18). The component costs included in the capital and operation costs for the battery energy storage subsystem (BESS) are expressed in Equation (8.19) and (8.20), respectively. The capital and operation costs for the hydrogen energy storage subsystem (HESS) are expressed in Equation (8.21) and (8.22), respectively.

$$C_I = \sum_{T=0}^{T=n} \frac{C_{CAPEX,BESS/HESS} + C_{OPEX,BESS/HESS}}{(1+r)^{(n-1)}} \tag{8.18}$$

$$C_{CAPEX,BESS} = C_{EB} + C_{CS} \tag{8.19}$$

$$C_{OPEX,BESS} = C_{OM,EB} + C_{OM,CS} \tag{8.20}$$

$$C_{CAPEX,HESS} = C_{BSV} + C_{DS} \tag{8.21}$$

$$C_{OPEX,HESS} = C_{OM,BSV} + C_{OM,DS} \tag{8.22}$$

The required number of the charger or dispenser is estimated using Equation (8.23). Where the required capacity of battery in kWh (P_{EB}) is calculated by using Equation (8.24). The lingering process time (t_{LP}) is assumed to be 3 minutes to allow the truck's driver to conduct the refuelling process. The battery performance is modelled and evaluated by using state of charge (SOC) as described by Ma et. al. [144] and Song et al. [145]. The battery is assumed to be able to discharge power (t_{EB}) for a maximum of 6 hours [142]. Hydrogen production from wind is modelled using model explained by Gunawan et. al [143]. The techno-economic parameters for refuelling infrastructure are presented in Table 8.3. The costs of installation, engineering and other systems are 20%, 15% and 50% of total capital costs, respectively [46], [177],[206].

$$N_{CS/DS} = \frac{\left(\frac{\bar{E}_{HDT}}{\dot{E}_{EL/H2}} + t_{LP}\right) \times x_{PH} \times N_{HDT}}{60} \quad (8.23)$$

$$P_{EB} = \frac{\tilde{E}_{HDT,EL} \times t_{EB}}{\eta_{EB}} \quad (8.24)$$

Table 8.3. Techno economic parameters for refuelling infrastructure

Parameters, Symbol	Value/ Unit/ Reference					
Equipment	**Electric battery (EB)**			**Buffer storage vessel (BSV)**		
Technology	Lithium Nickel Manganese Cobalt Oxide			Steel cylinder		
Lifetime, τ	20	years	[33]	20	years	[98]
Efficiency, η	90	%	[207]			
DoD	80	%	[207]			
Capital cost, C	-37.59 x Ln(P_{EB}) + 587	€/kWh	[142]	300 x m_{H2} x T	€	[140]
OandM cost, C_{OM}	2% x C_{EB}	€/ year	[142]	2% x C_{BSV}	€/ year	[98]
Equipment	**Charging system (CS)**			**Dispensing system (DS)**		
Technology	Fast charger			Hydrogen dispenser		
Capacity	350	kW_e	[208]	2	kg/min	[85]
Lifetime, τ	10	years	[208]	10	years	[42]
Capital cost, $C_{CU/DU}$	451	€/kW	[208]	67595	€/unit	[177]
OandM cost, C_{OM}	2% x C_{CS}	€/ year	[78]	2% x C_{DS}	€/ year	[46]

8.3.4. Heavy-duty truck

This study models heavy-duty trucks (HDTs) as four-axle rigid trucks, with weight of 32 tonnes and power of 460 hp (345 kW) from a 12.8-litre in-line 6-cylinder engine [61]. The Volvo FMX 460 Tipper, specifically designed for quarry activity, is used as a reference model for ICETs [209]. In an evaluation of energy consumption for HDTs, Smallbone et. al. found the operational range is crucial for new powertrains like BETs and FCETs [69].

The gravimetric (kg/km) and volumetric (l/km) energy densities of FCETs can significantly decrease for long working distances (km/day) compared to BETs. The current study applies the measured operational distance of HDTs performing quarry activities obtained from Robinson Quarry Masters Limited in Northern Ireland in 2019, as shown in Figure 8.3. The average annual distance and fuel economy are 54,229 km and 2.4 km/l, respectively. It is assumed that these numbers represent the annual quarry drive cycle that includes low speed driving and frequent idling during loading and unloading quarry in the rural or off-road zones [70], [210], [211]. The operational truck's weight is assumed to be limited to 80% of gross vehicle weight or equivalent to 25.6 tonnes [212]. Considering the base kerb weight is 14.9 tonnes, the remaining capacity for the payload is 10.7 tonnes per vehicle or 42% of the limited weight [213]. The discount rate and truck lifetime in this model are 7% and 10 years, respectively [208]. The vehicle cost is calculated based on major powertrain component cost (C_{MPC}) and retail price equivalent factor (F_{RPE}) to obtain the final vehicle costs that are close to the market prices as shown in Equation (8.25). The F_{RPE} for HDT applications is assumed to be 1.2 [214]–[216]. The technical and economic details of the powertrain options are provided in Table 8.4 and Table 8.5, respectively.

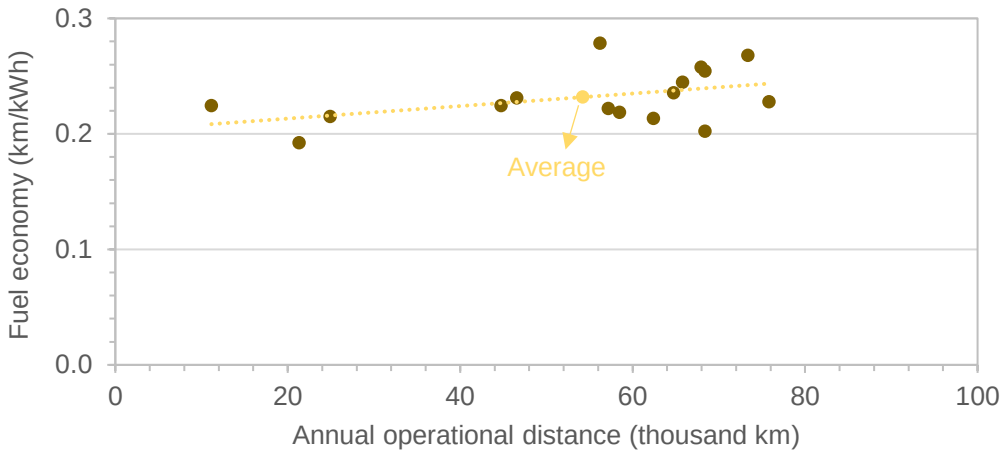

Figure 8.3. Typical operational distance in an operating quarry in Northern Ireland

Fuel cell stacks are capable of operating with 50% efficiency [204]. They are more efficient than diesel engines, which typically have efficiency of 35% [217]. In this study, fuel economy (km/kWh) is used to calculate fuel demand (kWh) by HDTs to perform at typical operational distances (km). By considering the fuel economy as shown in Table 8.4, the average daily fuel demand for quarry trucks can be calculated for each scenario. For a BET, dividing the daily distance of 150 km/day by fuel economy of 0.52 kWh/km results in a required battery capacity of nearly 300 kWh/BET. For recharging a BET, dividing the battery capacity of 300 kWh/BET by 350 kW_e fast charger results in a charging time of around 50 minutes/charge. Dividing the battery size of 300 kWh by the battery pack energy density of 0.2 kWh/kg results in a battery weight of 1.5 tonnes [218]. Estimating the volumetric energy density of 94 kWh/m^3, the size of battery is approximately 3 m^3 [219]. Assuming the weight of the electrical motor, inverter, and gearbox is 0.88 kg/kW_e, an additional weight of 0.35 tonnes is required for electrical motor rated power of 400 kW_e [218]. The required power of an electric motor is typically larger than an engine [204]. Due to a large electric motor is needed to apply the torque in proportion to vehicle acceleration and deceleration [212]. The total weight for a BET powertrain is 1.85 tonnes or slightly lighter than the weight of an ICET powertrain, which a 345-kW powertrain is typically weighted 2 tonnes [212]. Likewise, the total weight of the powertrain for PHETs, FCETs, and DFETs are assumed to be the same as for ICET [208]. Thus, this study does not include penalties for the over an hour refuelling duration or overweight powertrains.

$$C_V = \sum C_{MPC} \times F_{RPE} \tag{8.25}$$

Table 8.4. Technical parameters for each powertrain/ scenario

Parameter, Symbol	Unit	Values/ Reference									
		BET		PHET		ICET		DFET		FCET	
Operational parameters											
Fuel economy	km/kWh	0.52	[80]	0.41	[204]	0.40	[204]	0.40	[204]	0.47	[204]
Diesel ratio, R_{DF}	% E_{HDT}			60	[212]	100	[58]	70	[220]		
Electricity ratio, R_{EL}	% E_{HDT}	100	[58]	40	[212]						
Hydrogen ratio, R_{H2}	% E_{HDT}							30	[220]	100	[58]
Capacity of major powertrain components (MPCs)											
Engine	kW			345	[204]	345	[204]	345	[204]		
Diesel fuel tank	litres			270	[209]	270	[209]	270	[209]		
H_2 fuel tank (350 barg)	kg							15	[201]	30	[201]
Battery	kWh	300	[221]	25	[221]					12	[204]
Electric motor	kW	400	[70]	120	[70]					400	[204]
Fuel Cell	kW									350	[222]

Table 8.5. Economic parameters for each powertrain/ scenario

Parameter, Symbol	Unit	Values/ Reference									
		BET		PHET		ICET		DFET		FCET	
Operational parameter											
Maintenance cost	€/km	0.088	[208]	0.097	[208]	0.097	[208]	0.097	[208]	0.088	[208]
Cost of major powertrain components (MPCs)											
Base truck (glider kit)	k€/unit	78.3	[204]	78.3	[204]	78.3	[204]	78.3	[204]	78.3	[204]
Engine	€/kW			23	[70]	23	[70]	23	[70]		
Diesel fuel tank	€/litres			2.1	[70]	2.1	[70]	2.1	[70]		
H_2 fuel tank	€/kg							500	[204]	500	[204]
Battery	€/kWh	75	[29]	75	[29]					75	[204]
Electric motor	€/kW	12	[204]	12	[204]					12	[204]
Fuel Cell	€/kW									48	[204]

8.3.5. Life-cycle emission

This study also models the total life-cycle GHG emissions from well-to-wheel (WTW). WTW is the sum of well-to-tank (WTT) and tank-to-wheel (TTW) as illustrated in Figure 8.4. Palencia et. al. found that more than half of TTW emissions can be reduced with the penetration of electric and hydrogen vehicles in Japan by 2050 [223]. In another study, Osorio-Tejada et. al. emphasised that the fuel production process (WTT) has a significant impact on reducing total WTW emission for HDTs [224]. The same argument was also put forward by Lee et. al., who evaluated hydrogen produced from renewables and found it can further reduce life-cycle emission for HDTs than hydrogen produced from solely grid electricity [225].

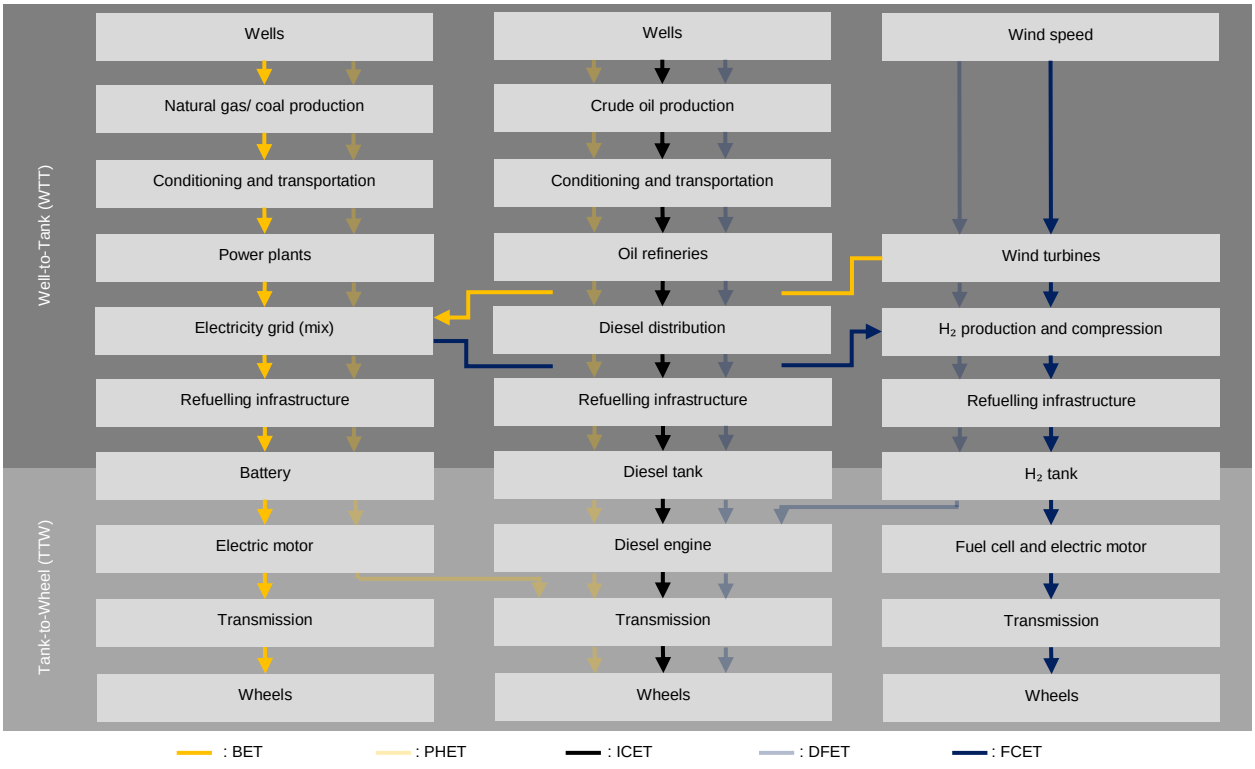

Figure 8.4. Processes involved in the life-cycle emission of well-to-wheel, reproduced from [58], [69], [71], [226]

In terms of tank-to-wheel emission, BETs and FCETs are categorised as zero-emission technologies. Still at the same relation to tank-to-wheel emission, PHETs and DFETs are

categorised as low-emission technologies. This study calculates the truck emission proportional to the diesel contribution of total energy demand for low emission technology. Particularly for DFETs, Liew et. al. found that adding a small amount of hydrogen results in a negligible effect on the combustion process and cylinder pressure in a spark-ignition (SI) engine [227]. In comparison, a compression-ignition (CI) engine enables a large share of hydrogen direct injection due to a higher limitation on compression ratio compared to SI engines [228]. The reduction of ten-fold in smoke and half of CO emission can be achieved at 30% hydrogen substitution ratio in a CI engine [229]. At idling and low load conditions, the addition of hydrogen can reduce nitrogen oxide (NO_x) emissions but can increase at the high load conditions due to higher temperature [230]. NO_x emitted from diesel engines consist of primarily nitric oxide (NO) and a small portion of nitrogen dioxide (NO_2) [231]. Another study by Liu et. al. suggested using Selective Catalytic Reduction (SCR) with a diesel-hydrogen dual-fuel engine to maximise NO_x reduction [231]. According to Monemian et. al., emissions from DFETs with a hydrogen ratio of 30% can meet Euro VI emission regulation after treatment [220]. The Volvo FMX reference ICET already implements Euro VI emission specification [232]. The emission in the Irish grid electricity is assumed to be reduced annually by 7% until 2030 [199]. The emission of diesel is also assumed to be reduced by 12% by 2030 due to the mandatory blend of biodiesel [233]. The life-cycle emission for all powertrain scenarios are listed in Table 8.6.

$$M_{WTW} = \sum_{T=0}^{T=n} \frac{E_{HDT} \times e_{WTW}}{(1+r)^{(n-1)}} \tag{8.26}$$

Table 8.6. Environmental parameters, calculated from [58], [234], [225], [235]

Emission, symbol, unit		1) ICET	2) BET	3) PHET	4) FCET	5) DFET
On-grid system						
WTT, e_{WTT}	gCO_2 eq./kWh	46	37	46	36	47
TTW, e_{TTW}	gCO_2 eq./kWh	239	0	109	0	82
WTW, e_{WTW}	gCO_2 eq./kWh	285	37	155	36	129
Off-grid system						
WTT, e_{WTT}	gCO_2 eq./kWh	46	0	31	0	36
TTW, e_{TTW}	gCO_2 eq./kWh	239	0	109	0	82
WTW, e_{WTW}	gCO_2 eq./kWh	285	0	140	0	118

8.3.6. Overall model

The integrated model of technical, economic and environmental models is summarised and illustrated in Figure 8.5. The overall model includes fuel production, required infrastructure, vehicle's powertrain, maintenance needed, and emission for each scenario. In the data preparation, the crucial data required are the hourly wind capacity factor, the total number of the truck, annual operational distance, and fuel economy for each powertrain. Electricity and hydrogen production can be theoretically calculated and sized to meet the annual energy demand from the HDTs. Based on its equipment size, the capital and operation costs of equipment and vehicle are calculated to obtain a total

cost of ownership (TCO). The TCO and well-to-wheel (WTW) emission is then used to calculate the total cost of carbon abatement (TCA).

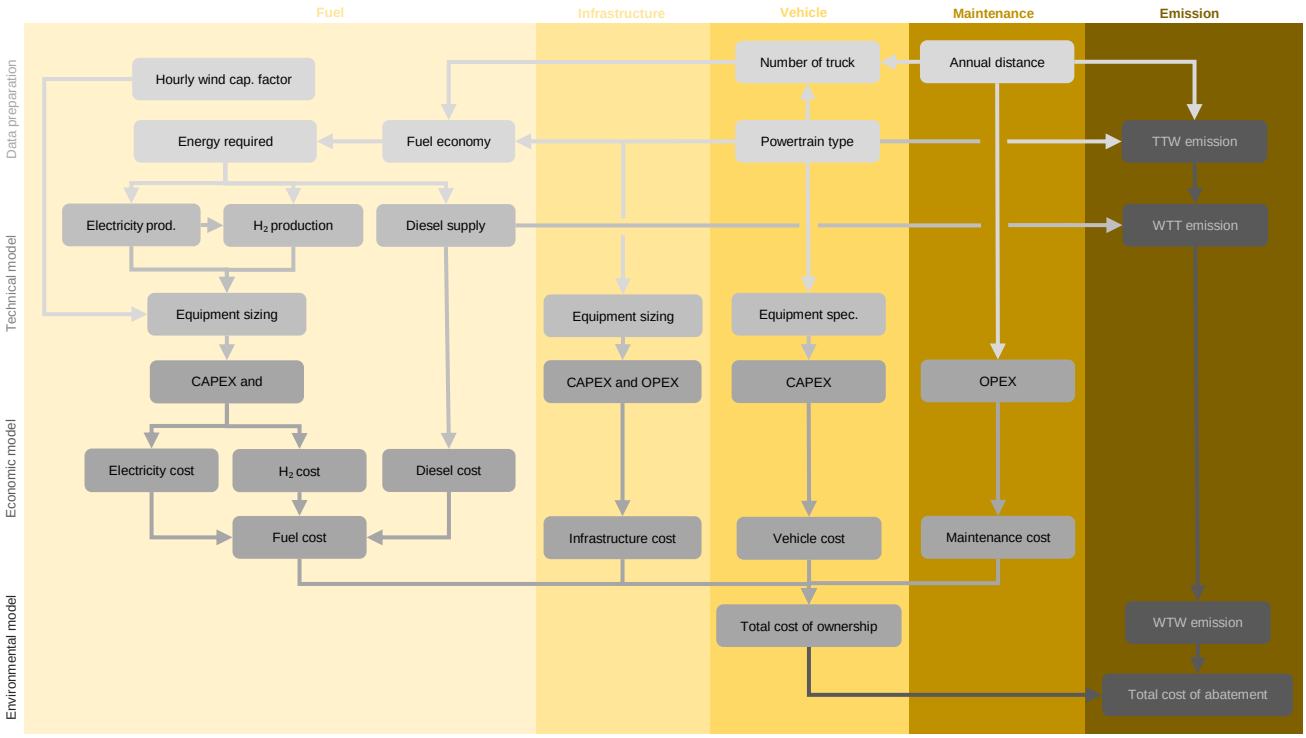

Figure 8.5. Overall algorithm to calculate the total cost of carbon abatement

8.4. Results and discussion

8.4.1. Refuelling performances for the on- and off-grid systems

The hourly refuelling performance of on-grid system for 100 HDTs in three days of winter are shown in Figure 8.6. During winter, when wind occurs relatively often, demand from BETs and PHETs can be met by wind and battery more frequently. In summer, the energy stored in the battery is at a minimum level. Therefore, fuel demand is met by grid electricity for BETs and by diesel and grid electricity for PHETs. The battery should be designed to store electricity up to 6 hours of the hourly average electricity demand for

BETs and PHETs. For hydrogen and DFETs, the hydrogen storage should be able to store hydrogen production up to 13 hours of the hourly average hydrogen demand for FCETs and DFETs.

Refuelling performances from the same energy demand and equipment sizes in off-grid system are shown in Figure 8.7. Red colours indicate the supplies that are unable to meet the demand for HDTs. It can be analysed that the wind for BETs can meet only 42% of annual electricity demand. It is because the wind electricity that can be stored is limited by battery size and the absence of grid electricity. On the other hand, the wind can only meet nearly 65% of the annual hydrogen demand for FCETs. This technical refuelling performance is an impact of the discontinuation of grid electricity supply and the size limitation of electrolyser to produce hydrogen during the available wind. Both systems are unable to supply the demand mostly during summer rather than winter due to insignificant wind occurrence.

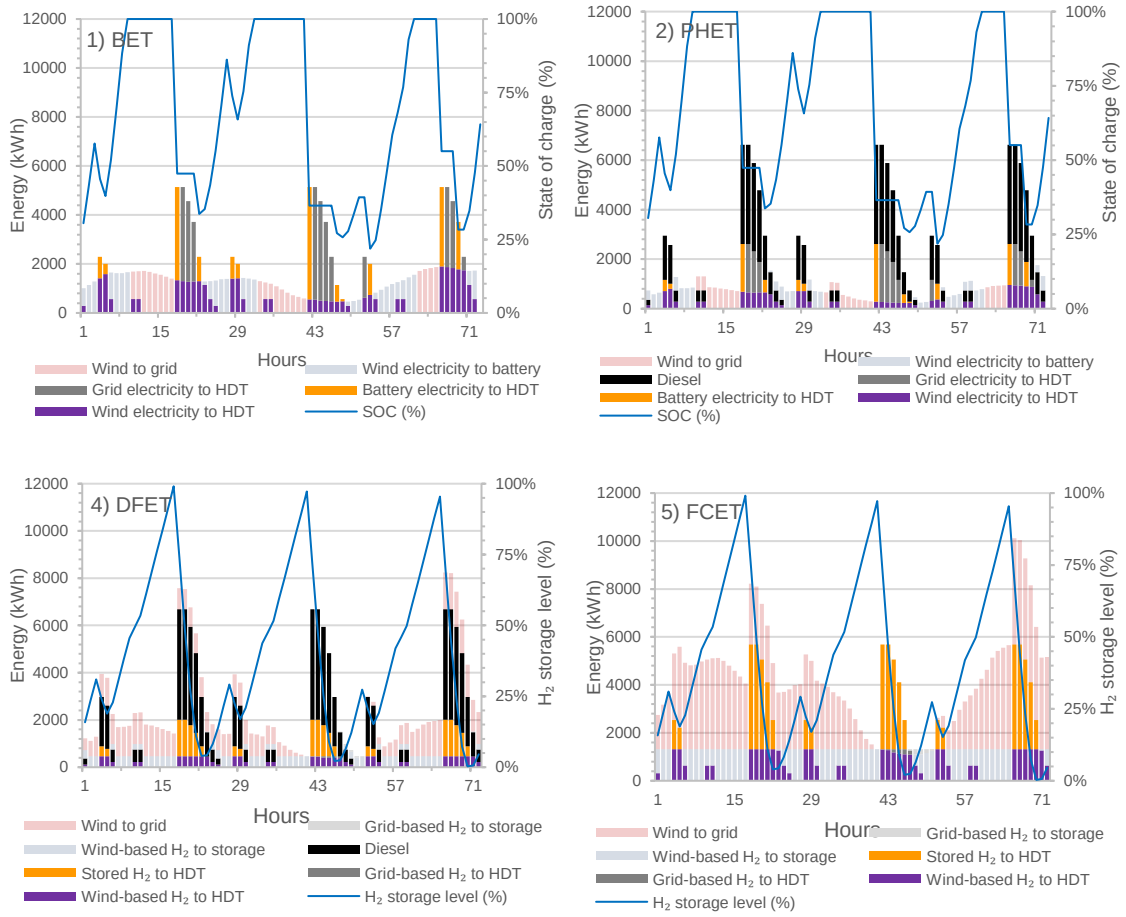

Figure 8.6. Refuelling performance of three summer days for on-grid system

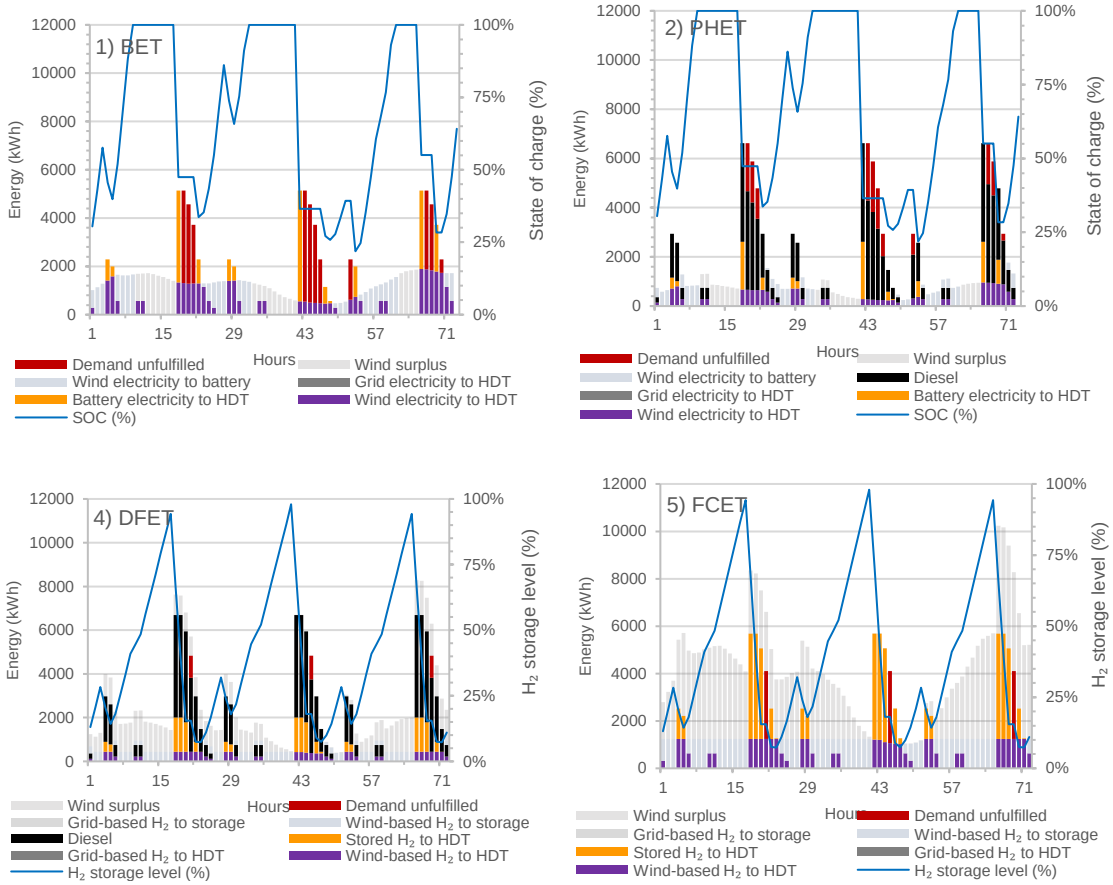

Figure 8.7. Refuelling performance of three summer days for off-grid system

8.4.2. Optimised equipment for off-grid systems

Either wind or battery capacity must be adjusted to meet the electricity demand for the BETs in off-grid system. The same approach is required to increase wind and electrolyser capacities for FCETs. This study implements a similar method introduced by Gunawan et. al [143]. For the BETs, the coverage of energy demand is iteratively calculated by increasing battery and wind capacity until all the demand is met with minimum TCO, as shown in Figure 8.8. For FCETs, electrolyser and wind capacities are enlarged until all the energy demand is met at minimum TCO as shown in Figure 8.9. The trade-off by increasing wind capacity is that the system generates more surplus energy at the site. This surplus wind reduces the usable electricity accounted for BETs

or FCETs. As a consequence, fuel costs for off-grid systems are higher compared to on-grid systems.

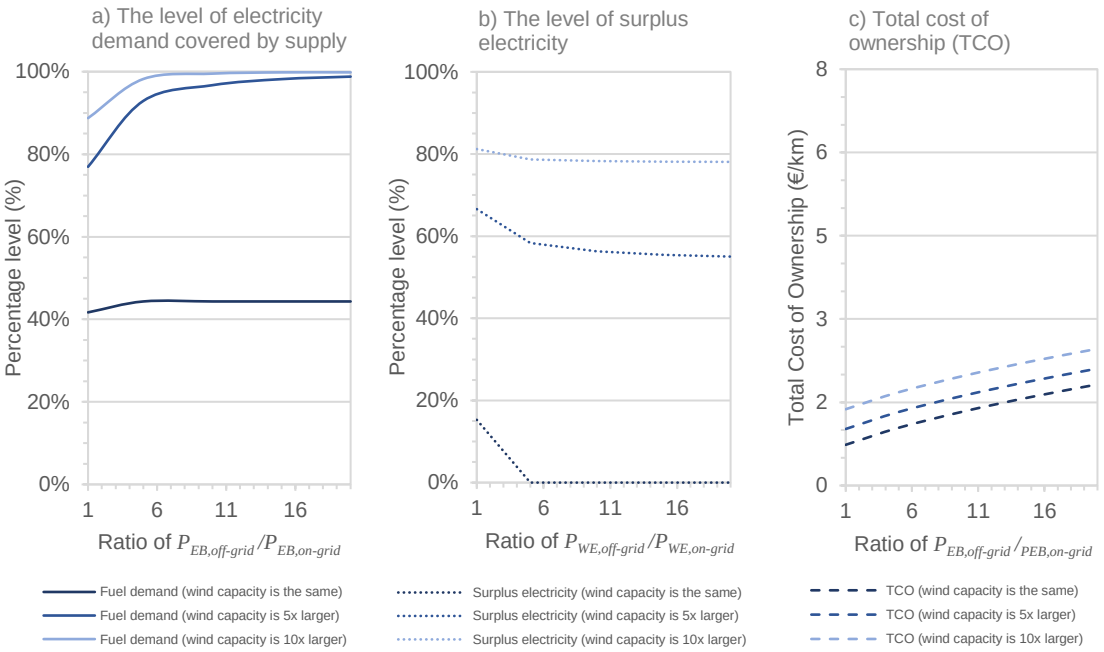

Figure 8.8. Impact of equipment sizes to (a) electricity demand, (b) surplus electricity, and (c) total cost of BETs ownership in an off-grid system

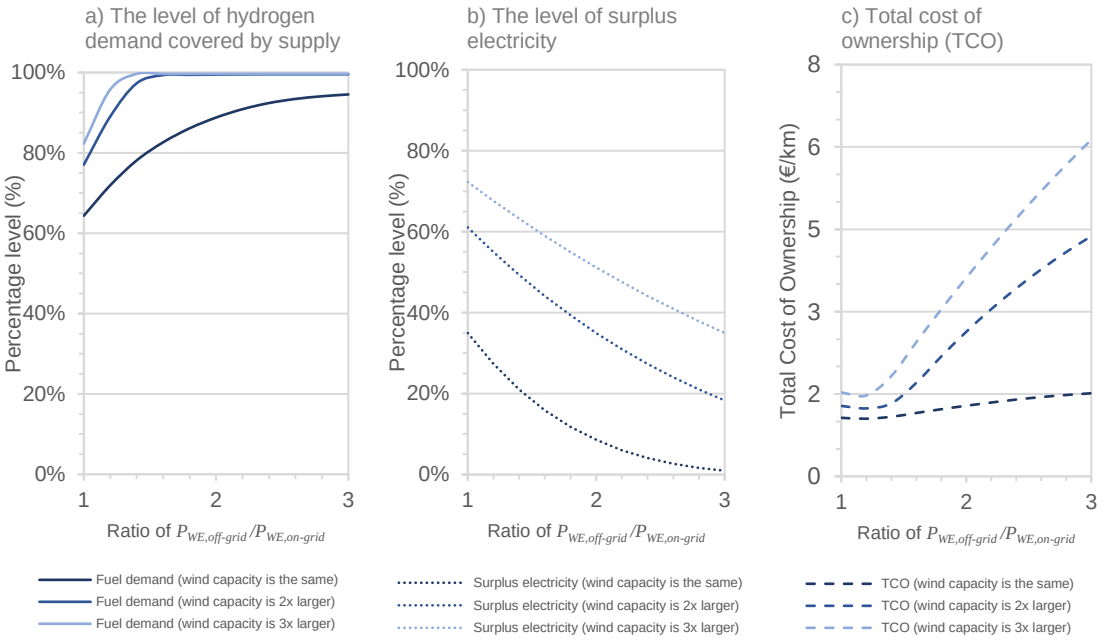

Figure 8.9. Impact of equipment sizes to (a) hydrogen demand, (b) surplus electricity, and (c) total cost of FCETs ownership in an off-grid system

8.4.3. Truck ownership costs for the on- and off-grid system

The total costs of ownership for fleets of 100 HDTs for all powertrains and systems are shown in Figure 8.10 It can be analysed that fuel cost is the most significant contributor for all powertrains in on-grid system except BET, which also dominated by infrastructure cost. For on-grid system, the BET has the lowest TCO of 0.82 €/km among ZLETs. The PHETs also show relatively low TCOs. However, the battery and charger costs affect the significant increase in infrastructure cost for BETs and PHETs in off-grid system. In off-grid system, DFETs shows better techno-economic performance than other powertrains even though the infrastructure cost also increases. The fuel cost for each powertrain is also shown in the same figure. The significant increase of fuel cost occurs on all ZLETs in off-grid system compared to on-grid system due to the escalation of required wind capacity and surplus wind energy.

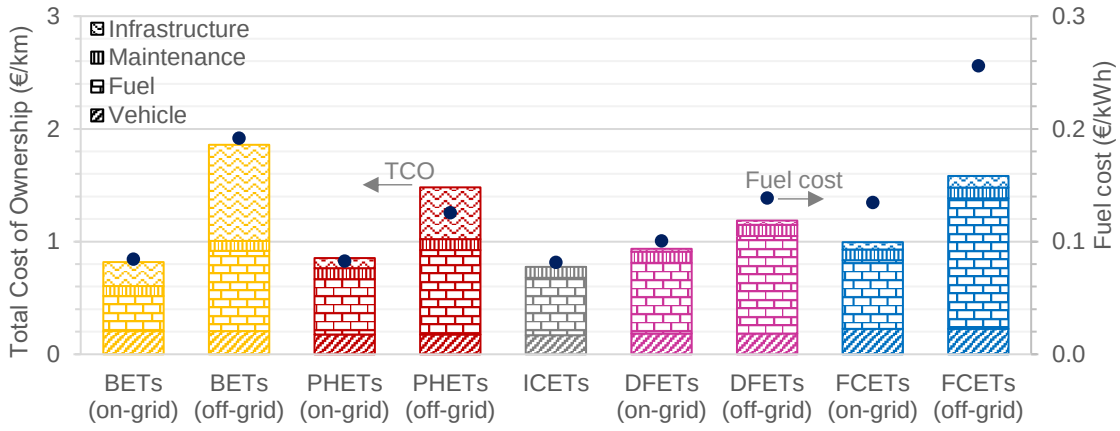

Figure 8.10. The total cost of ownership for on- and off-grid system

The impacts of the number of trucks on TCO and required wind capacities in on- and off-grid systems are shown in Figure 8.11. The TCOs for ZLETs are gradually reduced by increasing the number of trucks due to the system's economy of scale. Hydrogen-based trucks (FCETs, DFETs) require the most wind capacity in on-grid system among ZLETs due to the low overall energy efficiency. Conversely, battery-based trucks (BETs,

PHETs) require the least. In off-grid situations, zero-emissions vehicles (FCETs, BETs) require higher installed capacities than low-emissions vehicles (DFETs, PHETs).

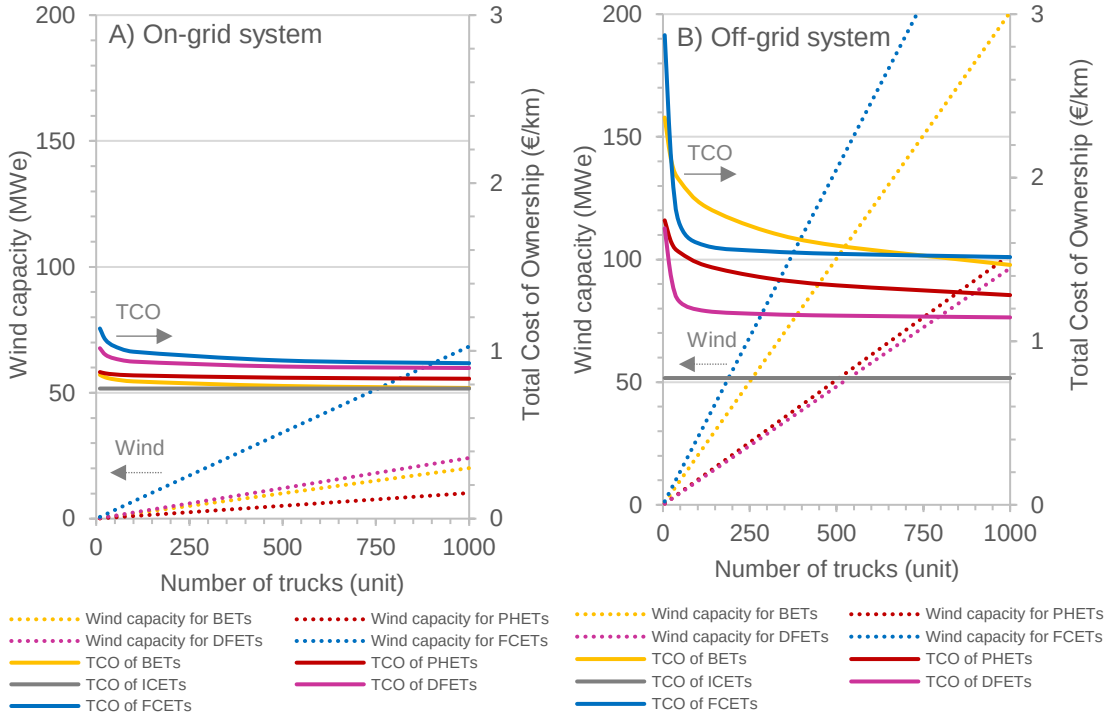

Figure 8.11. Dependence of the total cost of ownership and the required wind capacity on the number of trucks for on- and off-grid system

8.4.4. Carbon abatement costs for the on- and off-grid system

The total cost of carbon abatement for fleets of 100 HDTs for all powertrains and systems are shown in Figure 8.12. The TCAs are decreased by increasing the carbon tax since more expensive diesel results in a smaller gap between TCOs for ICETs and ZLETs. BETs obtain the lowest TCA for on-grid systems at 64 € per tonne of CO_2 at carbon tax of 80 € per tonne of CO_2 emitted. By using the same carbon tax, DFETs results in the lowest TCA for off-grid systems at 878 € per tonne of CO_2.TTW emissions are the largest contributor of emissions for ICETs, PHETs and DFETs due to diesel combustion. Only emissions for 2030 electricity generation are accounted for in WTT emission for on-grid BETs and FCETs. Off-grid systems exclude grid electricity supply, so all powertrains

result in lower WTT emission than on-grid systems. Depending on the diesel ratio, WTW emission varies from 0 to 29 kilotonnes. When all fuel is produced from renewables and zero-emission trucks such as BETs and FCETs are operated, zero WTW emissions can be achieved in off-grid systems. The results of total carbon abated and its costs for different number of HDTs are given in Figure 8.13. It can be seen that the more ICETs are replaced by ZLETs, the more carbon can be abated at lower costs.

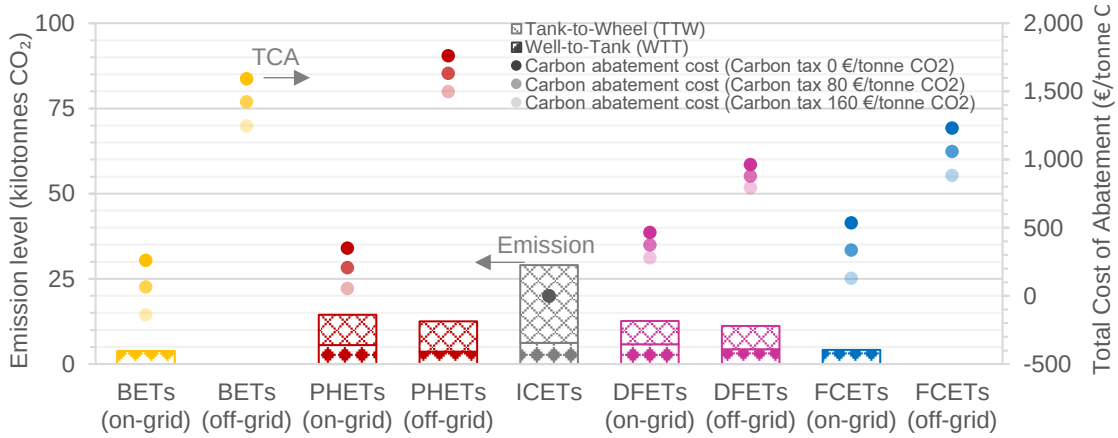

Figure 8.12. Emission level and total cost of carbon abatement for all scenarios

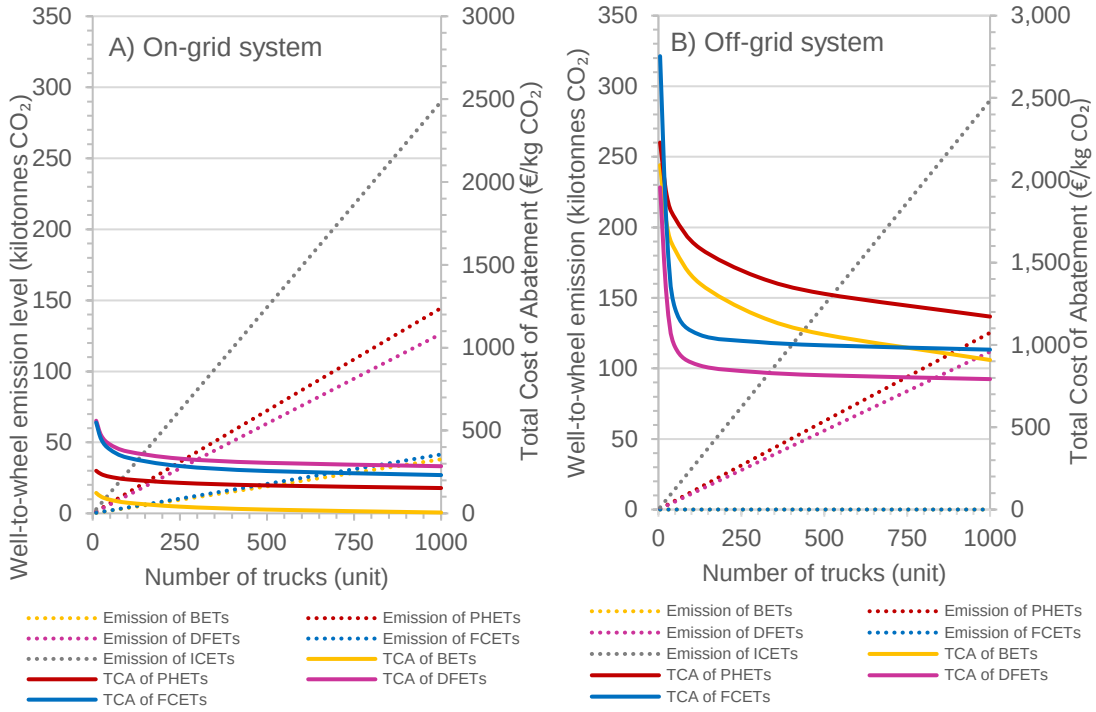

Figure 8.13. Dependence of the total cost of carbon abatement and the well-to-wheel emission on the number of trucks for on- and off-grid systems

8.4.5. Sensitivity analysis for the on- and off-grid system

The sensitivity analysis is performed for (1) technical parameters (wind capacity factor, electrolyser efficiency, and operational travel distance), (2) economic parameters (discount rate, electricity, and diesel prices, and (3) environmental parameters (fuel economy, diesel and grid emissions). The impact on TCA in percentage can be evaluated by changing the parameters' values by -10% and +10% of initial values as shown in Figure 8.14. In both on- and off-grid systems, diesel price and emissions impact all powertrains due to the fact that all TCAs are calculated relative to ICETs. The other sensitive parameters for the BETs and PHETs are electricity price for on-grid systems. The electrolyser efficiency can also broadly impact the TCA of DFETs and FCETs, particularly for on-grid systems.

Figure 8.14. Sensitivity analysis for technical, economic, and environmental parameters

8.5. Conclusions

This chapter presents the results of techno-econo-environmental modelling of producing electricity for fleets of (1) battery electric trucks (BETs) and (2) plug-in hybrid electric trucks (PHETs), supplying diesel for fleets of (3) internal combustion engine trucks (ICETs), and producing hydrogen for fleets of (4) diesel-hydrogen dual fuel engine trucks (DFETs) and (5) fuel cell electric trucks (FCETs). Fleets operating on and off the electricity grid are modelled. The key parameter used to evaluate alternative powertrains is the total cost of carbon abatement (TCA), calculated from the total cost of ownership (TCO) and well-to-wheel (WTW) emissions. The TCO submodel includes fuel production, required refuelling infrastructure, vehicle technology, and maintenance needed for each heavy-duty trucks' (HDTs) powertrain. Required data comprises hourly wind capacity

factor, number of trucks, annual operational distance, and fuel economy for each powertrain. Thus, electricity and hydrogen production capacity and their costs can be calculated and sized to meet the annual energy demand from the HDTs.

For on-grid systems, all ZLETs benefit from available and stable grid electricity. Equipment can be optimally sized based on energy demand with the availability of grid electricity. For off-grid systems, equipment to deliver the required electricity or hydrogen fuel must be enlarged to meet the entire HDTs' fuel demand. Otherwise, only 42% and 62% of total fuel demand can be met for BETs and FCET, respectively. The significant increase of wind capacities and battery sizes, in the case of BETs, in off-grid systems requires significant additional electricity and infrastructure costs. The increase of wind and electrolyser capacities are relatively small to satisfy all demand from DFETs and FCETs in an off-grid system.

TCO and TCA of all powertrains for on-grid systems are lower compared to those for off-grid systems. In contrast, emissions for all powertrains are lower off-grid compared to on-grid due to the GHG intensity of grid electricity. For 100 HDTs operating for relatively short distances, the minimum TCO and TCA for on-grid systems are found for BETs. Even though DFETs are less efficient than BETs, they are more likely to be used due to the lower TCO in off-grid systems. The more ICETs that are replaced by ZLETs, the lower the TCO and TCA that can be achieved due to economies of scale.

This study provides insight into direct coupling opportunities between wind energy and HDTs and challenges of harnessing variable power either with (i) batteries to supply BETs and PHETs continuously, or (ii) electrolysers to produce hydrogen for DFETs and FCETs. BETs require small wind capacity compared to FCETs in on-grid systems. However, BETs require much larger wind capacity and significant battery sizes in off-grid

systems. Therefore, BETs are more likely to be utilised by on-grid quarries, but not in off-grid ones.

Several areas can be further studied in the future, including (1) direct coupling between renewable power and heavy-duty transport for longer operational distance such as logistic or retail purposes, (2) additional renewable sources other than wind, and (3) hydrogen utilisation for other off-grid systems including isolated regions and islands.

8.6. Final remarks

This chapter presents the performances of full techno-econo-environmental modelling on hydrogen production from wind electricity and dispensing to hydrogen-fuelled trucks as well as comparison to the other trucks' technologies which fuelled by electricity. The typical operational distance of quarry trucks is 150 km/day. For this reason, all the emerging powertrain in ZLTEs are able to complete the typical quarry missions. TCA supports the evaluation on performances of carbon abatement for each technology. On- or off-grid system has significant impact to the either TCO or TCA.

In Chapter 9 the developed techno-econo-environmental model is assessed to the regional hydrogen hub for the wider applications on hydrogen vehicle types. Galway city in western Ireland is used as a case study to represent a typical small to medium size of European front city.

Chapter 9. Modelling a Regional Hydrogen Hub Incorporating Multiple Vehicle Fleets

9.1. Overview

This chapter presents the results of modelling of a regional hydrogen hub (RH2). Galway City and the renewable resources that surround it is taken as a case study of such an RH2. Hydrogen can be generated at one or more wind farms in the region to decarbonise multiple vehicle fleets that are currently fuelled by diesel. The hydrogen production capacity of an electrolyser size that meets the hydrogen demand is selected as the optimum size. The electrolyser operates by using (1) curtailed and (2) available wind. Three different scenarios are developed to evaluate the parameters, (I) scenario 1 represents a small scale RH2 with hydrogen capacity of less than 100 tonnes per year, (II) scenario 2 represents a medium scale RH2 of less than 500 tonnes per year, and (III) scenario 3 represents a large scale RH2 of up to 1,000 tonnes per year. The key parameters to evaluate the decarbonisation costs of multiple vehicles are the levelised cost of hydrogen fuel ($LCOH_F$), the total cost of ownership (TCO), and the total cost of carbon abatement (TCA). The TCOs (€/km) and TCAs (€/tCO_2) are calculated for hydrogen fuel cell electric buses (FCEBs), cars (FCECs) operating in taxi fleets, refuse collectors (FCERs), and a passenger ferry (FCEF). The methods used in this study can be applied in any comparable setting. Results show the calculated $LCOH_F$ for all

scenarios varies from 5 to 12 €/kg by 2030. At a large hydrogen hub, the TCOs of the multiple hydrogen fleets are found 14% to 50% more expensive than diesel fleets. The highest TCAs are found for hydrogen-fuelled taxis due to high operational cost while abating lower overall emissions than other vehicles.

9.2. Introduction

The objectives of this chapter are (1) to model a regional hydrogen hub (RH2) that consists of a wind-hydrogen system (WHS), hydrogen transportation by using tube trailer, and a hydrogen refuelling station (HRS), (2) to size the optimum electrolyser size for RH2 using the levelised costs of hydrogen (LCOH), and (3) to evaluate the total costs of vehicle ownership (TCO) and carbon abatement (TCA) for multiple hydrogen vehicles. The methodology in the following section gives a detailed description of the systems and scenarios, hydrogen supply, refuelling profile, hydrogen demand, greenhouse gas emission profile, and overall model. Afterwards, the results and discussion section covers electrolyser sizing for all scenarios of each electrolyser operation scenario, the capacity factor of each electrolyser operation scenario, the levelised cost of hydrogen fuel for all scenarios, and the total costs of vehicle and carbon abatement for all scenarios. Finally, the overall findings of the work are presented in the conclusions section.

9.3. Methodology

9.3.1. Systems and scenarios

A regional hydrogen hub (RH2) is an integrated system of infrastructure to produce, transport, and dispense hydrogen for hydrogen vehicles. The scale of this infrastructure

depends on the regional potential of hydrogen production and consumption. An RH2 is modelled to produce hydrogen (I) from either using only curtailed or available wind, (II) at a wind farm or a hydrogen refuelling station (HRS) and (III) for one type of vehicle or multiple types of vehicles. The hydrogen vehicles in this study comprise (1) the hydrogen fuel cell electric buses (FCEBs) for the city bus network, (2) fuel cell electric cars (FCECs) for the taxi fleet, (3) fuel cell electric refuse collectors (FCERs) for municipal waste collection, and (4) fuel cell electric passenger ferries (FCEFs) connecting the city's port and nearby islands.

The region around Galway city in Ireland is used as a case study for RH2. The city has approximately 80,000 inhabitants, which represents a small to medium-sized European waterfront city. The RH2 is evaluated based on 3 scenarios of the scale of hydrogen production and consumption, which are summarised in Table 9.1. In Scenario 1 (small hub), hydrogen is produced at a wind farm and transported using tube trailers to a HRS to supply several public city bus fleets. Scenario 2 (medium hub) has the same production and transportation arrangements as Scenario 1 but fuels more buses. Scenario 3 is a large hub that generates hydrogen onsite at a HRS that fuels multiple vehicle fleets. In scenario 3, hydrogen is produced using wind electricity from all nearby wind farms connected to the same transmission substation of 110 kV, located approximately 2 km from the proposed HRS.

Table 9.1. Description of scenarios

Scenario number	1	2	3
Scenario name	Small hub	Medium hub	Large hub
H_2 annual capacity	1 – 100 tonnes/year	100 – 500	500 – 1000
H_2 production site	Galway Wind Park	Galway Wind Park	A hypothetical HRS
Wind electricity sources	• Galway Wind Park	• Galway Wind Park	• Galway Wind Park • Lettergunnet • Knockalough • Letterpeck
H_2 end-users	• 5 FCEBs	• 40 FCEBs	• 50 FCEBs • 470 FCECs • 15 FCERs • 1 FCEF

Figure 9.1 shows the distribution of existing wind farms, 110 kV transmission lines and substation, the hypothetical HRS, taxi rank, bus depot, city port, and recycling centres. The red line illustrates the shortest hydrogen transportation route of 36 km for scenario 1 and 2 to connect the hydrogen production site at a wind farm and a HRS. A hypothetical HRS is intended to be built in the city centre nearby the bus depots, taxi rank, and city port. Thus, hydrogen can be supplied to the hydrogen-fuelled city buses, taxi fleets, refuse collectors, and a passenger ferry.

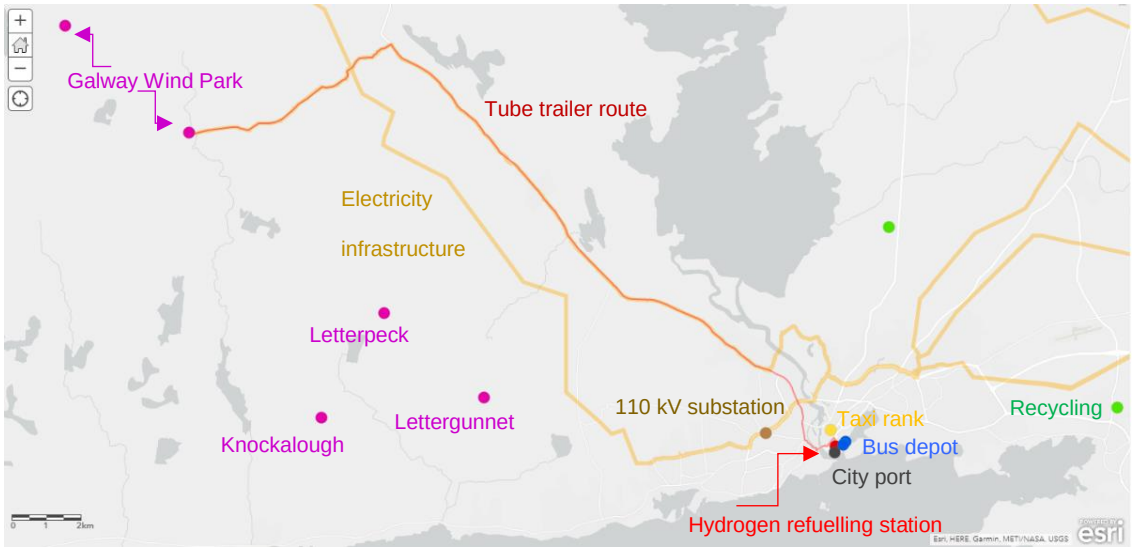

Figure 9.1. Regional power and transport infrastructures in Galway, Ireland

Figure 9.2.a. shows the required equipment to produce hydrogen off-site of the HRS for scenarios 1 and 2. The route of hydrogen transportation by tube trailers is shown in the same figure. In comparison to scenario 3, RH2 excludes the transportation system since hydrogen is produced on-site at the HRS as shown in Figure 9.2.b. The detailed method to calculate hydrogen production from a wind farm or transmission substation is described in the following hydrogen supply subsection. For transportation, this study uses the model previously described in Section 6.3.3. Hydrogen dispensing to meet the hydrogen demand for each vehicle is described in the refuelling profile subsection. The hydrogen demand subsection covers how to model the hydrogen demand for these hydrogen vehicles. Afterwards, the emission model is explained in the greenhouse gas emission profile subsection. Finally, all the involved models in this study are given in overall model subsection.

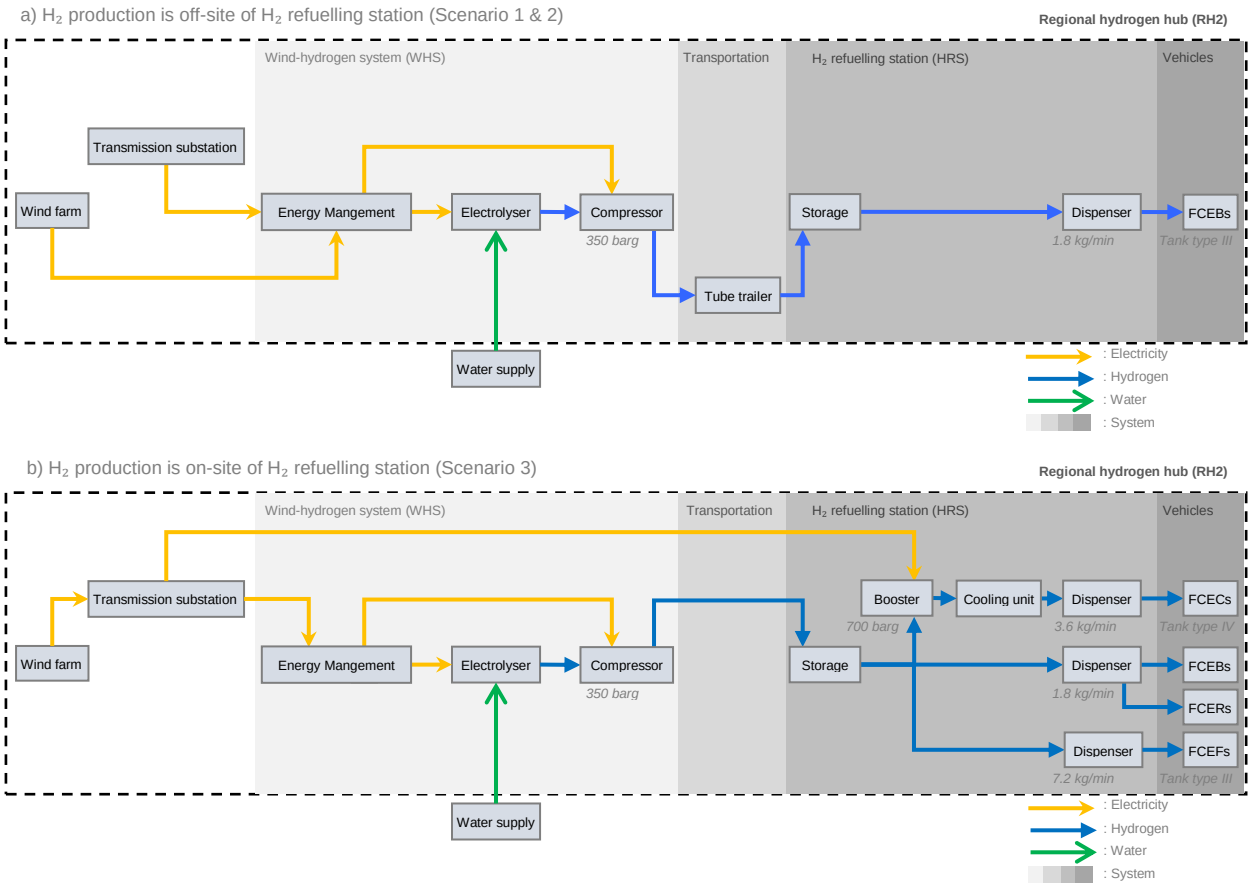

Figure 9.2. Block diagram of equipment for (a) hydrogen production is off-site of hydrogen refuelling station (Scenario 1 & 2), and (b) hydrogen production is on-site of hydrogen refuelling station (Scenario 3)

9.3.2. Hydrogen supply

In this study, the levelised cost of hydrogen fuel ($LCOH_F$) and production ($LCOH_P$) are previously described in Section 6.3.1 and can be calculated using Equation (6.2) and (6.3), respectively. The method to calculate hydrogen production is also previously given in Section 6.3.2 and calculated using Equation (6.6). In terms of the electrolyser sizing, the hydrogen production of an electrolyser size that meets the hydrogen demand is selected as the optimum size in this study. The following paragraph describes the wind electricity for electrolyser in RH2.

Two 110 kV transmission lines connect four existing wind farms to a 110 kV substation. The capacities and number of turbines for these wind farms listed in Table 9.2. The historical data of hourly generated wind electricity from 01/01/2020 to 31/12/2020 is obtained from the Single Electricity Market Operator (SEMO) [236]. The required data are the daily meter data (metered generation by unit), dispatch quantity, and actual availability. The hourly curtailed (CW) and exportable wind (EW) then can be calculated by using these three types of data following the model described in Section 3.3.3. for all wind farms, except Letterpeck wind farm, which due to its relatively small size is not recorded by SEMO. The Letterpeck and Lettergunnet wind farms are only separated by 1 km. The hourly curtailed and exportable wind electricity of Letterpeck ($E_{CW/EW,W4}$) is therefore calculated using Equation (9.1). Where $\lambda_{CW/EW,W2}$ is Lettergunnet hourly curtailed or exportable wind capacity factor and $P_{WF,W4}$ is the capacity of Letterpeck. The $\lambda_{CW/EW,W2}$ is calculated using Equation (9.2). Where $E_{CW/EW,W2}$ is curtailed and exportable wind electricity of Lettergunnet, $P_{WF,W2}$ is wind farm capacity of Lettergunnet, and t is the operational hours.

$$E_{CW/EW,W4(t)} = P_{WF,W4} \times \lambda_{CW/EW,W2(t)} \tag{9.1}$$

$$\lambda_{CW/EW,W2(t)} = \frac{E_{CW/EW,W2(t)}}{P_{WF,W2} \times t_{(t)}} \tag{9.2}$$

Table 9.2. Wind farms connected to 110 kV Salthill substation

No.	Name of wind farm	Capacity (MWe)	Turbines (unit)
W1	Galway Wind Park	169.0	58
W2	Lettergunnet	40.9	10
W3	Knockalough	35.2	11
W4	Letterpeck	16.1	7

In scenario 3, the hourly curtailed or exportable wind electricity delivered to the transmission substation (W5) is calculated using Equation (9.3). It represents the sum of all curtailed or all exportable electricity from all wind farms listed in Table 9.2.

$$E_{CW/EW,W5(n)} = \sum_{t=n}^{n}\left(E_{CW/EW,W1(n)} + E_{CW/EW,W2(n)} + E_{CW/EW,W3(n)} + E_{CW/EW,W4(n)}\right) \quad (9.3)$$

The economic lifetime of the system for all three scenarios is 20 years, with a discount rate of 5%. The curtailed, exportable and grid electricity prices are 2.5, 4.5 and 13 c/kWh, respectively. The techno-economic parameters in 2020 for the model are given in Table 9.3. The capital cost of a PEM electrolyser is expected to decrease by 51% to 2030 [140]. Additionally, the specific energy consumption of a PEM electrolyser is projected to improve by 9% in 2030, compared to 2020 [140]. The costs of high-pressure storage and precooling equipment are expected to decrease by 45% by 2030 [47]. Dispensers and compressors can even reduce 60% of the current cost [47].

For transporting hydrogen, the method previously described in Section 6.3.3. is used to model the hydrogen transportation for scenario 1 and 2. For dispensing hydrogen, the modelling of the HRS for all scenarios uses the model described in Section 6.3.4. In this study, all the hydrogen multiple fleets use hydrogen with a pressure of 350 barg, except FCECs that use 700 barg. Therefore, an additional compressor is located at the HRS for scenario 3. The modelling of the pre-cooling unit is described in the following subsection of the refuelling profile. This study excludes the capital cost for the 2-km grid connection between the transmission substation and HRS due to a lack of available data. However, the cost to install a 1,000 kVA connection in the United Kingdom is approximately € 335,000 [206].

Table 9.3. Techno-economic parameters of the hydrogen production site, transportation, and hydrogen refuelling station

	Units	Value	Ref.
Energy Management Unit (EMU)			
Technology		Converter and controller	
Efficiency		90%	[42]
CAPEX	€	10% x (C_{WE} + C_{EC})	[98]
Water electrolyser (WE)			
Technology		Proton exchange membrane	
Specific energy consumption, μ	kWh/kg	55	[140]
Stack replacement	years	20 (system), 5 (stack)	[31]
CAPEX, C_{CAPEX}	€	2498 x $P_{WE}^{0.925}$	[98]
OPEX, C_{OPEX}	€	0.2011 $P_{WE}^{-0.23}$ x $C_{CAPEX,WE}$	[115]
Electric compressor (EC)			
Technology		Reciprocating	
Specific energy consumption, μ	kWh/kg	1.7	[115]
Pressure, p	barg	300	[47]
CAPEX, C_{CAPEX}	€	4948 x $P_{WE}^{0.66}$	[98]
OPEX, C_{OPEX}	€	2% of C_{CAPEX}	[47]
Storage vessel (SV)			
Technology		Steel vessel	
Lifetime, τ	years	20	[98]
Working pressure, p	barg	350	[98]
CAPEX, C_{CAPEX}	€	350 x $\dot{M}_{H2}$	[140]
OPEX, C_{OPEX}	€	2% of C_{CAPEX}	[46]
Metallic tube trailer (TT)			
Capacity, $\dot{m}_{TT}$	kg	500	[125]
Pressure, p	barg	300	[125]
CAPEX, $C_{CAPEX,}$	€	232,000	[103]
OPEX, $\dot{C}_{OPEX}$	€/km	2.03	[103]
Retest cost, $C_{R,TT}$	€	30%xC_{TT}	[98]
Refrigeration unit (RU)			
Technology		Air-cooled refrigerator	
Ambient temp., T_{AMB}	°C	20	[237]
CAPEX, C_{CAPEX}	€	-39.89M_{CU}^2+5182 M_{CU} +112523	[47]
OPEX, C_{OPEX}	%	2	[47]
Heat exchanger (HX)			
Technology		Thermal mass	
CAPEX, C_{CAPEX}	€	5523 Q_{HE} + 60.078	[47]
OPEX, C_{OPEX}	%	2	[47]
Dispenser unit (DU)			
Technology		Hydrogen dispenser	
Pressure, p	barg	350/750	[177]
Flow rate, m''_{H2}	kg/min	2	[85]
Dispensing temp., T_{DU}	°C	-40	[177]
CAPEX (hose), C_{CAPEX}	€	35,048 (1), 67,595 (2)	[177]
OPEX, C_{OPEX}	%	2	[46]

9.3.3. Refuelling profile

The HRS refuelling profile for FCECs are obtained from the modelling work of Reddi et. al. [47]. For FCEBs, a previous model described in Section 6.3.4. is also used. The profile for FCERs is assumed to be the same as the profile for the heavy-duty truck as reported by International Council on Clean Transportation [78]. Finally, a study by Pfeifer et. al. shows a refuelling profile for FCEFs [88]. These refuelling profiles are reproduced and illustrated in Figure 9.3.

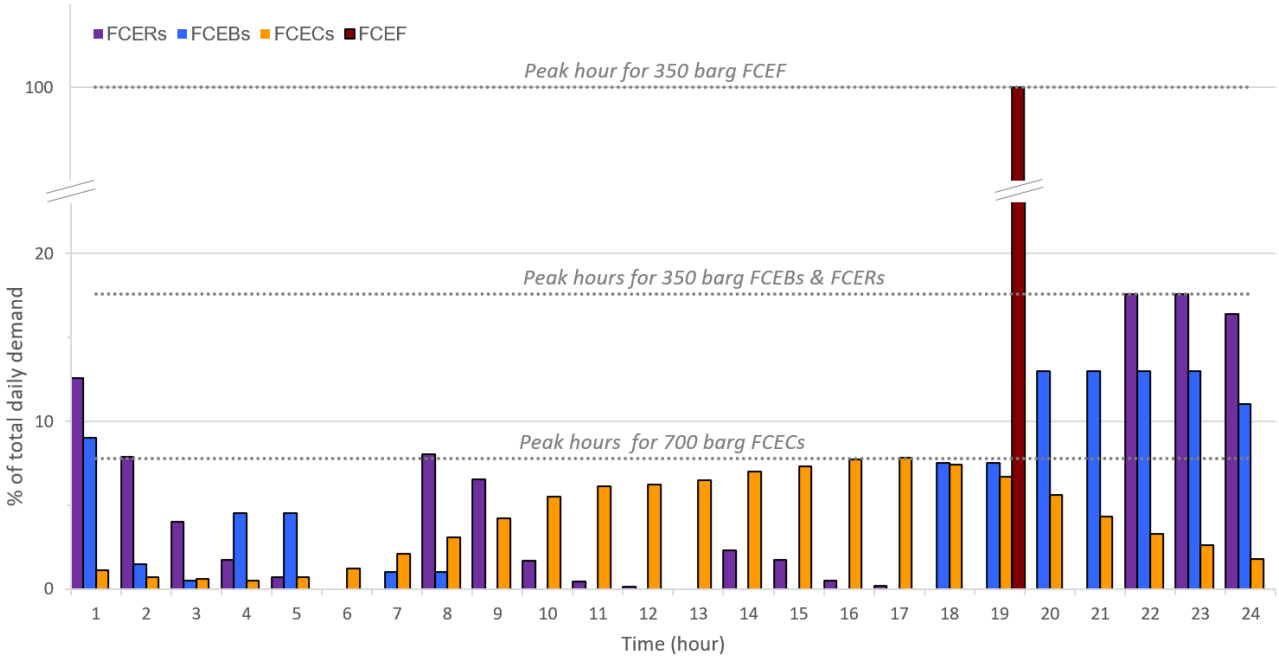

Figure 9.3. Daily refuelling profiles for all urban fleets

It is assumed that the FCEBs, FCECs, and FCERs regularly operate every day throughout the year except for 7 days of maintenance and public holidays. However, FCEF shows a seasonal characteristic, specifically taking more trips in summer than in winter [238], as illustrated in Figure 9.4. At the peak season in July, FCEF operates nine trips per day, which the hydrogen storage must accommodate. FCEF travels 45 km from

the city port to Inishmore in the Aran Islands. The techno-economic parameters of FCEF by Aarskog et. al. [239] are used to model FCEF in this study.

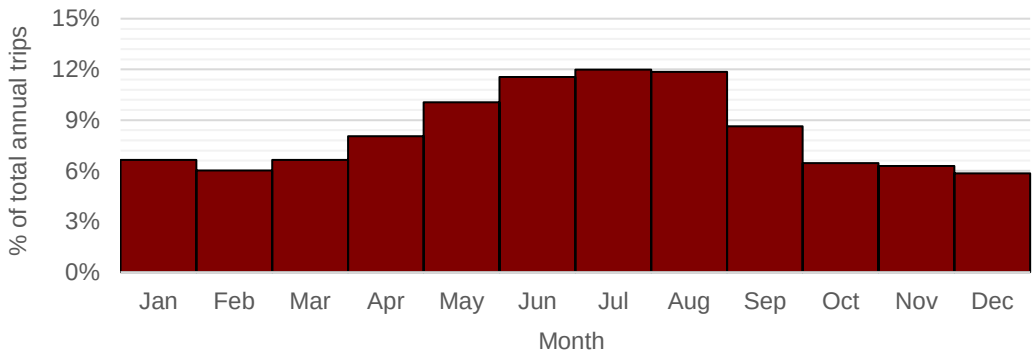

Figure 9.4. Monthly refuelling profile for hydrogen fuel cell electric ferry (FCEF)

There are three different maximum refuelling speeds in the commonly used SAE protocol for hydrogen refuelling dispensers. They are slow fuelling (30 g/s or 1.8 kg H2/min) for FCEBs and FCERs, normal fuelling (60 g/s or 3.6 kg/min) for FCECs, and fast fuelling (120 g/s 7.2 kg/min) for FCEF [165]. The differences in refuelling speeds are defined based on the type and maximum temperature of onboard hydrogen tanks. In general, there are four types of onboard hydrogen tanks. However, only type III and type IV are suitable for vehicular use [240]. They both use full composite wrapping, with metal liner (type III) for FCEBs, FCERs and FCEFs, and plastic liner (type IV) for FCECs. The impact of the mass flow rate and the inlet hydrogen temperature on the final temperature and state-of-charge of hydrogen tanks are stronger for type IV tanks than for type III [241]. Therefore, cooling demand is assumed to be not required for type 3 at 350 barg in this study. Moreover, a new approach with the addition of a pause during hydrogen refuelling can maintain the increase of temperature [242]. However, it is necessary to cool down the hydrogen in the pre-cooling unit from the ambient temperature of 20°C (T_{AMB}) to the dispensing temperature of -40°C (T_{DU}) for FCECs with type IV tanks at 700 barg [237]. So that a normal fuelling time can be safely achieved and a high temperature at hydrogen

tank of 85°C can be avoided [141]. A pre-cooling unit consists of a refrigerator and heat exchanger [85]. Equation (9.4) shows how the required electricity for the refrigeration unit is calculated. The capacity of refrigeration is calculated using Equation (9.5). In this model, the coefficient of Performance (CoP), specific heat ratio (k), specific heat of hydrogen (Cp_{H2}), and gas constant (R) are 1.1, 1.41, 14.7 kJ/kg·K, and 8.314 J/K·mol, respectively [180]. The cooling capacity of the heat exchanger is calculated using Equation (9.6).

$$E_{RU} = \dot{M}_{H2,HD} \times t_{OT} \times \frac{k}{k-1} \times \frac{R}{n_{H2}} \times \frac{T_{AMB} - T_{DU}}{3600} \times \frac{1}{CoP/24} \tag{9.4}$$

$$M_{RU} = m''_{H2,HD} \times N_{HA,HRS} \times Cp_{H2} \times (T_{AMB} - T_{DU}) \times \frac{1}{60} \times \frac{3412}{12000} \tag{9.5}$$

$$Q_{HX} = m'_{H2,HD} \times Cp_{H2} \times (T_{AMB} - T_{DU}) \tag{9.6}$$

9.3.4. Hydrogen demand

In this study, the total cost of vehicle ownership (TCO) is calculated using Equation (8.2) as described in Section 8.3.1. The operation of each FCEV is modelled using the available literature and listed in Table 9.4. The number of vehicles for each scenario is also given in the same table. The techno-economic parameters shown in Table 9.4 are for technology in the year 2020. The capital costs of hydrogen vehicles are projected to be reduced 14%-22% by 2030, compared to 2020 [88], [239].

Table 9.4. Technoeconomic parameters of the vehicle

	Units	FCEB	FCEC	FCER	FCEF
Reference		[200]	[50]	[243]	[88], [239]
Operational parameters	per unit				
Utilisation rate	km/day	250	279	125	45
Operational	day/year	358	358	358	362
Distance, *D*	km/year	89,500	100,000	44,750	16,308
H_2 vehicles	per unit				
Fuel economy$_2$, d'_{H2}	km/kg	10.0	109.0	9.0	1.1
CAPEX of H_2 vehicle	m€	0.60	0.07	0.30	5.12
OPEX of H_2 vehicle (annual)	% CAPEX	2%	2%	2%	2%
Diesel vehicles	per unit				
Fuel economy, d'_{HC}	km/l	2.0	13.6	1.8	0.2
CAPEX of diesel vehicle	m€	0.20	0.02	0.18	3.96
OPEX of diesel vehicle (annual)	% CAPEX	2%	2%	2%	2%

9.3.5. Emission profile

The total cost of carbon abatement (TCA) is calculated using Equation (8.1) as described in Section 8.3.1. Greenhouse gas (GHG) emission modelling uses the well-to-wheel (M_{WTW}) approach in tCO_2/km as shown in Equation (9.7). M_{WTW} is the sum of well-to-tank (M_{WTT}) emission, and tank-to-wheel (M_{TTW}), both of which are calculated using Equation (9.8). The specific WTT GHG emission ($\delta_{WTT,HC}$) for diesel is assumed at 52 gCO_2/kWh with specific energy ($\acute{E}$) of 10.18 kWh/l. The theoretical TTW emission from diesel combustion ($\gamma_{TTW,HC}$) is 2,640 gCO_2/l, or ($\delta_{TTW,HC}$) 264 gCO_2/kWh.

The average GHG intensity of electricity generation in Ireland (δ_{GE}) is 146 gCO_2/kWh. It is assumed that the maximum share of grid electricity in hydrogen production ($x_{WE,GE}$) is to 25%. Electrolyser efficiency (η_{WE}) is assumed at 69%. Specific fuel economy of hydrogen in km/kWh (d_{H2}) can be calculated by dividing fuel economy in km/kg (d'_{H2}) by the lower heating value of hydrogen (LHV_{H2} = 33.33 kWh/kg). The calculated specific emissions (*e*) in gCO_2/km for both diesel and hydrogen are given in Table 9.5.

$$M_{WTW} = \sum_{T=0}^{T=n} \frac{\left(M_{WTT} + M_{TTW}\right)}{\left(1+r\right)^{(T)}} \tag{9.7}$$

$$M_{WTT/TTW} = e_{WTT/TTW} \times \frac{D}{d'} \tag{9.8}$$

Table 9.5. Specific emission of each vehicle

Emission	Well-to-tank (WTT)		Tank-to-wheel (TTW)	
Fuel	Diesel ($e_{WTT,HC}$)	Hydrogen ($e_{WTT,H2}$)	Diesel ($e_{TTW,HC}$)	Hydrogen ($e_{TTW,H2}$)
Unit	(gCO_2/km)	(gCO_2/km)	(gCO_2/km)	(gCO_2/km)
Formula	$e_{WTT,HC} = \delta_{WTT,HC} / d' / \acute{E}$	$e_{WTT,H2} = \delta_{GE}$ x $x_{WE,GE} / \eta_{WE} / d$	$e_{TTW,HC} = \gamma_{TTW,HC} / d'$	-
FCEB	265	176	1,320	0
FCEC	39	16	194	0
FCER	291	197	1,451	0
FCEF	2,229	1,655	11,114	0

9.3.6. Overall model

The techno-economic and GHG emission performances of the regional hydrogen hub (RH2) are modelled in this study. The model uses the levelised cost of hydrogen fuel ($LCOH_F$), total capital expenditure (CAPEX), operational & maintenance expenditure (OPEX), the total cost of ownership (TCO), and total cost of carbon abatement (TCA) to evaluate the decarbonisation costs of multiple fleets. As shown in Figure 4.4, data preparation is needed for technical, economic, and emission models. These models are classified into two categories, supply and demand, as illustrated in the same figure.

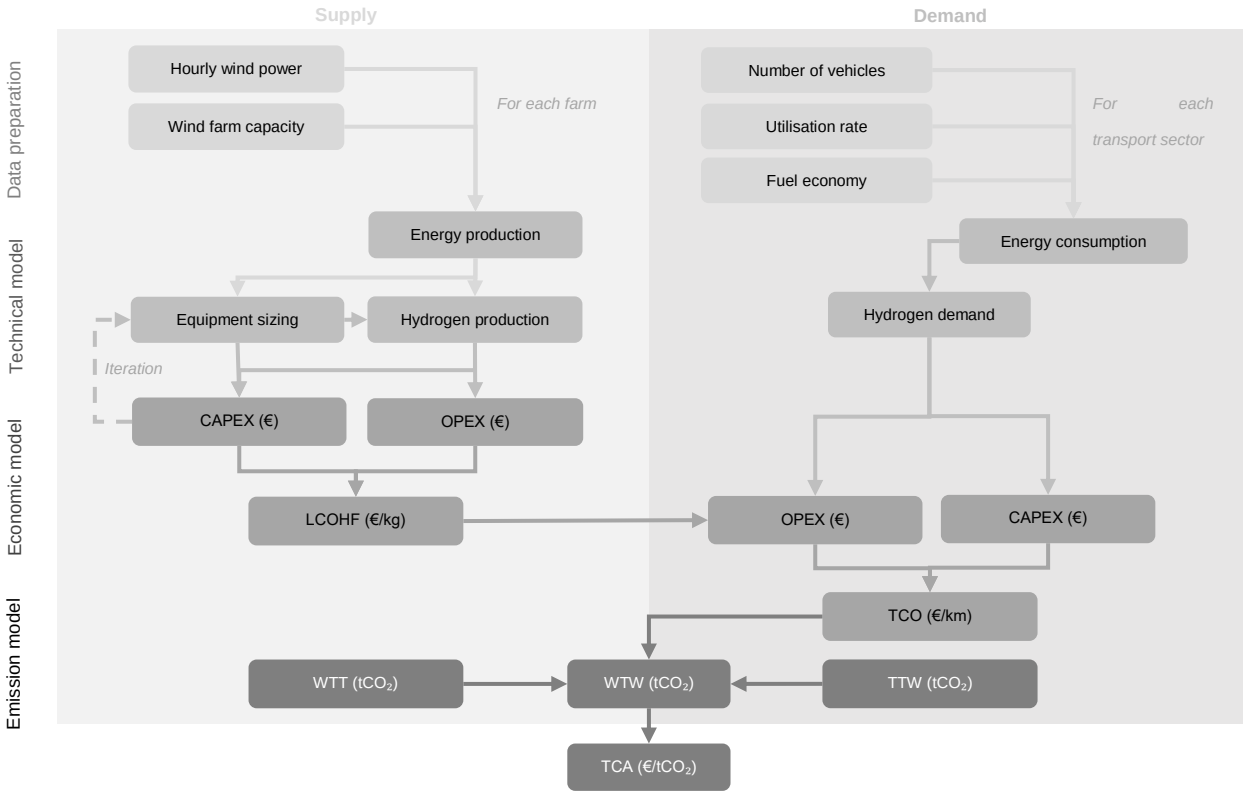

Figure 9.5. Overall model to calculate the total costs of carbon abatement

9.4. Results and discussion

9.4.1. Electrolyser sizing for all scenarios of each electrolyser operation scenario

Annual hydrogen production and $LCOH_P$ vary depending on electricity sources of RH2, as shown in Figure 9.6. The blue and red line colour represents the techno-economic performance of a wind farm and multiple wind farms, respectively. As shown in Figure 9.6.a, the optimum electrolyser sizes to meet the hydrogen demand in scenarios 1, 2 and 3 using curtailed wind are 0.7 MW_e, 6.5 MW_e, and 18 MW_e, respectively. In comparison, the optimum electrolyser to meet the same amount of hydrogen demand for

scenarios 1, 2 and 3 using available wind are 0.3 MW_e, 2.5 MW_e, and 6.5 MW_e, respectively, as shown in Figure 9.6.b.

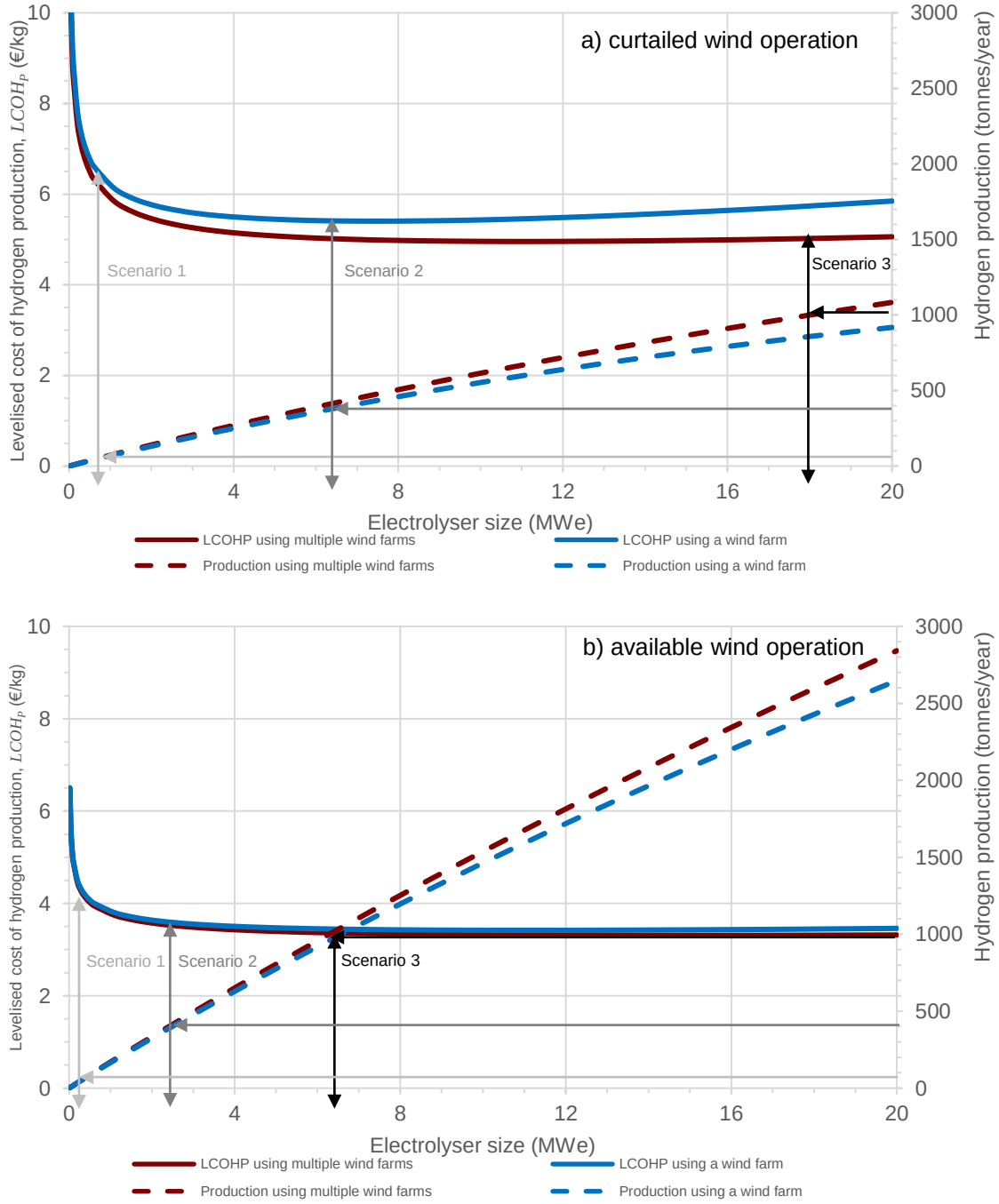

Figure 9.6. Impact of electrolyser size on $LCOH_F$ using a) curtailed wind operation and b) available wind (curtailed wind + exportable wind) for all scenarios

9.4.2. Capacity factor of each electrolyser operation scenario

At an optimum electrolyser size for scenario 2 using available wind, a 2.5-MW_e electrolyser can achieve a capacity factor of nearly 40% when operated by using curtailed wind only as shown in Figure 9.7.a. The input electricity comes from curtailed (92%) and grid (8%, to maintain minimum electrolyser operation) electricity. In contrast, the capacity factor of the electrolyser reaches 92% with available wind, as shown in Figure 9.7.b. Exportable wind replaces most grid electricity to maintain a minimum 5% of electrolyser nominal power. The shares of electricity using available wind operation are 37% for curtailed, 63% for exportable, and less than 1% for grid electricity.

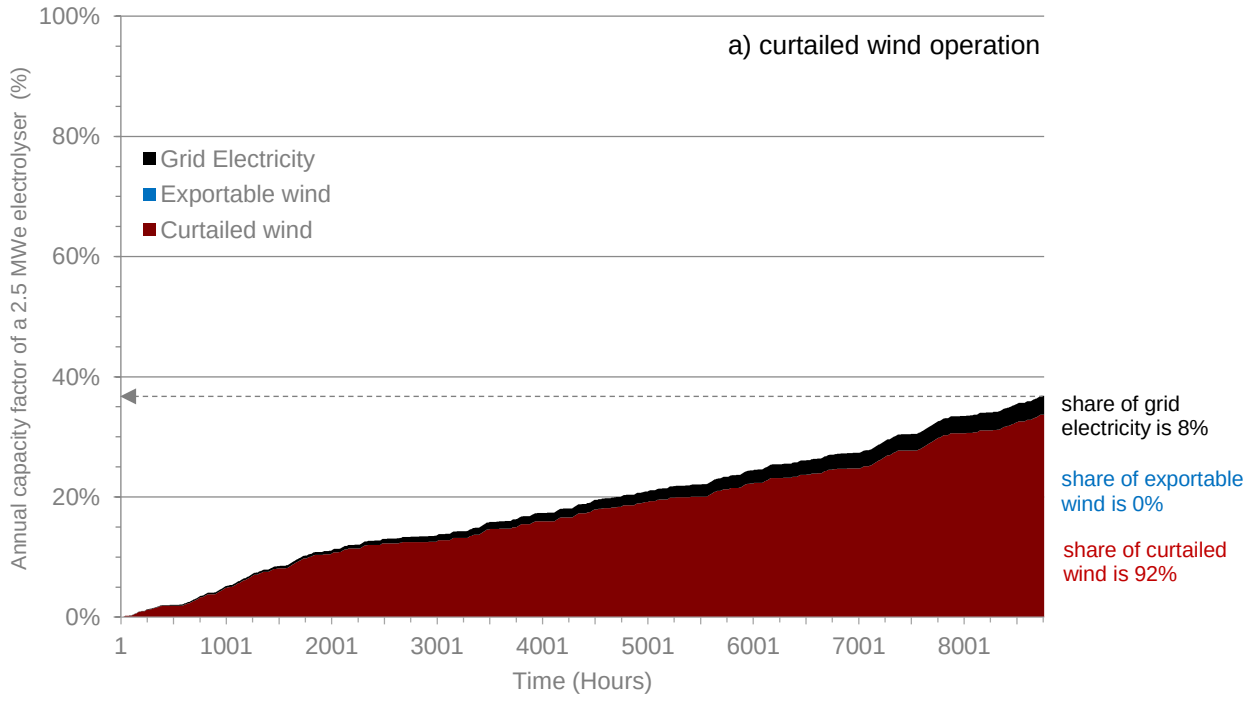

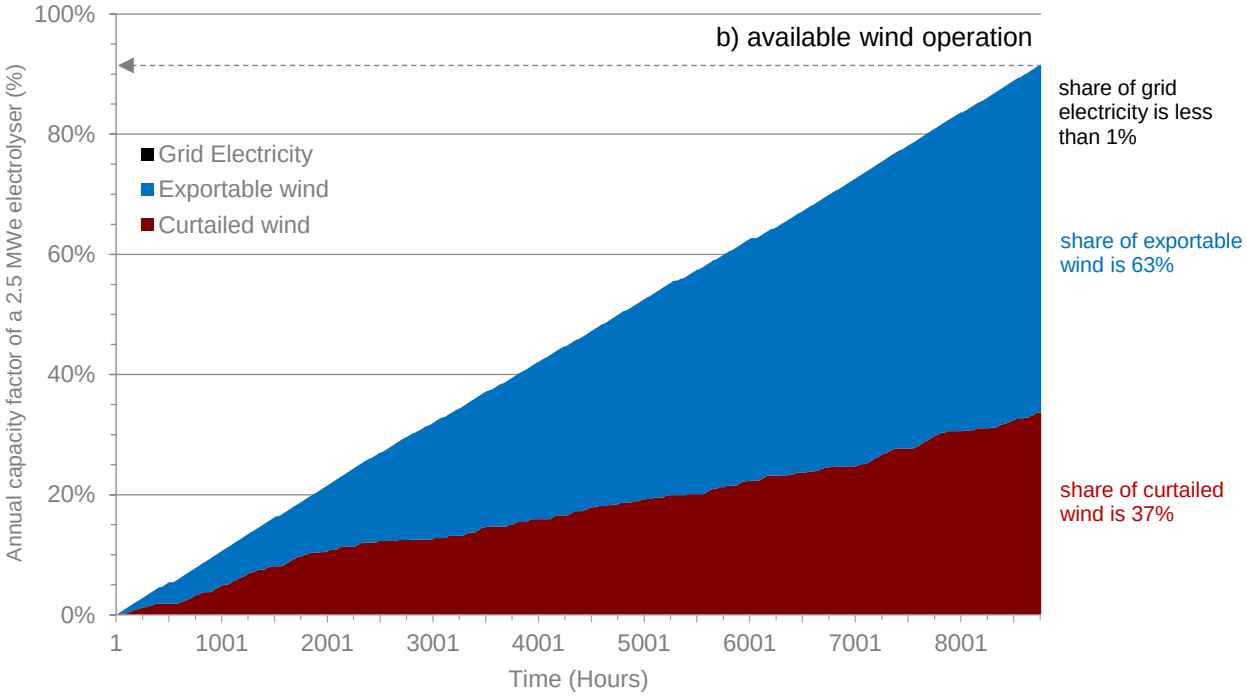

Figure 9.7. Share of electricity at a 2.5 MWe electrolyser of a sample wind farm by using a) curtailed wind operation and b) available wind operation (curtailed wind + exportable wind)

9.4.3. Levelised cost of hydrogen fuel for all scenarios

The $LCOH_P$ found through electrolyser sizing for each scenario in Section 9.4.1. is added to respective hydrogen transportation and dispensing costs to obtain $LCOH_F$ as shown in Figure 9.8. The $LCOH_F$ or total dispensed hydrogen fuel costs vary from 5 to 12 €/kg by 2030. The transportation and dispensing costs in scenario 1 are higher than scenario 2, due to the capacities of hydrogen transported and dispensed are lower than scenario 2. In scenario 3, the share of production cost in $LCOH_F$ is the same for all curtailed wind operation and for all available wind operation. The share of dispensing cost in $LCOH_F$ for FCEBs and FCERs are the same due to sharing the same 350-barg dispensers with 1.8 kg/min, which are also the largest refuelling capacity. In contrast, even though the refuelling capacity for FCECs are large, the dispensing costs are high due to the required extra compression to 700 barg and precooling. The highest dispensing cost is found at

the dispenser for FCEF due to its relative underutilisation. The addition of more hydrogen-fuelled ships would help to address this.

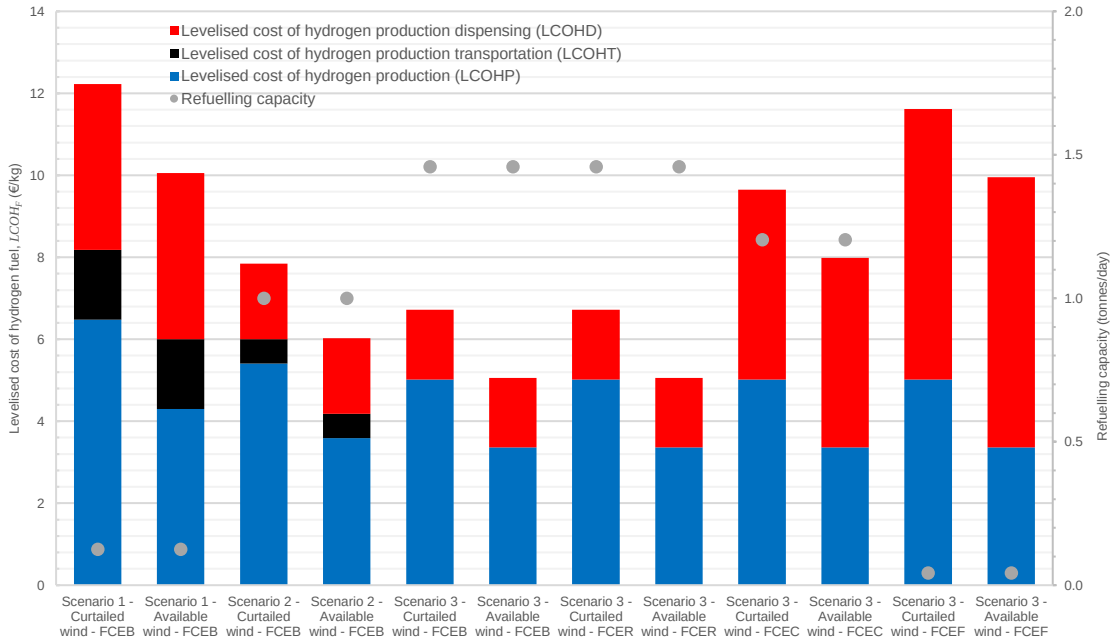

Figure 9.8. Levelised hydrogen fuel ($LCOH_F$) for all multiple vehicles in all scenarios by 2030

If newly developed glass-fibre tube trailers, which are capable of carrying 800 kg of hydrogen at a cost of 300,000 €/unit, are used [245], the $LCOH_T$ for scenario 1 increases by 19% and scenario 2 decreases by 33%. Thus, due to higher investment costs, the glass-fibre tube trailers are not suitable for delivering hydrogen of less than 50 tonnes/day, but are highly suitable for capacities larger than 300 tonnes/day.

9.4.4. Total costs of vehicle and carbon abatement for all scenarios

The total costs of ownership (TCOs) and carbon abatement (TCAs) are given in Figure 9.9. TCOs in scenario 1 show the most significant difference between TCOs for hydrogen and diesel-fuelled buses. TCOs for FCEBs in scenario 1 are 97% higher than diesel if using curtailed wind and 75% higher than diesel if using available wind. In scenario 2, the difference between TCOs for hydrogen and diesel is in the range of 34 to 52%. In

scenario 3, the TCOs of all hydrogen vehicles are 14% to 50% more expensive than diesel vehicles.

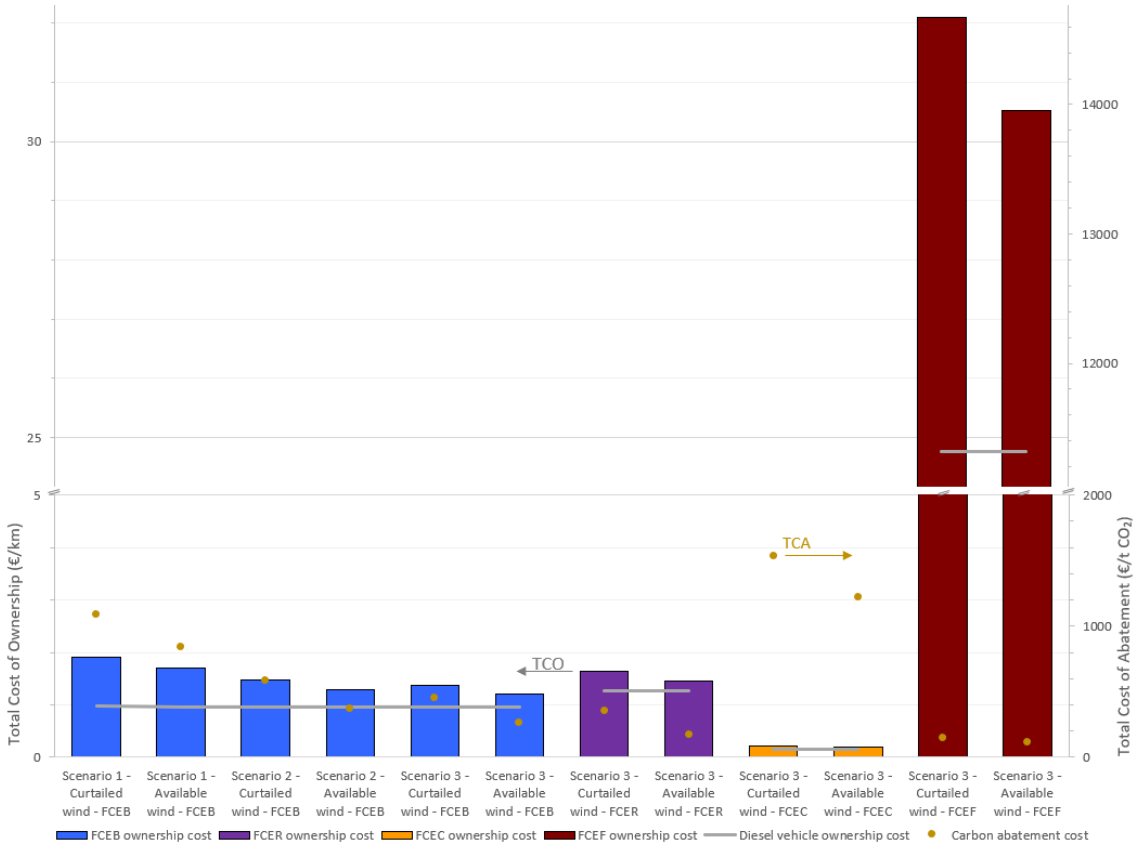

Figure 9.9. Total costs of vehicle ownership (TCO) and carbon abatement (TCA) for all scenarios by 2030

The costs of transitioning diesel to hydrogen fuel for city buses for all scenarios are between 263 and 1089 €/tCO_2. The TCAs for FCERs are 352 €/tCO_2 and 171 €/tCO_2 if using curtailed and available wind, respectively. The results also show that the most significant TCAs are for FCECs in scenario 3 due to it operates with high $LCOH_F$ while abating lower total emission than other vehicles. Finally, the TCAs for FCEF vary in the range of 119 to 151 €/tCO_2.

9.6. Conclusions

This study presents the results of modelling for a regional hydrogen hub (RH2). An RH2 is modelled to produce hydrogen (I) either from using only curtailed wind or the available wind, (II) at a wind farm or a hydrogen refuelling station (HRS) and (III) for one type of vehicle or multiple vehicles. The hydrogen vehicles in this study include hydrogen fuel cell electric buses (FCEBs), fuel cell electric taxi cars (FCECs), fuel cell electric refuse collectors (FCERs), and a fuel cell electric passenger ferry (FCEF). The key parameters of the levelised cost of hydrogen fuel (LCOHF), the total cost of ownership (TCO), and the total cost of carbon abatement (TCA) are used to evaluate three different sizes of RH2 (small, medium, and large) in Galway city.

Results show that the capacity factors of the electrolysers are 40% and 92% if operated with curtailed wind only and available wind, respectively. The low capacity factor for curtailed wind operation affects the need to have large electrolyser sizes to meet the hydrogen demand for the respective scenario. The optimum electrolyser sizes to meet the demand in scenarios 1, 2 and 3 using curtailed wind are 0.7 MW_e, 6.5 MW_e, and 18 MW_e, respectively. In contrast, the optimum electrolyser sizes using available wind for scenarios 1, 2 and 3 are 0.3 MW_e, 2.5 MW_e, and 6.5 MW_e, respectively. The $LCOH_F$ for all scenarios varies from 5 to 12 €/kg by 2030. Even though the total capital, operation, and maintenance expenditures of small RH2 are the lowest compared to the rest of the scenarios, it results in high $LCOH_F$ due to a lack of economies of scale. Moreover, the significant $LCOH_F$ can burden the TCOs. TCOs of scenario 1 are the highest among the evaluated scenarios. In scenario 3, the results show that the most significant TCAs are for FCECs due to high cost in operation while abating lower overall emission than other vehicles.

Future studies could explore new methods to reduce dispensing cost for 700 barg hydrogen. An international safety standard for hydrogen refuelling protocols for extra-large vehicles like maritime crafts is required, particularly for fast refuelling of 7.2 kg/min for a large onboard storage tank of more than 300 kg. The existing standards cover only limited vehicles, mainly road based. An improved algorithm for energy management to capture low wind electricity prices can potentially be investigated to obtain more cost reductions. In addition, a hydrogen-fuelled truck to haul tube trailer can also be evaluated to replace the diesel-fuelled trucks used in this study. An additional cost of a grid connection from transmission substation to HRS of approximately 2 km is also essential for future study. Different incentives or subsidies mechanism can also be explored to support the policymakers in providing a stimulating policy for renewable hydrogen.

9.7. Final remarks

This chapter presents the performances of techno-econo-environmental modelling on the regional hydrogen hub for the broader applications on multiple hydrogen vehicles. The Galway city in the west of Ireland is used as a case study to represent a typical small to medium sizes of European front city. According to the capacity scales of hydrogen production and consumption, scenarios are developed to evaluate the overall costs of hydrogen production, transportation, dispensing and consumption.

In Chapter 10, all the significant findings of the entire previous chapters and suggestions for future work are summarised in the conclusion.

Chapter 10. Conclusions

10.1. Overview

This chapter summarises all the significant contributions, the findings in the previous chapters, and the future studies. The essential contributions of the studies are listed in the contribution section. The overall conclusions are explained in the conclusion section. Finally, suggestions for future studies related to this research are provided in the future works section.

10.2.Contributions

The essential contributions of the research include:

1) An integrated model of renewable hydrogen supply chains that includes hydrogen production, transportation, dispensing and consumption.
2) Optimisation techniques for renewable hydrogen production from various renewable electricity sources, transportation using multiple distribution options, dispensing via various parameters, and consumption to a wide range of vehicle types.
3) A comprehensive modelling framework that includes technical, economic, and environmental aspects of the renewable hydrogen supply chain.

4) Assessment of the modelling framework for multiple configurations of equipment and value chains, technologies, time frames, capacities, and locations.

10.3. Conclusions

The significant findings in this thesis are classified into (1) hydrogen production, (2) hydrogen transportation, (3) hydrogen dispensing, (4) hydrogen consumption, (5) hydrogen costs, and (6) hydrogen demand. Each of these classifications is explained in the following paragraphs.

10.3.1. Hydrogen production

In terms of hydrogen production, the modelling works in this thesis find that wind and solar can produce 100% green hydrogen. The levelised costs of hydrogen (LCOH) is an essential parameter for equipment sizing in hydrogen production systems. For curtailed wind operation, the value of LCOH is mainly driven by the capital cost of electrolyser, which depends on the electrolyser size. Therefore, large hydrogen demand can lead to the use of a large electrolyser, which reduces the specific electrolyser cost. The optimum equipment sizes for producing hydrogen are selected at the minimum LCOH. Even though at its minimum LCOH, most of the hydrogen production costs are still expensive if current technologies are used, particularly for small wind and solar farms. Therefore, for small farms (< 5 MWe), it is important to consider increasing the capacity factor of electrolyser to full capacity. It is also clear that electricity price and capital costs of electrolyser contribute to the large share of hydrogen production costs. The expected reduction of these parameters in the next decade will significantly reduce hydrogen production cost.

10.3.2. Hydrogen transportation

Renewable electricity generators like wind and solar farms are well distributed across the EU. By producing hydrogen at renewable generation sites, hydrogen can be transported to the nearest hydrogen refuelling station. Tube trailers with capacity of 500 to 1,000 kg are sufficient for this purpose, depending on the scale of HRS. The optimum supply chain for this value chain can be investigated and modelled spatially. Additionally, a Geographic Information System can also optimise the costs of transporting hydrogen from production sites to consumption locations.

10.3.3. Hydrogen dispensing

Similar to production, the costs of hydrogen dispensing at a hydrogen refuelling station (HRS) also benefit from economies of scale. The larger the capacity of a HRS, the greater the cost reduction of dispensing each kilogram of hydrogen. Because most of the costs for HRS are invested in the equipment that can benefit from the economies of scale. The HRS equipment can be sized using the equivalent hydrogen demand from various types of hydrogen vehicles. However, the safety standards of dispensing hydrogen are still limited for several types of road vehicles. The standards should also include the dispensing criteria for maritime craft.

10.3.4. Hydrogen consumption

The modelling works in this thesis have shown that the potential of renewable energy is sufficient to meet demand from hydrogen blending, heating, and transportation. For hydrogen blending into the gas transmission network, the ability of the current gas network to receive such a large share of hydrogen is important. Also, insight into technical aspects like large storage for hydrogen is required to maintain the flow rate to exactly meet demand. When hydrogen production from onshore wind for hydrogen

blending does not meet the significant demand in a specific country, hydrogen for this purpose should also be produced using offshore wind. For transport, hydrogen can be an option to fuel heavy-duty transport and ferries, particularly in working environments where the electricity grid is unavailable. The total cost of vehicle ownership (TCO) is helpful for investigating the competitiveness between hydrogen-fuelled vehicles and other technologies. A competitive TCO of hydrogen vehicles is required for adoption of more hydrogen vehicles, leading to more hydrogen supply and demand capacities.

10.3.5. Hydrogen costs

The CAPEX and OPEX of hydrogen production, transportation, dispensing and vehicles can be significantly reduced in the next decade. Most of the CAPEX cost reduction will be due to the impact of mass production of the equipment. Therefore, more hydrogen projects and investments are required to achieve the substantial costs reduction of this hydrogen-related equipment. These projects must be supported by a wide range of research, including developing renewable hydrogen supply chains. Concerning the environment, the energy transition should be achieved with minimum costs. The costs of carbon abatement (TCA) can be used as a key parameter to evaluate the costs of transitioning from fossil fuel-based technology to zero- and -clean technologies. For example, TCAs for hydrogen-fuelled cars are relatively high due to high operational costs, while abating lower total emissions than other vehicles. Therefore, techno-economic modelling alone is not sufficient to investigate the decarbonisation performance by a specific technology. Energy transition-related modelling and research must always consider the techno-econo-environmental aspects.

10.3.6. Hydrogen demand

Hydrogen demand must also be continuously studied, developed, and supported. Otherwise, hydrogen supply will be challenging due to a lack of demand. Regional approaches are crucial to integrate multiple electricity sources with multiple vehicle types and fleets. This helps to increase the overall capacity of hydrogen demand rather than targeting a specific type of vehicle. Regional approaches like hydrogen hubs are vital to integrating multiple electricity sources for multiple vehicles at a large capacity.

10.4. Future works

Several suggestions for the improvement, addition, or extension of the current study in the future are described according to the category of (1) hydrogen production, (2) hydrogen transportation and storage, (3) hydrogen dispensing, and (4) hydrogen value chains. Each category is explained in each of the following paragraphs.

The opportunities for future studies in hydrogen production are:

- A combination of multiple electrolyser sizes in a hydrogen production system can be investigated to increase the overall capacity factor of electrolyser.
- Other renewable resources for hydrogen production can be investigated. These include electricity from offshore wind, floating PV, and bioenergy from biochemical or thermochemical processes.
- An improved algorithm for energy management to capture low wind electricity prices can potentially be investigated to obtain more cost reductions.

The opportunities for future studies in hydrogen transportation and storage are:

- Hydrogen-fuelled trucks to haul tube trailers can also be studied to replace the diesel-fuelled trucks.
- Alternative hydrogen transportation mechanisms such as transporting liquid hydrogen via trucks or ships, and hydrogen gas via dedicated pipelines are also necessary to be technically and economically compared to this study.
- The potential options for hydrogen storage to be studied are salt caverns to store hydrogen gas, hydrogen liquefaction, and liquid organic hydrogen carriers (LOHC).

The opportunities for future studies in hydrogen dispensing are:

- The HRSs equipped with PV arrays, batteries and/or fuel cells can also be studied to reduce carbon emissions from the operation of HRS.
- An additional cost of a grid connection from transmission substation to HRS is essential to be investigated, particularly for regional hydrogen hubs.
- Future studies can explore new methods or technologies to reduce dispensing cost at 700 barg hydrogen.
- A study on safety standards of hydrogen refuelling for extra-large vehicles like maritime crafts is required, particularly for fast refuelling of 7.2 kg/min for a large onboard storage tank of more than 300 kg.

The opportunities for future studies on hydrogen value chains are:

- Details of the required equipment and installation of hydrogen injection to the gas network are necessary to be investigated for a secure and stable hydrogen supply.
- Direct sector coupling between renewable power and heavy-duty transport for longer operational distance, such as logistics or retail purposes.

- Detailed techno-economic parameters of heating provided by hydrogen can be calculated and compared with fossil fuel-based technologies.
- Oxygen as a by-product of water electrolysis process may be evaluated for utilisation and value for multiple purposes in a future study, which may also reduce overall costs.

References

[1] Intergovernmental Panel on Climate Change, “Global warming of 1.5°C: An IPCC Special Report on the impacts of global warming of 1.5°C above pre-industrial levels and related global greenhouse gas emission pathways, in the context of strengthening the global response to the threat of climate change,” New York, USA. 2019., 1981. doi: 10.1038/291285a0.

[2] European Commission, “2030 Climate & Energy Framework,” Brussels, Belgium. 2014., 2014. [Online]. Available: http://data.consilium.europa.eu/doc/document/ST-169-2014-INIT/en/pdf

[3] European Commission, “‘Fit for 55’: delivering the EU’s 2030 Climate Target on the way to climate neutrality. Communication from the Commission to the European Parliament, the Council, the European Economic and Social Committee and the Committee of the Regions.,” Brussels, Belgium. 2021., 2021. [Online]. Available: https://eur-lex.europa.eu/legal-content/EN/TXT/?uri=CELEX:52021DC0550

[4] Energy Transition Commission, “Mission possible: Reaching Net-Zero Carbon Emissions from Harder-to-Abate Sectors by Mid-Century,” London, United Kingdom. 2018.

[5] European Comission, “A hydrogen strategy for a climate-neutral Europe,” Brussels, Belgium. 2020., 2020.

[6] M. Shahbaz *et al.*, “A state of the art review on biomass processing and conversion technologies to produce hydrogen and its recovery via membrane separation,” *International Journal of Hydrogen Energy*, vol. 45, no. 30, pp. 15166–15195, 2020, doi: 10.1016/j.ijhydene.2020.04.009.

[7] International Energy Agency, “The future of fuel: The future of hydrogen,” Paris, France. 2019., 2012. doi: 10.1016/S1464-2859(12)70027-5.

[8] M. Ahmed and I. Dincer, “A review on photoelectrochemical hydrogen production systems: Challenges and future directions,” *International Journal of Hydrogen Energy*, vol. 44, no. 5, pp. 2474–2507, 2019, doi: 10.1016/j.ijhydene.2018.12.037.

[9] M. Noussan, P. P. Raimondi, R. Scita, and M. Hafner, “The role of green and blue hydrogen in the energy transition—a technological and geopolitical perspective,” *Sustainability (Switzerland)*, vol. 13, no. 1, pp. 1–26, 2021, doi: 10.3390/su13010298.

[10] M. A. N. Idris Aminu, “Hydrogen from Waste Plastics by Two-Stage Pyrolysis/Low-Temperature Plasma Catalytic Processing,” *Energy Fuels*, [Online]. Available: https://pubs.acs.org/doi/pdf/10.1021/acs.energyfuels.0c02043

[11] SHELL; Wuppertal Institut, “The Shell Hydrogen Study: Energy of the Future? - Sustainable Mobility through Fuel Cells and H2,” Hamburg, Germany. 2017., 2017. [Online]. Available: https://www.shell.com/energy-and-innovation/the-energy-future/future-transport/hydrogen.html

[12] Global Energy Infrastructure, “Hydrogen – data telling a story.” https://globalenergyinfrastructure.com/articles/2021/03-march/hydrogen-data-telling-a-story/ (accessed May 05, 2021).

[13] Fuel Cells and Hydrogen Joint Undertaking (FCH JU), “Hydrogen Roadmap Europe,” Brussels, Belgium. 2019., 2019. doi: 10.2843/249013.

[14] Hydrogen Council, “Path to hydrogen competitiveness A cost perspective,” Brussels, Belgium. 2020., 2020. [Online]. Available: www.hydrogencouncil.com.

[15] European Commission, “Powering a climate-neutral economy: An EU Strategy for Energy System Integration EN,” Brussels, Belgium. 2020., 2020.

[16] J. Cihlar, A. Villar Lejarreta, A. Wang, F. Melgar, J. Jens, and P. Rio, “Hydrogen generation in Europe: Overview of costs and key benefits,” Luxembourg: Publications Office of the European Union, 2020, 2020.

[17] IRENA, “Green Hydrogen Cost Reduction: Scaling up Electrolysers to Meet the 1.5^{0}C Climate Goal,” Abu Dhabi, UEA. 2020., 2020. [Online]. Available: /publications/2020/Dec/Green-hydrogen-cost-reduction%0Ahttps://www.irena.org/-/media/Files/IRENA/Agency/Publication/2020/Dec/IRENA_Green_hydrogen_cost_2020.pdf

[18] H. Holttinen, “Design and operation of power systems with large amounts of wind power,” VTT Technical Research Centre of Finland Ltd: Espoo, Finland, 2012. [Online]. Available: http://www.vttresearch.com/impact/publications

[19] EirGrid SONI, “Annual Renewable Energy Constraint and Curtailment Report 2018,” EirGrid: Dublin, Ireland, 2019. [Online]. Available: http://www.soni.ltd.uk/media/documents/Operations/Annual Renewable Constraint and Curtailment Report 2014.pdf

[20] WindEurope, “WindEurope Views on Curtailment of Wind Power and its Links to Priority Dispatch,” 2016.

[21] M. Beccali, S. Brunone, P. Finocchiaro, and J. M. Galletto, “Method for size optimisation of large wind-hydrogen systems with high penetration on power grids,” *Applied Energy*, vol. 102, pp. 534–544, 2013, doi: 10.1016/j.apenergy.2012.08.037.

[22] G. Zhang and X. Wan, “A wind-hydrogen energy storage system model for massive wind energy curtailment,” *International Journal of Hydrogen Energy*, vol. 39, no. 3, pp. 1243–1252, 2014, doi: 10.1016/j.ijhydene.2013.11.003.

[23] Renewable Power Generation Costs | IRENA, *Renewable Power Generation Costs in 2020*. 2020. [Online]. Available: https://www.irena.org/-/media/Files/IRENA/Agency/Publication/2018/Jan/IRENA_2017_Power_Costs_2018.pdf

[24] International Renewable Energy Agency - IRENA, *Future of solar photovoltaic*, vol. November. Abu Dhabi, UEA. 2019., 2019. [Online]. Available: https://www.irena.org/-/media/Files/IRENA/Agency/Publication/2019/Oct/IRENA_Future_of_wind_2019.pdf

[25] Y. Zhou and A. Gu, “Learning curve analysis of wind power and photovoltaics technology in US: Cost reduction and the importance of research, development and demonstration,” *Sustainability (Switzerland)*, vol. 11, no. 8, 2019, doi: 10.3390/su11082310.

[26] D. S. Mallapragada, D. D. Pilas, and P. G. Fernandez, “System implications of continued cost declines for wind and solar on driving power sector decarbonization,” MIT Energy Initiative,Cambridge, USA. 2020., 2020.

[27] Y. Kikuchi, T. Ichikawa, M. Sugiyama, and M. Koyama, “Battery-assisted low-cost hydrogen production from solar energy: Rational target setting for future technology systems,” *International Journal of Hydrogen Energy*, vol. 44, no. 3, pp. 1451–1465, 2019, doi: 10.1016/j.ijhydene.2018.11.119.

[28] G. Dispenza, F. Sergi, G. Napoli, V. Antonucci, and L. Andaloro, “Evaluation of hydrogen production cost in different real case studies,” *Journal of Energy Storage*, vol. 24, no. April, p. 100757, 2019, doi: 10.1016/j.est.2019.100757.

[29] G. Berckmans, M. Messagie, J. Smekens, N. Omar, L. Vanhaverbeke, and J. van Mierlo, “Cost projection of state of the art lithium-ion batteries for electric vehicles up to 2030,” *Energies*, vol. 10, no. 9, 2017, doi: 10.3390/en10091314.

[30] S. McDonagh, P. Deane, K. Rajendran, and J. D. Murphy, “Are electrofuels a sustainable transport fuel? Analysis of the effect of controls on carbon, curtailment, and cost of hydrogen,” *Applied Energy*, vol. 247, no. March, pp. 716–730, 2019, doi: 10.1016/j.apenergy.2019.04.060.

[31] O. Schmidt, A. Gambhir, I. Staffell, A. Hawkes, J. Nelson, and S. Few, “Future cost and performance of water electrolysis: An expert elicitation study,” *International Journal of Hydrogen Energy*, vol. 42, no. 52, pp. 30470–30492, 2017, doi: 10.1016/j.ijhydene.2017.10.045.

[32] Z. Abdin and W. Mérida, “Hybrid energy systems for off-grid power supply and hydrogen production based on renewable energy: A techno-economic analysis,” *Energy Conversion and Management*, vol. 196, no. June, pp. 1068–1079, 2019, doi: 10.1016/j.enconman.2019.06.068.

[33] V. Papadopoulos, J. Desmet, J. Knockaert, and C. Develder, “Improving the utilization factor of a PEM electrolyzer powered by a 15 MW PV park by combining wind power and battery storage – Feasibility study,” *International Journal of Hydrogen Energy*, vol. 43, no. 34, pp. 16468–16478, 2018, doi: 10.1016/j.ijhydene.2018.07.069.

[34] Z. N. Ashrafi, M. Ghasemian, M. I. Shahrestani, E. Khodabandeh, and A. Sedaghat, “Evaluation of hydrogen production from harvesting wind energy at

high altitudes in Iran by three extrapolating Weibull methods," *International Journal of Hydrogen Energy*, vol. 43, no. 6, pp. 3110–3132, 2018, doi: 10.1016/j.ijhydene.2017.12.154.

[35] C. J. Quarton and S. Samsatli, "Power-to-gas for injection into the gas grid: What can we learn from real-life projects, economic assessments and systems modelling?," *Renewable and Sustainable Energy Reviews*, vol. 98, no. September, pp. 302–316, 2018, doi: 10.1016/j.rser.2018.09.007.

[36] T. T. Q. Vo, A. Xia, D. M. Wall, and J. D. Murphy, "Use of surplus wind electricity in Ireland to produce compressed renewable gaseous transport fuel through biological power to gas systems," *Renewable Energy*, vol. 105, pp. 495–504, 2017, doi: 10.1016/j.renene.2016.12.084.

[37] A. Singlitico, J. Goggins, and R. F. D. Monaghan, "Evaluation of the potential and geospatial distribution of waste and residues for bio-SNG production: A case study for the Republic of Ireland," *Renewable and Sustainable Energy Reviews*, vol. 98, no. August 2018, pp. 288–301, 2018, doi: 10.1016/j.rser.2018.09.032.

[38] A. Singlitico, J. Goggins, and R. F. D. Monaghan, *Life cycle assessment-based multiobjective optimisation of synthetic natural gas supply chain: a case study for the Republic of Ireland (in press)*.

[39] Gas Networks Ireland, "Vision 2050: A Net Zero Carbon Gas Network for Ireland."

[40] M. Cavana and P. Leone, "Solar hydrogen from North Africa to Europe through greenstream: A simulation-based analysis of blending scenarios and production plant sizing," *International Journal of Hydrogen Energy*, vol. 46, no. 43, pp. 22618–22637, 2021, doi: 10.1016/j.ijhydene.2021.04.065.

[41] M. Gökçek and C. Kale, “Techno-economical evaluation of a hydrogen refuelling station powered by Wind-PV hybrid power system: A case study for İzmir-çeşme,” *International Journal of Hydrogen Energy*, vol. 43, no. 23, pp. 10615–10625, 2018, doi: 10.1016/j.ijhydene.2018.01.082.

[42] M. Gökçek and C. Kale, “Optimal design of a Hydrogen Refuelling Station (HRFS) powered by Hybrid Power System,” *Energy Conversion and Management*, vol. 161, no. December 2017, pp. 215–224, 2018, doi: 10.1016/j.enconman.2018.02.007.

[43] H. Sun, C. He, X. Yu, M. Wu, and Y. Ling, “Optimal siting and sizing of hydrogen refueling stations considering distributed hydrogen production and cost reduction for regional consumers,” *International Journal of Energy Research*, vol. 43, no. 9, pp. 4184–4200, 2019, doi: 10.1002/er.4544.

[44] R. Moradi and K. M. Groth, “Hydrogen storage and delivery: Review of the state of the art technologies and risk and reliability analysis,” *International Journal of Hydrogen Energy*, vol. 44, no. 23, pp. 12254–12269, 2019, doi: 10.1016/j.ijhydene.2019.03.041.

[45] K. Reddi, A. Elgowainy, N. Rustagi, and E. Gupta, “Techno-economic analysis of conventional and advanced high-pressure tube trailer configurations for compressed hydrogen gas transportation and refueling,” *International Journal of Hydrogen Energy*, vol. 43, no. 9, pp. 4428–4438, 2018, doi: 10.1016/j.ijhydene.2018.01.049.

[46] T. Mayer, M. Semmel, M. A. Guerrero Morales, K. M. Schmidt, A. Bauer, and J. Wind, “Techno-economic evaluation of hydrogen refueling stations with liquid or gaseous stored hydrogen,” *International Journal of Hydrogen Energy*, vol. 44, no. 47, pp. 25809–25833, 2019, doi: 10.1016/j.ijhydene.2019.08.051.

[47] K. Reddi, A. Elgowainy, N. Rustagi, and E. Gupta, “Impact of hydrogen refueling configurations and market parameters on the refueling cost of hydrogen,” *International Journal of Hydrogen Energy*, vol. 42, no. 34, pp. 21855–21865, 2017, doi: 10.1016/j.ijhydene.2017.05.122.

[48] M. Iordache, D. Schitea, and I. Iordache, “Hydrogen refuelling station infrastructure roll-up, an indicative assessment of the commercial viability and profitability in the Member States of Europe Union,” *International Journal of Hydrogen Energy*, vol. 42, no. 50, pp. 29629–29647, 2017, doi: 10.1016/j.ijhydene.2017.09.146.

[49] C. He, H. Sun, Y. Xu, and S. Lv, “Hydrogen refueling station siting of expressway based on the optimization of hydrogen life cycle cost,” *International Journal of Hydrogen Energy*, vol. 42, no. 26, pp. 16313–16324, 2017, doi: 10.1016/j.ijhydene.2017.05.073.

[50] S. Campíñez-Romero, A. Colmenar-Santos, C. Pérez-Molina, and F. Mur-Pérez, “A hydrogen refuelling stations infrastructure deployment for cities supported on fuel cell taxi roll-out,” *Energy*, vol. 148, no. 2018, pp. 1018–1031, 2018, doi: 10.1016/j.energy.2018.02.009.

[51] F. Grüger, L. Dylewski, M. Robinius, and D. Stolten, “Carsharing with fuel cell vehicles: Sizing hydrogen refueling stations based on refueling behavior,” *Applied Energy*, vol. 228, no. April, pp. 1540–1549, 2018, doi: 10.1016/j.apenergy.2018.07.014.

[52] N. Liu, F. Xie, Z. Lin, and M. Jin, “Evaluating national hydrogen refueling infrastructure requirement and economic competitiveness of fuel cell electric long-haul trucks,” *Mitigation and Adaptation Strategies for Global Change*, 2019, doi: 10.1007/s11027-019-09896-z.

[53] J. Z. Thellufsen and H. Lund, “Cross-border versus cross-sector interconnectivity in renewable energy systems,” *Energy*, vol. 124, pp. 492–501, 2017, doi: 10.1016/j.energy.2017.02.112.

[54] M. Victoria, K. Zhu, T. Brown, G. B. Andresen, and M. Greiner, “The role of storage technologies throughout the decarbonisation of the sector-coupled European energy system,” *Energy Conversion and Management*, vol. 201, no. August, p. 111977, 2019, doi: 10.1016/j.enconman.2019.111977.

[55] M. Felgenhauer and I. R. Witzmann, “Battery and Fuel cell Electric Vehicles in the Context of the Energy Transition,” Technical University of Munich, Germany. 2016., 2016.

[56] O. Ruhnau, S. Bannik, S. Otten, A. Praktiknjo, and M. Robinius, “Direct or indirect electrification? A review of heat generation and road transport decarbonisation scenarios for Germany 2050,” *Energy*, vol. 166, pp. 989–999, 2019, doi: 10.1016/j.energy.2018.10.114.

[57] X. Yue, J. P. Deane, B. O’Gallachoir, and F. Rogan, “Identifying decarbonisation opportunities using marginal abatement cost curves and energy system scenario ensembles,” *Applied Energy*, vol. 276, no. August 2019, p. 115456, 2020, doi: 10.1016/j.apenergy.2020.115456.

[58] B. Helgeson and J. Peter, “The role of electricity in decarbonizing European road transport – Development and assessment of an integrated multi-sectoral model,” *Applied Energy*, vol. 262, no. February 2019, p. 114365, 2020, doi: 10.1016/j.apenergy.2019.114365.

[59] T. Inkinen and E. Hämäläinen, “Reviewing truck logistics: Solutions for achieving low emission road freight transport,” *Sustainability (Switzerland)*, vol. 12, no. 17, pp. 1–11, 2020, doi: 10.3390/SU12176714.

[60] H. Liimatainen, P. Greening, P. Dadhich, and A. Keyes, “Possible impact of long and heavy vehicles in the United Kingdom-A commodity level approach,” *Sustainability (Switzerland)*, vol. 10, no. 8, pp. 1–19, 2018, doi: 10.3390/su10082754.

[61] B. Sen, T. Ercan, O. Tatari, and Q. P. Zheng, “Robust Pareto optimal approach to sustainable heavy-duty truck fleet composition,” *Resources, Conservation and Recycling*, vol. 146, no. March, pp. 502–513, 2019, doi: 10.1016/j.resconrec.2019.03.042.

[62] Z. Gao *et al.*, “The evaluation of developing vehicle technologies on the fuel economy of long-haul trucks,” *Energy Conversion and Management*, vol. 106, pp. 766–781, 2015, doi: 10.1016/j.enconman.2015.10.006.

[63] A. Elgowainy *et al.*, “Cost of ownership and well-to-wheels carbon emissions/oil use of alternative fuels and advanced light-duty vehicle technologies,” *Energy for Sustainable Development*, vol. 17, no. 6, pp. 626–641, 2013, doi: 10.1016/j.esd.2013.09.001.

[64] E. Mulholland, J. Teter, P. Cazzola, Z. McDonald, and B. P. Ó Gallachóir, “The long haul towards decarbonising road freight – A global assessment to 2050,” *Applied Energy*, vol. 216, no. November 2017, pp. 678–693, 2018, doi: 10.1016/j.apenergy.2018.01.058.

[65] Yvonne Ruf; Markus Baum; Thomas Zorn; Alexandra Menzel; Johannes Rehberger, “Fuel Cells Hydrogen Trucks: Heavy-Duty’s High Performance Green Solution,” FCH 2 JU.Brussels, Belgium. 2020., 2019.

[66] H. Liimatainen, O. van Vliet, and D. Aplyn, “The potential of electric trucks – An international commodity-level analysis,” *Applied Energy*, vol. 236, no. August 2018, pp. 804–814, 2019, doi: 10.1016/j.apenergy.2018.12.017.

[67] T. Brown, D. Schlachtberger, A. Kies, S. Schramm, and M. Greiner, “Synergies of sector coupling and transmission reinforcement in a cost-optimised, highly renewable European energy system,” *Energy*, vol. 160, pp. 720–739, 2018, doi: 10.1016/j.energy.2018.06.222.

[68] S. Mojtaba Lajevardi, J. Axsen, and C. Crawford, “Comparing alternative heavy-duty drivetrains based on GHG emissions, ownership and abatement costs: Simulations of freight routes in British Columbia,” *Transportation Research Part D: Transport and Environment*, vol. 76, no. September, pp. 19–55, 2019, doi: 10.1016/j.trd.2019.08.031.

[69] A. Smallbone, B. Jia, P. Atkins, and A. P. Roskilly, “The impact of disruptive powertrain technologies on energy consumption and carbon dioxide emissions from heavy-duty vehicles,” *Energy Conversion and Management: X*, vol. 6, no. January, p. 100030, 2020, doi: 10.1016/j.ecmx.2020.100030.

[70] H. Zhao, A. Burke, and L. Zhu, “Analysis of Class 8 hybrid-electric truck technologies using diesel, LNG, electricity, and hydrogen, as the fuel for various applications,” *2013 World Electric Vehicle Symposium and Exhibition, EVS 2014*, no. Epa 2010, pp. 1–16, 2014, doi: 10.1109/EVS.2013.6914957.

[71] M. el Hannach, P. Ahmadi, L. Guzman, S. Pickup, and E. Kjeang, “Life cycle assessment of hydrogen and diesel dual-fuel class 8 heavy duty trucks,” *International Journal of Hydrogen Energy*, vol. 44, no. 16, pp. 8575–8584, 2019, doi: 10.1016/j.ijhydene.2019.02.027.

[72] J. J. S. Guilbaud, “Hybrid Renewable Power Systems for the Mining Industry: System Costs, Reliability Costs, and Portfolio Cost Risks,” University College London, 2016.

[73] OECD, “Mining and Green Growth in the EECCA region,” Paris, France. 2019., 2019.

[74] L. Delevinge, W. Glazener, L. Gregoir, and K. Henderson, “Climate risk and decarbonization: What every mining CEO needs to know,” New York, United States. 2020., 2020.

[75] A. Phadke, M. McCall, and D. Rajagopal, “Reforming electricity rates to enable economically competitive electric trucking,” *Environmental Research Letters*, vol. 14, no. 12, 2019, doi: 10.1088/1748-9326/ab560d.

[76] P. K. Rose and F. Neumann, “Hydrogen refueling station networks for heavy-duty vehicles in future power systems,” *Transportation Research Part D: Transport and Environment*, vol. 83, no. May, p. 102358, 2020, doi: 10.1016/j.trd.2020.102358.

[77] P. Sterchele, K. Kersten, A. Palzer, J. Hentschel, and H. M. Henning, “Assessment of flexible electric vehicle charging in a sector coupling energy system model – Modelling approach and case study,” *Applied Energy*, vol. 258, no. November 2019, p. 114101, 2020, doi: 10.1016/j.apenergy.2019.114101.

[78] International Council on Clean Transportation, “Electrifying EU City Logistics: An analysis of energy demand and charging cost,” Washington, DC, United States. 2020.

[79] U. Bünger and J. Michalski, “The Impact of E-Mobility in a Future Energy System Dominated by Renewable Electricity,” *Chemie-Ingenieur-Technik*, vol. 90, no. 1, pp. 113–126, 2018, doi: 10.1002/cite.201700084.

[80] V. Keller *et al.*, “Electricity system and emission impact of direct and indirect electrification of heavy-duty transportation,” *Energy*, vol. 172, pp. 740–751, 2019, doi: 10.1016/j.energy.2019.01.160.

[81] S. Kuczynski, M. Łaciak, A. Olijnyk, A. Szurlej, and T. Włodek, “Thermodynamic and technical issues of hydrogen and methane-hydrogen mixtures pipeline transmission,” *Energies*, vol. 12, no. 3, 2019, doi: 10.3390/en12030569.

[82] L. Ma and C. Spataru, “The use of natural gas pipeline network with different energy carriers,” *Energy Strategy Reviews*, vol. 8, pp. 72–81, 2015, doi: 10.1016/j.esr.2015.09.002.

[83] S. Samsatli, I. Staffell, and N. J. Samsatli, “Optimal design and operation of integrated wind-hydrogen-electricity networks for decarbonising the domestic transport sector in Great Britain,” *International Journal of Hydrogen Energy*, vol. 41, no. 1, pp. 447–475, 2016, doi: 10.1016/j.ijhydene.2015.10.032.

[84] A. P. Pereira and S. Samsatli, “Optimal Design and Operation of Heat Networks Utilising Hydrogen as an Energy Carrier,” *Computer Aided Chemical Engineering*, vol. 40, pp. 2527–2532, 2017, doi: 10.1016/B978-0-444-63965-3.50423-2.

[85] A. Elgowainy, K. Reddi, D. Y. Lee, N. Rustagi, and E. Gupta, “Techno-economic and thermodynamic analysis of pre-cooling systems at gaseous hydrogen refueling stations,” *International Journal of Hydrogen Energy*, vol. 42, no. 49, pp. 29067–29079, 2017, doi: 10.1016/j.ijhydene.2017.09.087.

[86] C. You and J. Kim, “Optimal design and global sensitivity analysis of a 100% renewable energy sources based smart energy network for electrified and hydrogen cities,” *Energy Conversion and Management*, vol. 223, no. July, p. 113252, 2020, doi: 10.1016/j.enconman.2020.113252.

[87] M. Kim and J. Kim, “An integrated decision support model for design and operation of a wind-based hydrogen supply system,” *International Journal of Hydrogen Energy*, vol. 42, no. 7, pp. 3899–3915, 2017, doi: 10.1016/j.ijhydene.2016.10.129.

[88] A. Pfeifer, P. Prebeg, and N. Duić, “Challenges and opportunities of zero emission shipping in smart islands: A study of zero emission ferry lines,” *eTransportation*, vol. 3, 2020, doi: 10.1016/j.etran.2020.100048.

[89] H. Hao, Z. Mu, Z. Liu, and F. Zhao, “Abating transport GHG emissions by hydrogen fuel cell vehicles: Chances for the developing world,” *Frontiers in Energy*, vol. 12, no. 3, pp. 466–480, 2018, doi: 10.1007/s11708-018-0561-3.

[90] G. Morrison, J. Stevens, and F. Joseck, “Relative economic competitiveness of light-duty battery electric and fuel cell electric vehicles,” *Transportation Research Part C: Emerging Technologies*, vol. 87, no. June 2017, pp. 183–196, 2018, doi: 10.1016/j.trc.2018.01.005.

[91] N. Liu, F. Xie, Z. Lin, and M. Jin, “Evaluating national hydrogen refueling infrastructure requirement and economic competitiveness of fuel cell electric long-haul trucks,” *Mitigation and Adaptation Strategies for Global Change*, vol. 25, no. 3, pp. 477–493, 2020, doi: 10.1007/s11027-019-09896-z.

[92] IRENA, *Renewable capacity statistics 2019, International Renewable Energy Agency (IRENA), Abu Dhabi*. 2019.

[93] M. Turner, Y. Zhang, and O. Rix, “70 By 30: A 70% Renewable Electricity Vision for Ireland in 2030,” Baringa Partners LLP: London, UK, 2018. [Online]. Available: http://www.eirgridgroup.com/site-files/library/EirGrid/EirGrid-Tomorrows-Energy-Scenarios-Report-2017.pdf

[94] Department of Communications Climate Action & Environment of Government of Ireland, “Renewable Electricity Support Scheme (RESS),” Government of Ireland: Dublin, Ireland, 2020. [Online]. Available: https://www.dccae.gov.ie/documents/RESS Design Paper.pdf

[95] E. V. Mc Garrigle, J. P. Deane, and P. G. Leahy, “How much wind energy will be curtailed on the 2020 Irish power system?,” *Renewable Energy*, vol. 55, no. 2013, pp. 544–553, 2013, doi: 10.1016/j.renene.2013.01.013.

[96] M. Melaina, O. Antonia, and M. Penev, “Blending Hydrogen into Natural Gas Pipeline Networks: A Review of Key Issues,” Colorado, 2013. doi: 10.2172/1068610.

[97] SEAI, “Energy in Ireland,” 2019.

[98] E. Tractebel, Engie, and Hinicio, “Study on Early Business Cases for H2 in Energy Storage and More Broadly Power To H2 Applications,” Brussels, Belgium, 2017. [Online]. Available: http://www.hinicio.com/inc/uploads/2017/07/P2H_Full_Study_FCHJU.pdf%0Ahttp://www.fch.europa.eu/sites/default/files/P2H_Full_Study_FCHJU.pdf%0Ahttp://www.hinicio.com/file/2018/06/P2H_Full_Study_FCHJU.pdf

[99] M. Götz *et al.*, “Renewable Power-to-Gas: A technological and economic review,” *Renewable Energy*, vol. 85, pp. 1371–1390, 2016, doi: 10.1016/j.renene.2015.07.066.

[100] W. Kuckshinrichs, T. Ketelaer, and J. C. Koj, “Economic analysis of improved alkaline water electrolysis,” *Frontiers in Energy Research*, vol. 5, no. FEB, 2017, doi: 10.3389/fenrg.2017.00001.

[101] S. H. Siyal, D. Mentis, and M. Howells, “Economic analysis of standalone wind-powered hydrogen refueling stations for road transport at selected sites in Sweden,” *International Journal of Hydrogen Energy*, vol. 40, no. 32, pp. 9855–9865, 2015, doi: 10.1016/j.ijhydene.2015.05.021.

[102] L. Viktorsson, J. T. Heinonen, J. B. Skulason, and R. Unnthorsson, “A step towards the hydrogen economy - A life cycle cost analysis of a hydrogen refueling station,” *Energies*, vol. 10, no. 6, pp. 1–15, 2017, doi: 10.3390/en10060763.

[103] Scottish Entreprise, “Constrained Renewables and Green Hydrogen Production Study Final Report,” Scottish Entreprise: Glasgow, UK, 2018.

[104] G. Glenk and S. Reichelstein, “Economics of converting renewable power to hydrogen,” *Nature Energy*, vol. 4, no. 3, pp. 216–222, 2019, doi: 10.1038/s41560-019-0326-1.

[105] J. Proost, “State-of-the art CAPEX data for water electrolysers, and their impact on renewable hydrogen price settings,” *International Journal of Hydrogen Energy*, vol. 44, no. 9, pp. 4406–4413, 2019, doi: 10.1016/j.ijhydene.2018.07.164.

[106] J. Linnemann and R. Steinberger-Wilckens, “Realistic costs of wind-hydrogen vehicle fuel production,” *International Journal of Hydrogen Energy*, vol. 32, no. 10–11, pp. 1492–1499, 2007, doi: 10.1016/j.ijhydene.2006.10.029.

[107] C. J. Greiner, M. KorpÅs, and A. T. Holen, “A Norwegian case study on the production of hydrogen from wind power,” *International Journal of Hydrogen Energy*, vol. 32, no. 10–11, pp. 1500–1507, 2007, doi: 10.1016/j.ijhydene.2006.10.030.

[108] SEM Committee, “SEM Monitoring Report : Q3 2018 November 2018,” 2018.

[109] D. Parra, L. Valverde, F. J. Pino, and M. K. Patel, “A review on the role, cost and value of hydrogen energy systems for deep decarbonisation,” *Renewable and Sustainable Energy Reviews*, vol. 101, no. July 2018, pp. 279–294, 2019, doi: 10.1016/j.rser.2018.11.010.

[110] SEAI, “Electricity & Gas Prices in Ireland,” Sustainable Energy Authority of Ireland, Sustainable Energy Authority of Ireland: Dublin, Ireland, 2018.

[111] SEM Committee, “Single Electricity Market Performance,” SEM Committee: Dublin, Ireland, 2019. [Online]. Available: https://www.semcommittee.com/sites/semc/files/media-files/MMU public report Jan 19.pdf

[112] A. Louw *et al.*, “Global Trends in Renewable Energy Investment 2018,” Frankfurt School of Finance & Management gGmbH.: Frankfurt, Germany, 2018. doi: 10.3928/00220124-20081201-03.

[113] National Competitiveness Council, “Costs of Doing Business in Ireland 2018,” 2018.

[114] L. Bertuccioli, A. Chan, D. Hart, F. Lehner, B. Madden, and E. Standen, “Study on development of water electrolysis in the EU - Final Report,” 2014.

[115] A. Buttler and H. Spliethoff, “Current status of water electrolysis for energy storage, grid balancing and sector coupling via power-to-gas and power-to-liquids: A review,” *Renewable and Sustainable Energy Reviews*, vol. 82, no. 2017, pp. 2440–2454, 2018, doi: 10.1016/j.rser.2017.09.003.

[116] S. Hall, “Fans, Blowers, and Compressors,” in *Rules of Thumb for Chemical Engineers*, Gulf Professional Publishing, 2012, p. 123.

[117] A. Léon, “Hydrogen Storage,” in *Hydrogen Technology: Mobile and Portable Applications*, Springer, 2008, p. 86.

[118] G. Saur, “Wind-To-Hydrogen Project: Electrolyzer Capital Cost Study. Technical Report NREL/TP-550-44103,” 2008.

[119] Y. Jiang, Z. Deng, and S. You, “Size optimization and economic analysis of a coupled wind-hydrogen system with curtailment decisions,” *International Journal of Hydrogen Energy*, vol. 44, no. 36, pp. 19658–19666, 2019, doi: 10.1016/j.ijhydene.2019.06.035.

[120] “TSC-Part-B-Glossary,” *Single Electricity Market Operator*, 2018. www.sem-o.com/MarketDevelopment/MarketRules/Glossary.docx. (accessed Aug. 10, 2018).

[121] EirGrid and SONI, “Annual Renewable Energy Constraint and Curtailment Report 2014,” pp. 1–28, 2015.

[122] R. O’Shea, D. Wall, I. Kilgallon, and J. D. Murphy, “Assessment of the impact of incentives and of scale on the build order and location of biomethane facilities and the feedstock they utilise,” *Applied Energy*, vol. 182, no. 2016, pp. 394–408, 2016, doi: 10.1016/j.apenergy.2016.08.063.

[123] A. Singlitico, I. Kilgallon, J. Goggins, and R. F. D. Monaghan, “GIS-based techno-economic optimisation of a regional supply chain for large-scale deployment of bio-SNG in a natural gas network,” *Applied Energy*, vol. 250, no. April, pp. 1036–1052, 2019, doi: 10.1016/j.apenergy.2019.05.026.

[124] GNI (UK) Limited, “Northern Ireland Gas Capacity Statement 2018/19,” 2018.

[125] Françoise Barbier, “Hydrogen Distribution Infrastructure for an Energy System: Present Status and Perspectives of Technologies,” no. 278796, pp. 1–33, 2013.

[126] SEAI, “Wind Mapping System,” 2016. http://maps.seai.ie/wind/ (accessed Oct. 10, 2019).

[127] RenewableUK, “Onshore Wind Farms in the UK,” 2016. https://www.arcgis.com/home/item.html?id=8bad1da3b2d14a90bf22a7d0b52dc9b3 (accessed Oct. 10, 2019).

[128] Geofabrik GmbH, “OpenStreetMap Data Extracts,” 2019. http://download.geofabrik.de/ (accessed Jan. 10, 2019).

[129] Gas Networks Ireland, “The future of transport - Case Study: Comparison of a natural gas truck versus a diesel truck,” Gas Networks Ireland: Cork, Ireland, 2014.

[130] S. Roberts and T. Williams, “Common Arrangements for Gas: Final Report on the Requirements for a Single Natural Gas Quality Standard for Northern Ireland and the Republic of Ireland,” no. December, 2008.

[131] J. Leicher, T. Nowakowski, A. Giese, and K. Görner, “Power-to-gas and the consequences: Impact of higher hydrogen concentrations in natural gas on industrial combustion processes,” *Energy Procedia*, vol. 120, pp. 96–103, 2017, doi: 10.1016/j.egypro.2017.07.157.

[132] H. de Vries, A. V. Mokhov, and H. B. Levinsky, “The impact of natural gas/hydrogen mixtures on the performance of end-use equipment: Interchangeability analysis for domestic appliances,” *Applied Energy*, vol. 208, no. September, pp. 1007–1019, 2017, doi: 10.1016/j.apenergy.2017.09.049.

[133] M. Andersson, J. Larfeldt, A. Larsson, and D. Studie Har Finansierats, “Co-firing with hydrogen in industrial gas turbines (Sameldning med vätgas i industriella gasturbiner),” Sweden, 2013.

[134] Commission for Regulation of Utilities, “Gas Networks Ireland Transmission Tariffs and Allowed Revenue 2019/20,” no. May, pp. 0–13, 2019.

[135] Commission for Regulation of Utilities, “Biogas injection into the Natural Gas Grid,” 2013.

[136] European Commission, “Quarterly Report on European Gas Markets (Q1 to Q4 in 2019),” Brussels, Belgium. 2019., 2019.

[137] European Network of Transmission System Operators for Gas (ENTSOG), “The European Natural Gas Network 2019,” Brussels, Belgium. 2019., 2019.

[138] Joint Research Centre (JRC) EU Science Hub, “EU Photovoltaic Geographical Information System (PVGIS): PV Performance tool.” https://re.jrc.ec.europa.eu/pvg_tools/en/#PVP (accessed Mar. 15, 2021).

[139] M. Almaktar, A. M. Elbreki, and M. Shaaban, “Revitalizing operational reliability of the electrical energy system in Libya: Feasibility analysis of solar generation in local communities,” *Journal of Cleaner Production*, vol. 279, p. 123647, 2021, doi: 10.1016/j.jclepro.2020.123647.

[140] European Energy Research Alliance, “Key Performance Indicators (KPIs) for FCH Research and Innovation, 2020 - 2030,” Brussels, Belgium. 2020., 2020.

[141] D. Apostolou and G. Xydis, “A literature review on hydrogen refuelling stations and infrastructure. Current status and future prospects,” *Renewable and Sustainable Energy Reviews*, vol. 113, no. May 2018, p. 109292, 2019, doi: 10.1016/j.rser.2019.109292.

[142] L. Rowland, “2020 Energy Storage Assessment Study: Black Hills Energy,” Colorado, USA. 2020., 2020.

[143] T. A. Gunawan, A. Singlitico, P. Blount, J. Burchill, J. G. Carton, and R. F. D. Monaghan, “At What Cost Can Renewable Hydrogen Offset Fossil Fuel Use in

Ireland’s Gas Network?,” *Energies*, vol. 13, no. 7, p. 1798, Apr. 2020, doi: 10.3390/en13071798.

[144] T. Ma and M. S. Javed, “Integrated sizing of hybrid PV-wind-battery system for remote island considering the saturation of each renewable energy resource,” *Energy Conversion and Management*, vol. 182, no. December 2018, pp. 178–190, 2019, doi: 10.1016/j.enconman.2018.12.059.

[145] Z. Song, S. Feng, L. Zhang, Z. Hu, X. Hu, and R. Yao, “Economy analysis of second-life battery in wind power systems considering battery degradation in dynamic processes: Real case scenarios,” *Applied Energy*, vol. 251, no. March, p. 113411, 2019, doi: 10.1016/j.apenergy.2019.113411.

[146] World Bank, “Renewable energy desalination: an emerging solution to close the water gap in MENA,” Washington, DC, United States. 2012., 2013.

[147] P. Palenzuela, D. C. Alarcón-Padilla, and G. Zaragoza, “Large-scale solar desalination by combination with CSP: Techno-economic analysis of different options for the Mediterranean Sea and the Arabian Gulf,” *Desalination*, vol. 366, pp. 130–138, 2015, doi: 10.1016/j.desal.2014.12.037.

[148] E. El-Bialy, S. M. Shalaby, A. E. Kabeel, and A. M. Fathy, “Cost analysis for several solar desalination systems,” *Desalination*, vol. 384, pp. 12–30, 2016, doi: 10.1016/j.desal.2016.01.028.

[149] MARCOGAZ, “Overview of Available Test Results and Regulatory Limits for Hydrogen Admission into Existing Natural Gas Infrastructure and End Use.”

[150] Energy Co-operatives Ireland, “Energy Co-operatives Ireland: Who We Are.” https://www.energyco-ops.ie/who-we-are/ (accessed Aug. 12, 2021).

[151] S. Galls and G. Nth, “Valentia Island Hydrogen Energy Opportunities Feasibility Study,” Dublin, Ireland. 2019.

[152] CSO, “Environmental Indicators Ireland: EU Greenhouse gas emissions per capita 2017,” *2019*. https://www.cso.ie/en/releasesandpublications/ep/p-eii/eii19/greenhousegasesandclimatechange/ (accessed Nov. 20, 2019).

[153] SEAI, “CO_2 Emissions: Share of energy related CO_2 by sector in 2017.” https://www.seai.ie/data-and-insights/seai-statistics/key-statistics/co2/ (accessed Nov. 20, 2019).

[154] European Environment Agency, *Transport and environment: on the way to a new common transport policy*, no. 1. European Environment Agency: Copenhagen, Denmark, 2019.

[155] Global Solution Networks, “C40 Cities Climate Leadership Group - Cities Confronting Climate Change Lighthouse Case Study,” Global Solution Networks: Toronto, Canada, 2014.

[156] C40 Cities, “Green and Healthy Streets: Fossil-Fuel-Free Streets Declaration - Planned Actions to Deliver Commitments,” C40 Cities Climate Leadership Group: New York, USA, 2018.

[157] N. Pocard and C. Reid, “Fuel Cell Electric Buses: an Attractive Value Proposition for Zero-Emission Buses in the United Kingdom,” Ballard Power Systems Inc.: Burnaby, Canada, 2016., 2016. [Online]. Available: http://www.fuelcellbuses.eu/sites/default/files/Ballard - fuel cell electric buses.pdf

[158] CIVITAS, “Smart Choices for cities: Alternative Fuel Buses,” CIVITAS Secretariat: Brussels, Belgium, 2017. [Online]. Available: http://civitas.eu/sites/default/files/civ_pol-08_m_web.pdf

[159] K. K. Müller, F. Schnitzeler, A. Lozanovski, S. Skiker, and M. Ojakovoh, “Clean Hydrogen in European Cities,” EvoBus GmbH: Stuttgart, Germany, 2017. [Online]. Available: https://www.fuelcellbuses.eu/sites/default/files/documents/Final Report_CHIC_28022017_Final_Public.pdf

[160] K. Kendall, M. Kendall, B. Liang, and Z. Liu, “Hydrogen vehicles in China: Replacing the Western Model,” *International Journal of Hydrogen Energy*, vol. 42, no. 51, pp. 30179–30185, 2017, doi: 10.1016/j.ijhydene.2017.10.072.

[161] International Energy Agency, “Fuel cell electric vehicles stock by region and by mode, 2020,” 2021. https://www.iea.org/data-and-statistics/charts/fuel-cell-electric-vehicles-stock-by-region-and-by-mode-2020 (accessed Sep. 28, 2021).

[162] Central Statistics Office, “Projected Population by Sex, Age, Criteria for Projection, Regional Authority and Year,” 2017. https://statbank.cso.ie/ (accessed Jun. 10, 2020).

[163] Northern Ireland Statistics and Research Agency, “2017 Mid Year Population Estimates for Northern Ireland,” 2017. https://www.nisra.gov.uk/publications/2017-mid-year-population-estimates-northern-ireland-new-format-tables (accessed Jun. 10, 2020).

[164] S. Adams *et al.*, “Impact of Electrolysers on the Network,” Scottish and Southern Electricity Networks: Perth, UK, 2016.

[165] B. Reuter, M. Faltenbacher, O. Schuller, N. Whitehouse, and S. Whitehouse, “New Bus Refuelling for European Hydrogen Bus Depots,” thinkstep AG: Leinfelden-Echterdingen, Germany, 2017. [Online]. Available: http://www.fch.europa.eu/sites/default/files/NewBusFuel Press Release 14102016 Final version.pdf#

[166] S. Pfenninger and I. Staffell, “Long-term patterns of European PV output using 30 years of validated hourly reanalysis and satellite data,” *Energy*, vol. 114, pp. 1251–1265, 2016, doi: 10.1016/j.energy.2016.08.060.

[167] Sustainable Energy Authority of Ireland, “Wind Mapping System - Wind Atlas,” 2017. https://gis.seai.ie/wind/ (accessed Jan. 20, 2019).

[168] S. M. H. Erfani, S. Danesh, S. M. Karrabi, R. Shad, and S. Nemati, “Using applied operations research and geographical information systems to evaluate effective factors in storage service of municipal solid waste management systems,” *Waste Management*, vol. 79, pp. 346–355, 2018, doi: 10.1016/j.wasman.2018.08.003.

[169] International Council on Clean Transportaion, “Developing hydrogen fueling infrastructure for fuel cell vehicles: A status update,” no. October, pp. 1–22, 2017.

[170] CSO, “Transport Omnibus 2017: Bus Éireann fleet 2017,” *2018*. https://www.cso.ie/en/releasesandpublications/ep/p-tranom/transportomnibus2017/publictransport/ (accessed Jan. 20, 2020).

[171] Department for Infrastructure, “Northern Ireland Transport Statistics 2018 - 2019,” Department for Infrastructure: Belfast, UK, 2019.

[172] S. Carr, F. Zhang, F. Liu, Z. Du, and J. Maddy, “Optimal operation of a hydrogen refuelling station combined with wind power in the electricity market,” *International Journal of Hydrogen Energy*, vol. 41, no. 46, pp. 21057–21066, 2016, doi: 10.1016/j.ijhydene.2016.09.073.

[173] A. Lozanovski, N. Whitehouse, N. Ko, and S. Whitehouse, “Sustainability assessment of fuel cell buses in public transport,” *Sustainability (Switzerland)*, vol. 10, no. 5, pp. 1–15, 2018, doi: 10.3390/su10051480.

[174] L. Eudy, M. Post, L. Eudy, and M. Post, “Fuel Cell Buses in U.S. Transit Fleets: Current Status 2016,” National Renewable Energy Laboratory: Golden, Colorado, USA, 2016.

[175] L. Eudy, M. Post, L. Eudy, and M. Post, “Fuel Cell Buses in U.S. Transit Fleets: Current Status 2016,” National Renewable Energy Laboratory: Golden, Colorado, USA, 2016.

[176] CIVITAS, “Smart choices for cities - Clean buses for your city,” CIVITAS: Brussels, Belgium, 2013.

[177] A. Mayyas and M. Mann, “Manufacturing competitiveness analysis for hydrogen refueling stations,” *International Journal of Hydrogen Energy*, vol. 44, no. 18, pp. 9121–9142, 2019, doi: 10.1016/j.ijhydene.2019.02.135.

[178] B. Reuter, M. Faltenbacher, O. Schuller, N. Whitehouse, and S. Whitehouse, “New Bus Refuelling for European Hydrogen Bus Depots - Guidance Document on Large Scale Hydrogen Bus Refuelling,” thinkstep AG: Leinfelden-Echterdingen, Germany, 2017.

[179] M. Dolman, “Operators ’ guide to fuel cell bus deployment,” The Fuel Cells and Hydrogen Joint Undertaking (FCH JU): Brussels, Belgium, 2018., 2018.

[180] T.-P. Cheng, “Hydrogen Delivery Infrastructure Options Analysis,” Nexant, Inc.: San Francisco, USA, 2010. [Online]. Available: https://www.energy.gov/sites/prod/files/2014/03/f11/delivery_infrastructure_analysis.pdf

[181] M. Joos and I. Staffell, “Short-term integration costs of variable renewable energy: Wind curtailment and balancing in Britain and Germany,” *Renewable and*

Sustainable Energy Reviews, vol. 86, no. January, pp. 45–65, 2018, doi: 10.1016/j.rser.2018.01.009.

[182] I. Gonzalez Aparicio, A. Zucker, F. Careri, F. Monforti, T. Huld, and J. Badger, *EMHIRES dataset Part I: Wind power generation. European Meteorological derived High resolution RES generation time series for present and future scenarios*. 2016. doi: 10.2790/831549.

[183] Fnavia Nordexfrance, “The Wind Farms in France.”

[184] Geopunt Vlaanderen, “The Wind Farms in Belgium.”

[185] Utrecht University, “The Wind Farms in the Netherlands.”

[186] ESRI Germany, “The Wind Farms in Germany.”

[187] Dublin bus, “Corporate Information.” https://www.dublinbus.ie/About-Us/ (accessed Feb. 12, 2019).

[188] Civitas, “Munich.” https://civitas.eu/eccentric/munich (accessed Feb. 12, 2019).

[189] wikipedia, “Transport in Berlin.” https://en.wikipedia.org/wiki/Transport_in_Berlin (accessed Feb. 12, 2019).

[190] Sustainable bus, “Germany 2030: 3,000 electric buses in 5 biggest cities.” https://www.sustainable-bus.com/news/germany-electric-bus-biggest-cities-3000-berlin-hamburg-cologne-frankfurt-munich/ (accessed Feb. 12, 2019).

[191] Smart Freight Centre, “Global Logistics Emissions Council Framework for Logistics Emissions Accounting and Reporting Version 2.0,” Amsterdam, Netherland. 2019.ISBN 978-90-82-68790-3.

[192] International Council on Clean Transportation, “The European Commission’s Proposed CO2 Standards For Heavy-Duty Vehicles,” Washington, D.C., United States. 2018.

[193] The European Parliament and the Council of the European Union, “Regulation (EU) 2019/1242 of the European Parliament and of the Council of 20 June 2019 Setting CO2 emission performance standards for new heavy-duty vehicles and amending Regulations (EC) No 595/2009 and (EU) 2018/956 of the European Parliament,” *Official Journal of the European Union*, vol. L 198, no. April, pp. 202–240, 2019.

[194] C. Hank *et al.*, “Economics & carbon dioxide avoidance cost of methanol production based on renewable hydrogen and recycled carbon dioxide-power-to-methanol,” *Sustainable Energy and Fuels*, vol. 2, no. 6, pp. 1244–1261, 2018, doi: 10.1039/c8se00032h.

[195] P. Markewitz *et al.*, “Carbon capture for CO2 emission reduction in the cement industry in Germany,” *Energies*, vol. 12, no. 12, pp. 1–25, 2019, doi: 10.3390/en12122432.

[196] A. Hoekstra, A. Vijayashankar, and V. L. Sundrani, “Modelling the Total Cost of Ownership of Electric Vehicles in the Netherlands,” *EVS 2017 - 30th International Electric Vehicle Symposium and Exhibition*, no. January, 2017.

[197] Y. Chen and M. Melaina, “Model-based techno-economic evaluation of fuel cell vehicles considering technology uncertainties,” *Transportation Research Part D: Transport and Environment*, vol. 74, no. August 2019, pp. 234–244, 2019, doi: 10.1016/j.trd.2019.08.002.

[198] Irish Petroleum Industry Association, “What determines pump prices?,” Dublin, Ireland. 2018., 2018.

[199] Department of Communications Climate Action and Environment, “National Energy & Climate Plan 2021-2030,” 2020.

[200] T. A. Gunawan, I. Williamson, D. Raine, and R. F. D. Monaghan, “Decarbonising city bus networks in Ireland with renewable hydrogen,” *International Journal of Hydrogen Energy*, Dec. 2020, doi: 10.1016/j.ijhydene.2020.11.164.

[201] J. Kast, G. Morrison, J. J. Gangloff, R. Vijayagopal, and J. Marcinkoski, “Designing hydrogen fuel cell electric trucks in a diverse medium and heavy duty market,” *Research in Transportation Economics*, vol. 70, no. November 2016, pp. 139–147, 2018, doi: 10.1016/j.retrec.2017.07.006.

[202] Ioannis Tsiropoulos, Dalius Tarvydas, and Andreas Zucker, “Cost development of low carbon energy technologies: Scenario-based cost trajectories to 2050, 2017 edition,” Brussels, Belgium. 2018., 2018. doi: 10.2760/23266.

[203] International Renewable Energy Agency, “Renewable Energy Technologies: Cost Analysis Series - Wind Power,” Abu Dhabi, UEA. 2012., 2012. doi: 10.1007/978-3-642-20951-2_8.

[204] International Council on Clean Transportation, “Transitioning to zero-emission heavy-duty freight vehicles,” Washington, DC, United States of America. 2017., 2017.

[205] E. Çabukoglu, G. Georges, L. Küng, G. Pareschi, and K. Boulouchos, “Battery electric propulsion: an option for heavy-duty vehicles? Results from a Swiss case-study,” *Transportation Research Part C: Emerging Technologies*, vol. 88, no. September 2017, pp. 107–123, 2018, doi: 10.1016/j.trc.2018.01.013.

[206] S. Wainwright, J. Peters, and D. Glave, “Clean Power for Transport Infrastructure Deployment,” Luxembourg: Publications Office of the European Union, 2017., 2017. [Online]. Available: https://www.docutren.com/pdf/boletin/IIIA 1332(1).pdf

[207] G. Lorenzi and C. A. S. Silva, “Comparing demand response and battery storage to optimize self-consumption in PV systems,” *Applied Energy*, vol. 180, pp. 524–535, 2016, doi: 10.1016/j.apenergy.2016.07.103.

[208] D. Hall and N. Lutsey, “Estimating the infrastructure needs and costs for the launch of zero-emission trucks,” Washington DC, USA. 2019., 2019.

[209] Volvo Trucks, “The new Volvo FMX 440 19.5 Cu.m Tipper: The Mining & Construction Expert,” New Delhi, India. 2020.

[210] The European Parliament and the Council of the European Union, “Commission Regulation (EU) No 2017/2400,” *Official Journal of the European Union*, vol. 349, no. 582, 2017.

[211] J. Seo, J. Park, Y. Oh, and S. Park, “Estimation of total transport CO2 emissions generated by medium- and heavy-duty vehicles (MHDVs) in a sector of Korea,” *Energies*, vol. 9, no. 8, 2016, doi: 10.3390/en9080638.

[212] National Academy of Sciences, “Technologies and Approaches to Reducing the Fuel Consumption of Medium- and Heavy-Duty Vehicles. Chapter: 4 Power Train Technologies for Reducing Load-Specific Fuel Consumption.,” Page 79. National Academies Press, Washington DC, USA. 2010.

[213] C. D. Nikolas Hill, John Norris, Felix Kirsch, E. (Ricardo-AEA), Neil McGregor (Ricardo UK), and I. S. (TEPR) Pastori (TRT), “Light weighting as a means of improving Heavy Duty Vehicles’ energy efficiency and overall CO2 emissions,” Didcot, United Kingdom. 2015., 2015.

[214] K. Schubert, R., Chan, M., and Law, “Commercial Medium- and Heavy-Duty Truck Fuel Efficiency Technology Study – Report #1,” (Report No. DOT HS 812 177). Washington, DC: National Highway Traffic Safety Administration. 2015., 2015. [Online]. Available: https://www.nhtsa.gov/sites/nhtsa.dot.gov/files/812146-commercialmdhd-truckfuelefficiencytechstudy-v2.pdf

[215] R. Vijayagopal and A. Rousseau, “Electric truck economic feasibility analysis,” *World Electric Vehicle Journal*, vol. 12, no. 2, 2021, doi: 10.3390/wevj12020075.

[216] R. A. Vijayagopal R., Prada D. N., “Fuel Economy and Cost Estimates for Medium- and Heavy-Duty Trucks,” (Report No. ANL/ESD-19/8). Lemont, Illnois: Argonne National Laboratory. 2019.

[217] U.S. Environmental Protection Agency, “Final Rulemaking to Establish Greenhouse Gas Emissions Standards and Fuel Efficiency Standards for Medium- and Heavy-Duty Engines and Vehicles,” EPA-420-R-11-901. Washington DC, USA. 2011.

[218] B. Sharpe, “Zero-emission tractor-trailers in Canada,” Washington DC, USA. 2019., 2019.

[219] S. Sabihuddin, A. E. Kiprakis, and M. Mueller, “A numerical and graphical review of energy storage technologies,” *Energies*, vol. 8, no. 1, pp. 172–216, 2015, doi: 10.3390/en8010172.

[220] E. Monemian, A. Cairns, M. Gilmore, D. Newman, and K. Scott, “Evaluation of intake charge hydrogen enrichment in a heavy-duty diesel engine,” *Proceedings of the Institution of Mechanical Engineers, Part D: Journal of Automobile Engineering*, vol. 232, no. 1, pp. 139–147, 2018, doi: 10.1177/0954407017738375.

[221] B. Sen, T. Ercan, and O. Tatari, “Does a battery-electric truck make a difference? – Life cycle emissions, costs, and externality analysis of alternative fuel-powered Class 8 heavy-duty trucks in the United States,” *Journal of Cleaner Production*, vol. 141, no. 2017, pp. 110–121, 2017, doi: 10.1016/j.jclepro.2016.09.046.

[222] L. Fulton and M. Miller, “Strategies for transitioning to low-carbon emission trucks in the United States,” Davis, United States of America. 2015., 2015.

[223] J. C. González Palencia, M. Araki, and S. Shiga, “Energy consumption and CO2 emissions reduction potential of electric-drive vehicle diffusion in a road freight vehicle fleet,” *Energy Procedia*, vol. 142, pp. 2936–2941, 2017, doi: 10.1016/j.egypro.2017.12.420.

[224] J. L. Osorio-Tejada, E. Llera-Sastresa, and A. H. Hashim, “Well-to-wheels approach for the environmental impact assessment of road freight services,” *Sustainability (Switzerland)*, vol. 10, no. 12, 2018, doi: 10.3390/su10124487.

[225] D. Y. Lee, A. Elgowainy, A. Kotz, R. Vijayagopal, and J. Marcinkoski, “Life-cycle implications of hydrogen fuel cell electric vehicle technology for medium- and heavy-duty trucks,” *Journal of Power Sources*, vol. 393, no. May, pp. 217–229, 2018, doi: 10.1016/j.jpowsour.2018.05.012.

[226] R. Edwards *et al.*, “Well-to-Wheels analysis of future automotive fuels and powertrains in the European context WELL-TO-TANK (WTT) Report Version 4.a,” 2013. doi: 10.2790/95629.

[227] C. Liew *et al.*, “An experimental investigation of the combustion process of a heavy-duty diesel engine enriched with H2,” *International Journal of Hydrogen Energy*, vol. 35, no. 20, pp. 11357–11365, 2010, doi: 10.1016/j.ijhydene.2010.06.023.

[228] H. L. Yip *et al.*, “A review of hydrogen direct injection for internal combustion engines: Towards carbon-free combustion,” *Applied Sciences (Switzerland)*, vol. 9, no. 22, pp. 1–30, 2019, doi: 10.3390/app9224842.

[229] X. Liu, A. Srna, H. L. Yip, S. Kook, Q. N. Chan, and E. R. Hawkes, “Performance and emissions of hydrogen-diesel dual direct injection (H2DDI) in a single-cylinder compression-ignition engine,” *International Journal of Hydrogen Energy*, vol. 46, no. 1, pp. 1302–1314, 2021, doi: 10.1016/j.ijhydene.2020.10.006.

[230] S. R. Jhang, K. S. Chen, S. L. Lin, Y. C. Lin, and W. L. Cheng, “Reducing pollutant emissions from a heavy-duty diesel engine by using hydrogen additions,” *Fuel*, vol. 172, pp. 89–95, 2016, doi: 10.1016/j.fuel.2016.01.032.

[231] S. Liu *et al.*, “An experimental investigation of NO2 emission characteristics of a heavy-duty H2-diesel dual fuel engine,” *International Journal of Hydrogen Energy*, vol. 36, no. 18, pp. 12015–12024, 2011, doi: 10.1016/j.ijhydene.2011.06.058.

[232] Volvo Trucks, “Tailoring your Volvo FM,” Gothenburg, Sweden. 2020.

[233] Sustainable Energy Authority of Ireland, “National Energy Projections to 2030,” Dublin, Ireland. 2018., 2018.

[234] Sustainable Energy Authority of Ireland, “Energy in Ireland: 2020 Report,” Dublin, Ireland. 2020., 2020.

[235] E. Çabukoglu, G. Georges, L. Küng, G. Pareschi, and K. Boulouchos, “Fuel cell electric vehicles: An option to decarbonize heavy-duty transport? Results from a Swiss case-study,” *Transportation Research Part D: Transport and Environment*, vol. 70, no. March, pp. 35–48, 2019, doi: 10.1016/j.trd.2019.03.004.

[236] Single Electricity Market Operator, “SEMO: Dynamic Reports.” https://www.sem-o.com/market-data/dynamic-reports/index.xml (accessed Feb. 10, 2021).

[237] C. Blazquez-Diaz, “Techno-economic modelling and analysis of hydrogen fuelling stations,” *International Journal of Hydrogen Energy*, vol. 44, no. 2, pp. 495–510, 2019, doi: 10.1016/j.ijhydene.2018.11.001.

[238] Aran Island Ferries, “Inis Mór Timetable 2021,” 2021. https://www.aranislandferries.com/times_mor.php (accessed Mar. 01, 2021).

[239] F. G. Aarskog, J. Danebergs, T. Strømgren, and Ø. Ulleberg, “Energy and cost analysis of a hydrogen driven high speed passenger ferry,” *International Shipbuilding Progress*, vol. 67, no. 1, pp. 93–119, 2020, doi: 10.3233/ISP-190273.

[240] M. Li *et al.*, “Review on the research of hydrogen storage system fast refueling in fuel cell vehicle,” *International Journal of Hydrogen Energy*, vol. 44, no. 21, pp. 10677–10693, 2019, doi: 10.1016/j.ijhydene.2019.02.208.

[241] R. Ortiz Cebolla, B. Acosta, N. de Miguel, and P. Moretto, “Effect of precooled inlet gas temperature and mass flow rate on final state of charge during hydrogen vehicle refueling,” *International Journal of Hydrogen Energy*, vol. 40, no. 13, pp. 4698–4706, 2015, doi: 10.1016/j.ijhydene.2015.02.035.

[242] X. Wu, J. Liu, J. Shao, and G. Deng, “Fast filling strategy of type III on-board hydrogen tank based on time-delayed method,” *International Journal of Hydrogen Energy*, no. xxxx, pp. 1–9, 2021, doi: 10.1016/j.ijhydene.2021.01.094.

[243] Ballard, “‘Zero Emission’ Fuel Cell Electric Refuse Collection Vehicles,” Burnaby, Canada. 2021.

[245] Godula-Jopek, Agata. Hydrogen Production: by Electrolysis. Wiley VCH Verlag GmbH & Co. Weinheim, Germany. 2015.

APPENDIX A

The Decision Support Tool (DST) of Community Hydrogen Forum (CH2F)

A.1. Antwerpen, Belgium

The estimated number of buses is 424 units.

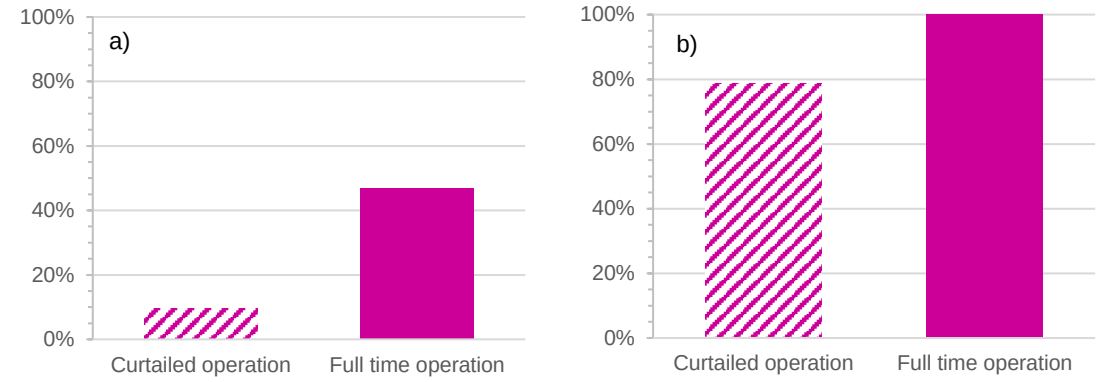

Figure A.0.1. The percentage of city bus fuel in Antwerpen displaceable by renewable hydrogen in Dublin for different electrolyser operation modes by using a) wind electricity and b) wind and solar electricity

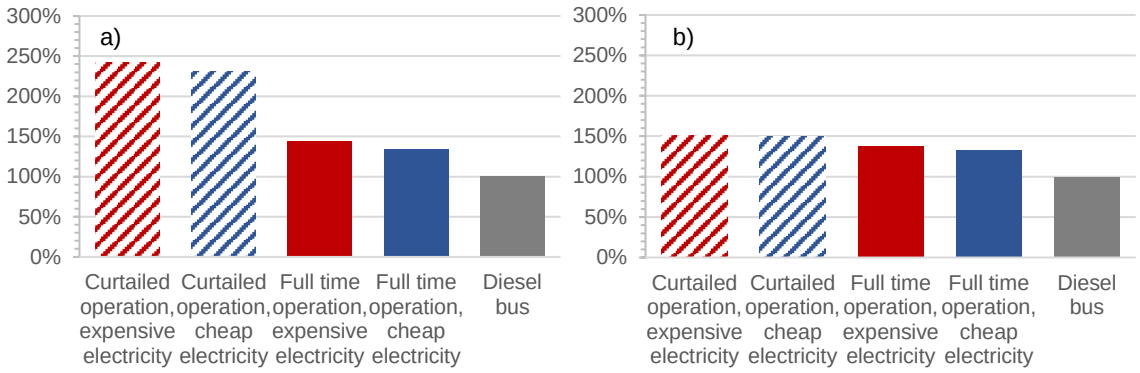

Figure A.0.2. The percentage of operational costs for hydrogen buses in Antwerpen for different electricity prices and electrolyser operation modes by using a) wind electricity and b) wind and solar electricity, relative to diesel

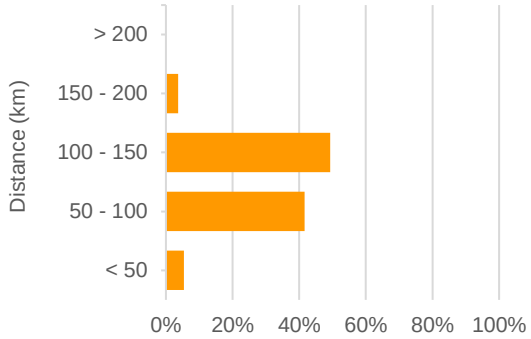

Figure A.0.3. Distances from hydrogen sources to city bus fleet in Antwerpen

A.2. Brussel, Belgium

The estimated number of buses is 235 units.

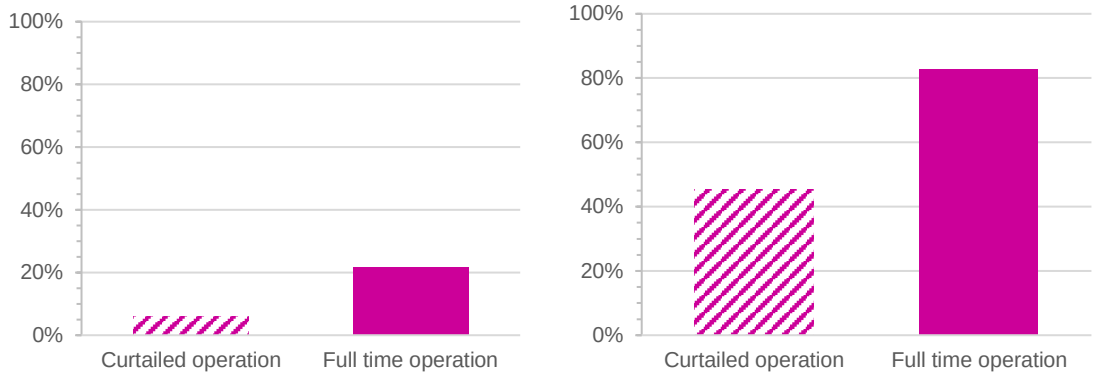

Figure A.0.4. The percentage of city bus fuel in Brussel displaceable by renewable hydrogen in Dublin for different electrolyser operation modes by using a) wind electricity and b) wind and solar electricity

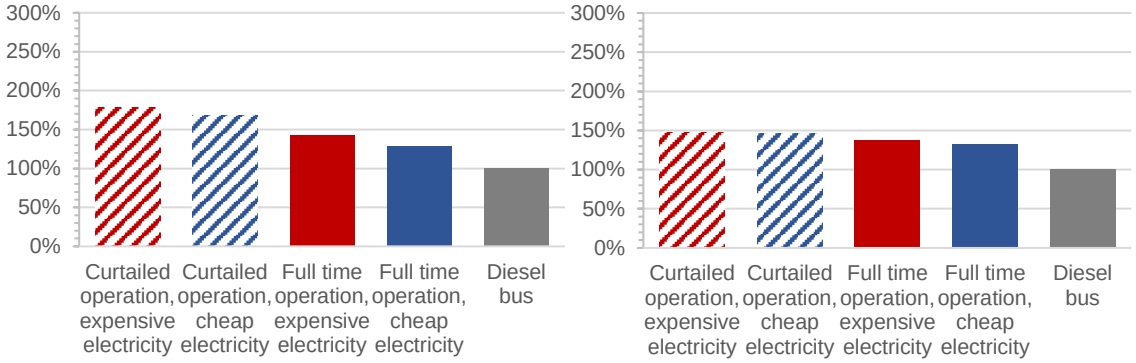

Figure A.0.5. The percentage of operational costs for hydrogen buses in Brussel for different electricity prices and electrolyser operation modes by using a) wind electricity and b) wind and solar electricity, relative to diesel

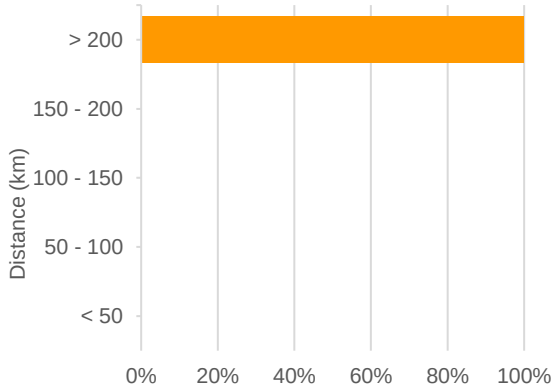

Figure A.0.6. Distances from hydrogen sources to city bus fleet in Brussel

A.3. Berlin, Germany

The estimated number of buses is 1,357 units.

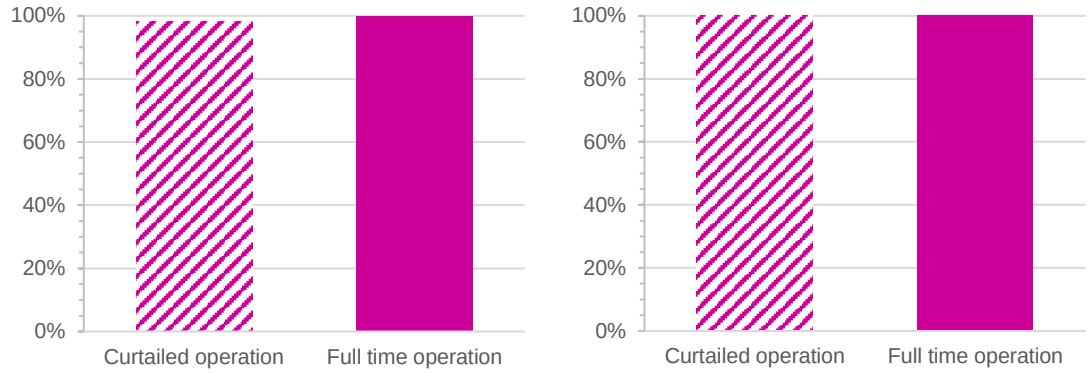

Figure A.0.7. The percentage of city bus fuel in Berlin displaceable by renewable hydrogen in Dublin for different electrolyser operation modes by using a) wind electricity and b) wind and solar electricity

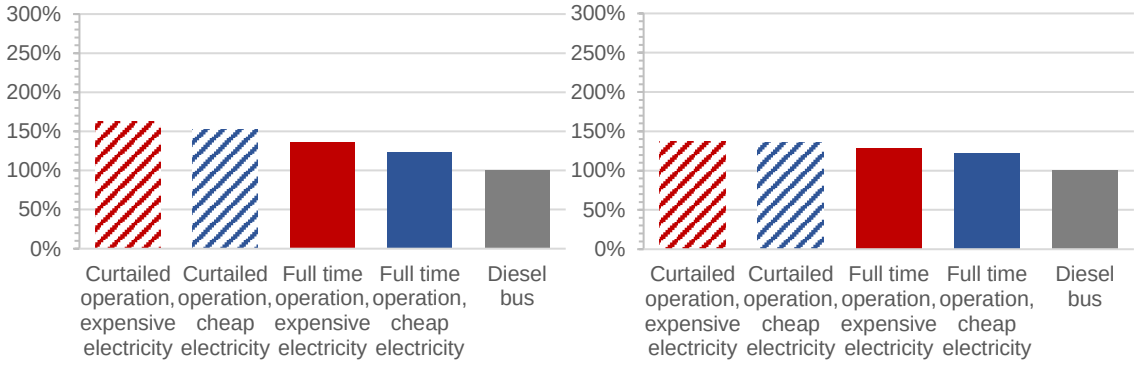

Figure A.0.8. The percentage of operational costs for hydrogen buses in Berlin for different electricity prices and electrolyser operation modes by using a) wind electricity and b) wind and solar electricity, relative to diesel

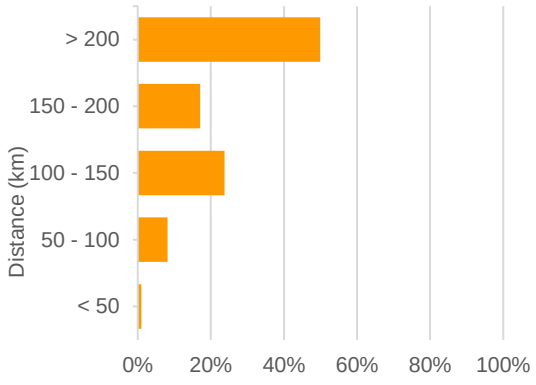

Figure A.0.9. Distances from hydrogen sources to city bus fleet in Berlin

A.4. Bremen, Germany

The estimated number of buses is 430 units.

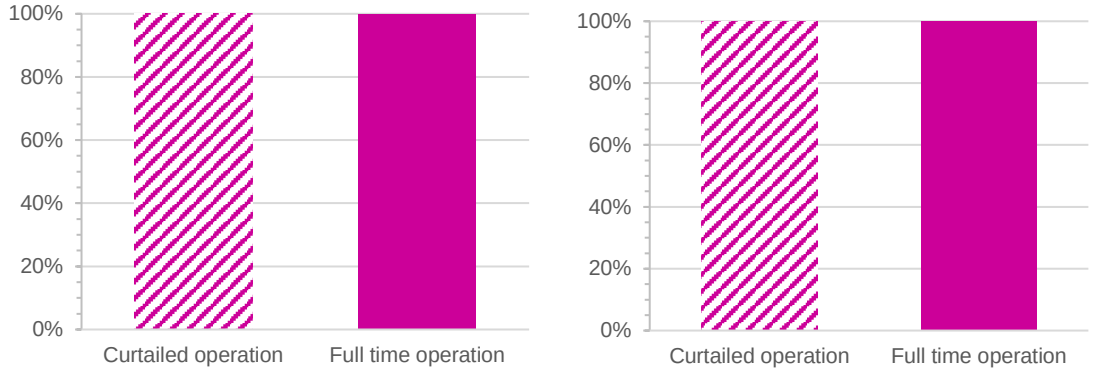

Figure A.0.10. The percentage of city bus fuel in Bremen displaceable by renewable hydrogen in Dublin for different electrolyser operation modes by using a) wind electricity and b) wind and solar electricity

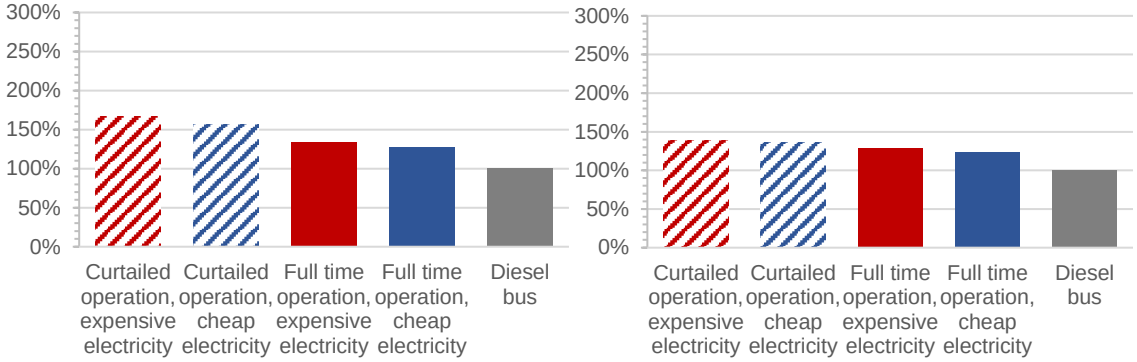

Figure A.0.11. The percentage of operational costs for hydrogen buses in Bremen for different electricity prices and electrolyser operation modes by using a) wind electricity and b) wind and solar electricity, relative to diesel

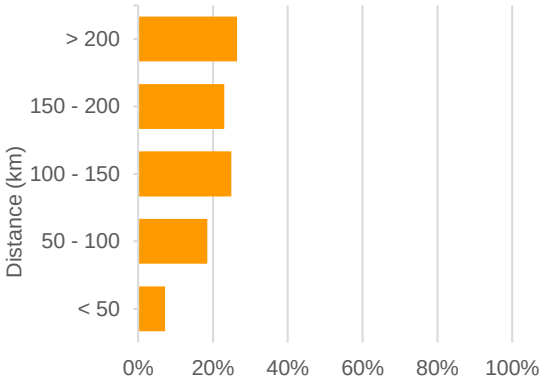

Figure A.0.12. Distances from hydrogen sources to city bus fleet in Bremen

A.5. Dortmund, Germany

The estimated number of buses is 435 units.

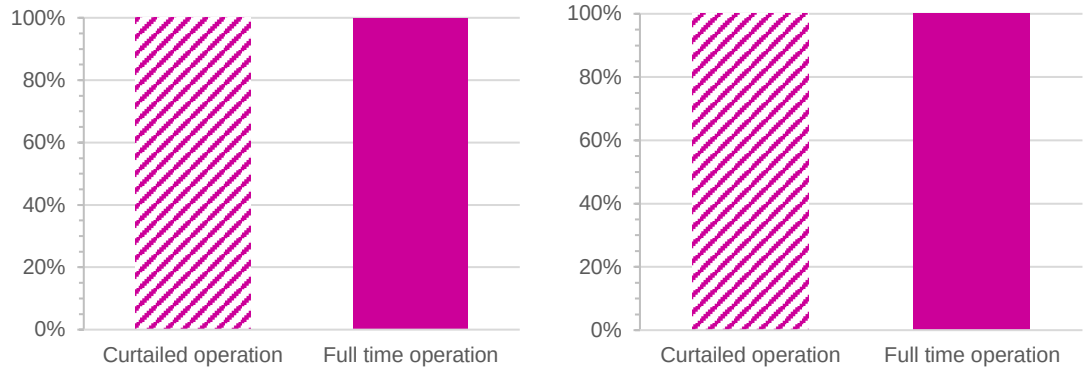

Figure A.0.13. The percentage of city bus fuel in Dortmund displaceable by renewable hydrogen in Dublin for different electrolyser operation modes by using a) wind electricity and b) wind and solar electricity

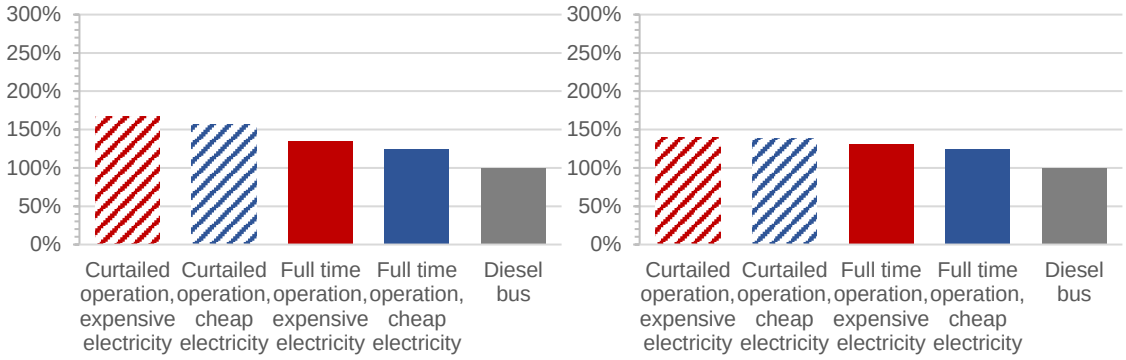

Figure A.0.14. The percentage of operational costs for hydrogen buses in Dortmund for different electricity prices and electrolyser operation modes by using a) wind electricity and b) wind and solar electricity, relative to diesel

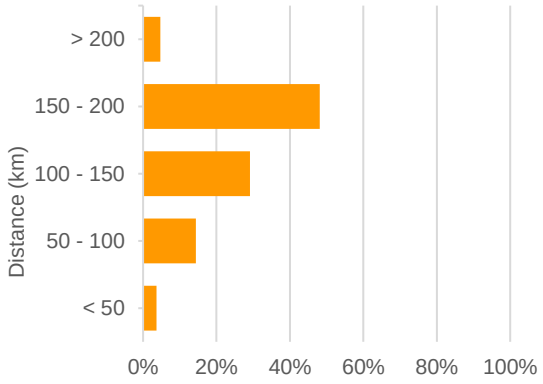

Figure A.0.15. Distances from hydrogen sources to city bus fleet in Dortmund

A.6. Dresden, Germany

The estimated number of buses is 427 units.

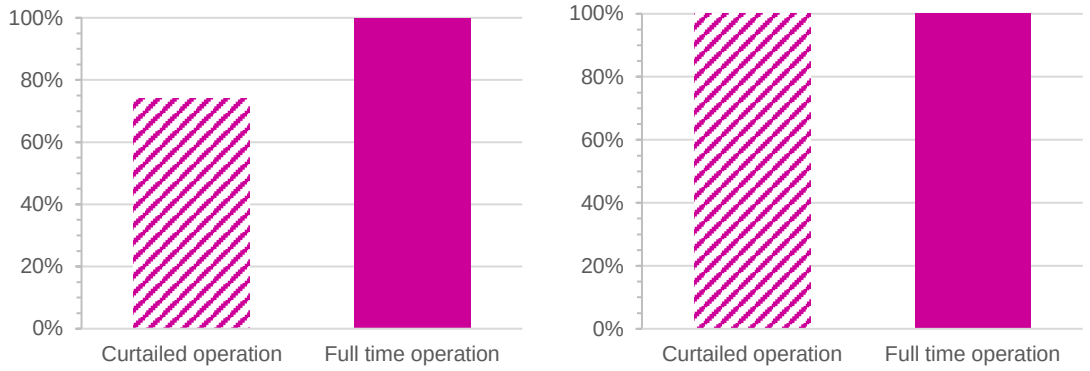

Figure A.0.16. The percentage of city bus fuel in Dresden displaceable by renewable hydrogen in Dublin for different electrolyser operation modes by using a) wind electricity and b) wind and solar electricity

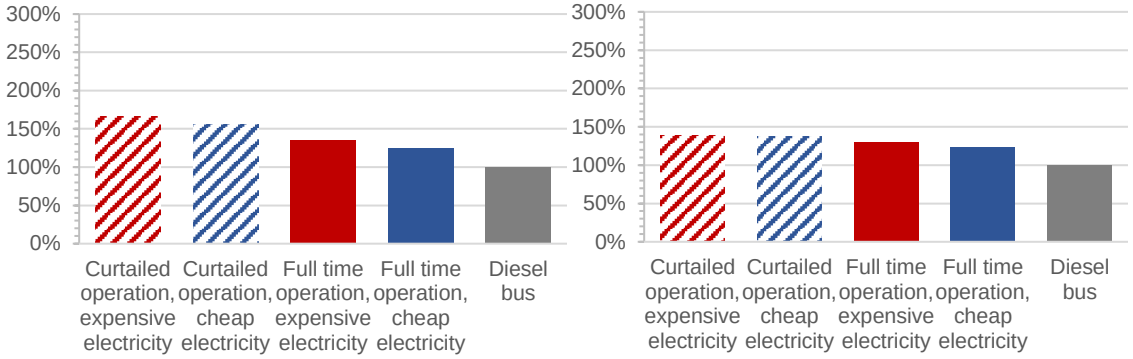

Figure A.0.17. The percentage of operational costs for hydrogen buses in Dresden for different electricity prices and electrolyser operation modes by using a) wind electricity and b) wind and solar electricity, relative to diesel

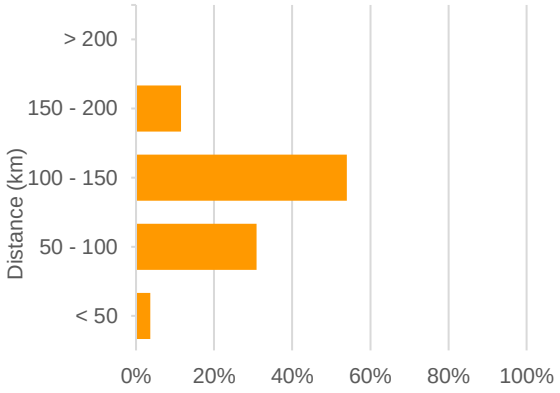

Figure A.0.18. Distances from hydrogen sources to city bus fleet in Dresden

A.7. Duisburg, Germany

The estimated number of buses is 420 units.

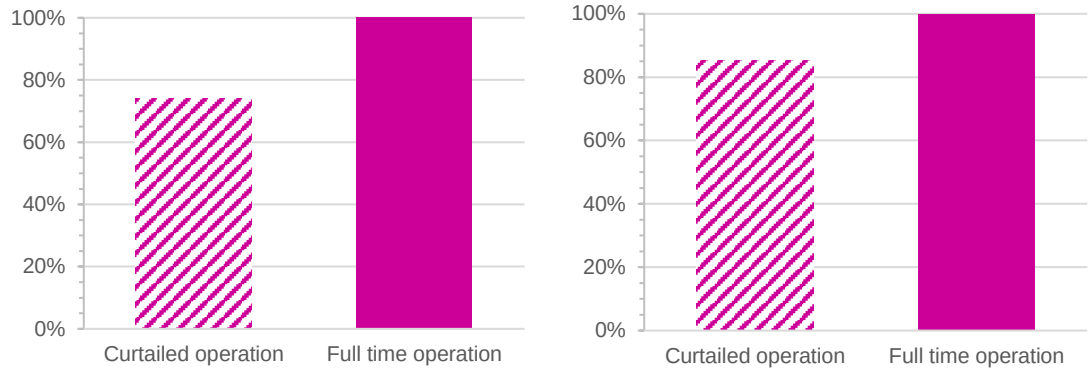

Figure A.0.19. The percentage of city bus fuel in Duisburg displaceable by renewable hydrogen in Dublin for different electrolyser operation modes by using a) wind electricity and b) wind and solar electricity

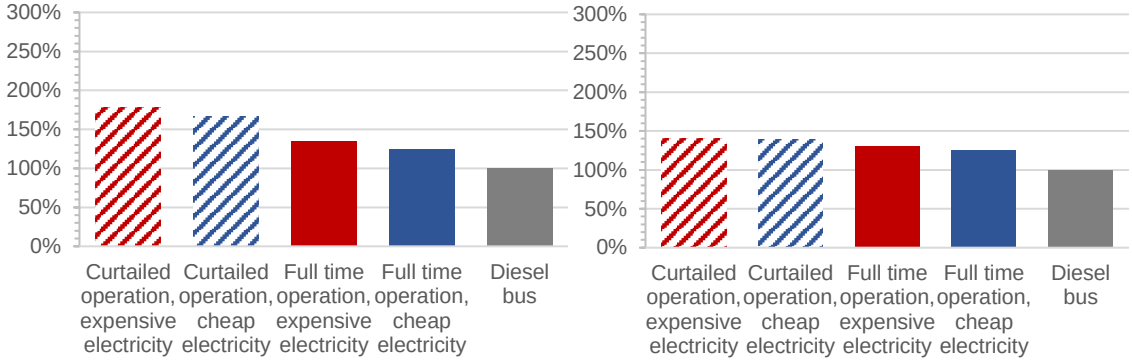

Figure A.0.20. The percentage of operational costs for hydrogen buses in Duisburg for different electricity prices and electrolyser operation modes by using a) wind electricity and b) wind and solar electricity, relative to diesel

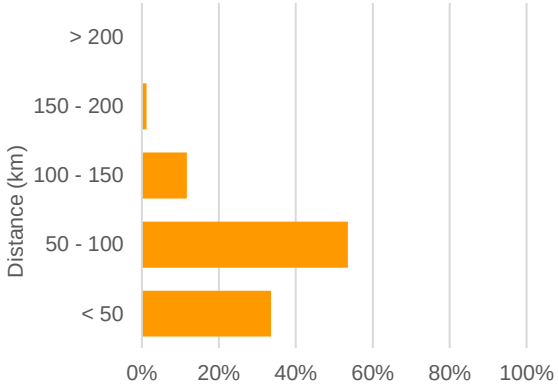

Figure A.0.21. Distances from hydrogen sources to city bus fleet in Duisburg

A.8. Düsseldorf, Germany

The estimated number of buses is 439 units.

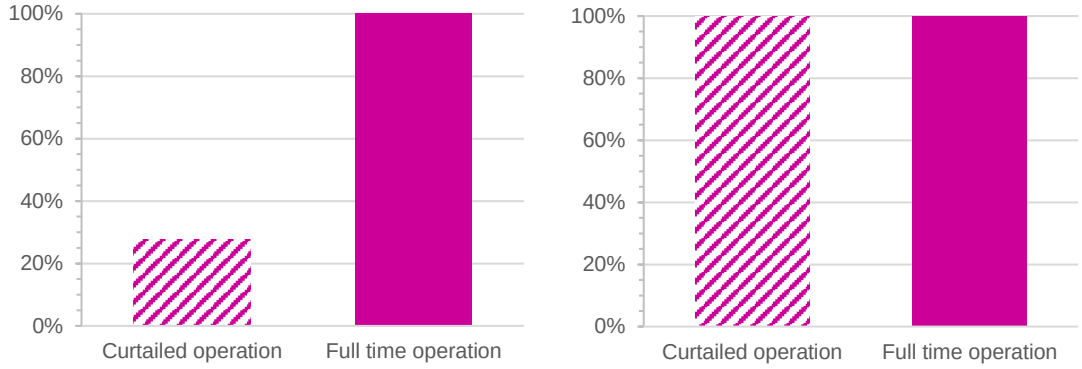

Figure A.0.22. The percentage of city bus fuel in Düsseldorf displaceable by renewable hydrogen in Dublin for different electrolyser operation modes by using a) wind electricity and b) wind and solar electricity

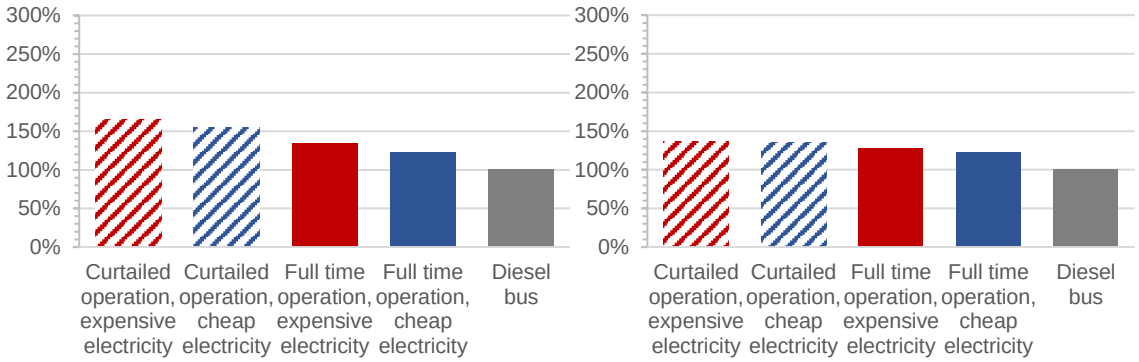

Figure A.0.23. The percentage of operational costs for hydrogen buses in Düsseldorf for different electricity prices and electrolyser operation modes by using a) wind electricity and b) wind and solar electricity, relative to diesel

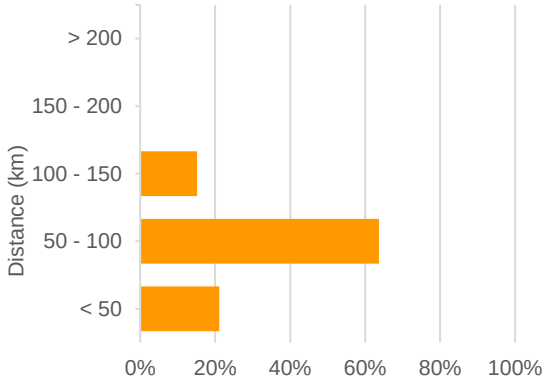

Figure A.0.24. Distances from hydrogen sources to city bus fleet in Düsseldorf

A.9. Essen, Germany

The estimated number of buses is 434 units.

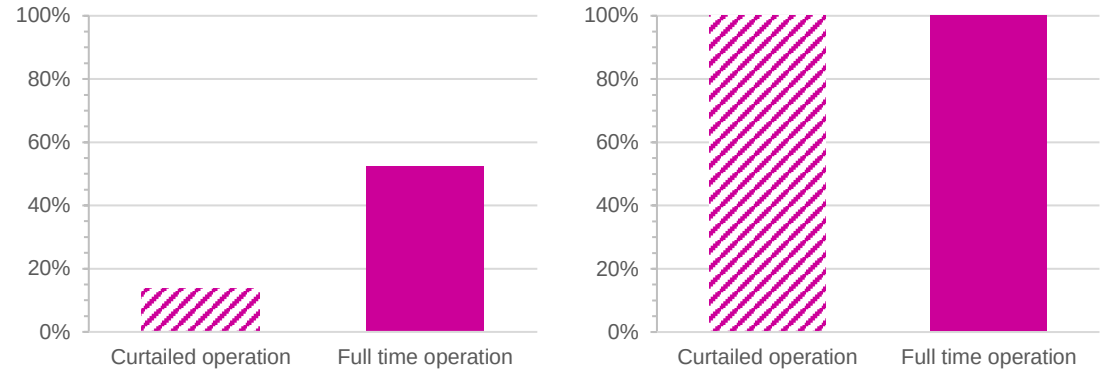

Figure A.0.25. The percentage of city bus fuel in Essen displaceable by renewable hydrogen in Dublin for different electrolyser operation modes by using a) wind electricity and b) wind and solar electricity

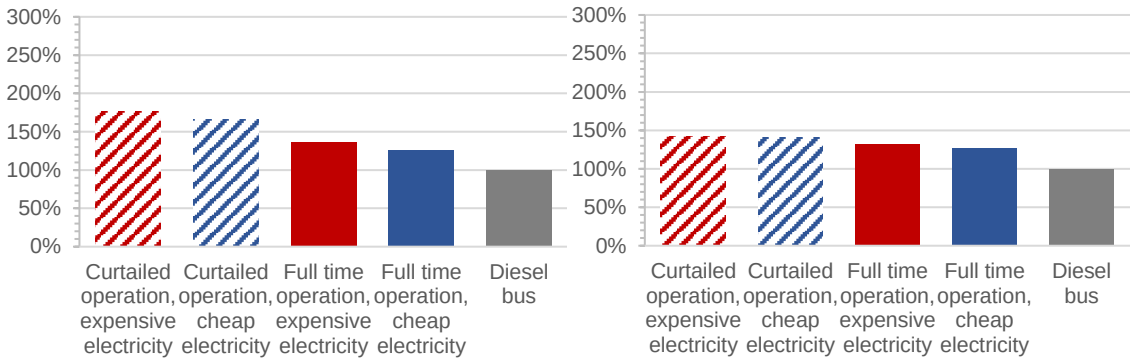

Figure A.0.26. The percentage of operational costs for hydrogen buses in Essen for different electricity prices and electrolyser operation modes by using a) wind electricity and b) wind and solar electricity, relative to diesel

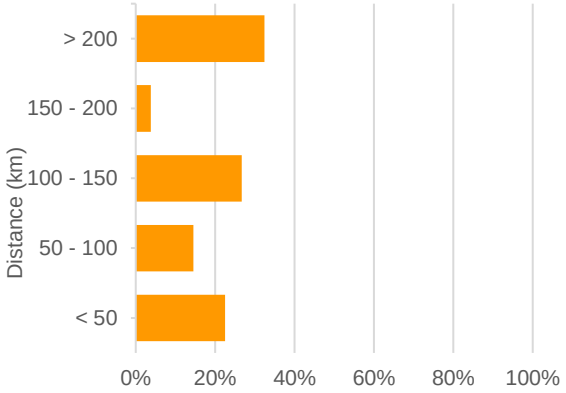

Figure A.0.27. Distances from hydrogen sources to city bus fleet in Essen

A.10. Frankfurt, Germany

The estimated number of buses is 457 units.

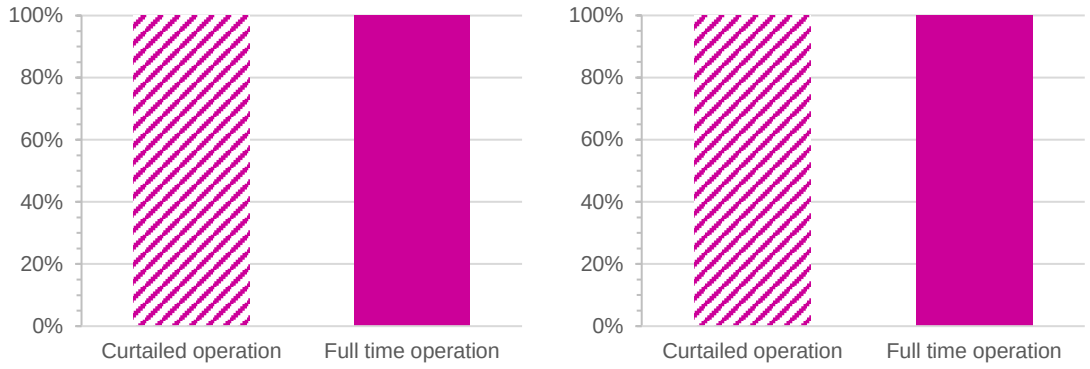

Figure A.0.28. The percentage of city bus fuel in Frankfurt displaceable by renewable hydrogen in Dublin for different electrolyser operation modes by using a) wind electricity and b) wind and solar electricity

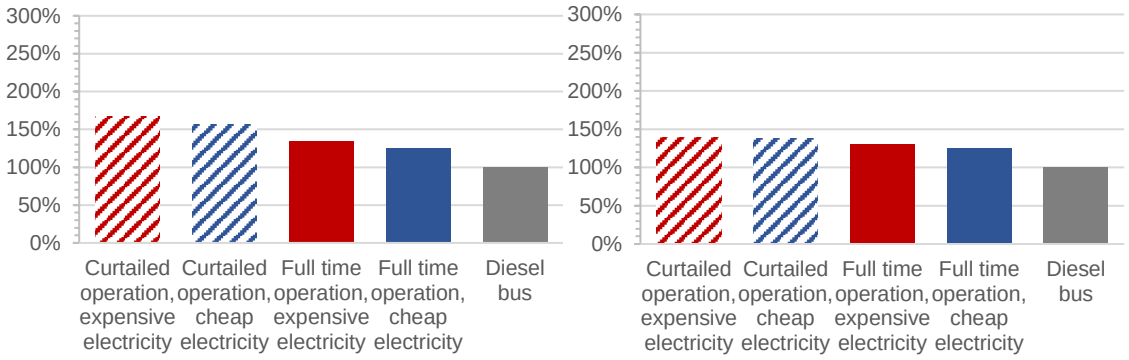

Figure A.0.29. The percentage of operational costs for hydrogen buses in Frankfurt for different electricity prices and electrolyser operation modes by using a) wind electricity and b) wind and solar electricity, relative to diesel

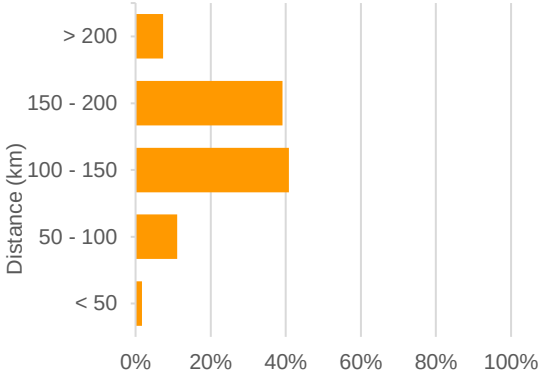

Figure A.0.30. Distances from hydrogen sources to city bus fleet in Frankfurt

A.11. Hamburg, Germany

The estimated number of buses is 457 units.

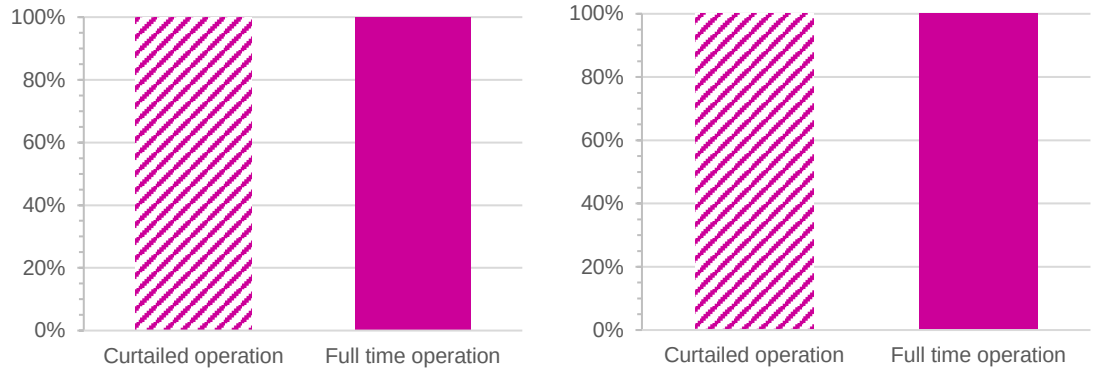

Figure A.0.31. The percentage of city bus fuel in Hamburg displaceable by renewable hydrogen in Dublin for different electrolyser operation modes by using a) wind electricity and b) wind and solar electricity

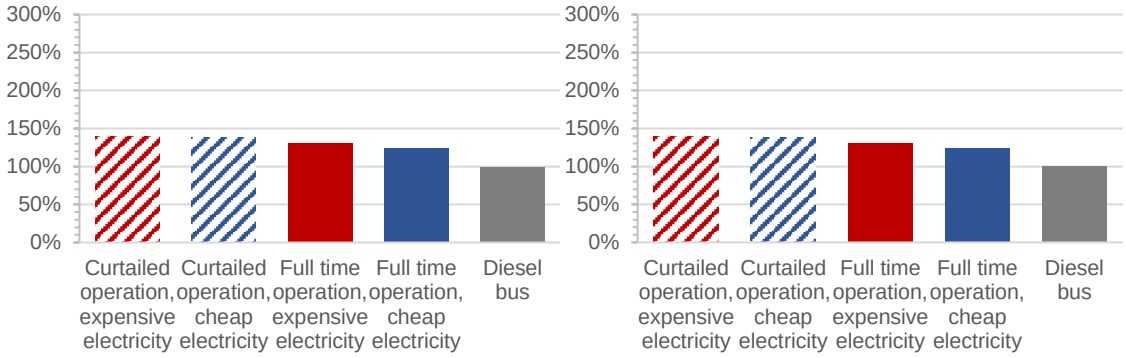

Figure A.0.32. The percentage of operational costs for hydrogen buses in Hamburg for different electricity prices and electrolyser operation modes by using a) wind electricity and b) wind and solar electricity, relative to diesel

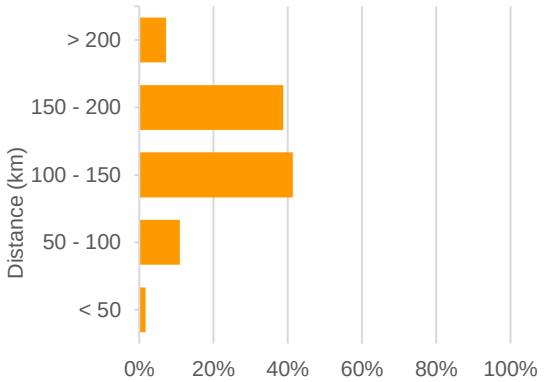

Figure A.0.33. Distances from hydrogen sources to city bus fleet in Hamburg

A.12. Hannover, Germany

The estimated number of buses is 425 units.

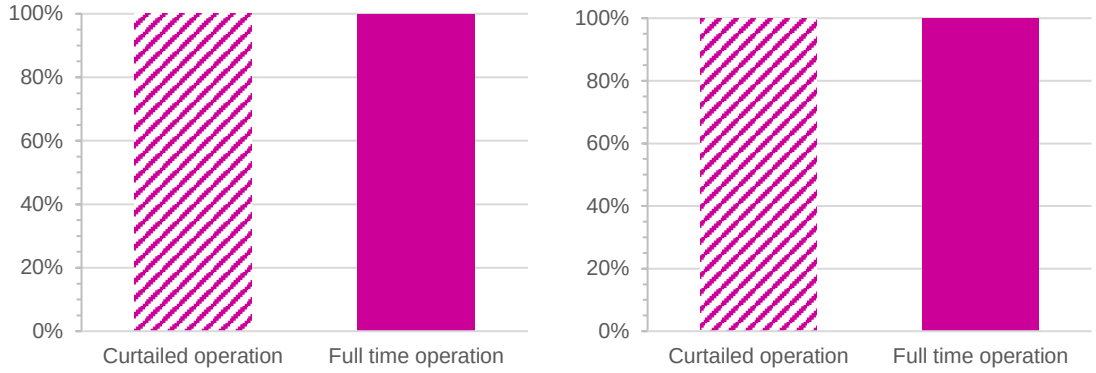

Figure A.0.34. The percentage of city bus fuel in Hannover displaceable by renewable hydrogen in Dublin for different electrolyser operation modes by using a) wind electricity and b) wind and solar electricity

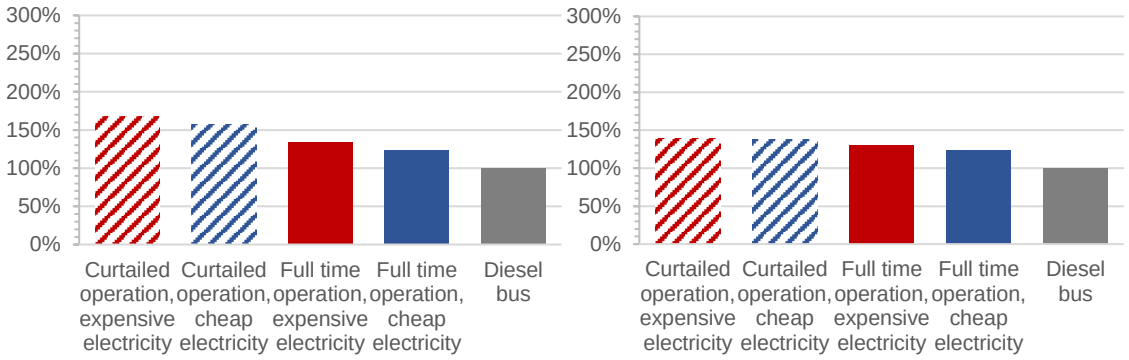

Figure A.0.35. The percentage of operational costs for hydrogen buses in Hannover for different electricity prices and electrolyser operation modes by using a) wind electricity and b) wind and solar electricity, relative to diesel

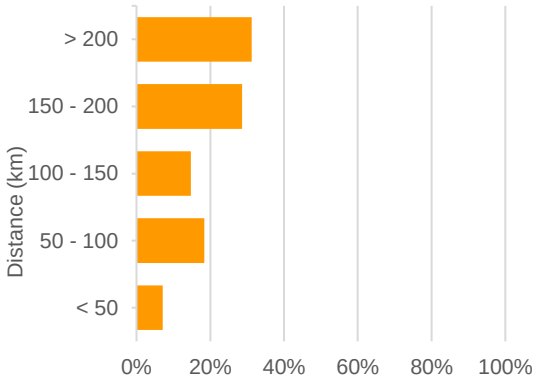

Figure A.0.36. Distances from hydrogen sources to city bus fleet in Hannover

A.13. Köln, Germany

The estimated number of buses is 522 units.

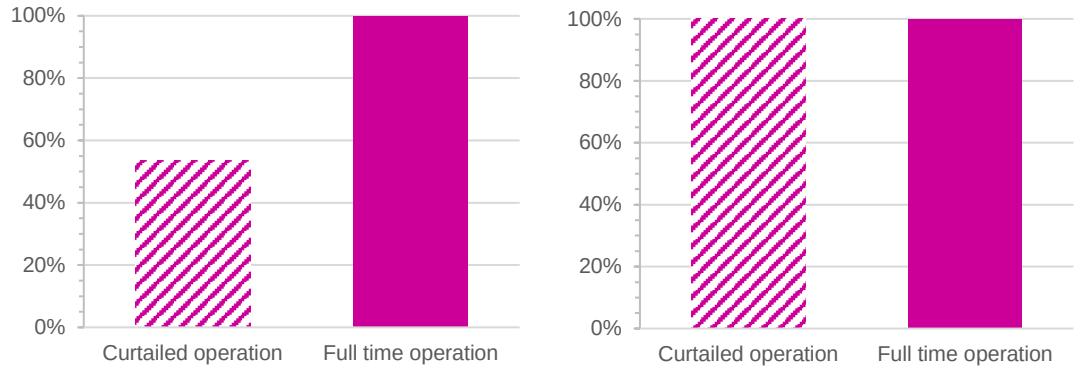

Figure A.0.37. The percentage of city bus fuel in Köln displaceable by renewable hydrogen in Dublin for different electrolyser operation modes by using a) wind electricity and b) wind and solar electricity

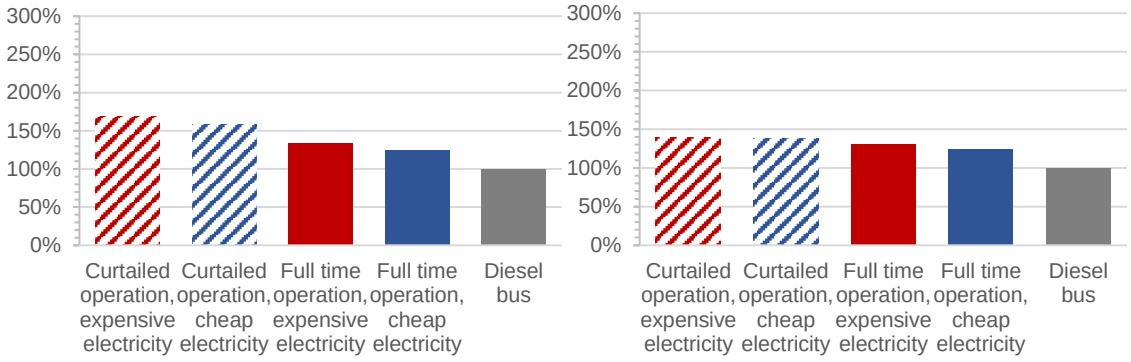

Figure A.0.38. The percentage of operational costs for hydrogen buses in Köln for different electricity prices and electrolyser operation modes by using a) wind electricity and b) wind and solar electricity, relative to diesel

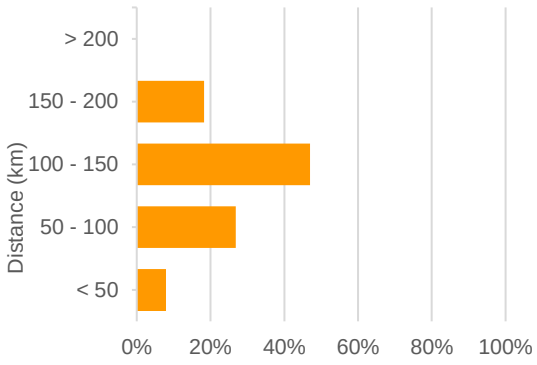

Figure A.0.39. Distances from hydrogen sources to city bus fleet in Köln

A.14. Leipzig, Germany

The estimated number of buses is 427 units.

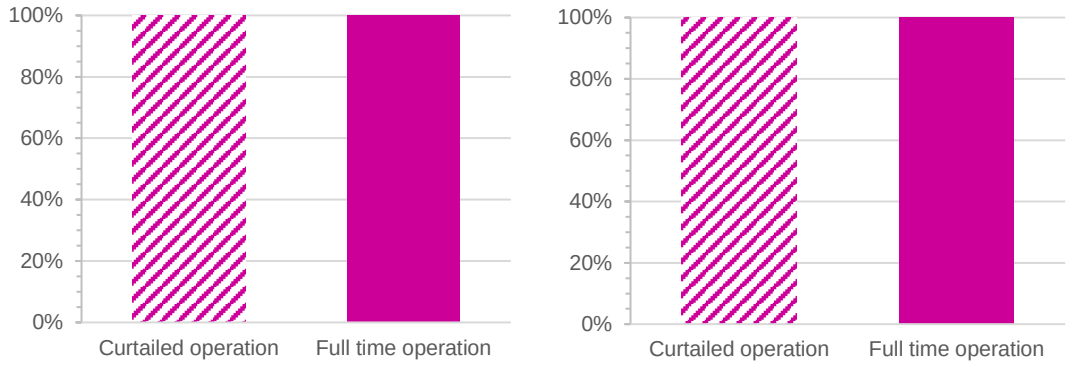

Figure A.0.40. The percentage of city bus fuel in Leipzig displaceable by renewable hydrogen in Dublin for different electrolyser operation modes by using a) wind electricity and b) wind and solar electricity

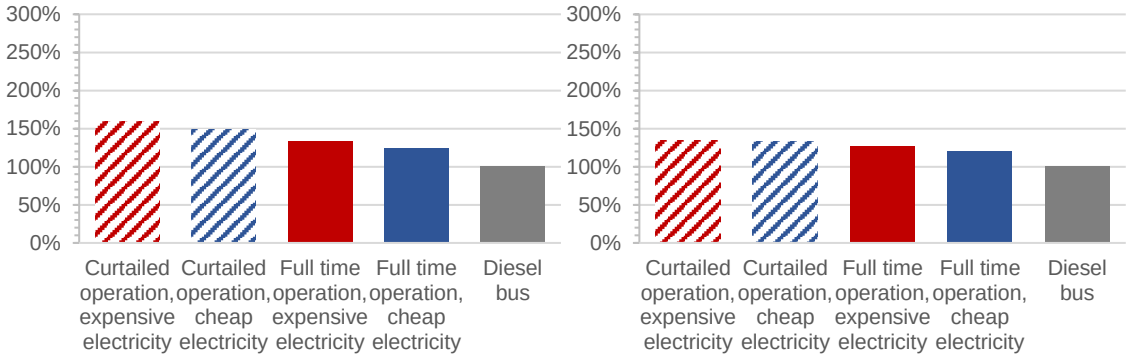

Figure A.0.41. The percentage of operational costs for hydrogen buses in Leipzig for different electricity prices and electrolyser operation modes by using a) wind electricity and b) wind and solar electricity, relative to diesel

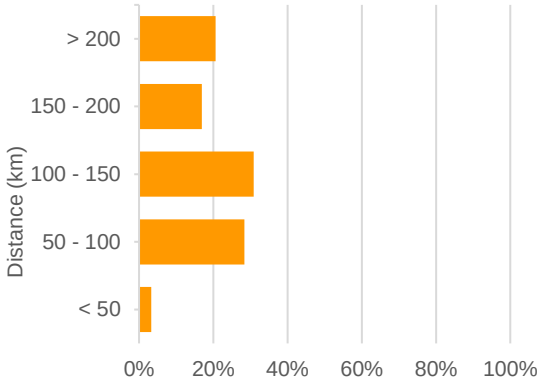

Figure A.0.42. Distances from hydrogen sources to city bus fleet in Leipzig

A.15. München, Germany

The estimated number of buses is 606 units.

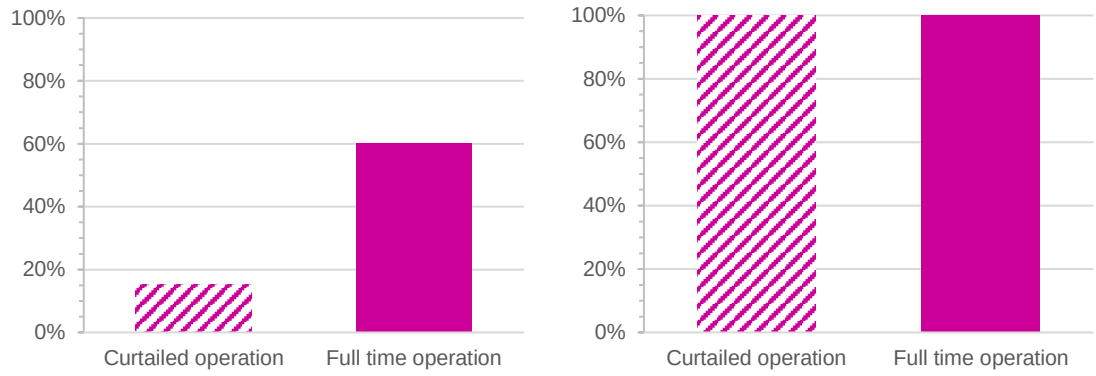

Figure A.0.43. The percentage of city bus fuel in München displaceable by renewable hydrogen in Dublin for different electrolyser operation modes by using a) wind electricity and b) wind and solar electricity

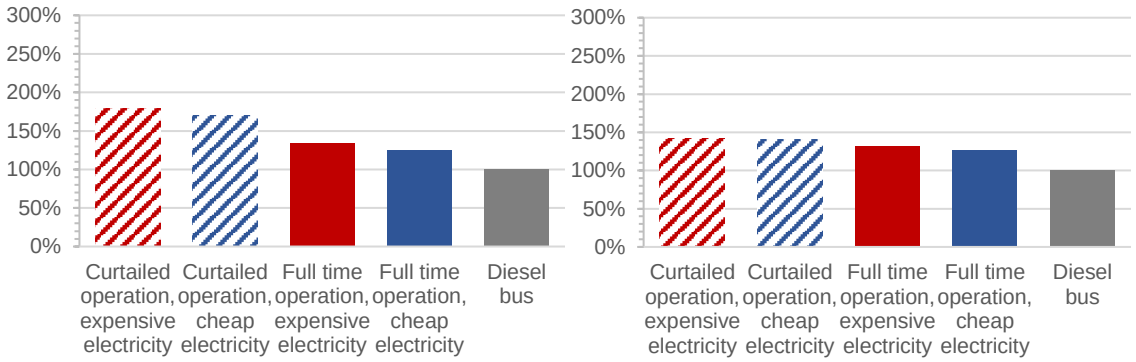

Figure A.0.44. The percentage of operational costs for hydrogen buses in München for different electricity prices and electrolyser operation modes by using a) wind electricity and b) wind and solar electricity, relative to diesel

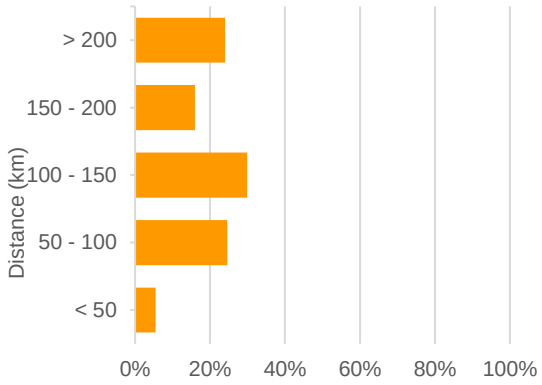

Figure A.0.45. Distances from hydrogen sources to city bus fleet in München

A.16. Nürnberg, Germany

The estimated number of buses is 422 units.

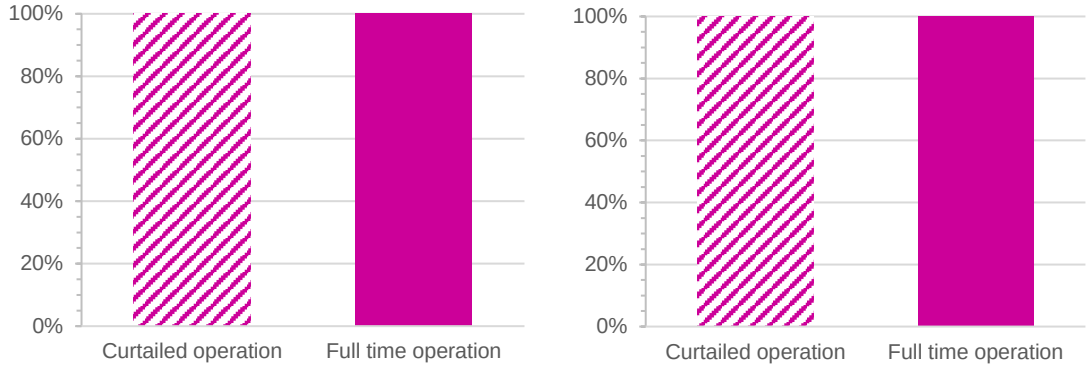

Figure A.0.46. The percentage of city bus fuel in Nürnberg displaceable by renewable hydrogen in Dublin for different electrolyser operation modes by using a) wind electricity and b) wind and solar electricity

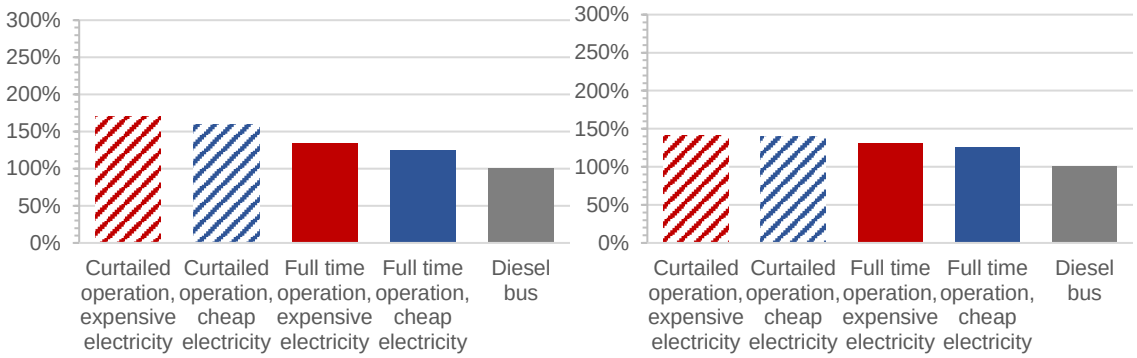

Figure A.0.47. The percentage of operational costs for hydrogen buses in Nürnberg for different electricity prices and electrolyser operation modes by using a) wind electricity and b) wind and solar electricity, relative to diesel

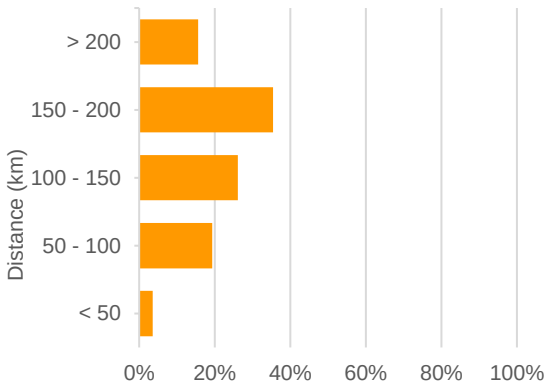

Figure A.0.48. Distances from hydrogen sources to city bus fleet in Nürnberg

A.17. Lille, France

The estimated number of buses is 495 units.

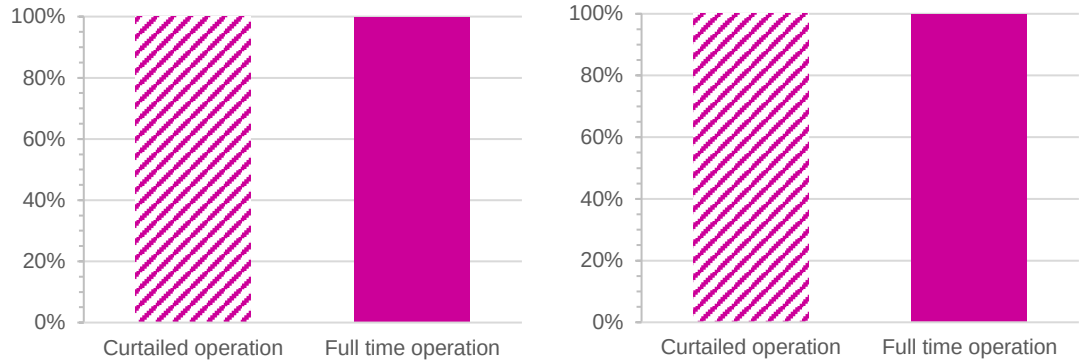

Figure A.0.49. The percentage of city bus fuel in Lille displaceable by renewable hydrogen in Dublin for different electrolyser operation modes by using a) wind electricity and b) wind and solar electricity

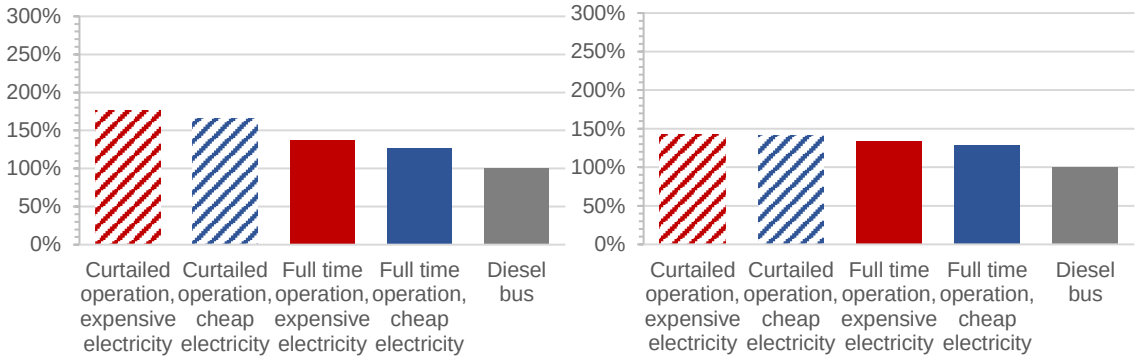

Figure A.0.50. The percentage of operational costs for hydrogen buses in Lille for different electricity prices and electrolyser operation modes by using a) wind electricity and b) wind and solar electricity, relative to diesel

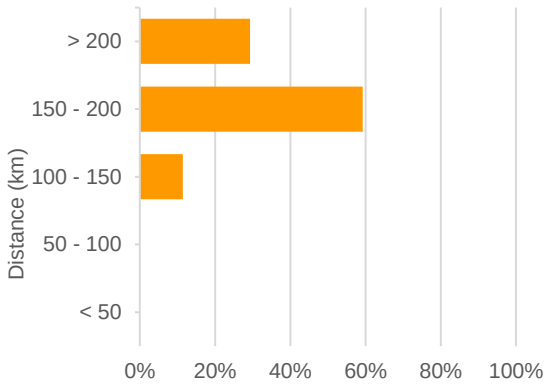

Figure A.0.51. Distances from hydrogen sources to city bus fleet in Lille

A.18. Paris, France

The estimated number of buses is 5,147 units.

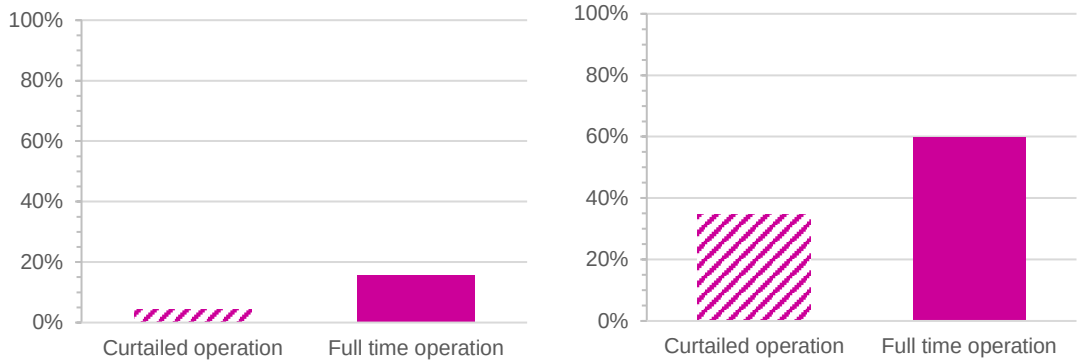

Figure A.0.52. The percentage of city bus fuel in Paris displaceable by renewable hydrogen in Dublin for different electrolyser operation modes by using a) wind electricity and b) wind and solar electricity

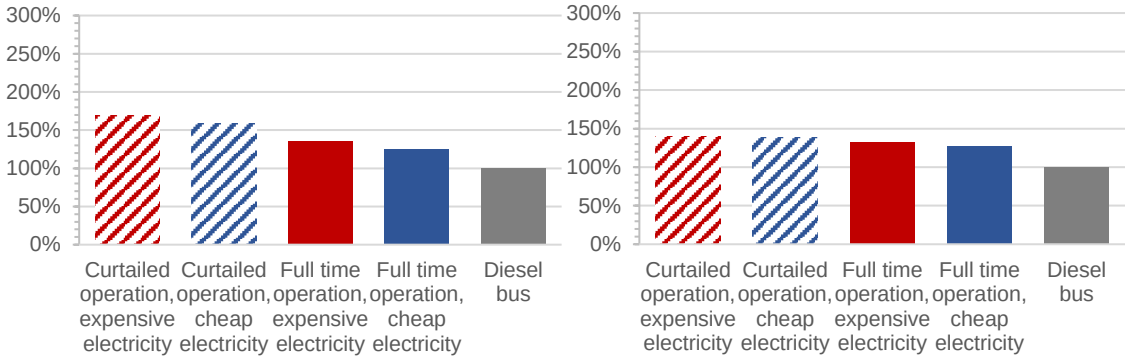

Figure A.0.53. The percentage of operational costs for hydrogen buses in Paris for different electricity prices and electrolyser operation modes by using a) wind electricity and b) wind and solar electricity, relative to diesel

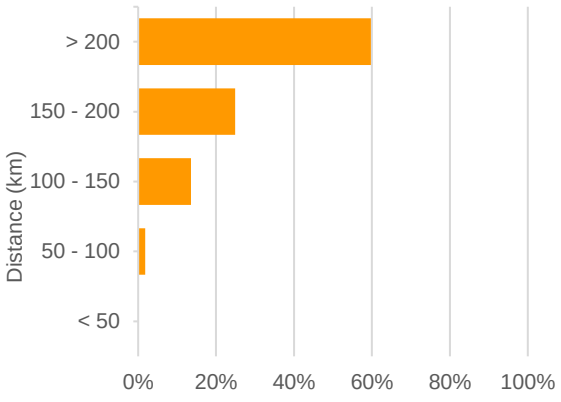

Figure A.0.54. Distances from hydrogen sources to city bus fleet in Paris

A.19. Strasbourg, France

The estimated number of buses is 405 units.

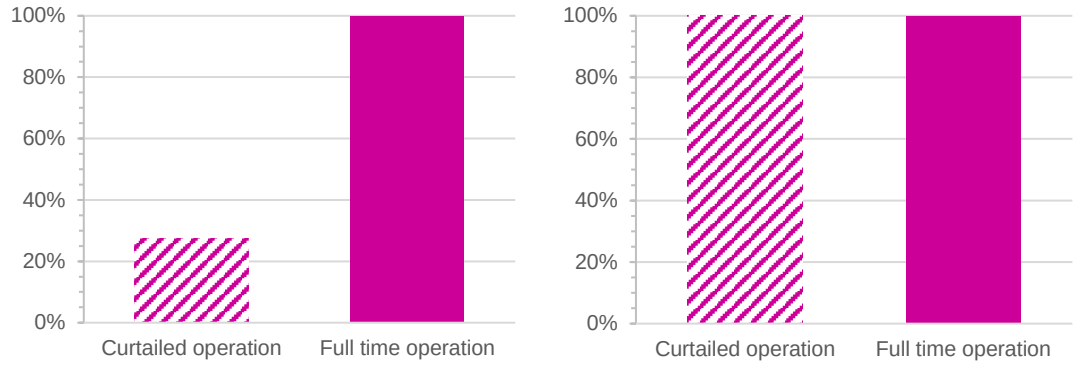

Figure A.0.55. The percentage of city bus fuel in Strasbourg displaceable by renewable hydrogen in Dublin for different electrolyser operation modes by using a) wind electricity and b) wind and solar electricity

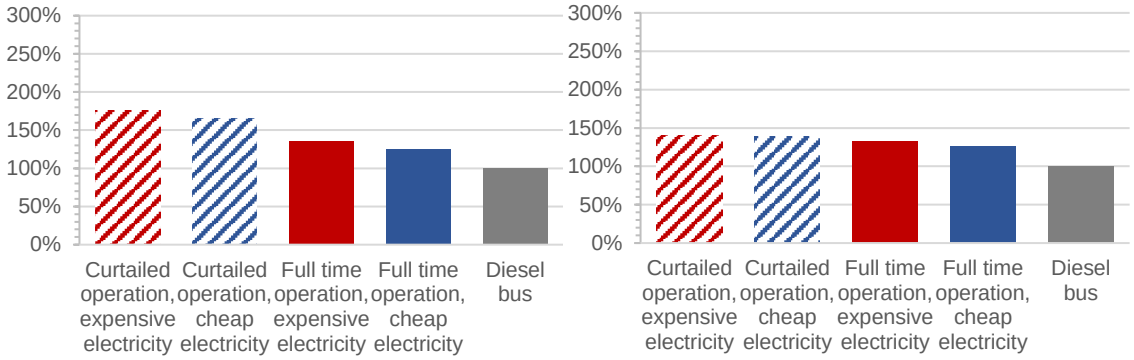

Figure A.0.56. The percentage of operational costs for hydrogen buses in Strasbourg for different electricity prices and electrolyser operation modes by using a) wind electricity and b) wind and solar electricity, relative to diesel

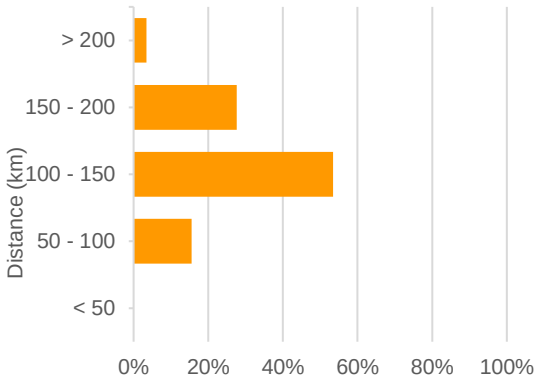

Figure A.0.57. Distances from hydrogen sources to city bus fleet in Strasbourg

A.20. Bradford, United Kingdom

The estimated number of buses is 426 units.

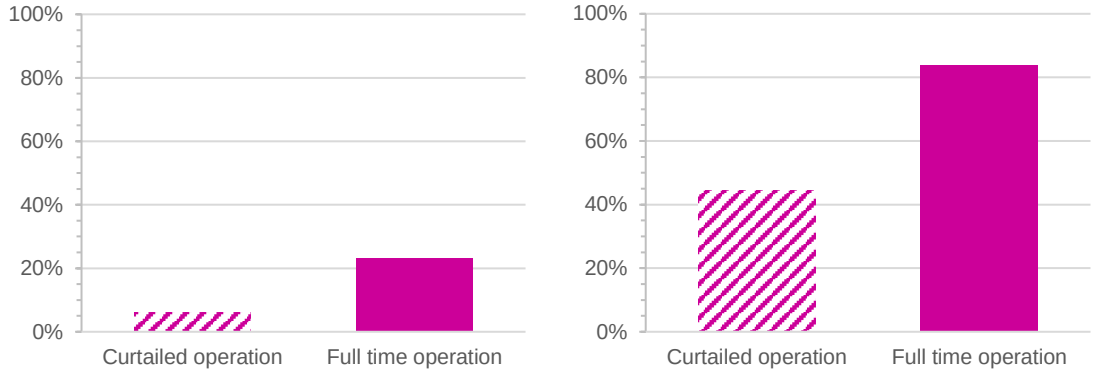

Figure A.0.58. The percentage of city bus fuel in Bradford displaceable by renewable hydrogen in Dublin for different electrolyser operation modes by using a) wind electricity and b) wind and solar electricity

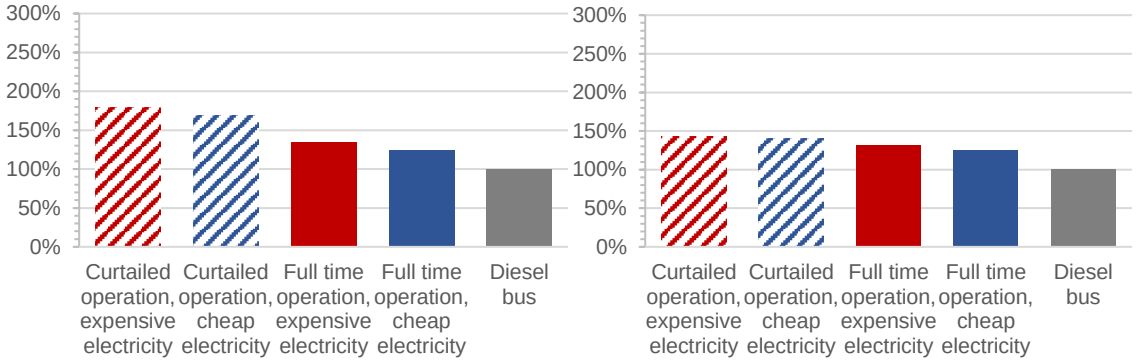

Figure A.0.59. The percentage of operational costs for hydrogen buses in Bradford for different electricity prices and electrolyser operation modes by using a) wind electricity and b) wind and solar electricity, relative to diesel

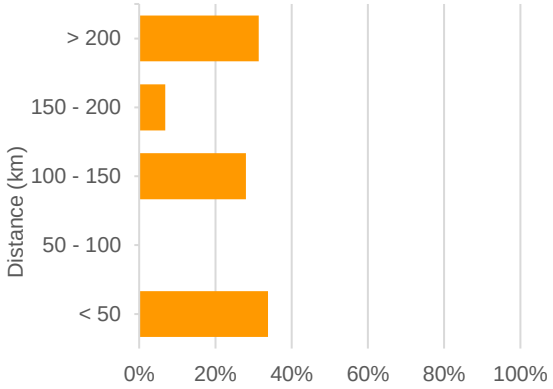

Figure A.0.60. Distances from hydrogen sources to city bus fleet in Bradford

A.21. Bristol, United Kingdom

The estimated number of buses is 412 units.

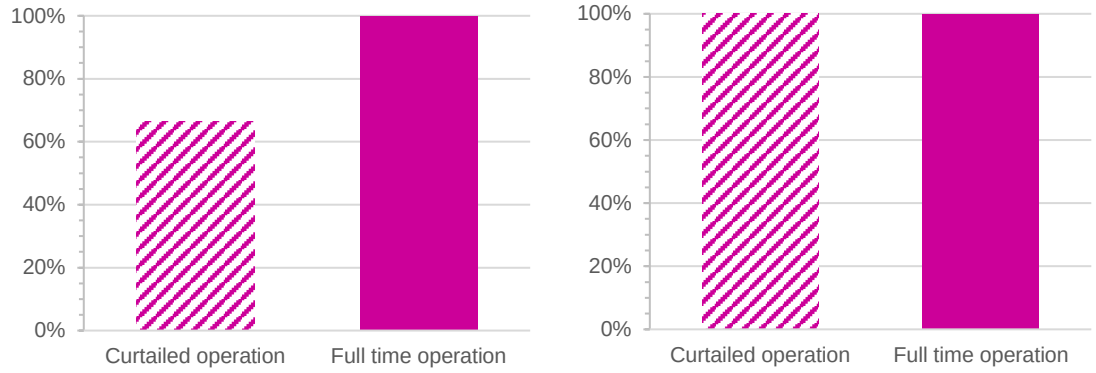

Figure A.0.61. The percentage of city bus fuel in Bristol displaceable by renewable hydrogen in Dublin for different electrolyser operation modes by using a) wind electricity and b) wind and solar electricity

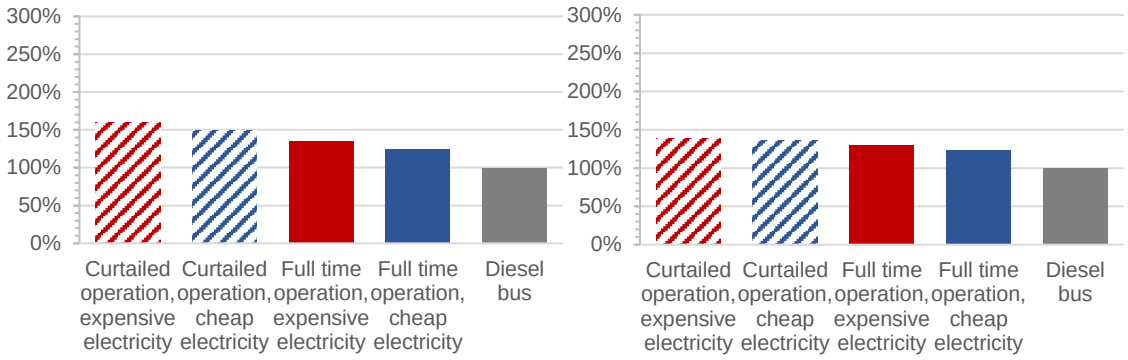

Figure A.0.62. The percentage of operational costs for hydrogen buses in Bristol for different electricity prices and electrolyser operation modes by using a) wind electricity and b) wind and solar electricity, relative to diesel

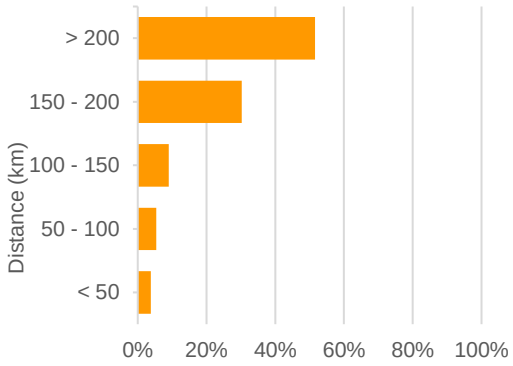

Figure A.0.63. Distances from hydrogen sources to city bus fleet in Bristol

A.22. Edinburgh, United Kingdom

The estimated number of buses is 420 units.

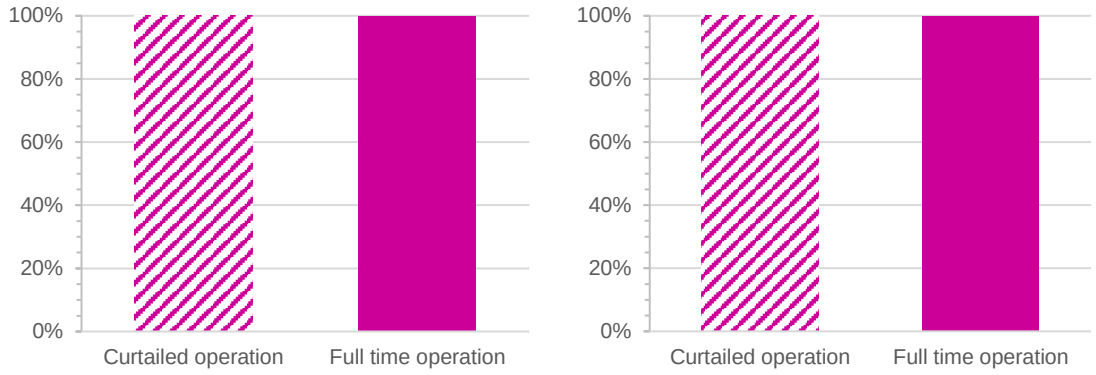

Figure A.0.64. The percentage of city bus fuel in Edinburgh displaceable by renewable hydrogen in Dublin for different electrolyser operation modes by using a) wind electricity and b) wind and solar electricity

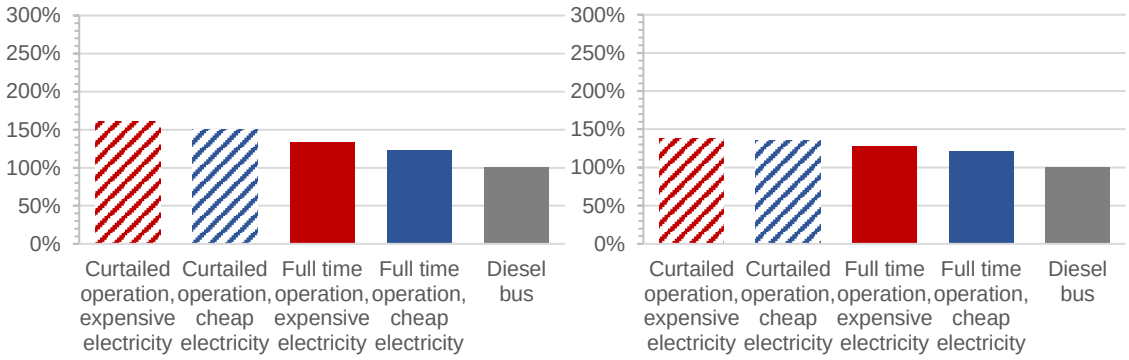

Figure A.0.65. The percentage of operational costs for hydrogen buses in Edinburgh for different electricity prices and electrolyser operation modes by using a) wind electricity and b) wind and solar electricity, relative to diesel

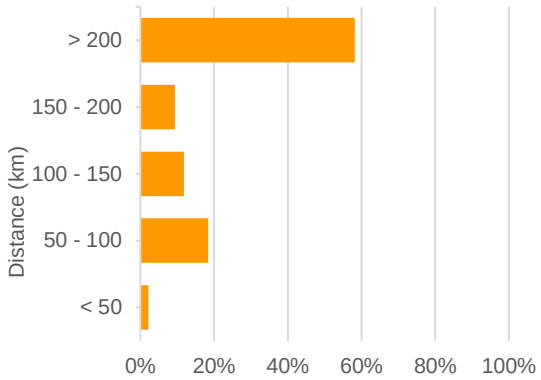

Figure A.0.66. Distances from hydrogen sources to city bus fleet in Edinburgh

A.23. Glasgow, United Kingdom

The estimated number of buses is 439 units.

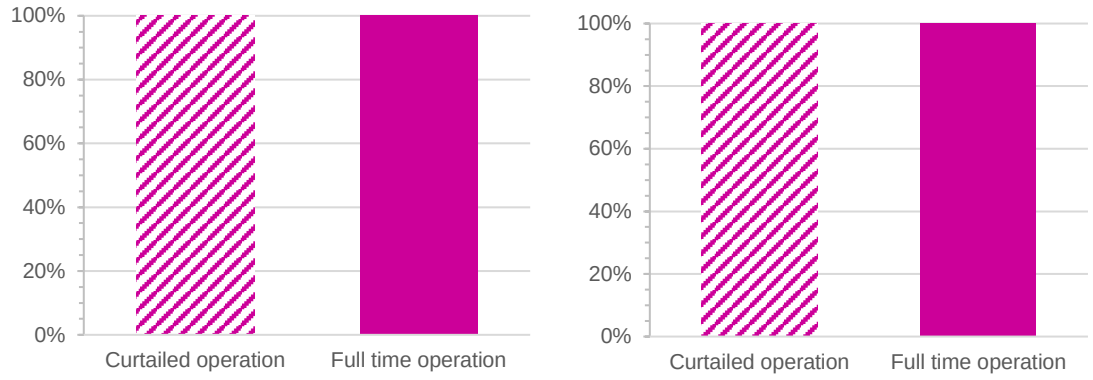

Figure A.0.67. The percentage of city bus fuel in Glasgow displaceable by renewable hydrogen in Dublin for different electrolyser operation modes by using a) wind electricity and b) wind and solar electricity

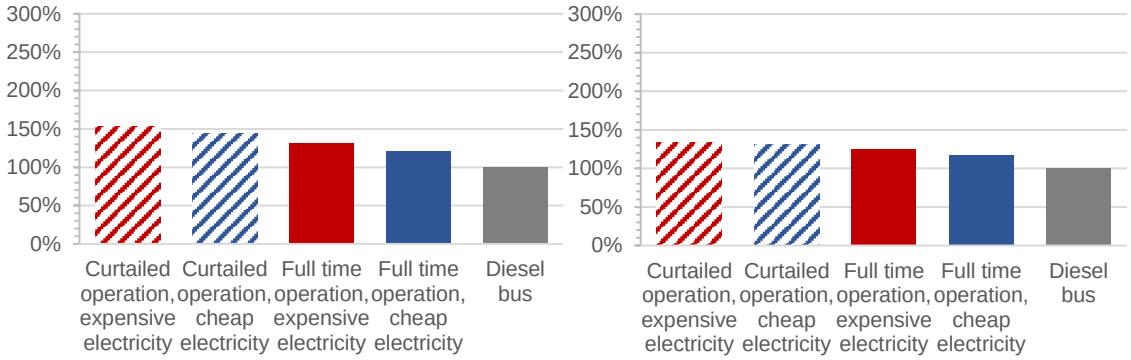

Figure A.0.68. The percentage of operational costs for hydrogen buses in Glasgow for different electricity prices and electrolyser operation modes by using a) wind electricity and b) wind and solar electricity, relative to diesel

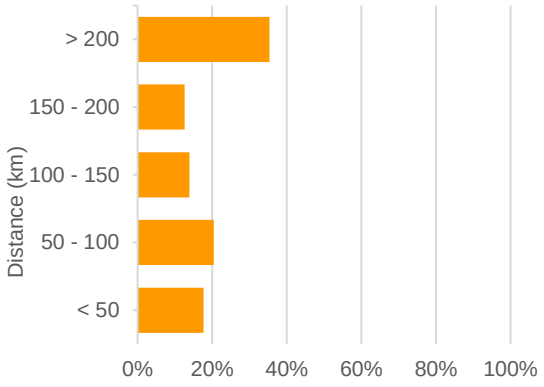

Figure A.0.69. Distances from hydrogen sources to city bus fleet in Glasgow

A.24. Belfast, United Kingdom

The estimated number of buses is 1,000 units.

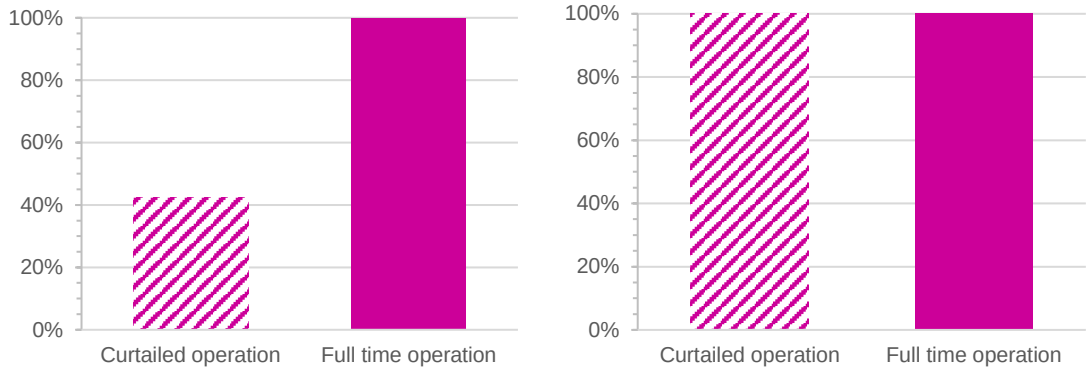

Figure A.0.70. The percentage of city bus fuel in Belfast displaceable by renewable hydrogen in Dublin for different electrolyser operation modes by using a) wind electricity and b) wind and solar electricity

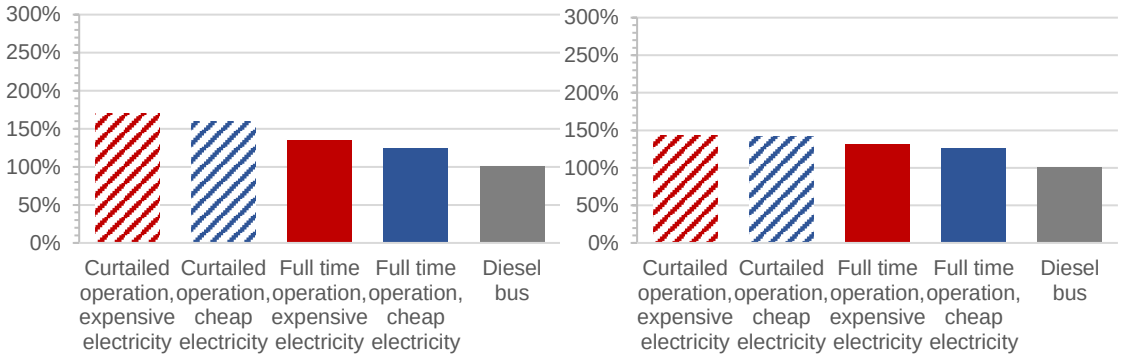

Figure A.0.71. The percentage of operational costs for hydrogen buses in Belfast for different electricity prices and electrolyser operation modes by using a) wind electricity and b) wind and solar electricity, relative to diesel

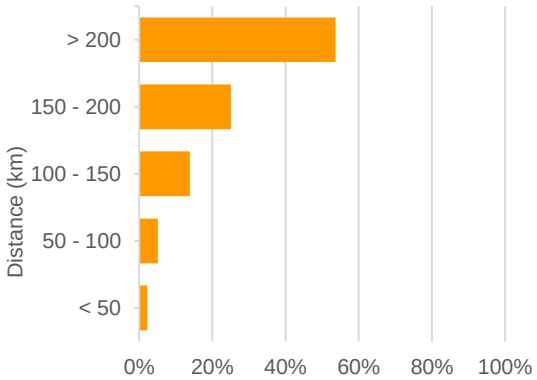

Figure A.0.72. Distances from hydrogen sources to city bus fleet in Belfast

A.25. Nottingham, United Kingdom

The estimated number of buses is 448 units.

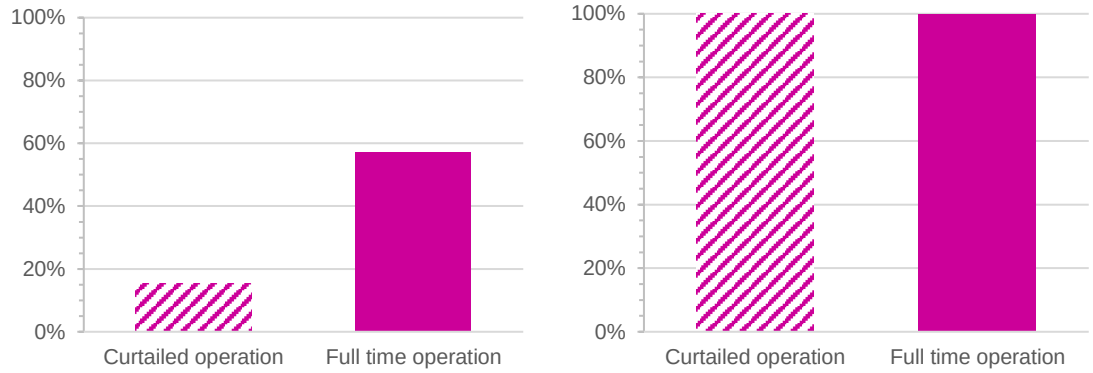

Figure A.0.73. The percentage of city bus fuel in Nottingham displaceable by renewable hydrogen in Dublin for different electrolyser operation modes by using a) wind electricity and b) wind and solar electricity

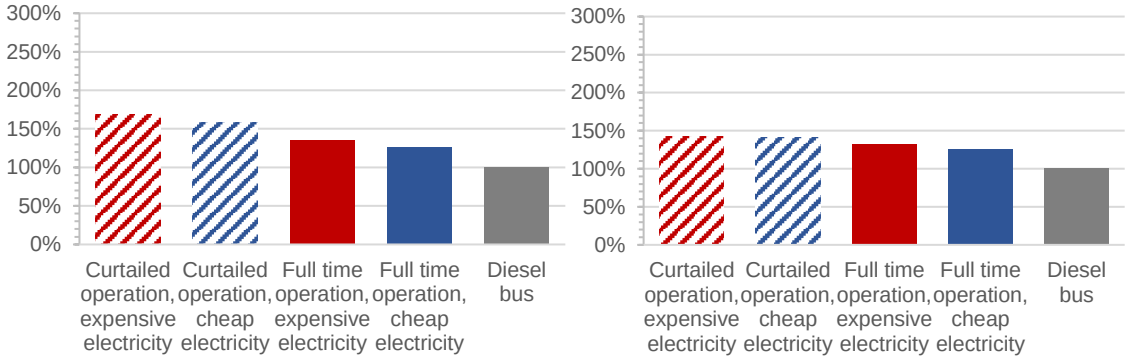

Figure A.0.74. The percentage of operational costs for hydrogen buses in Nottingham for different electricity prices and electrolyser operation modes by using a) wind electricity and b) wind and solar electricity, relative to diesel

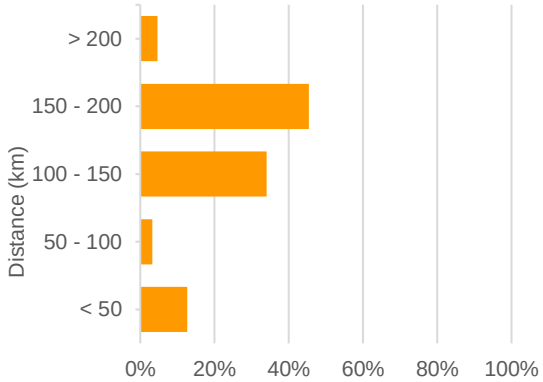

Figure A.0.75. Distances from hydrogen sources to city bus fleet in Nottingham

A.26. Kirklees, United Kingdom

The estimated number of buses is 410 units.

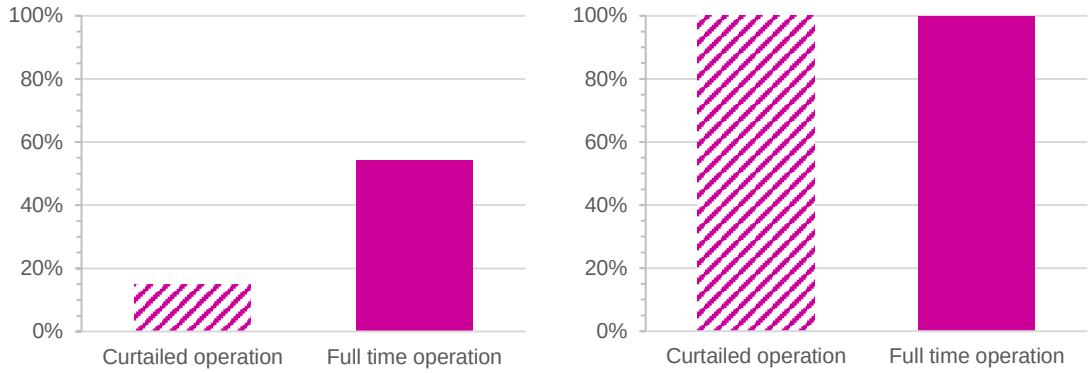

Figure A.0.76. The percentage of city bus fuel in Kirklees displaceable by renewable hydrogen in Dublin for different electrolyser operation modes by using a) wind electricity and b) wind and solar electricity

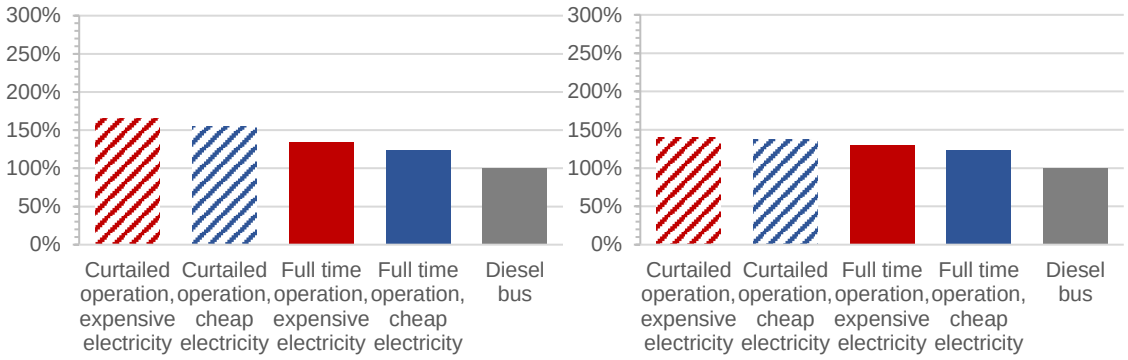

Figure A.0.77. The percentage of operational costs for hydrogen buses in Kirklees for different electricity prices and electrolyser operation modes by using a) wind electricity and b) wind and solar electricity, relative to diesel

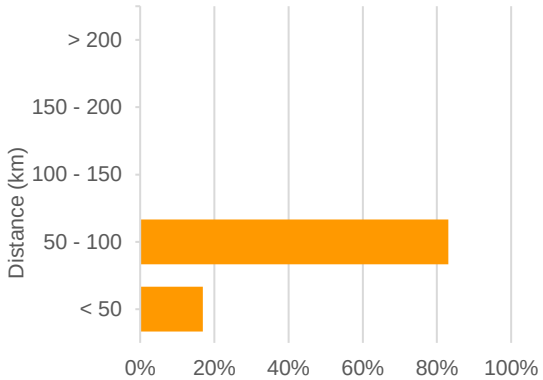

Figure A.0.78. Distances from hydrogen sources to city bus fleet in Kirklees

A.27. Leeds, United Kingdom

The estimated number of buses is 469 units.

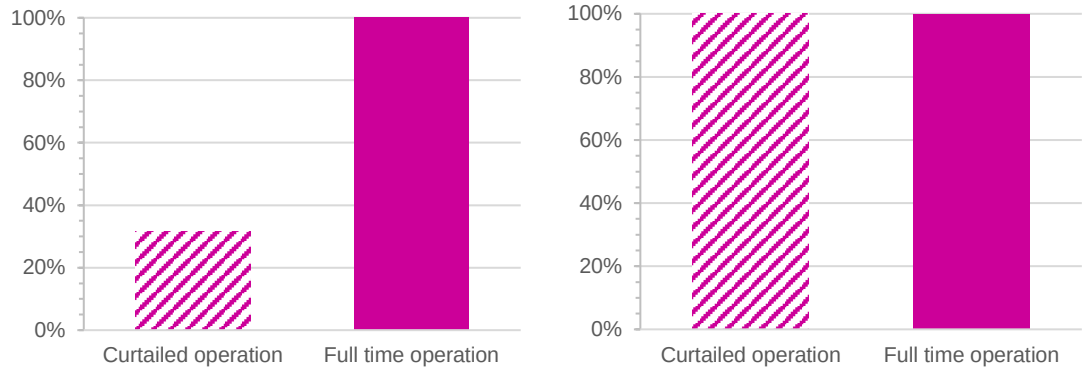

Figure A.0.79. The percentage of city bus fuel in Leeds displaceable by renewable hydrogen in Dublin for different electrolyser operation modes by using a) wind electricity and b) wind and solar electricity

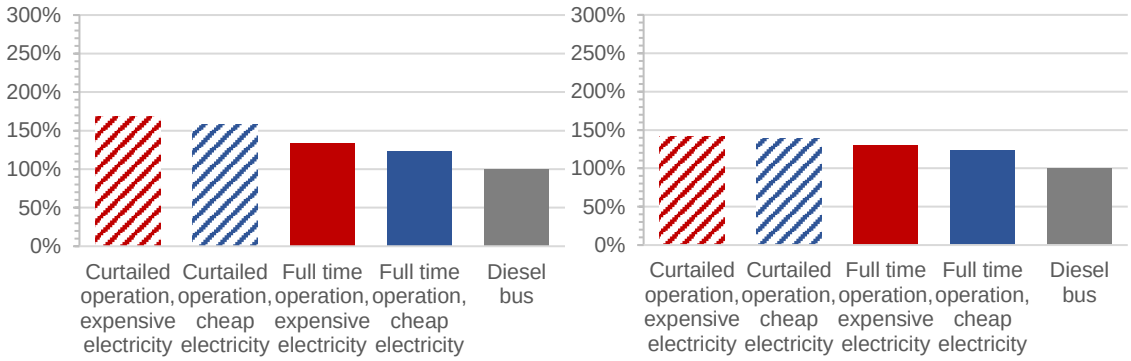

Figure A.0.80. The percentage of operational costs for hydrogen buses in Leeds for different electricity prices and electrolyser operation modes by using a) wind electricity and b) wind and solar electricity, relative to diesel

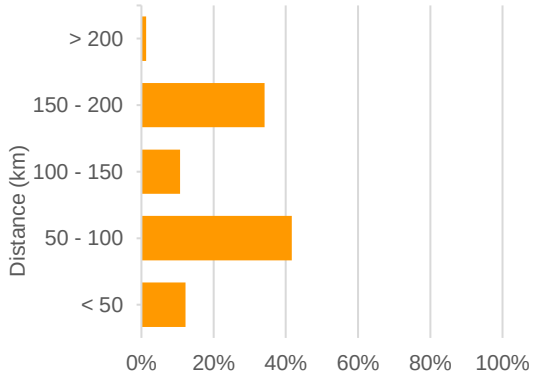

Figure A.0.81. Distances from hydrogen sources to city bus fleet in Leeds

A.28. Leicester, United Kingdom

420

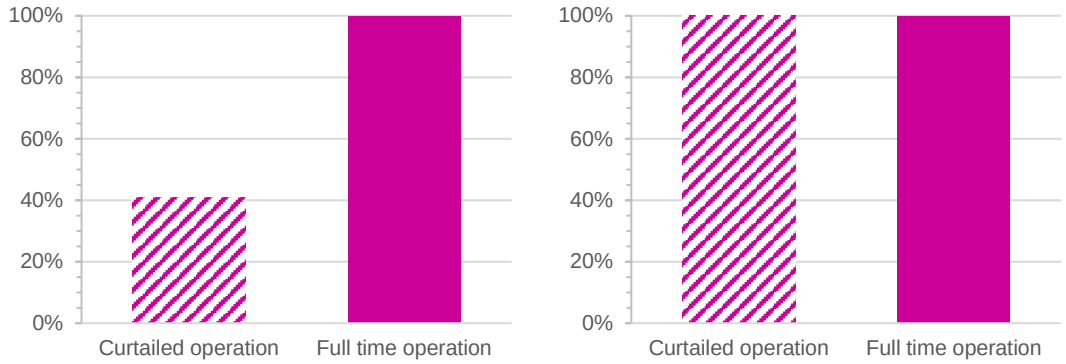

Figure A.0.82. The percentage of city bus fuel in Leicester displaceable by renewable hydrogen in Dublin for different electrolyser operation modes by using a) wind electricity and b) wind and solar electricity

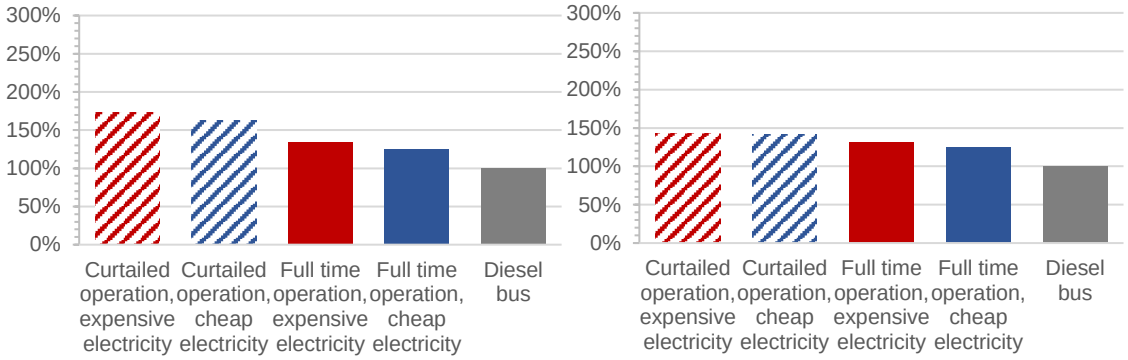

Figure A.0.83. The percentage of operational costs for hydrogen buses in Leicester for different electricity prices and electrolyser operation modes by using a) wind electricity and b) wind and solar electricity, relative to diesel

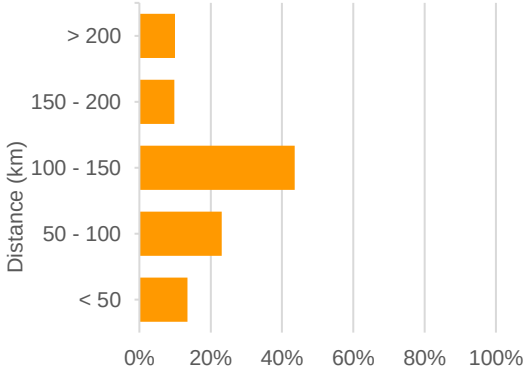

Figure A.0.84. Distances from hydrogen sources to city bus fleet in Leicester

A.29. Liverpool, United Kingdom

The estimated number of buses is 529 units.

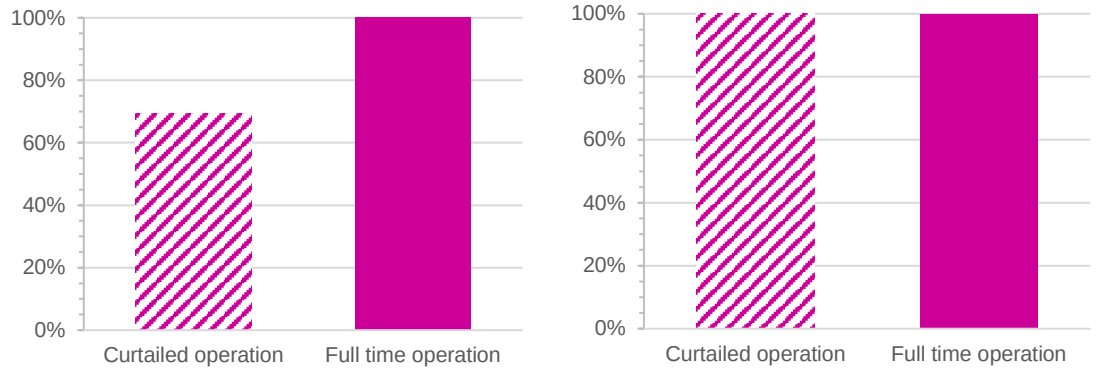

Figure A.0.85. The percentage of city bus fuel in Liverpool displaceable by renewable hydrogen in Dublin for different electrolyser operation modes by using a) wind electricity and b) wind and solar electricity

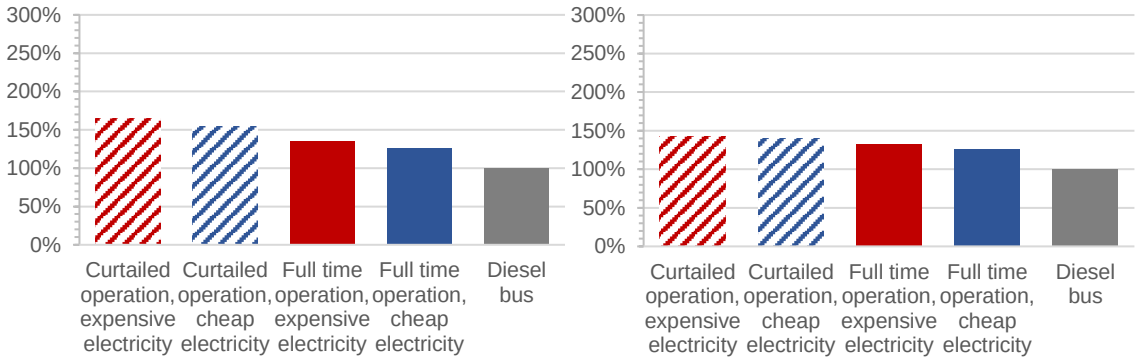

Figure A.0.86. The percentage of operational costs for hydrogen buses in Liverpool for different electricity prices and electrolyser operation modes by using a) wind electricity and b) wind and solar electricity, relative to diesel

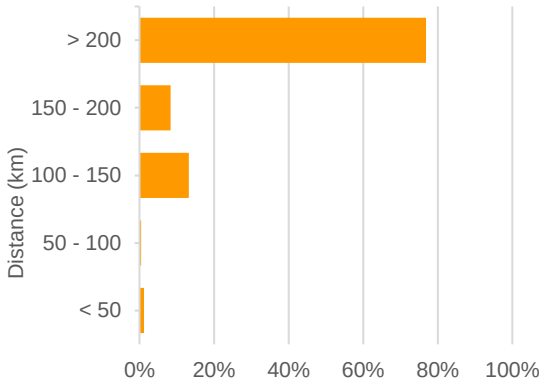

Figure A.0.87. Distances from hydrogen sources to city bus fleet in Liverpool

A.30. London, United Kingdom

The estimated number of buses is 8,000 units.

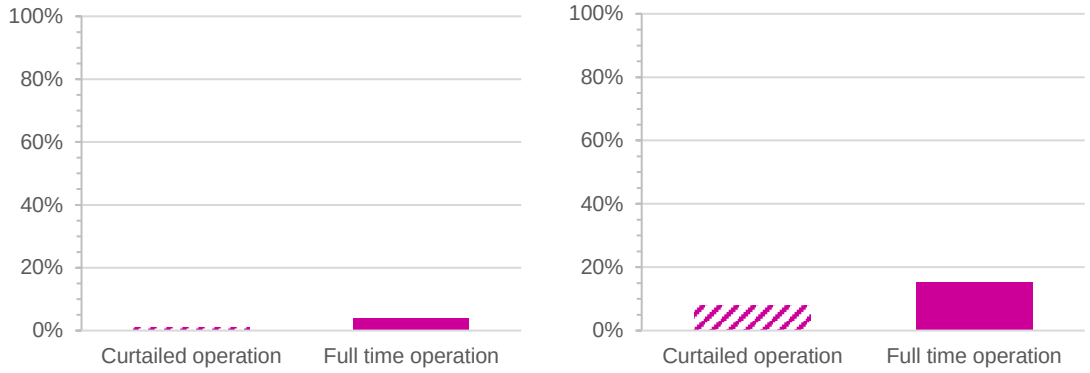

Figure A.0.88. The percentage of city bus fuel in London displaceable by renewable hydrogen in Dublin for different electrolyser operation modes by using a) wind electricity and b) wind and solar electricity

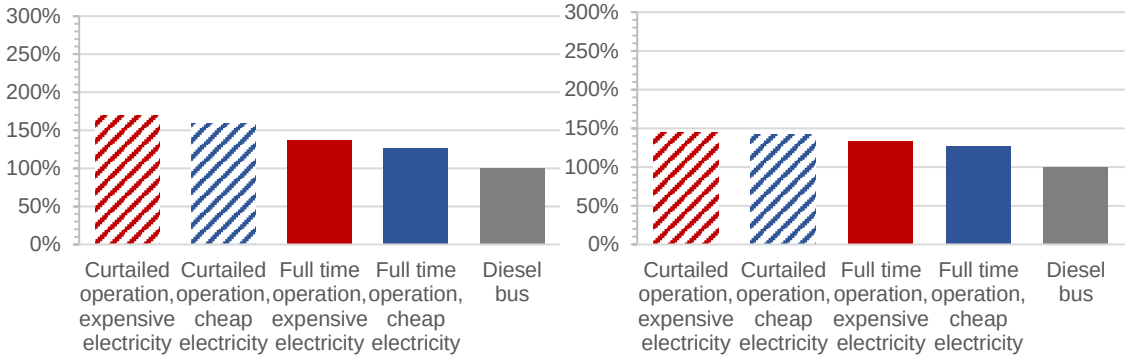

Figure A.0.89. The percentage of operational costs for hydrogen buses in London for different electricity prices and electrolyser operation modes by using a) wind electricity and b) wind and solar electricity, relative to diesel

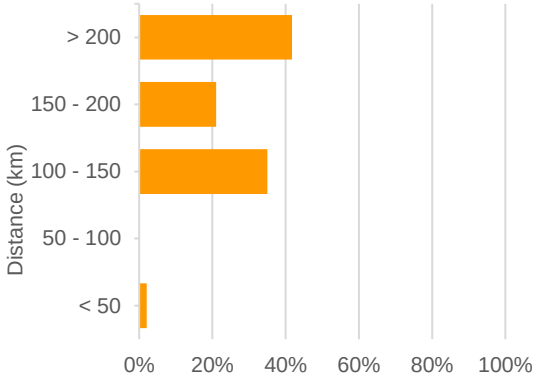

Figure A.0.90. Distances from hydrogen sources to city bus fleet in London

A.31. Portsmouth, United Kingdom

The estimated number of buses is 427 units.

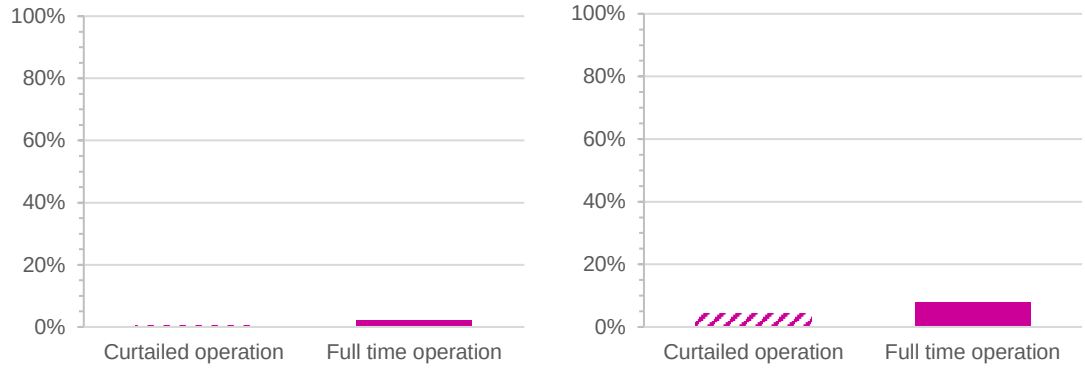

Figure A.0.91. The percentage of city bus fuel in Portsmouth displaceable by renewable hydrogen in Dublin for different electrolyser operation modes by using a) wind electricity and b) wind and solar electricity

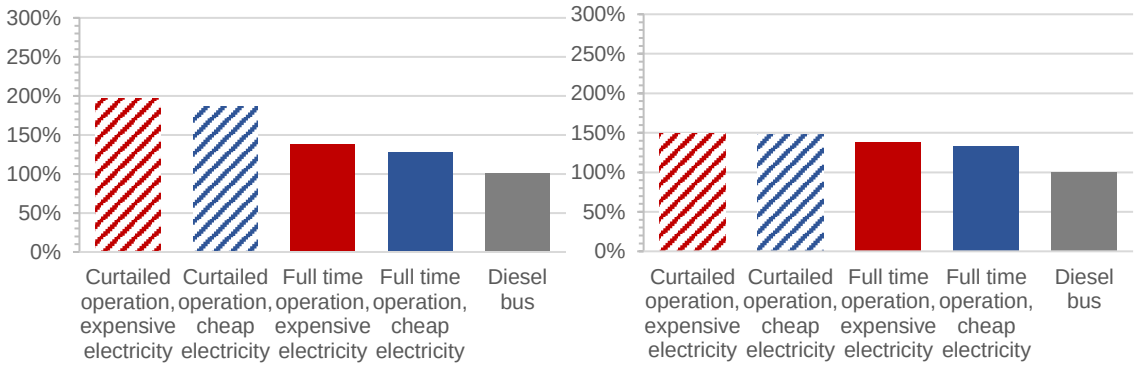

Figure A.0.92. The percentage of operational costs for hydrogen buses in Portsmouth for different electricity prices and electrolyser operation modes by using a) wind electricity and b) wind and solar electricity, relative to diesel

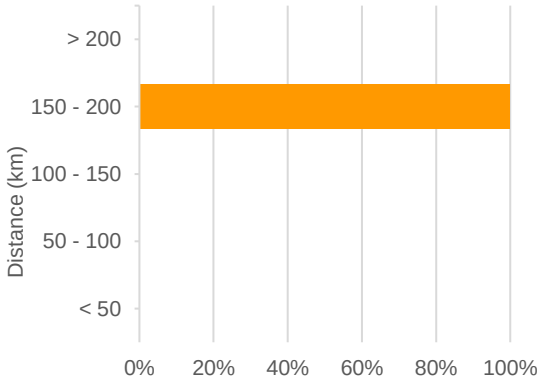

Figure A.0.93. Distances from hydrogen sources to city bus fleet in Portsmouth

A.32. Sheffield, United Kingdom

The estimated number of buses is 432 units.

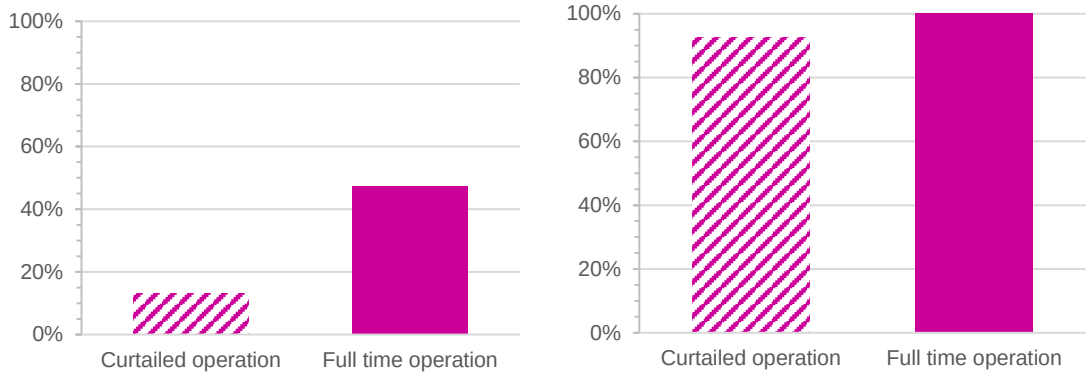

Figure A.0.94. The percentage of city bus fuel in Sheffield displaceable by renewable hydrogen in Dublin for different electrolyser operation modes by using a) wind electricity and b) wind and solar electricity

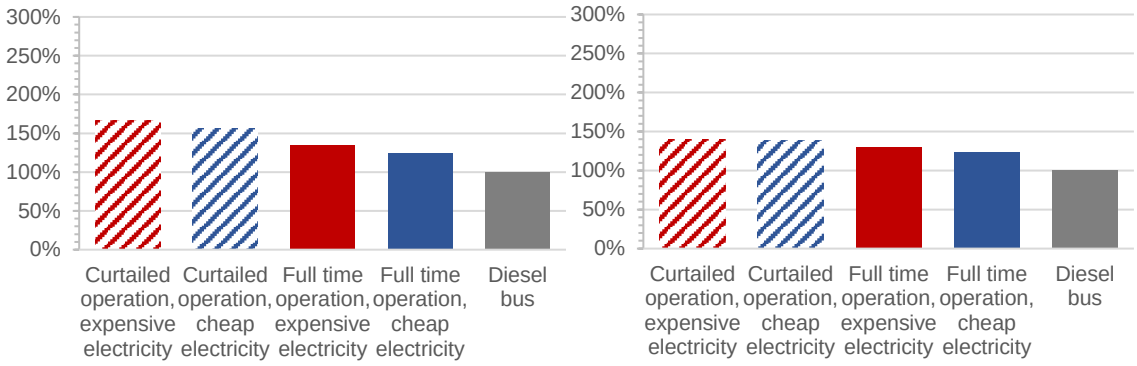

Figure A.0.95. The percentage of operational costs for hydrogen buses in Sheffield for different electricity prices and electrolyser operation modes by using a) wind electricity and b) wind and solar electricity, relative to diesel

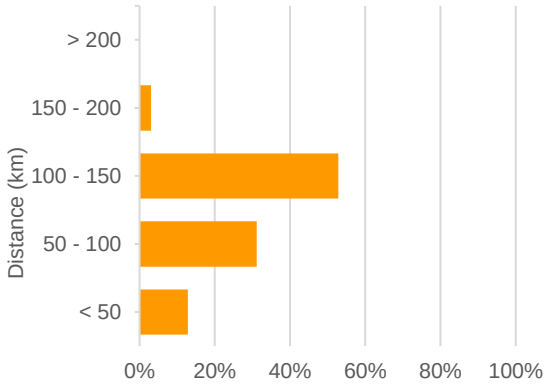

Figure A.0.96. Distances from hydrogen sources to city bus fleet in Sheffield

A.33. Tyneside, United Kingdom

The estimated number of buses is 483 units.

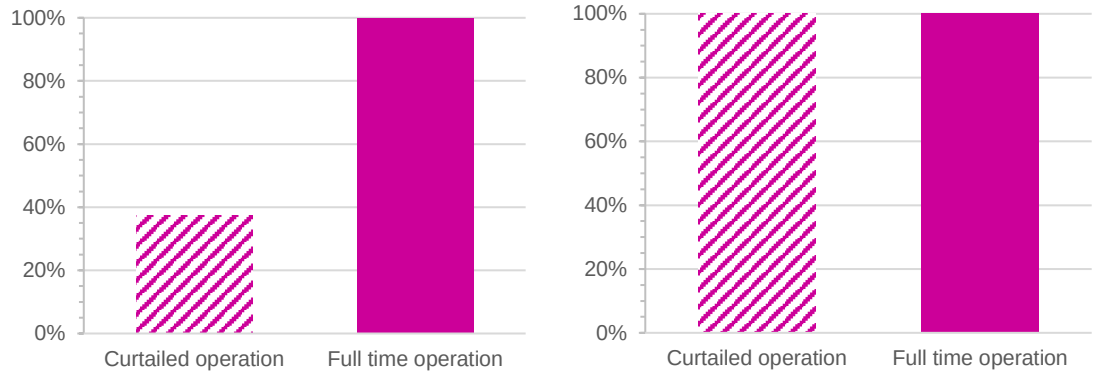

Figure A.0.97. The percentage of city bus fuel in Tyneside displaceable by renewable hydrogen in Dublin for different electrolyser operation modes by using a) wind electricity and b) wind and solar electricity

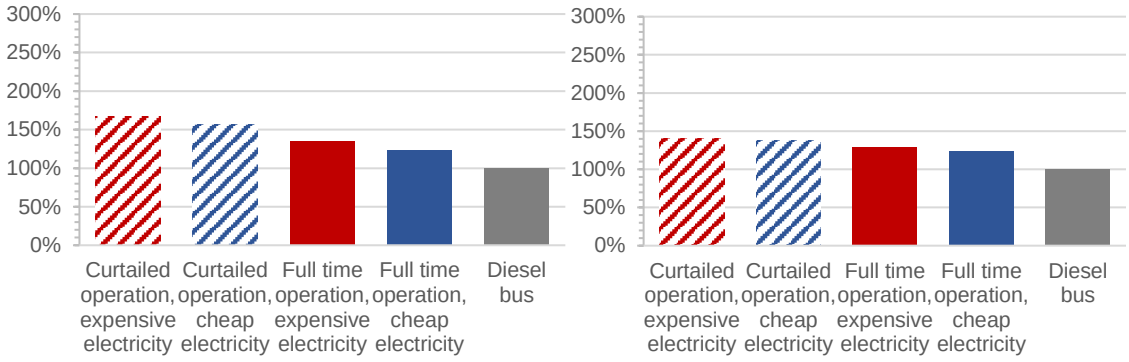

Figure A.0.98. The percentage of operational costs for hydrogen buses in Tyneside for different electricity prices and electrolyser operation modes by using a) wind electricity and b) wind and solar electricity, relative to diesel

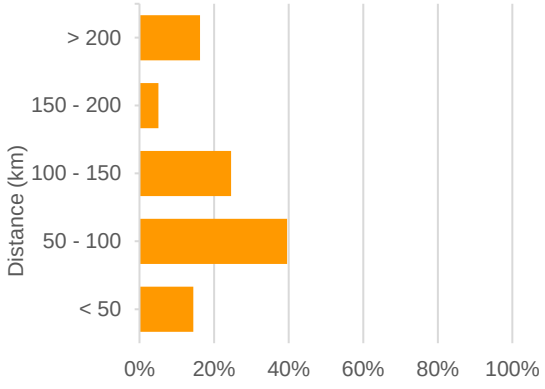

Figure A.0.99. Distances from hydrogen sources to city bus fleet in Tyneside

A.34. Luxembourg, Luxembourg

The estimated number of buses is 360 units.

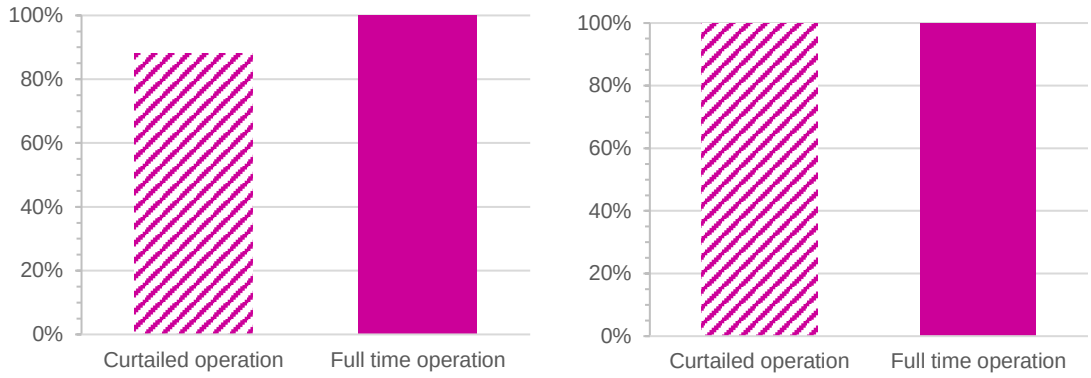

Figure A.0.100. The percentage of city bus fuel in Luxembourg displaceable by renewable hydrogen in Dublin for different electrolyser operation modes by using a) wind electricity and b) wind and solar electricity

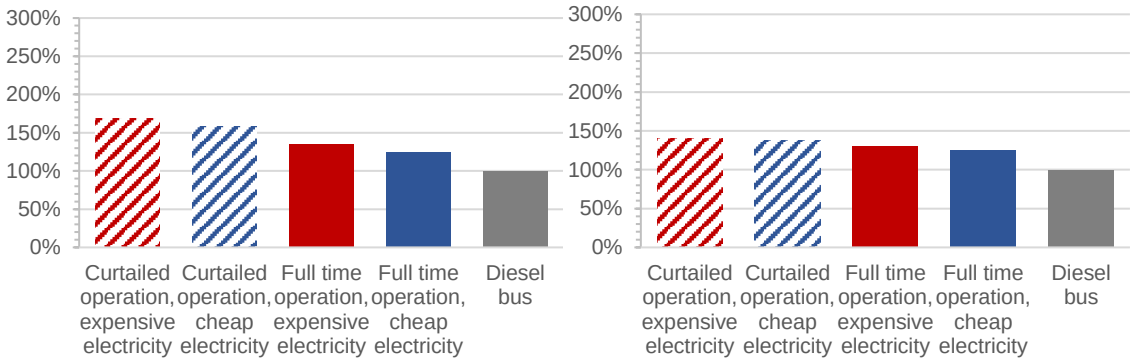

Figure A.0.101. The percentage of operational costs for hydrogen buses in Luxembourg for different electricity prices and electrolyser operation modes by using a) wind electricity and b) wind and solar electricity, relative to diesel

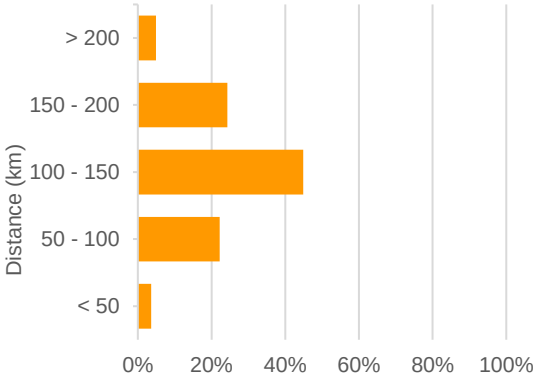

Figure A.0.102.Distances from hydrogen sources to city bus fleet in Luxembourg

A.35. Amsterdam, Netherland

The estimated number of buses is 478 units.

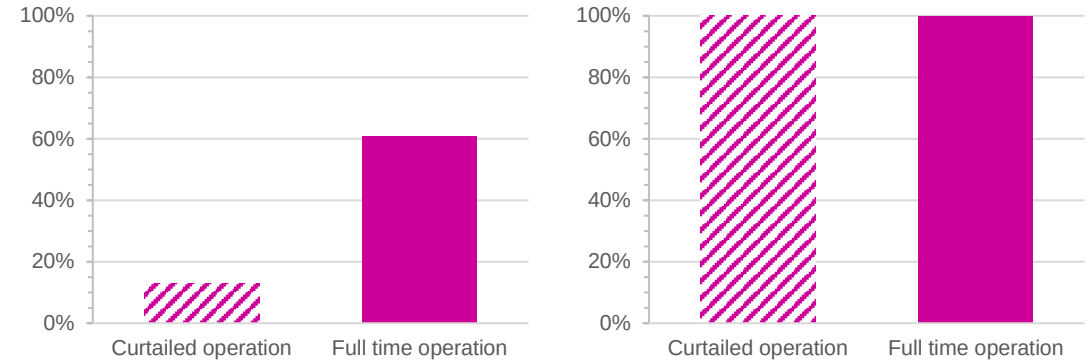

Figure A.0.103. The percentage of city bus fuel in Amsterdam displaceable by renewable hydrogen in Dublin for different electrolyser operation modes by using a) wind electricity and b) wind and solar electricity

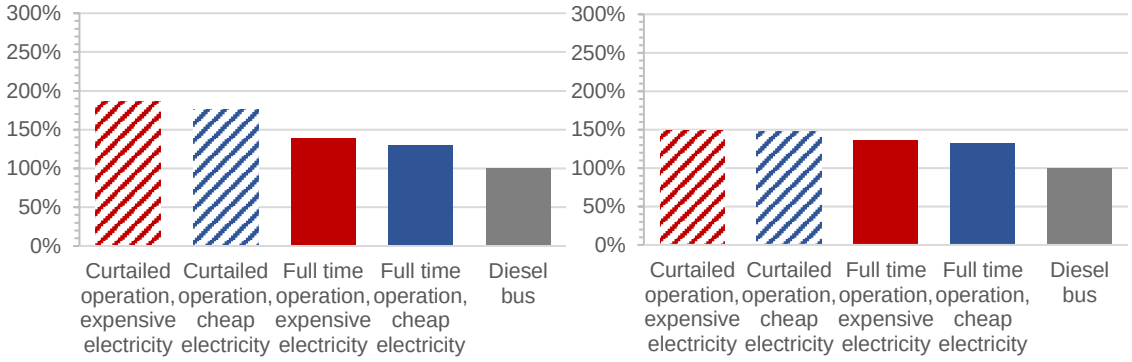

Figure A.0.104. The percentage of operational costs for hydrogen buses in Amsterdam for different electricity prices and electrolyser operation modes by using a) wind electricity and b) wind and solar electricity, relative to diesel

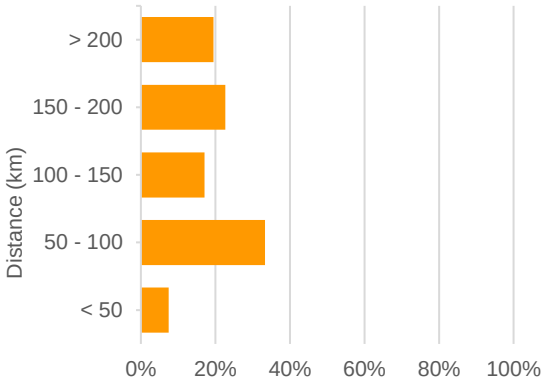

Figure A.0.105. Distances from hydrogen sources to city bus fleet in Amsterdam

A.36. Rotterdam, Netherland

The estimated number of buses is 442 units.

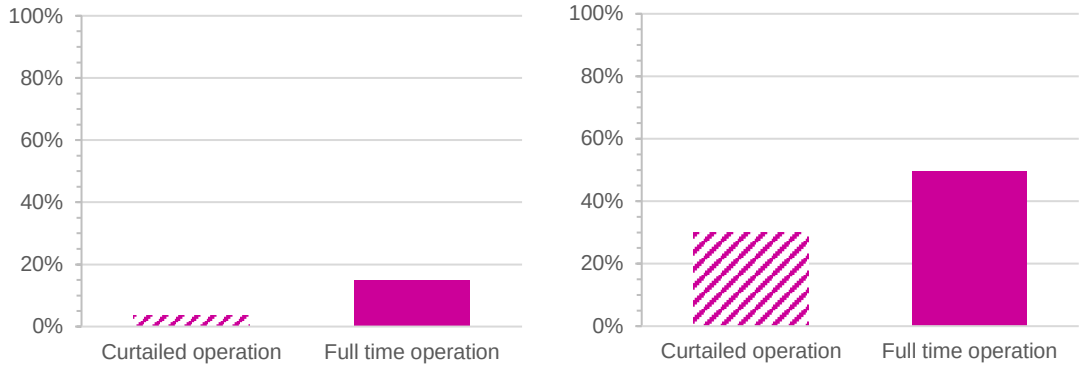

Figure A.0.106. The percentage of city bus fuel in Rotterdam displaceable by renewable hydrogen in Dublin for different electrolyser operation modes by using a) wind electricity and b) wind and solar electricity

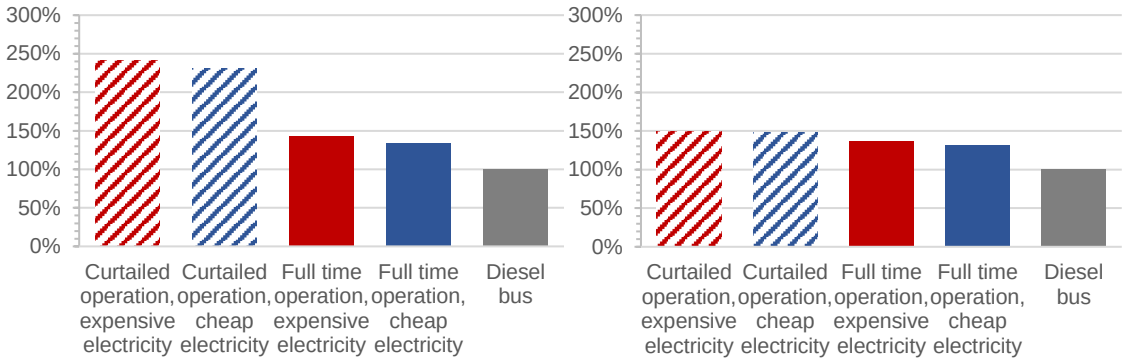

Figure A.0.107. The percentage of operational costs for hydrogen buses in Rotterdam for different electricity prices and electrolyser operation modes by using a) wind electricity and b) wind and solar electricity, relative to diesel

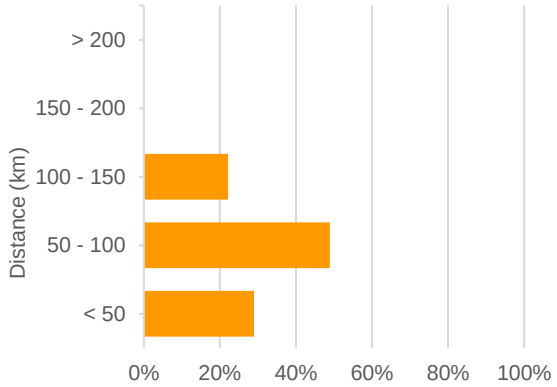

Figure A.0.108. Distances from hydrogen sources to city bus fleet in Rotterdam